



UNIVERSITY OF IOANNINA
SCHOOL OF PHYSICAL SCIENCES
DEPARTMENT OF CHEMISTRY

DETECTION, PHOTOLYTIC FATE AND REMOVAL OF ANTIDEPRESSANTS IN AQUEOUS ENVIRONMENT

Cristina Jiménez Holgado

CHEMIST, MSc

DOCTORAL THESIS

2021

Ioannina

With the co-financing of the European Union program "Horizon 2020" (Marie Skłodowska-Curie grant agreement No 765860)





ΠΑΝΕΠΙΣΤΗΜΙΟ ΙΩΑΝΝΙΝΩΝ
ΣΧΟΛΗ ΘΕΤΙΚΩΝ ΕΠΙΣΤΗΜΩΝ
ΤΜΗΜΑ ΧΗΜΕΙΑΣ

DETECTION, PHOTOLYTIC FATE AND REMOVAL OF ANTIDEPRESSANTS IN AQUEOUS ENVIRONMENT

Cristina Jiménez Holgado

ΧΗΜΙΚΟΣ, MSc

ΔΙΔΑΚΤΟΡΙΚΗ ΔΙΑΤΡΙΒΗ

2021

Ιωάννινα

Με τη συγχρηματοδότηση του προγράμματος της Ευρωπαϊκής Ένωσης «Ορίζων 2020» (Marie Skłodowska-Curie grant agreement No 765860)



«Η έγκριση της διδακτορικής διατριβής από το Τμήμα Χημείας της Σχολής Θετικών Επιστημών, του Πανεπιστημίου Ιωαννίνων δεν υποδηλώνει αποδοχή των γνώμων του συγγραφέα Ν. 5343/32, άρθρο 202, παράγραφος 2»

Ορισμός Τριμελούς Συμβουλευτικής Επιτροπής από τη Συνέλευση: 976/27-04-2018

Μέλη Τριμελούς Συμβουλευτικής Επιτροπής:

Επιβλέπων:

Associate Professor, Sakkas Vasilios, University of Ioannina

Μέλη:

Professor AlbanisTriantafyllos, University of Ioannina

Professor Prodromidis Mamantos, University of Ioannina

Ημερομηνία ορισμού θέματος: 28-05-2021

Θέμα: « Detection, Photolytic Fate And Removal Of Antidepressants In Aqueous Environment »

ΟΡΙΣΜΟΣ ΕΠΤΑΜΕΛΟΥΣ ΕΞΕΤΑΣΤΙΚΗΣ ΕΠΙΤΡΟΠΗΣ από τη Συνέλευση: 1041/19-07-2021

1. Associate Professor, Sakkas Vasilios, University of Ioannina (Supervisor)
2. Professor AlbanisTriantafyllos, University of Ioannina (member of Advisory Committee)
3. Professor Prodromidis Mamantos, University of Ioannina (member of Advisory Committee)
4. Professor Stalikas Constantine University of Ioannina (member of Evaluation Committee)
5. Professor Stathopoulos Vasileios, National and Kapodistrian University of Athens (member of Evaluation Committee)
6. Professor Calza Paola, Università degli Studi di Torino, (member of Evaluation Committee)
7. Professor Richard Claire, Université Clermont Auvergne, UFR Sciences et Technologies (member of Evaluation Committee)

Έγκριση Διδακτορικής Διατριβής με βαθμό «ΑΡΙΣΤΑ, 10» στις 15-09-2021

Η Πρόεδρος του Τμήματος Χημείας
Λουλούδη Μαρία, Καθηγήτρια

Η Γραμματέας του Τμήματος
Ξανθή Τουτουτζόγλου

To my parents Magdalena and Manuel.

Acknowledgements

I would first like to thank my advisor Dr. Vasilios Sakkas for giving me this great opportunity to work in his lab. I learned a lot from his insight and advice how to be a successful research scientist. Thanks to him for his patience and direction throughout my thesis experience. Thanks also to all the people that I had the opportunity to work with in the lab: Christophoros, Loukia, Thalia, Giannis, Anna, Irene and a special thanks to Merina Kalaboka for teaching me her knowledges and for her great support inside and outside the lab.

During this period I had the opportunity to travel and work in different places in Europe. I would like to thank Prof. Vasileios Stathopoulos for hosted me in Chalkida and for his kindness reception and for making me feel like at home. As well, I wish to thank Prof. Claire Richard for hosted me in Clermont-Ferrand and for her professionalism and for helping me to understand a completely different field of my studies. And finally, I would like to thank to Prof. Debora Fabbri and Prof. Paola Calza for hosted me in Turin in the kindness possible way and for all their guidance and their scientific knowledge.

Last but not least, a big thanks to Dimitra, Alice, Iván, Nuno, Masho and to all my fellow ESRs and friends, for all the great moments during these three years. I am really happy to have met with all of you and it would not be the same without you.

Finally and most important, I would like to thank my family, for their love and constant support and encouragement not only in this period but in all areas of life. Without whom I would never have come this far. This work is yours.

INDEX

Thesis Abstract	7
List of publications	9
Abbreviations and acronyms	11
Chapter 1. Introduction. State of the art	13
1.1. Emerging contaminants.....	13
1.1.1. Effects of ECs in human health and environment.....	14
1.1.2. Legislation of emerging contaminants	16
1.2. Pharmaceuticals.....	19
1.2.1. Effects of PhACs in the environment and in human health.....	20
1.3. Selection of target emerging contaminants	22
1.3.1. Psychiatric pharmaceuticals	22
1.3.1.1. Antidepressants.....	23
1.3.1.2. Antipsychotics	24
1.4. Extraction techniques of micropollutants	25
1.4.1. Fabric Phase Sorptive Extraction (FPSE)	27
1.4.1.1. FPSE media.....	29
1.4.1.2. Design and preparation of the sol solution for the substrate's sol-gel coating procedure	31
1.5. Liquid chromatographic analysis	33
1.5.1. LC-Detectors.....	35
1.5.2. Mass spectrometer	36
1.5.3. Ion sources for mass spectrometry	38
1.5.4. Electrospray ionization (ESI)	39
1.5.5. Mass analyzers	41
1.5.6. High resolution mass spectrometry	42

1.5.7. Orbitrap mass analyzer	43
1.6. Fate and remediation methods of CE in the environment: Advanced Oxidation Processes.....	45
1.6.1. Degradation by UV-photolysis	47
1.6.2. Photocatalysis	50
References.....	52

Chapter 2. Development of a green analytical microextraction method for the determination of three psychoactive drugs 66

2.1. Abstract	66
2.2. Introduction	67
2.3. Materials and methods	69
2.3.1. Reagents	69
2.3.2. Sample collection	70
2.3.3. HPLC analysis	71
2.3.4. Preparation of sol-gel sorbent-coated FPSE media.....	72
2.3.4.1. Pretreatment of media for sol-del coatings.....	72
2.3.4.2. Preparation of the sol-gel solutions for coating on the substrate surface	73
2.3.4.3. Fabric Phase Sorptive Extraction process	73
2.4. Results and discussion.....	75
2.4.1. Selection of FPSE substrate and sol-gel coating.....	75
2.4.2. Optimization of the experimental conditions.....	75
2.4.2.1. Preliminary experiments.....	76
2.4.2.2. Experimental design optimization.....	77
2.4.3. Analytical performance	80
2.4.4. Applications in environmental samples	81
2.5. Conclusions.....	82
Supplementary Material	85
References.....	87

Chapter 3. Phototransformation of three psychoactive drugs in presence of sedimental water extractable organic matter	91
3.1. Abstract	91
3.2. Introduction	92
3.3. Materials and methods	94
3.3.1. Sediment sampling and analysis	94
3.3.2. Chemicals and preparation of solutions	95
3.3.3. Water extractable organic matter extraction	96
3.3.4. DOC analyses.....	96
3.3.5. Optical analyses	97
3.3.6. Irradiations.....	97
3.3.7. HPLC Analyses	98
3.3.8. Ecotoxicity assessment.....	99
3.4. Results and discussion.....	100
3.4.1. Main characteristics of the sediments	100
3.4.2. Extraction and characterization of WEOM from sediments.....	101
3.4.3. Photoproduction of reactive species upon WEOM irradiation.....	102
3.4.4. Irradiation of drugs in the presence of WEOM.....	104
3.4.5. Drugs photoproducts.....	106
3.4.6. Prediction of ecotoxicity assessment	111
3.5. Conclusions.....	114
Supplementary material	116
References.....	121
Chapter 4. Exploring the photolytic and photocatalytic transformation of Sertraline: kinetics, degradation mechanism and toxicity assessment	127
4.1. Abstract	128
4.2. Introduction	128

4.3. Experimental details.....	130
4.3.1. Reagents	130
4.3.2. Irradiation procedures.....	131
4.3.2.1. Direct and indirect photolysis	131
4.3.2.2. Photocatalytic procedures	131
4.3.3. Analytical procedures	132
4.3.4. Toxicity.....	134
4.4. Results and discussion.....	134
4.4.1. Photolytic degradation	134
4.4.2. Photocatalytic performance	137
4.4.3. Structural elucidation of the transformation products	139
4.4.3.1. Hydroxylated compounds.....	141
4.4.3.2. Dechlorinated compounds.....	143
4.4.3.3. Compounds at lower molecular weight.....	143
4.4.4. Toxicity of sertraline and its TPs	145
4.5. Conclusions.....	147
Supplementary material	150
References.....	170

Chapter 5. Exploring the photolytic and photocatalytic transformation of Citalopram: kinetics, degradation mechanism and toxicity assessment 175

5.1. Abstract	175
5.2. Introduction	176
5.3. Materials and methods	178
5.3.1. Reagents and materials	178
5.3.2. Sample collection	178
5.3.3. Irradiation procedures.....	179
5.3.3.1. Natural sunlight irradiation.....	179

5.3.3.2. Simulated solar irradiation.....	179
5.3.3.3. Photocatalytic experiments	180
5.3.4. Analytical procedures.....	180
5.3.5. Identification of by-products	181
5.3.6. Toxicity measurements	182
5.4. Results and discussion.....	182
5.4.1. Irradiation experiments.....	183
5.4.1.1. Natural sunlight experiments.....	183
5.4.1.2. Simulated solar irradiation experiments.	185
5.4.1.3. Photocatalytic experiments	186
5.4.2. Identification and evolution of TPs	188
5.4.3. Toxicity assessment.....	194
5.5. Conclusions.....	196
Supplementary Materials.....	201
References.....	213
Chapter 6. Exploring the photolytic and photocatalytic transformation of Clozapine: kinetics, degradation mechanism and toxicity assessment	217
6.1. Introduction	217
6.2. Materials and methods	219
6.2.1. Materials.....	219
6.2.2. Sample collection	219
6.2.3. Irradiation experiments.....	220
6.2.3.1. Natural solar light.....	220
6.2.3.2. Artificial solar irradiation	221
6.2.3.3. Photocatalysis	222
6.2.4. Irradiation experiments.....	223
6.2.5. Toxicity.....	224

6.3. Results and Discussion	225
6.3.1. Natural sunlight Irradiation	225
6.3.2. Artificial solar irradiation	227
6.3.3. Photocatalysis	229
6.3.4. Toxicity assessment.....	231
6.4. Conclusions.....	232
References.....	234
Chapter 7. General conclusions	239
Summary of PhD activities	237

Thesis Abstract

The data presented in this PhD thesis is part of a multidisciplinary project that received funding from the European Union's Horizon 2020 Research and Innovation program under the Marie Skłodowska-Curie-Grant Agreement No 765860 (AQUALity). My individual project involves the research fields of Analytical Chemistry, Chemometrics tools, Materials Chemistry and Environmental Chemistry. The goals of this individual PhD project, were divided in different tasks accordingly to the following specific aims:

- The development of environmentally friendly practices for CECs determination
- The elucidation of the significance of photochemical reactions on their contribution to the abiotic transformation of CECs
- Via direct or indirect pathways
- Toxicity assessment
- And the application of this knowledge to real environmental waters such as hospital and WWTP effluent water from Ioannina, and Pamvotis Lake water, which it is a lake located in Ioannina as well.

The first main objective of this thesis was to develop a green analytical microextraction method for the determination and quantification of three different target pharmaceuticals (sertraline, citalopram and clozapine), belonging to the family of psychiatric drugs and are considered as contaminants of emerging concern. After that, their photolytic fate in the environment was investigated, and drugs were irradiated under different conditions (Xe-lamp and artificial and natural solar irradiation) and in different matrices (Milli-Q water, hospital effluent, WWTP, and Pamvotis Lake water) via direct or indirect pathways. As well, drugs were irradiated in the presence of organic

matter (WEOM) extracted under mild conditions from sediment of Lake Pamvotis. Moreover, Advance Oxidation Processes (AOPs) such as TiO₂ were applied for the abatement of pollution. Drugs photoproducts were identified by means of HPLC-HRMS and photodegradation pathways were proposed. Finally, toxicity assessment was followed based on *Vibrio fischeri* and US EPA ECOSAR computer mode.

List of publications

P1. Cristina Jiménez-Holgado, Christoforos Chrimatopoulos, Vassilis Stathopoulos, Vasilios Sakkas, Investigating the Utility of Fabric Phase Sorptive Extraction and HPLC-UV-Vis/DAD to Determine Antidepressant Drugs in Environmental Aqueous Samples, *Separations* 2020, 7, 39; [doi:10.3390/separations7030039](https://doi.org/10.3390/separations7030039)

P2. Maria Kalaboka, Christoforos Chrimatopoulos, **Cristina Jiménez-Holgado**, Vasiliki Boti, Vasilios Sakkas * and Triantafyllos Albanis. Exploring the efficiency of UHPLC-orbitrap MS for the determination of 20 pharmaceuticals and acesulfame k in hospital and urban wastewaters with the aid of FPSE. *Separations* 2020, 7, 46; [doi:10.3390/separations7030046](https://doi.org/10.3390/separations7030046)

P3. Jimenez-Holgado Cristina, Sakkas Vasilios Richard, Claire. Phototransformation of Three Psychoactive Drugs in Presence of Sedimental Water Extractable Organic Matter. *Molecules*, 2021, 1-17, doi.org/10.3390/molecules26092466

P4. Jimenez-Holgado Cristina, Calza Paola, Marco Coha, Chrimatopoulos Christoforos, Claudio Medana, Sakkas Vasilios, “Study of the Photoinduced Transformations of Sertraline in Aqueous Media”. *Science of the Total Environment*, 756, 2021, [DOI: 10.1016/j.scitotenv.2020.143805](https://doi.org/10.1016/j.scitotenv.2020.143805)

P5. Cristina Jiménez-Holgado, Paola Calza, Debora Fabbri , Federica Dal Bello, Claudio Medana, Vasilios Sakkas, “Exploring the photolytic and photocatalytic transformation of the antidepressant Citalopram: kinetics, degradation mechanism and toxicity assessment”. *Molecules*. Submitted.

Abbreviations and acronyms

POPs	Non-polar hazardous substances
CAS	Chemical Abstract Services
PFOS	Perfluorooctane sulfonates
DEET	N,N-diethyl-m-toluamide
WTD	Water Framework Directive
PS	Priority Substances
CEC	Contaminant of Emerging Concern
LC–MS/MS	Liquid chromatography tandem mass spectrometry
PhACs	Pharmaceutically Active Compounds
SER	Sertraline
CIT	Citalopram
CLO	Clozapine
SSRI	Selective Serotonin Reuptake Inhibitors
OECD	Organization for Economic Co-operation and Development countries (OECD)
HPLC	High performance liquid chromatography
MS	Mass Spectrometric
GC	Gas chromatography
TCA	Tricyclic Antidepressants
MAOI	Monoamine Oxidase Inhibitors
LLE	liquid-liquid extraction
SPE	Solid Phase Extraction
MSPE	Magnetic Solid Phase Extraction
FPSE	Fabric Phase Sorptive Extraction
PhACs	Pharmaceutically Active Compounds
MTMOS	Methyl-trimethoxysilane,
TEOS	Tetra-ethoxysilane
TMOS	Tetra-methoxysilane
C8-TMOS	octyl-trimethoxysilane
C18-TMOS	3-octadecyl-trimethoxysilane
3-APT MOS	Aminopropyl-trimethoxysilane
PTMOS	Phenyl-trimethoxysilane
PEG	Polyethylene glycol
PDMS	Polydimethylsiloxane
PTMEG	Polytetrahydrofuran polymers
TFA	Trifluoroacetic Acid
MTMS	Methyltrimethoxysilane
ToF	Time-of-flight
API	Atmospheric Pressure Ionization
ESI	Electrospray Ionization
APCI	Atmospheric Pressure Chemical Ionization
APPI	Atmospheric Pressure Photoionization
WWTP	Waste Water Treatment Plant

Abbreviations and acronyms (continued)

DWTP	Drinking Water Treatment Plants
AOPs	Advanced Oxidation Processes
ROS	reactive oxygen species
UV	Ultraviolet

Chapter 1. Introduction. State of the art

1.1. Emerging contaminants

The advancement of modern technologies, as well as the science that underpins them, is the bedrock of human progress. At both, global and individual levels, technological advancements have increased human welfare in terms of health, longevity, and general living conditions. The continual expansion of the chemical industry, as well as the employment of chemicals in many aspects of life, contributed to a clean impression of chemistry in our society during the first half of the twentieth century. Nowadays, the chemical industry is an important part of the economy in industrialized countries, and it is regarded as a key sector that contributes considerably to gross domestic product. According to the World Health Organization (WHO), more than 100,000 chemicals are released into the global environment every year as a result of their production, use, and disposal. Non-polar hazardous substances (POPs) and heavy metals were the subject of attention and recognition until the 1990s. However, as a result of technology manufacturing or human use, a new class of contaminants has emerged as an environmental issue, and there is widespread agreement that this type of contamination may require legislative intervention. The new class of contaminants, the so-called "emerging contaminants" (ECs), are defined as anthropogenic chemicals or substances of natural origin, which are currently not regulated but might be submitted to future regulations because they can pose risks to human health or the environment, as their persistence or toxicity

might alter the metabolism of a living being [1]. These are not necessarily new contaminants; emerging data on legacy compounds can also introduce new regulations or make the existing ones stricter. It is an extremely complex field of study, as 100 million chemicals are registered in the Chemical Abstract Services (CAS) database, and this number increases each year. Routine monitoring programs, determining whether compounds have the potential to be harmful to humans or the environment and, as a result, to what extent they should be regulated, their occurrence in environmental compartments, and techniques for treating environmental media to remove or transform them are all areas where knowledge is being developed [2]. The main CEs are divided into categories and are summarized in Table 1.1.

ECs from which originate before their transport to surface waters, groundwater, sediments, and drinking water are varied and include discharges or leaks of domestic, hospital or industrial wastewater containing pharmaceutical or personal care compounds, pesticide applications to agricultural land, parks, gardens, urban infrastructure, and the transport network, discharges or leaks of domestic, sewage sludge application to land, pharmaceutical and pesticides used to treat animals and solid waste disposal [3].

1.1.1. Effects of ECs in human health and environment

The increased consumption of these substances in developed countries raises the risk of environmental contamination and negative impacts on human health and environments [2]. These effects on human and environmental health are largely uncertain and there is not enough information about their fate, change, or degradation along the course they take. The effects of ECs on human health, environmental waters, and living organisms such as invertebrates and fishes, are important even at relatively low levels of exposure, because certain ECs can have an effect on biological systems [3,4]. ECs have been shown to have a wide variety of health impacts on humans and other animals. It has been noticed that this substance has the potential to cause cancer or have hazardous effects in both animals and humans, but the most common concern is endocrine disruption [5–8].

Table 1.1. Representative list of ECs.

Category	Compound Examples
Per fluorinated Compounds	Perfluorooctane sulfonates (PFOS), perfluorooctanoic acid
Pesticides	Organophosphorus pesticides, thiocarbamates
Food additives	Sucralose, triacetin
Nanoparticles	Titanium dioxide, fullerenes
Algal toxins	Microcystine
Antifouling compounds	Organotins (dibutyltin and triphenyltin ions), cybutryne
Insect repellents	N,N-diethyl-m-toluamide (DEET).
Flame retardants	Tetrabromobisphenol A, Hexabromocyclododecane
Surfactants	Alkylphenol ethoxylates, alkylphenols (nonylphenol and octylphenol), alkylphenol carboxylates
Antiseptic additives	Triclosan, triclocarban
Plasticizers	Bisphenol A
Steroids & hormones	Estradiol, estrone, estriol, diethylstilbestrol
Water (disinfection)	2,2,2-Trichloroacetamide, chloroacetaldehyde
Fragrances	Nitro, polycyclic, and macrocyclic musks
Drugs of abuse	Morphine, dihydrocodeine, cocaine
Sunscreen agents	2-ethyl-hexyl-4-trimethoxycinnamate, octocrylene
Analgesics, anti-inflammatory drugs	Ibuprofen, acetaminophen, codeine, aspirin, diclofenac
Veterinary and human antibiotics	Trimethoprim, sulfamethoxazole, erythromycin
Psychiatric drugs	Citalopram, Clozapine, Sertraline, Risperidone, carbamazepine
β -Blockers	Metoprolol, propranolol, timolol, bisoprolol
Lipid regulators	Gemfibrozil, bezafibrate, clofibrac acid, fenofibrac acid,
X-ray contrast agent	Iopromide, iothalamic acid, diatrizoic acid
Gasoline additives	tert-Butyl methyl ether, dialkyl ethers

The negative effects of a chemical can be assessed in a variety of ways. The acute toxicity of a chemical refers to its ability to cause harm as a result of a single short exposure. This is likely to be important in accidents and spills where the health effect is immediate. Chronic toxicity is the ability of a chemical to cause harm after repeated or prolonged exposure, such as in an industrial setting. The main effects are:

- toxicity (ability to cause unspecified harm)
- carcinogenicity (ability to produce tumors)
- mutagenicity (ability to cause alteration of genetic material)
- teratogenicity (effects on the fetus)

Genotoxic carcinogens, which are considered to be the most harmful to people, cause cancer by interfering with genetic information in the cells they affect. Other potential adverse effects include allergies, immune system disruption, and neurological system disruption. Toxic effects can be utilized in monitoring studies to help prioritize contaminants.

1.1.2. Legislation of emerging contaminants

To preserve the environment and human health, numerous laws have been implemented around the world to establish permissible amounts of pollutants in water, air, and soil, as well as effective control measures. The Water Framework Directive (WFD) aims to enhance water quality in all EU countries. According to the WFD, ecological and chemical factors must be considered in order to obtain good surface water quality. The ecological aspect is measured by aquatic plant life and fish, whereas the chemical aspect is measured by the presence of particular compounds in sediment, water, and biota [9].

Directive 2000/60/EC established a framework for the protection of inland surface water, transitional waters, coastal waters, and groundwater that prevents further deterioration and protects and improves the status of aquatic ecosystems, promotes long-term water use, and aims at

enhanced protection and improvement of the aquatic environment through specific measures [10,11].

Directive 2008/105/EU, amending Directive 2000/60/EC, established the first list of 33 priority substances/groups of chemicals (PSs) to be monitored in 2008 [12]. The list included 33 substances, including herbicides, pesticides, metals, alkylphenols, organic compounds, polycyclic aromatic hydrocarbons, benzo(a)pyrene, and polycyclic aromatic hydrocarbons, as well as another list of substances that would be reviewed for possible classification as priority substances or priority hazardous substances. However, these regulations did not involve any pharmaceutical substances. In 2013, the Directive 2013/39/EU[13] on priority compounds in the context of water policy, revising Directives 2000/60/EC and 2008/105/EU, marked a watershed moment in the control of medicines in the environment. The Directive 2013/39/EU revised previous documents by recommending the monitoring of 45 contaminants and emphasizing the need for new water treatment methods [13]. The new directive was very useful because it allowed the inclusion of emerging contaminants to the list of priority substances based on the findings of various studies, and, specifically in the case of pharmaceuticals, these agents are mentioned as contaminants of emerging concern for the first time. Furthermore, the Directive 2013/39/EU on advanced water policy established a first Watch List as a guideline of substances for which Union-wide monitoring data must be acquired in order to help future prioritizing exercises in the EU, with the complete list published in Decision 2015/495/EU.

This Watch List included ten chemicals/groups of compounds (a total of 17 organic substances). The significance of these provisions was demonstrated by the inclusion of three pharmaceuticals, diclofenac, 17-estradiol, and 17-ethynylestradiol, on the first watch list in order to collect monitoring data to aid in the determination of appropriate measures to address the risk posed by these substances [14]. The matrices that should be monitored, as well as the possible techniques of analysis for each substance/group of compounds, are also mentioned in Decision 2015/495/EU [14]. Liquid chromatography tandem mass spectrometry (LC-MS/MS) is the recommended analytical methodology for most Watch List CECs in the Decision 2015/495/EU [14].

The European Union recently proposed a second Watch List in Decision 2018/840/EU. Five compounds from the first Watch List were removed from the second Watch List (diclofenac, oxadiazon, triallate, EHMC, and BHT), while three new substances were added: two antibiotics, amoxicillin and ciprofloxacin, and the insecticide metaflumizone [10,15]. A summary of all regulations related to water quality and pharmaceutical compound lists as well as artificial sweeteners are summarized in Table 1.2.

Table 1.2. Main Directives and Regulation of environmental interest from EU related to target emerging contaminants.

Regulation	Ref.	Content
2000/60/EC	[11]	Establishing a framework for Community action in the field of water policy
2008/105/EU	[12]	Establishing environmental quality standards in the field of water policy, amending and subsequently repealing Council Directives 82/176/EEC, 83/513/EEC, 84/156/EEC, 84/491/EEC
2013/39/EU	[13]	Establishing a framework as regards priority substances in the field of water policy amending Directives 2000/60/EC and 2008/105/EC
2015/495/EU	[14]	Establishing a watch list of substances for Union-wide monitoring in the field of water policy pursuant to Directive 2008/105/EC of the European Parliament and of the Council
2018/840/EU	[15]	Establishing a watch list of substances for Union-wide monitoring in the field of water policy pursuant to Directive 2008/105/EC of the European Parliament and of the Council and repealing Commission Implementing Decision (EU) 2015/495
2001/83/EU	[16]	Establishing a Community code relating to medicinal products for human use
2001/82/EU	[17]	Establishing a Community code relating to veterinary medicinal products
2004/27/EC	[18]	Establishing a Community code relating to medicinal products for human use, amending Directive 2001/83/EC . Introduces specific precautions relating to the disposal of unused medicinal products
91/271/CEE	[19]	Establishing a framework concerning urban wastewater treatment

1.2. Pharmaceuticals

Pharmaceuticals are another major group of anthropogenic contaminants found in the aquatic environment, as a result of population increase and economic activity[8]. These compounds are used for treatment (cure/mitigation), diagnosis, alteration, and prevention of diseases. They are either designed to be highly active and interact with receptors in humans and animals, or they are aimed to be toxic to a wide variety of pathogenic organisms. Although studies on safety and toxicity are utilized to investigate the impacts of pharmaceuticals, the potential environmental consequences of their manufacture and use are less well understood and have only recently become a research topic of interest. In these chemicals, there is no persistent class of substances with identical chemical, structural, biological, or toxicological properties. As a result, they are classified according to their function and biological effect (e.g., antibiotics, analgesics, anti-neoplastics, anti-inflammatory substances, antihistamines, X-ray contrast media, surface disinfectants, etc.). These compounds are also called as Pharmaceutically Active Compounds (PhACs) because they are complex compounds with various physicochemical and biological properties and functionalities, which are pharmacologically active, resistant to degradation, highly persistent in aqueous medium, and potentially capable of causing harmful effects in aquatic organisms and harming human health [21].

In Europe, their use is continuously rising with 3000 compounds already on the market [22]. Pharmaceuticals can enter into the aquatic environment via a variety of methods, including animal and human waste, improper residential or industrial discharge, and landfill leaching [8], depending on the drug and its qualities. Over the last few decades, a wide range of studies have reported their existence in water systems of various types, at concentrations ranging from ng/L to a few g/L [23–31], raising worries about their possible impacts on human health, particularly after long-term exposure to low level concentrations.

Pharmaceutical contaminants, according to Rivera-Utrilla et al.[21], are classified based on: (a) having molecular masses <500 Da, although larger for some compounds, (b) containing chemically complex molecules with a large variety of structures, shapes, molecular masses, and functionalities, and (c) consisting of polar compounds having more than one ionizable group. Pharmaceuticals can also (d) exhibit properties and a degree of ionization that depends on the medium's pH, and (e) have lipophilic properties, while some may also have moderate water solubility. They also share (f) the ability to persist in nature, accumulate in life forms, and remain biologically active. Finally, these molecules tend to adsorb and spread in a live body, altering their chemical structure biologically [22]. The aquatic and terrestrial environments are threatened by metabolites, environmental transformation products (TPs) and parent PhACs.

1.2.1. Effects of PhACs in the environment and in human health

The extensive range of pharmaceutical structures associated with diverse biological activities, their surface-active nature, and persistence, not only of the parent chemicals but also of their metabolites, result in adverse effect in the environment, as well as potential dangers to human health[2]. Once they enter into the environment, these compounds become the target of diverse biotic factors (living organisms) and abiotic factors (sunlight, pH, temperature, salts, metals, other chemical compounds, and so on) that can potentially modify their properties and are converted into metabolites through a number of physical, chemical, and biological processes, which are often more persistent and toxic than the original compound [32,33].

Pharmaceuticals exist in the environment as complex mixtures, and their interaction with wildlife that may have high similarity with the molecular targets molecules, the so-called non-target organisms [34], may occur at relevant environmental concentrations due to combined and synergistic effects known as the "cocktail effect" [35]. Hormones and steroids are one of the major pharmaceuticals that affects the environmental. Exogenous natural or synthetic hormones have been shown in several studies to have a negative influence on the normal reproductive physiology of

several species, inducing direct effects on the gonads such as feminization, demasculinization, or size reduction. The main sex hormones found in water are 17 α -ethinyl estradiol, 17 α -estradiol, 17 β -estradiol, estrone, 17 α -testosterone, and 17 β -testosterone or androstenedione [36–42].

In addition, non-steroidal anti-inflammatory drugs (NSAIDs) which are widely used to relieve pain, reduce inflammation, and bring down a high temperature, have also been reported to cause oxidative stress, cyto-/genotoxicity, and even teratogenesis in a variety of aquatic species, including *Hyalella azteca*, *Danio rerio*, *Cyprinus carpio*, and *Xenopus laevis* [43–45]. A good example of this is the deaths of significant numbers of vultures in Central Asia caused by the ingestion of diclofenac by feeding on a putrefied body of a cattle which before was treated with this specific drug [46]. As a consequence, the death of vultures could cause an ecological imbalance that perhaps becomes a potential threat to human health.

Furthermore, the presence of pharmaceuticals in the environment has been linked to a wide range of toxic effects, including mortality, molting errors, hatching, variations in the rhythm of life, anatomical deformities, sublethal changes in plant growth, changes in biogeochemical cycles, changes in the sexual ratio of higher organisms, disinfectant damage to microbial communities, and trophic relationships[10,47,48].

Although the risks for humans are less evident than those for the environment, there are still significant concern about specific types of molecules, particularly as a consequence of European research (BIO IS, 2014), which shows that there is no clear short-term evidence of health effects on humans. Antibiotics, antiparasiticides, antifungals, and anticancer drugs are pharmaceutical categories that are especially designed to kill the target organism or cells and if they are exposed to the environment, they can have a substantial impact on human health. Humans may be exposed to pharmaceutical metabolites through drinking water. Although these drugs in drinking water are at much lower concentration than those used in therapy, drinking water regulations for most pharmaceuticals have yet to be established, even if the harmful effects produced on human health arising from these low concentrations in drinking water is extremely unlikely [49].

Furthermore, pharmaceutical effects can have an indirect impact on human populations through the food chain, for example if a crucial prey species is damaged[50]. According to several studies [51–55], PhACs can accumulate in fish and other aquatic species; therefore, exposure to these PhACs through consumption by organisms at higher trophic levels, including humans, must be assessed. Due to the lack of information on the accumulation of human pharmaceuticals in terrestrial wildlife and the other features mentioned above, it has recently become an important research concern.

1.3. Selection of target emerging contaminants

The NORMAN list of CECs was investigated; it contains 1036 compounds, including the most commonly discussed emerging substances and pollutants. Due to this, 41 pollutants of emerging concern were chosen as part of the AQUALity project to investigate their occurrence in the environment, photochemistry, potential removal technologies, and toxicity. Three contaminants: sertraline (SER), citalopram (CIT) and clozapine (CLO), classified as psychoactive drugs, were selected for their determination in environmental aqueous solutions (Chapter 2), detailed photochemical studies (Chapter 3, 4, 5, and 6) and their removal from the environment through Advanced Oxidation Processes (Chapter 4 and 5).

1.3.1. Psychiatric pharmaceuticals

My individual project focuses on three psychiatric compounds, which are one important class of pharmaceuticals that has recently received attention because of the global prevalence of psychiatric disorders. According to their therapeutic use, there are four main groups: antidepressants, anxiolytics, sedatives and hypnotics and antipsychotics[35]. The consumption of antidepressant drugs doubled in Organization for Economic Co-operation and Development countries (OECD) between 2000 and 2017 and is represented in Figure 1.1. This could be due to

increased awareness of depression, the availability of treatments, the evolution of clinical standards, and shifts in patient and provider attitudes[56]. Furthermore, their high consumption could be attributable to the increased insecurity caused by the European financial crisis, which could contribute to a variety of neurological problems [57–59].

As I mentioned before, the three target analytes of my project belong to antidepressant and antipsychotic groups, which are going to be explained in more detail below.

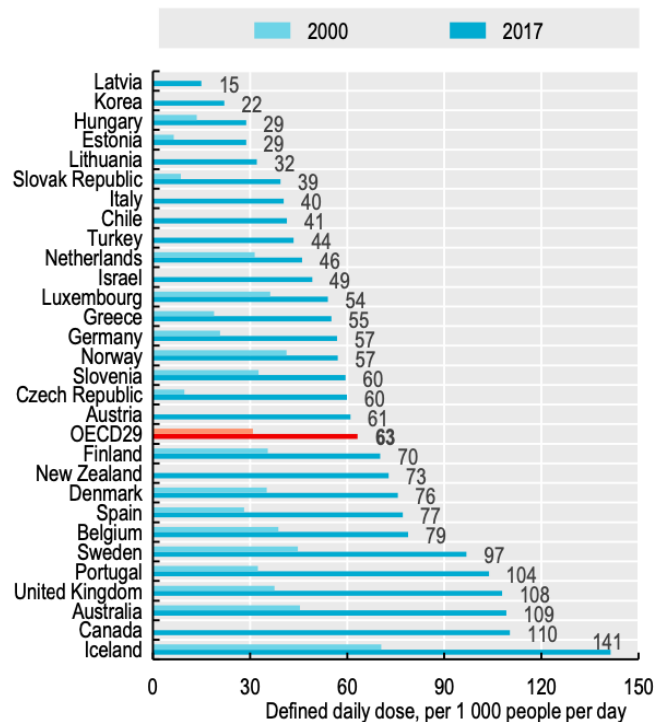


Figure 1.1.Antidepressant drug consumption between 2000 and 2017 [60].

1.3.1.1. Antidepressants

Antidepressants are used to treat depression by acting on multiple neurotransmitter systems, namely serotonin, norepinephrine, and dopamine. The three most important groups in which they are classified are: selective serotonin reuptake inhibitors (SSRI), where sertraline and citalopram are included, tricyclic antidepressants (TCA) and monoamine oxidase inhibitors (MAOI). The first antidepressants that were successfully utilized were tricyclic antidepressants [35]. However,

in addition to their initial activity, they exhibit neuropharmacological effects. SSRIs are nowadays recognized as a therapeutic breakthrough in psychopharmacology. The SSRI works by modifying the levels of the neurotransmitter serotonin, specifically by inhibiting the activity of the serotonin transporter in cell membranes, resulting in higher serotonin levels [35]. This class of antidepressants is largely prescribed to treat depression, anxiety, panic disorder, obsessive-compulsive disorder, eating disorders and social phobia. The antidepressants investigated in this study are sertraline (SER) and citalopram (CIT), both SSRIs. Below, their structures (Figure 1.2) and their main physical-chemical properties (Table 1.3) are shown.

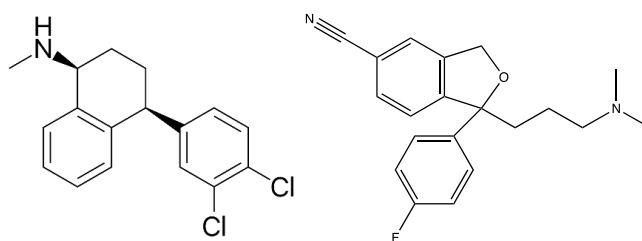


Figure 1.2. Structure of SER (right) and CIT (left).

Table 1.3. Main physical-chemical properties of SER and CIT.

Compound	MW (g/mole)	pKa	LogK _{ow}
Sertraline	306,23	9.87	5.10
Citalopram	324,39	9.78	3.76

1.3.1.2. Antipsychotics

Antipsychotics or neuroleptics are used to treat several psychiatric disorders, including schizophrenia, mania, dementia and delusional disorder. There are two groups: typical and atypical antipsychotics. The typical antipsychotic pharmaceuticals are the first generation of antipsychotics and they are chlorpromazine, haloperidol, flupenthixol, perphenazine, thioridazine, thiothixene and

trifluoperazine. The atypical antipsychotics, the second generation, include olanzapine, quetiapine, risperidone, aripiprazole, ziprasidone and clozapine. This last group represents a new generation of drugs prescribed for schizophrenia and delusional disorders[61]. The antipsychotics pharmaceuticals act by regulating serotonin and dopamine levels in the brain [62]. The representative compound of this category studied in this work was clozapine (CLO) and its structure (Figure 1.3) and physical-chemical properties (Table 1.4) are shown below.

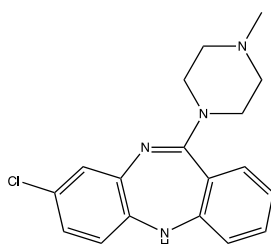


Figure 1.3. Structure of CLO.

Table 1.4. Main physical-chemical properties of CLO.

Compound	MW (g/mole)	pKa	LogK _{ow}
Clozapine	326.8	7.50	3.23

1.4. Extraction techniques of micropollutants

As I mention before, in recent years there has been a concerning overconsumption of psychiatric drugs. A wide spectrum of psychoactive drugs has already been discovered in surface waters and wastewater at concentrations ranging from a few ng/L to several tens of g/L [63–66]. As a result, identifying and quantifying of such pharmaceuticals in natural water is now critical, with concentration levels recorded as high as 78.3 g/L [65]. Numerous analytical procedures for the determination of these drugs have been published in the literature. High performance liquid

chromatography (HPLC) equipped with a UV–Vis or a mass spectrometric detector (MS) are the most widely utilized [67–75]. Gas chromatography (GC) coupled to MS [76–79] or tandem MS [80] has also been described, as well as the capillary electrophoretic method (CE) [81]. The limiting of the target compound's volatility is a significant disadvantage of GC approaches [82]. In comparison, HPLC can analyze both volatile and non-volatile chemicals, making it a user-friendly separation technology [83].

Because most samples cannot be directly injected into the chromatographic instrument, sample pretreatment is the most critical stage in the chromatographic analysis. Several sample preparation methods combined with HPLC for the detection and preconcentration of antidepressant in biological fluids have been published.

Extraction technique is the separation, isolation, and recovery of a substance from a chemical system by transferring it from one phase (liquid, solid, or suspension) to another phase (liquid). Compounds are extracted from liquid and solid environmental matrices by partitioning them into a single immiscible with water solvent and aqueous phase, or by retaining them on a column or a solid phase substrate, or, in rare cases, by evaporation to dry and selective reconstitution of the analyzed compounds.

Traditional extraction procedures, such as liquid-liquid extraction (LLE) and solid phase extraction (SPE), were established decades ago and have been since applied to sample processing. Traditional sample preparation approaches, on the other hand, have significant limitations, including: (a) excessive solvent consumption and waste production, (b) laboratory time-consuming routine, (c) frequent sample contamination, and (d) analytical errors due to the operator's handling necessary to complete these techniques. As a result, today's scientific focus is on analytical procedures that use minimal amounts of organic solvents, alternative non-chlorinated solvents, and the capacity to automatically deliver accurate, selective, and repeatable results. The progress in the traditional extraction technique resulted in a number of different methods using solid phase sorbent materials, like magnetic solid phase extraction (MSPE). Although MSPE avoid some of the limitations explained

before, still it has some drawbacks in sample preparation: low selectivity and stability in strong acidic aqueous media and in many sample matrices where they have a poor dispersion ability.

The most commonly used procedures are liquid–liquid extraction (LLE) [84] and solid-phase extraction (SPE) [85]. Fabric-Phase Sorptive Extraction (FPSE) has lately attracted the scientific community's interest, particularly in its application for the identification of pharmaceutical substances in biological samples. For this reason, in this project, we have developed a new green analytical microextraction method, FPSE, for the determination of the target compound in aqueous matrices.

1.4.1. Fabric Phase Sorptive Extraction (FPSE)

Kabir and Furton first proposed FPSE as a two-step, novel and green sample preparation technique [86]. FPSE successfully combines the advantages of sol–gel sorbents used in microextraction with a wide range of fabric substrates, resulting in a highly efficient and environmentally friendly sample pretreatment approach [87,88]. FPSE is able to overcome the two major fundamental limitations of other sorptive extraction techniques: the low sorbent capacity and the long sample preparation time. These two parameters are determined by the sorbent's thermodynamics, whereas the latter is also determined by kinetics. The maximum amount of analytes that can be extracted by unit mass of sorbent under a specific set of extraction conditions is determined by the sorbent's thermodynamic characteristics. Sorbent loading should be maximized since it allows for the accumulation of a greater mass of analyte under equilibrium extraction circumstances. However, the maximal sorbent loading capacity of a microextraction device is determined by the substrate type and design [89]. Kinetics, on the other hand, governs the rate of extraction and thus the time required to reach the extraction equilibrium. These factors are linked because increasing surface area allows for direct interaction with analytes during the extraction process and allows for larger sorbent loading without changing the coating method. As a result, more target analytes are adsorbed by the sorbent, and the extraction equilibrium time is reduced. Sol-gel

coating technology was used to address this issue. The strong connection between sol-gel coated sorbent and the substrate suggested by Malik et al.[90] results in a high level of solvent and chemical stability. Furthermore, the wide range of sorbent materials with high analyte retention capacity that may be employed makes sol-gel technology a versatile and practical coating process. Other advantages of this technique are: (a) The media can be direct immersed into the sample, (b) easy method, low cost and used of the minimal quantity of solvent, (c) versatility election of the organic solvent that can be utilized as eluent, (d) increased efficiency by magnetic stirring or sonication, (e) minimization of sample preparation processes, lowering sample pretreatment time and potential sources of mistakes, (f) as a sorbent, a variety of efficient sol-gel coatings can be used and (g) FPSE media have a high chemical resistance due to a strong chemical connection between the sorbent phase and the substrate [91].

This microextraction technique is capable of extracting a range of wide polarity analyzers, depending on the physicochemical properties of the colloidal gel. The porous network of the sol-gel coating, the permeability of the fabric substrate and the high active surface of the FPSE device, result in a very high sample loading capacity and high sensitivity in a relatively short time. The desorption of the analytes from the FPSE media is much faster, with no significant possibility of reabsorption and is accomplished by immersing the coated fabric in organic solvents. It is noteworthy that it allows a wide range of target compounds to be extracted directly from the sample, without any pretreatment[87].

As extraction medium, FPSE uses a natural or synthetic fabric substrate (cellulose, polyester, or fiberglass) that has been chemically coated with a sol-gel organic-inorganic hybrid sorbent. The FPSE technique generally consists of the following steps: first, the material is cleaned and conditioned to eliminate any impurities and to activate the surface of the material. After that, the FPSE media can then be directly immersed into the sample (blood, urine, milk, or environmental aqueous water) containing the target analytes and without any pretreatment for the extraction of the analytes. The FPSE media is removed after the extraction, and the analytes are eluted with a

small quantity of solvent into another vial. Then, the retained analytes are back extracted into that eluting system and the solvent is injected into the chromatographic system for the analysis. The FPSE process is presented below step by step (Figure 1.4). The FPSE medium can be washed with the solvent solution and reused, or it can be dried on a watch glass and stored in an airtight glass container for later use [92–94].

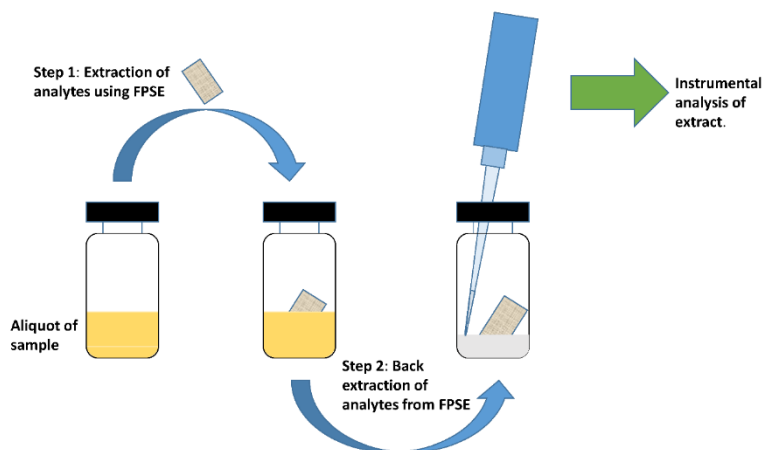


Figure 1.4. Schematical procedure of FPSE [94].

1.4.1.1. FPSE media

Fabric Phase Extraction media are made up of three basic components: (a) a fabric substrate, (b) a sol-gel inorganic precursor/organically modified inorganic precursor, (c) and a sol-gel active inorganic/inorganic polymer. Each component of the FPSE medium is detailed in detail below.

a) Fabric substrate

The most common substrates for FPSE media are cellulose, polyester, and fiberglass textiles. These materials have active functional groups that are chemically linked to the sol-gel sorbent network during the coating process. The amount of sorbent loading per unit area is determined by the concentration of sol-gel active functional groups as well as the amount of sorbent loading on the FPSE medium.

b) Organically/inorganic modified sol-gel precursor.

The inorganic/organically modified sol-gel precursor is also important in the sol-gel sorbent coating process. By inserting the inorganic/organic polymer into the networks in random positions, this precursor is responsible for the creation of 3D networks of sol-gel sorbent. It also functions as a ligand in sol-gel sorbent networks with fabric substrates. The most used precursors in the literature are: methyl-trimethoxysilane (MTMOS), tetra-ethoxysilane (TEOS), tetra-methoxysilane (TMOS), octyl-trimethoxysilane (C8-TMOS), 3-octadecyl-trimethoxysilane (C18-TMOS), aminopropyl-trimethoxysilane (3-APTMO), phenyl-trimethoxysilane (PTMOS), tetra-methoxygermane, titanium isopropoxide and zirconium isopropoxide[92].

c) Sol-gel active inorganic/organic polymer

Sol-gel active organic polymers such as polyethylene glycol (PEG) and polytetrahydrofuran polymers (PTMEG), as well as inorganic polymers such as polydimethylsiloxane (PDMS) and polydimethyldiphenylsiloxane, are incorporated into the sol-gel networks via the sol-gel process and are the primary source of selectivity and affinity toward the analytes of interest. Each polymer utilized in the sol-gel sorbent coating method has a unique structure and properties, resulting in various intermolecular interactions between polymers[92]. Figure 1.5 shows a schematic representation of sol-gel sorbent coated FPSE media.

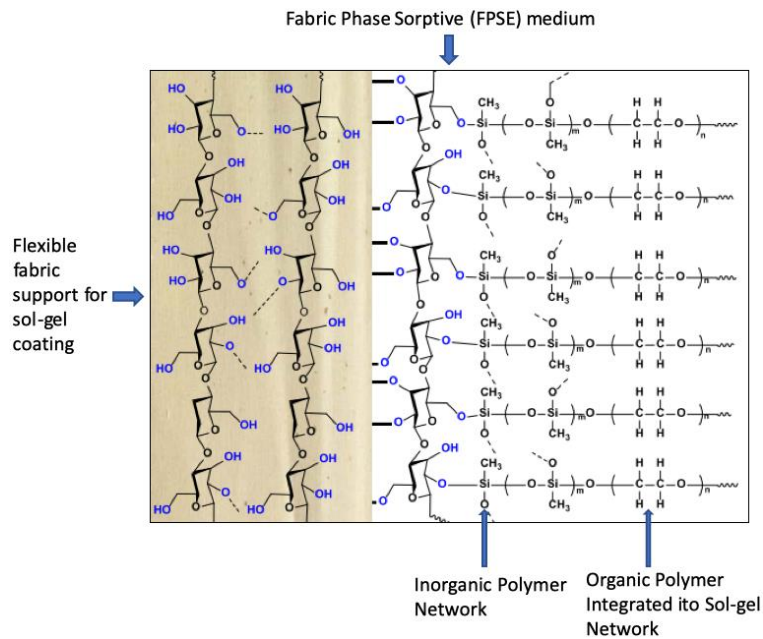


Figure 1.5. Schematic representation of FPSE medium and its different coating parts [92].

1.4.1.2. Design and preparation of the sol solution for the substrate's sol-gel coating procedure

The sol solution is an important parameter in the formation of sol-gel sorbents because its composition and relative ratios of components influence the porosity, selectivity, and specificity of the resulting sorbent[75]. The nature of the target analytes and the sample matrix determine the design of the sol solution. The choice of the sol-gel active organic polymer, the inorganic or organically modified inorganic sol-gel precursor, the solvent/solvent system, the catalyst, the amount of water, and an appropriate relative molar ratio of the constituents, must all be considered when creating an effective sol-gel sorbent.

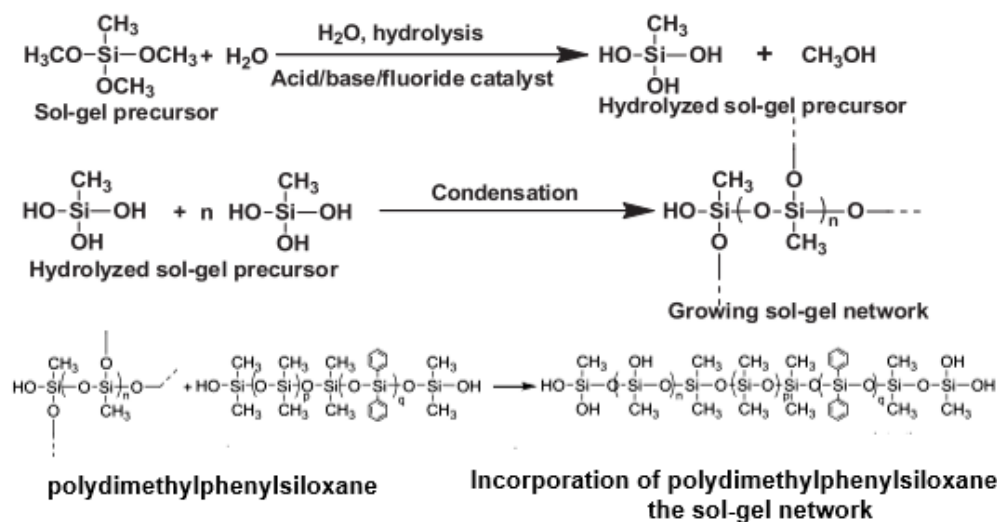


Figure 1.6 Chemical reactions involved in the sol-gel coating (poly-dimethyldiphenylsiloxane) [88].

The major advantages of sol-gel technology for sorbent-based microextractions include robust coating retention on the substrate due to chemical bonding, as well as a large reduction in extraction equilibrium time and quick mass transfer due to the porous structure [88].

The transfer of a liquid colloidal solution named as “sol” into a solid “gel” substrate is known as the sol-gel process. In this technique, the following primary sets of reactions occur [93,95]:

- Sol-gel precursor hydrolysis catalytically.
- Hydrolyzed Sol-gel active organic polymer is randomly incorporated into the developing sol-gel network.
- Sol-gel active organic polymer is randomly incorporated into the developing sol-gel network.
- Polycondensation immobilization of the forming sol-gel network on the substrate surface.

The sol-gel precursor is usually methyltrimethoxysilane (MTMS), while the sol-gel catalyst is trifluoroacetic acid (TFA) (95%-5% H₂O). The three methoxy groups of MTMS are hydrolyzed to generate hydroxyl groups during hydrolysis, and then polycondensation begins to form a 3D network. Sol-gel active organic polymer enters the network at random during the synthesis of the 3D network.

Finally, through polycondensation, the sol-gel sorbent network chemically bonds to the fabric substrate via the fabric hydroxyl groups. Figure 1.6 depicts a schematic illustration of sol-gel reactions as well as a schematic representation of sol-gel coating on fabric medium (Figure 1.7).

In conclusion, the aim was to develop a green analytical microextraction technique, called FPSE, for the determination and quantification of the three target analytes in different aqueous media. In Chapter 2 this technique is explained in detail.

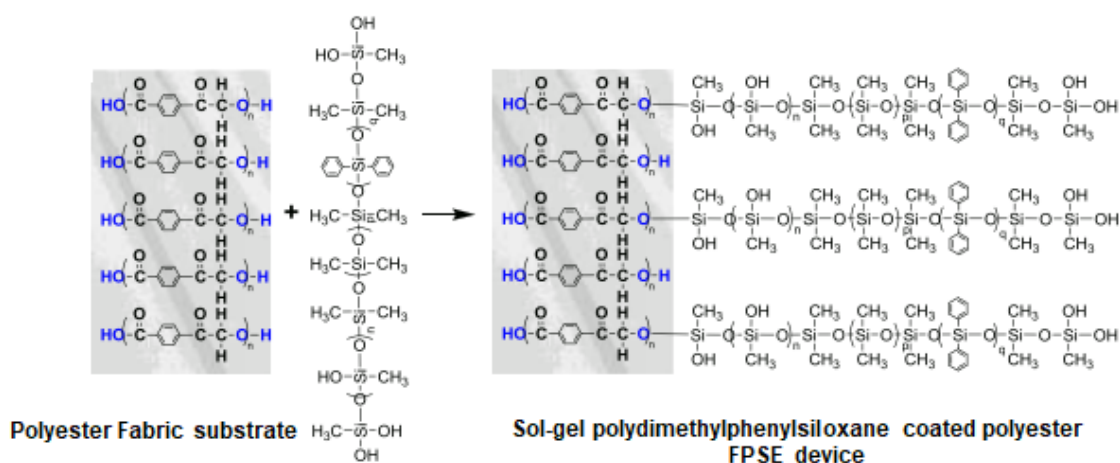


Figure 1.7. Schematic representation of sol-gel poly(dimethyldiphenylsiloxane) coating on a polyester fabric [92].

1.5. Liquid chromatographic analysis

Chromatography is a method of separating chemicals, which is based on the different distribution of the components of a mixture between a mobile and a static phase. Depending on the nature of the mobile phase, chromatography is characterized as gaseous or liquid. Liquid chromatography is a powerful analytical tool capable of identifying both polar and non-polar organic compounds in levels of ng/L without the need for derivatization, in a wide range of matrices including water bodies (wastewater, surface water, groundwater, and drinking water), solid samples (sewage sludge, manure, soil, or sediments), biological fluids (blood, plasma, urine), and environmental samples.

Emerging contaminants (ECs), as previously documented, can be detected at very low concentration levels up to ng/L in a variety of media, both natural and anthropogenic such as wastewater, rivers, lakes, soil, air, or live creatures. Since detection techniques in past decades were not capable to detect concentration levels in the range of g/L to ng/L in environmental or biological samples, most pollutants were unreported and were not categorized as emerging contaminants. Liquid chromatography, usually coupled with mass spectrometry (LC-MS), is a powerful tool for performing environmental analysis [96].

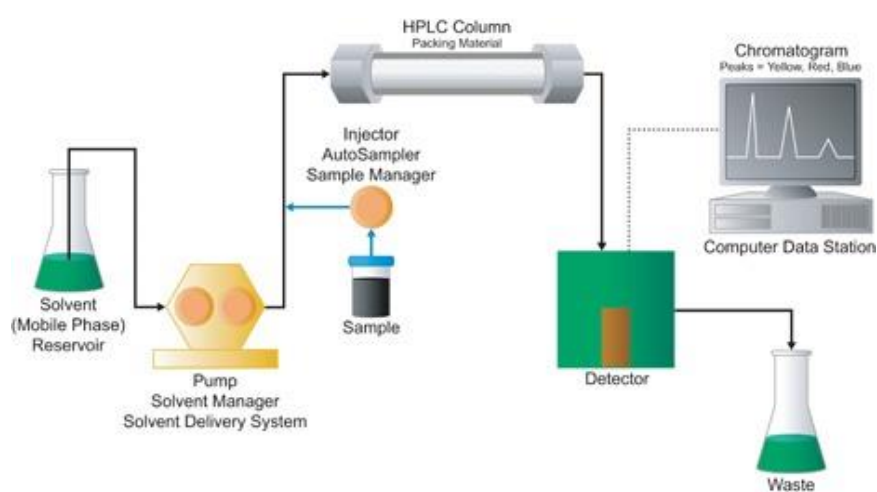


Figure 1.8. Liquid chromatographic system[97].

High-performance liquid chromatography(HPLC), also known as high-resolution liquid chromatography, uses very thin packing particles and a relatively high pressure for analytical separations of solutions, detection, and quantification, providing fast analysis times and a very high resolution [96]. Figure 1.8 depicts the fundamental components of a typical chromatographic system.

The stationary phase in liquid chromatography is commonly a packed chromatographic column made up of irregularly or spherically shaped particles. Once the sample is introduced, the mobile phase passes through the equipment carrying the sample. Because of variations in ion-exchange, adsorption, partitioning, or size as the sample moves through this system, the compounds interact with the stationary phase, resulting in the retention of distinct solutes by this phase. As a result, there is a variation in the rate of transit for these components, allowing the compounds to be

separated. A separation requires not only a difference in retention, but also that the peaks of two neighboring compounds be sufficiently narrow to allow this difference to be seen. There are a number of factors that influence chromatographic efficiency: column length, tube diameter and particle size of the column, uniformity in size, shape, and packing material of the column, flow rate and linear velocity, temperature and rate of solute diffusion, mobile phase and the initial injection volume [97].

Reversed-phase liquid chromatography, which utilizes a non-polar (hydrophobic) stationary phase, such as a C18 sorbent, and a polar (aqueous) mobile phase, such as water, is the most frequently used separation technique for quantitative analysis. Then, reversed-phase chromatography appears to be more adaptable for a wide range of substances, using low-cost solvents that are also safer than those used in normal-phase chromatography.

1.5.1. LC-Detectors

One of the most significant advantages of liquid chromatography is that it provides a platform compatible with a wide range of detectors. Typical LC detectors include the following:

- UV detector
 - o Single wavelength (filter)
 - o Variable wavelength (monochromator)
 - o Multiple wavelengths (Photodiode array detector (PDA))
- Fluorescence
- Electrochemical detector
- Mass spectrometry

Chromatographic system's detectors are responsible for recording the sample compounds that have previously been separated in a chromatographic column and transferring this information to a data output device. The combination of LC techniques and mass spectrometry has been formed

as a result of advancements in chromatographic systems due to the development of new apparatus (MS) [98]. Due to the sensitive and highly specific character of mass spectrometry compared to other chromatographic detectors, coupling it to chromatographic procedures has long been desirable. The combination of LC and MS takes advantage of both LC's power and versatility as a separation technique and MS's value as a sensitive and selective detection and identification tool. These two methodologies' inherent qualities have resulted in the advanced development of a potent analytical chemistry instrument with applications in environmental chemistry, biomedical and clinical toxicology, forensic science, and food analysis, among other fields.

1.5.2. Mass spectrometer

Due to its high sensitivity, selectivity, mass accuracy, and throughput capabilities, mass spectrometry (MS) is one of the most powerful analytical instruments, and its application is growing in a variety of scientific fields. Analytical and environmental chemistry [99,100], food authentication and food safety [101,102], biomedical and clinical research [103–105], forensic science [106,107], sports doping control [108], and pharmaceutical manufacturing industries [109], are only a few of the applications.

Mass spectrometry is an analytical technique that can precisely quantify the atomic or molecular weight of ionized atoms or molecules, represented as mass-to-charge ratio (m/z) values. The sample introduction, the source where ionization happens, the mass analyzer, and the detector are the four basic components of a conventional mass spectrometer. For data output, it has also been linked to a computer recorder (Figure 1.9).

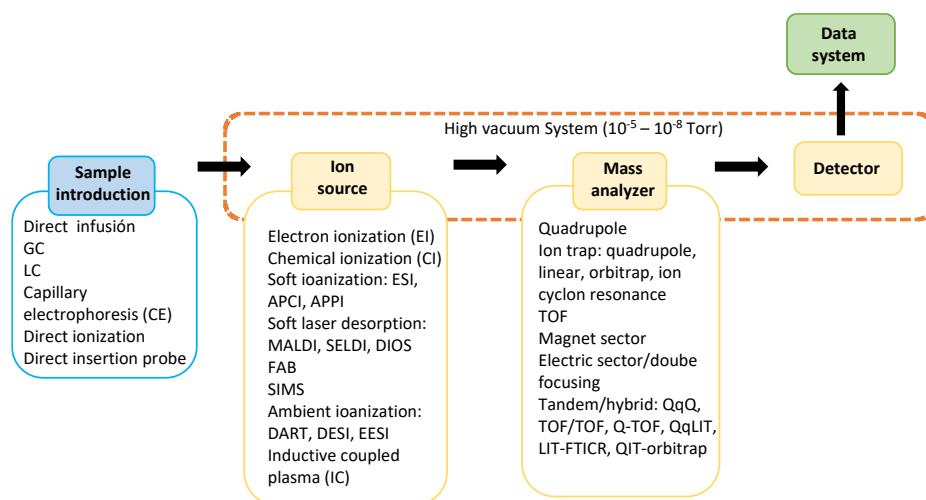


Figure 1.9. Basic Components of a Mass Spectrometer.

Although mass spectrometers come in a variety of shapes and sizes, they consistently share three characteristics (Figure 1.9). Firstly, it is a method for ionizing atoms or molecules in the sample. Because electric fields employed in mass spectrometers cannot steer neutral species, it is required to create ions. There are a variety of ways to do this, which are referred to as ion sources collectively.

The mass analyzer is the second component of all mass spectrometers. The m/z ratio of ions can be measured using numerous different methods. The most common mass analyzers are time-of-flight (ToF), magnetic sector, and quadrupole mass analyzers, each one with its own set of advantages and disadvantages.

A method for detecting or counting the amount of ions for a certain m/z value is the final component common to all mass spectrometer systems. These detectors come in a variety of shapes and sizes, the most common being electron multipliers, Faraday cups, channel trons, and channel plates. Each has its own set of strengths and weaknesses[110,111].

Finally, how to couple the ion source to the sample in order to produce the ions for measurement must be considered, especially because all mass spectrometers must be operated under vacuum. The sample will be held under vacuum in some situations, at atmospheric pressure in others (usually referred to as ambient MS techniques), and others will contain some other kind of

separation technology before being introduced to the ionization chamber. The sections that follow will go through these three common mass spectrometer components in greater depth.

1.5.3. Ion sources for mass spectrometry

Prior to analysis in the mass spectrometer, the studied samples are ionized in the ion sources. Mass spectrometry employs a variety of ionization processes. The internal energy transferred during the ionization process, as well as the physicochemical qualities of the analyte that can be ionized, are the most significant factors to consider. Some ionization processes are quite energetic, resulting in a high fragmentation. Other methods are milder, producing ions of the molecular species. Only gas-phase ionization is acceptable for electron ionization, chemical ionization, and field ionization; hence their employment is restricted to substances that are sufficiently volatile and thermally stable.

However, several molecules are thermally labile or do not have enough vapor pressure. Molecules of these substances must be extracted directly from the condensed to the gas phase. There are two types of direct ion sources: liquid-phase ion sources and solid-state ion sources. The analyte is in solution in liquid-phase ion sources. This solution is transported as droplets into the source where ions are generated at atmospheric pressure (API) by nebulization and focused into the mass spectrometer via vacuum pumping stages (Figure 1.10). This class includes electrospray (ESI), atmospheric pressure chemical ionization (APCI), and atmospheric pressure photoionization sources (APPI). The analyte is in an involatile deposit in solid-state ion sources. It is created through a variety of processes, the most common of which involves the introduction of a matrix, which can be either solid or viscous fluid. Ion production is frequently associated with gas-phase ion–molecule processes [112].

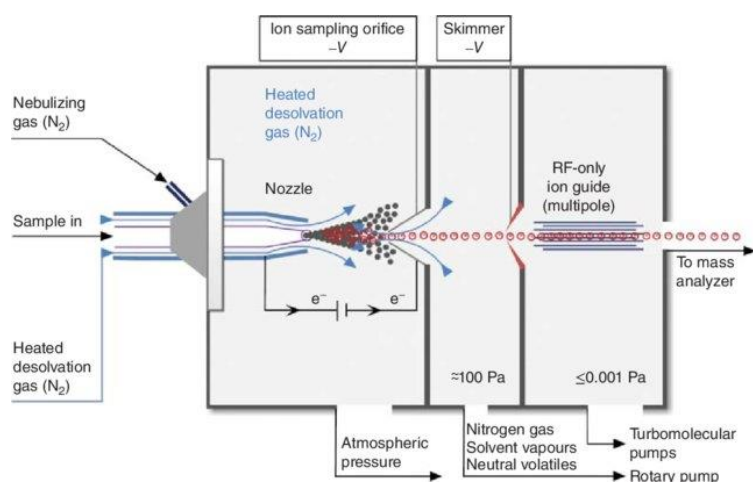


Figure 1.10. Atmospheric Pressure Ionization mode (API) with an electro spray ionization (ESI) inlet [113].

Electrospray Ionization (ESI) and Atmospheric Pressure Chemical Ionization (APCI) are the two most commonly used APIs for LC nowadays. ESI occurs in the liquid phase and is primarily used with polar molecules. APCI, on the other hand, occurs in the gas phase and can be used to ionize less polar molecules. Atmospheric Pressure Photoionization (APPI) is a less common ionization technique for LC-MS. In comparison to ESI and APCI, APPI is the last soft ionization technology that can ionize less polar and nonpolar molecules that ESI and APCI cannot. Figure 1.11 depicts the application of various ionization technologies based on the polarity and molecular weight of target chemical compounds.

1.5.4. Electrospray ionization (ESI)

ESI employs electrical energy to aid the transfer of ions from solution to gaseous phase prior to mass spectrometric analysis. ESI has emerged as an important ionization technique for the on-line linking of liquid phase separation technologies with mass spectrometry (MS). It is a simple and precise technology that works with small and large molecules, works at atmospheric pressure, and is likely the most gentle ionization technique available for MS.

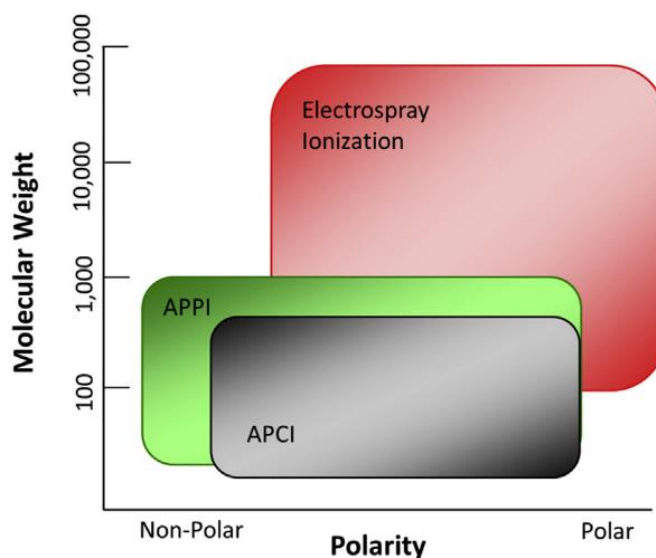


Figure 1.11. Application of atmospheric pressure ionization (API) techniques depending of polarity and molecular weight[108].

ESI is considered a “soft” ionization source under typical conditions, which means that relatively little energy is transferred to the analyte, and hence little fragmentation occurs. Increased ESI “in-source” fragmentation can be achieved by increasing voltages within the source to promote collisions with nitrogen molecules [109].

Electrospray ionization (ESI) is a procedure in which a high potential is applied to a liquid to produce a fine aerosol (Figure 1.12). Typically, a liquid sample is delivered into a spray needle/capillary at a flow rate of 1–1,000 L/min. A voltage of 3–6 kV is applied to this capillary in order to establish an electric field gradient. The voltage, which can be either negative or positive depending on the nature of the analyte, generates charged droplets that are sprayed out of the needle tip into the atmosphere (nebulization) in the shape of a Taylor cone. During the nebulization process, the presence of a sheath gas (nitrogen) flowing around the needle at atmospheric pressure aids in the size reduction of the droplets due to evaporation. As the solvent evaporates, the charge intensity on the droplet's surface rapidly increases and the droplet eventually splits into one or more charged ions. The charged droplets pass through a curtain of heated inert gas (nitrogen) or a heated

capillary, allowing the analyte to enter the gas phase as a single or multiple charges and becoming a gas phase ion [115].

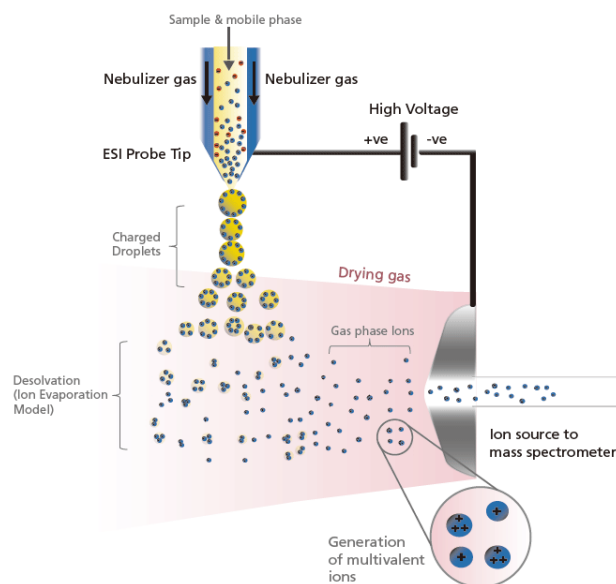


Figure 1.12. Schematic illustration of an Electro spray Ionization in a positive mode [114].

1.5.5. Mass analyzers

Most mass analyzers operate at high vacuum or low pressure to ensure that charged particles do not deviate considerably from their paths due to collisions with the residual gas. Analyzers can operate in continuous mode (i.e., magnetic sector, quadrupole), pulsed mode (i.e., time of flight), or ion trapping mode, depending on the operation of mass analysis (i.e., quadrupole traps, ion cyclotron, orbitrap).

There are tandem/hybrid arrangements, often known as MS/MS systems, in addition to single MS. For measuring organic compounds, single mass analyzers such as the magnetic sector, quadrupole, and time-of-flight (ToF), were extensively utilized, but the quadrupole model has gradually increased its share due to its lower cost. Aside from these mass analyzers, an ion trap MS system, which temporarily collects ions of a specific range before separating them by mass, and a tandem/hybrid MS system, which combines multiple MS units, have also been designed. Each of

these MS systems takes advantage of their unique capabilities and are utilized to achieve a multitude of analytical goals. HRMS coupled with Orbitrap has been used in current survey and is described in the following section. The basic types of mass analyzers are summarized in Table 1.5.

Table 1.5. Most common used mass analyzers [111].

Acronym	Mass analyzer	Principle
B	Magnetic sector	Deflection of a continuous ion beam; separation by momentum in magnetic field due to Lorentz force
TOF	Time-of-flight	Time dispersion of a pulsed ion beam; separation by time-of-flight
Q	Linear quadrupole	Continuous ion beam in linear radio frequency quadrupole field; s due to instability of ion trajectories
LIT	Linear quadrupole ion trap	Continuous ion beam delivers ions for trapping; storage, and eventually separation in linear radio frequency quadrupole field by resonant excitation
QIT	Quadrupole ion trap	Trapped ions; separation in three-dimensional radio frequency quadrupole field by resonant excitation
FT-ICR	Fourier transform-ion cyclotron resonance	Trapped ions in magnetic field (Lorentz force); separation by cyclotron frequency, image current detection and Fourier transformation of a transient signal
Orbitrap	Orbitrap	Axial oscillation in inhomogeneous electric field; detection of frequency after Fourier transformation of a transient signal

1.5.6. High resolution mass spectrometry

The use of high-resolution mass spectrometry (HRMS) in research has increased data collection capabilities for both targeted and untargeted analyses [101,116,117]. HRMS can distinguish between two peaks with minor m/z variations. Furthermore, HRMS instruments have high mass precision and can measure the mass of a molecule with an accuracy of 0.0001 Da or less (within 1 ppm) compared to the precise mass, in contrast to low resolution mass spectrometers that only report whole mass values. As a result, HRMS can be used to identify molecules that have the same whole mass but different exact masses, enhancing the detection of features in untargeted studies [118].

HRMS has been a milestone in the identification of untargeted compounds, with time-of-flight (ToF), quadrupole-TOF (QTOF), and Orbitrap spectrometers increasingly being used. As well, the development of tandem MS systems, such as the triple and quadrupole linear ion trap (QLIT-MS/MS), has enhanced the quantitative and qualitative performance of target analyses [119].

Low-resolution mass spectrometers, such as quadrupole filters and ion traps, have unit mass resolutions (≈ 1000 resolving power), while high-resolution ones, such as time-of-flight instruments have power resolutions of tens of thousands. Other HRMS, such as Orbitrap, which have a mass resolving power of the order of hundreds of thousands, while Fourier transform ion cyclotron resonance mass spectrometer (FT-ICR) achieve a resolving power of hundreds of thousands to millions [119]. The additional advantage is that, while low resolution mass spectrometry can effectively identify small molecules, larger molecules yield more accurate mass data in HRMS analyses, which may be utilized to identify these organic molecules with greater precision.

1.5.7. Orbitrap mass analyzer

Orbitrap is a novel type of mass analyzer that has received great attention due to its analytical performance in terms of mass accuracy, resolution, space charge capacity, and linear dynamic range, as well as its small size and low cost. The orbitrap mass analyzer, invented by Makarov, is based on the Paul trap, which employs a wire stretched along the axis of an outer cylinder enclosing the

trapping chamber. Two types of orbitrap hybrids have been used in this work. During my secondment at Clermont Ferrand in France, products were identified by HRMS performed on an Orbitrap Q-Exactive, and during my stay in Turin, Italy, an LTQ Orbitrap mass spectrometer was used. The only difference is that in the latter, the mass analyzer orbitrap is combined with a linear ion trap LTQ, while the Q-Exactive is a hybrid quadrupole-Orbitrap mass spectrometer.

Ions generated by the ion source are trapped in the LTQ/quadrupole and analyzed using the MS and MSⁿ scan methods. The Orbitrap mass analyzer is based on spectrometer principles and is represented in the Figure 1.13.

The LTQ or Q-Executive Orbitrap hybrid includes three basic components: (a) a linear ion trap LTQ or a quadrupole for sample ionization, selection and fragmentation, (b) a device for storage (curved linear trap), and (c) an Orbitrap analyzer for Fourier-based analysis [120].

The Orbitrap mass analyzer, which is made up of two electrodes, one external and one central, operates as both an analyzer and a detector. Ions generated by ESI are collected in the LTQ or quadrupole, then axially ejected to the curved linear storage trap (C-trap), which is employed as store and collision cell of the ions before injection into the orbital trap. By rapidly raising the electric field, the ions transported from the C-Trap are caught in the orbital trap ("electrodynamic squeezing"). Once the ions are captured, they fluctuate around the central electrode and between the two outside electrodes. Because the ions are different, they oscillate at different frequencies, causing a mass separation. The signals from the orbital trap's outer electrodes are amplified and translated into a frequency spectrum using a fast Fourier transform, which is then converted into a mass spectrum. As a result, the Orbitrap mass analyzer acts as a Fourier Transform (FT) mass analyzer, similar to the well-known FT-ion cyclotron resonance (ICR) technology, but with the benefit of a smaller instrument size and simpler instrument operation [121].

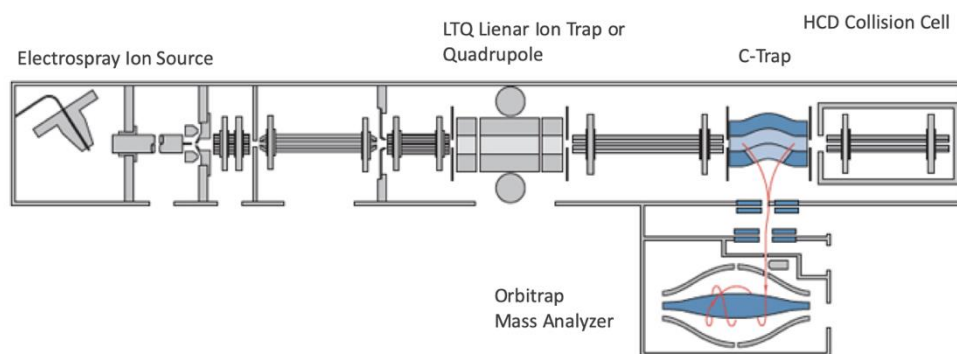


Figure 1.13. Schematic picture of a linear trap or quadrupole -Orbitrap hybrid mass spectrometer.

1.6. Fate and remediation methods of CE in the environment: Advanced Oxidation Processes

According to EU legislation, wastewater treatment is mandatory and it is known that the primary obstacle to preventing water body contamination is WWTPs [122]. Although WWTPs are the major CECs pollution sources, traditional physical and biological treatment procedures on which they rely are unable to remove them due to CEC's physicochemical properties (e.g., water solubility, vapor pressure, and polarity) [50] and they are discharged directly into the environment. Once released in the surface water, they can undergo several transformations processes such as hydrolysis, biodegradation, adsorption and photolysis [123,124]. Surface water photochemical reactions, which include direct and indirect photolysis, play a crucial aspect in their environmental attenuation. Another obstacle to prevent unintentional human exposure to CECs are the Drinking Water Treatment Plants (DWTPs) and several studies have demonstrated that traditional treatments such as coagulation, filtration, flocculation and chlorination have low removal efficiency as well [125,126], while advanced treatment technologies such as ozonation and activated carbon adsorption can efficiently remove them [125,127,128]. Furthermore, while these procedures are effective, they may involve the use of costly chemicals and equipment. As a result, more efficient, cost-effective treatment solutions for a wide range of chemicals that minimize waste and energy consumption must be developed. Advanced Oxidation Processes (AOPs) are one potential choice

among the alternatives [129]. AOPs are an effective, promising and green technologies for removing persistent organic pollutants from water and wastewaters as well as for pretreatment to minimize the concentrations of toxic organic compounds that inhibit the biological processes of wastewater treatment [130,131]. It is based on the production in situ of a potent reactive oxygen species (ROS), such as hydroxyl radicals ($\bullet\text{OH}$) or sulfate radical ($\text{SO}_4\bullet^-$), which are highly reactive and non-selective substances used to degrade organic compounds present in a medium. Moreover, these ROS do not produce additional waste, are not corrosive to equipment, are not hazardous, and have a very limited existence [132,133]. All AOPs involve two steps: the production of ROS in situ and its reaction with the target compound. The performance of an AOP depends on the nature of CE and the characteristics of the water matrix [134]. AOPs combine different processes such as photolysis, Fenton and like reactions, ozonation, ozonation with H_2O_2 and/or ultraviolet (UV) radiation, photocatalysis activated by semiconductors such as TiO_2 , sonolysis and electrochemical oxidation among other (Table 1.6).

Table 1.6. Different Advanced Oxidation Processes and sources of radicals [133].

Advanced Oxidation Processes (AOPs)	Source of Radicals
O ₃ -based	O ₃
	O ₃ /H ₂ O ₂
	O ₃ /UV
	O ₃ / H ₂ O ₂ /UV
Photolysis	UV irradiation
H ₂ O ₂ -based	H ₂ O ₂ /UV
	H ₂ O ₂ /Fe ⁺² (Fenton)
	H ₂ O ₂ /Fe ⁺³ (Fenton-Like)
	H ₂ O ₂ /Fe ⁺² /UV (Photo-Fenton)
Heterogeneous photocatalysis	TiO ₂ /UV
	TiO ₂ /UV/ H ₂ O ₂
Sonochemical oxidation	Ultrasounds (water sonolysis)
Electrochemical oxidation	Electricity (water electrolysis)

Although the advantages of using AOPs have already been mentioned, their uses present some drawbacks, which include: the inability to treat large volumes of low-concentration drugs, as occurs in the environment under real conditions; its effectiveness is restricted by the presence of organic matter or inorganic ions, which limit the reaction rates of radicals; the use of costly reagents (for example, H_2O_2); and the consumption of energy (generation of O_3 or UV radiation) [133,135]. It is also important to highlight that studies have shown that AOPs can produce a variety of toxic intermediates that are sometimes even more toxic than the parent compounds [33,135,136], therefore the toxicity of the by-products must be assessed.

1.6.1. Degradation by UV-photolysis

Photolysis is the degradation of a compound caused by UV light absorption [137]. More specific, the degradation of micropollutants in water occurs in two ways, direct and indirect photolysis. Direct photolysis occurs when the molecule absorbs photons providing the energy required to reach from the ground state (S_0) to their excited states, forming free radicals that undergo a series of chain reactions and indirectly photolysis [138]. Initially, the singlet excited state (S_1) of the molecule is produced, which is converted to the relative stable triplet excited state (T_1) very quickly. At this state, it could undergo direct degradation (pathway 1 in Figure 1.14), or/and interact with dissolved oxygen ($^3\text{O}_2$), which can interact in two ways: when the electron transfer goes from T_1 to $^3\text{O}_2$ with the superoxide radical anion ($\text{O}_2^{\bullet-}$) (photooxidation, path 2) or when the energy is transferred from T_1 to $^3\text{O}_2$ for the formation of singlet oxygen ($^1\text{O}_2$) (path 3) [8].

In the case of indirect photolysis, photoactive compounds known as photosensitizers absorb sunlight [139]. These molecules generate reactive transients such the hydroxyl radical ($\bullet\text{OH}$) [140–142], hydrogen peroxide (H_2O_2) and superoxide radical anion (O_2^-) [143], singlet oxygen ($^1\text{O}_2$) [144,145] and chromophoric dissolved organic (CDOM) triplet states ($^3\text{CDOM}^*$) [146], when exposed

to sunlight, which might induce pollutant transformation[142]. Because they can assist in the generation of the above-mentioned reactive species, natural water components such as nitrates, bicarbonate, and especially dissolved organic matter, which is by far the main sunlight absorber in natural waters, play a significant role in the photolytic degradation of organic compounds [147].

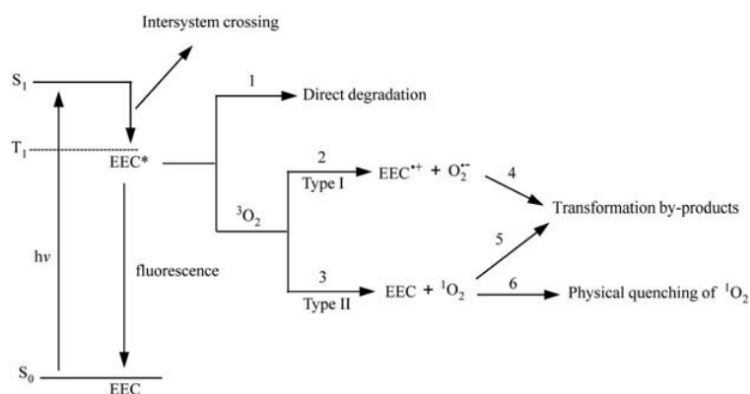
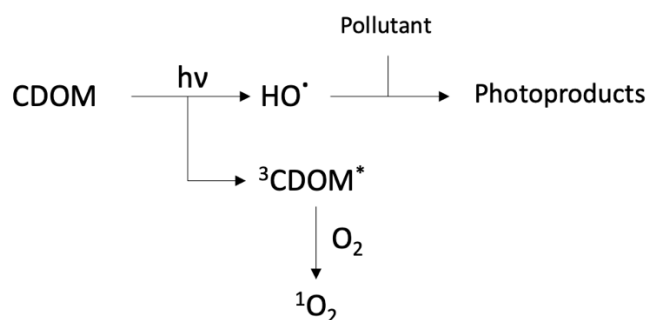


Figure 1.14. Mechanisms of direct photolysis of CEC [8].

When the mentioned photosensitizers are exposed to light, they produce the photoreactive transient $\bullet\text{OH}$, which can form another transient ($\text{CO}_3\bullet^-$, carbonate radical) when they react with inorganic carbon species (HCO_3^- and CO_3^{2-})[148]. Irradiated CDOM can also generate reactive triplet states (${}^3\text{CDOM}^*$), which when combined with dissolved O_2 produce singlet oxygen (${}^1\text{O}_2$) [149,150] (Scheme 1.1). The transients are mainly scavenged/quenched by natural water components, despite the fact that they play a crucial role in the indirect phototransformation of contaminants.

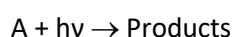


Scheme 1.1. Main photochemical processes involving $\text{HO}\bullet$, ${}^3\text{CDOM}^*$, and ${}^1\text{O}_2$ in surface fresh waters.

The efficiency of such procedures is determined by several variables including the intensity and wavelength of UV irradiation, as well as the water matrix. UV irradiation is characterized as a set of electromagnetic radiations with different wavelengths (e.g., 10-400 nm), including UV-A (365 nm), UV-B (302 nm), UV-C (254 nm), and Vacuum UV. Recently, sunlight has been evaluated as a renewable energy source [117,138,151].

The main advantages of this category of AOP include that it is a green and sustainable method of degradation, as well as the requirement of a low cost of operation and maintenance. However, the treatment with UV alone presents some drawbacks. For example, the presence of some organic compounds could act as photosensitizers, thus increasing the turbidity of the medium and therefore, reducing the efficiency of the process [132,133,135]. However, the use of UV radiation alone is rarely applied as an advanced oxidation process (AOP).

As we have already seen, pollutants in the environment can be directly photolyzed by radiation from the sun. Rate laws (also known as differential rate laws) or rate equations are mathematical expressions that define the relationship between the rate of a chemical reaction and its reactant concentration, that allow to calculate the life of photolysis (time to decay to 1/e of an initial concentration) or how quickly this process happens. Considering a pollutant A, which is released into the environment and is photolabile. This pollutant A can absorb a photon of the solar radiation, $h\nu$, and it is a first order reaction because it depends on the concentration of A. The units are given by 1/s. It is a unimolecular reaction and other reactants may be present, though these reactions will be of zero order since their concentrations do not affect the rate of the A reaction. Thus, the rate law for a first-order elementary reaction with regard to a reactant A is given by:



The rate of concentration loss of pollutant A, [A] is:

$$d[A] / dt = -k[A](1)$$

where k is the rate constant. The rate law is a differential equation, which means it defines how the concentration of a reactant changes over the time. The rate law can be integrated to generate an integrated rate equation that directly connects the concentrations of reactants or products with time. After integrating Equation (1), it is possible to write the final equations in two forms:

$$[A]_t = [A]_0 e^{-kt} \quad (2)$$

$$\ln [A] = -k t + \ln [A]_0 \quad (3)$$

$[A]_t$ is the concentration of the target pollutant at a particular time t , and $[A]_0$ represents the initial concentration of A. To represent it graphically, a plot of $\ln[A]$ vs t will result in a straight line with slope of $-k$. The integrated first-order rate law, on the other hand, is commonly represented as an exponential decay equation. The half-life of a first-order reaction can be obtained by using:

$$t_{1/2} = \ln 2 / k \quad (4)$$

It can be seen that the half-life of a first-order reaction is inversely proportional to the rate constant k . A fast reaction (shorter half-life) will have a higher k and on the contrary, a slow reaction (longer half-life) will have a lower k .

1.6.2. Photocatalysis

Among all oxidative treatments, photocatalytic methods have received a great interest over the last decades for the removal of pollutants in water. Photocatalysis is the activation of a photocatalytic material or substance by light photons, which accelerate the rate of a chemical reaction without consuming it. The photocatalyst might be dissolved in liquid (homogeneous photocatalysis) or particles suspended in liquid or anchored on surfaces (heterogeneous photocatalysis) [152]. This part is going to focus on heterogeneous photocatalysis.

The heterogeneous photocatalytic oxidation process is based on the use of near UV light to photoexcite semiconductor catalysts in the presence of oxygen in order to attack organic molecules in water or air for purification and disinfection. There are several photocatalysts such as ZnO, Fe₂O₃,

CdS, GaP, Cu₂O, TiO₂ and ZnS that were successfully used for the removal of a wide range of organic compounds under optimal conditions. Among these photocatalysts, TiO₂ is the most widely used, due to its high photocatalytic activity, nontoxic properties, abundance and low cost, among other properties [153,154]. The photocatalytic behavior of TiO₂ involves the generation of photo-generated electrons in the conduction band of the catalysts, which leads to the formation of highly oxidative holes in the valence band, where an interaction with the adsorbed water, for example surface hydroxyl, occurs to form the highly reactive hydroxyl radicals [155]. Furthermore, the excited electrons may be trapped by O₂ and create superoxide radical ions [156]. Organic molecules are then degraded by the holes in the TiO₂ surface as well as by radicals in the bulk solution [153].

This process has mainly two limitations when applied on a large scale for the removal of pollutants: the first is the separation of the colloidal catalyst from the water suspension after treatment, and the second is based on the mass transfer limitation of the immobilized catalyst on the substrate [129]. Although the extensive research in the field of photocatalysis, this technique is barely used in industrial or WWTPs due to the poor quantum yield for the formation of OH radicals.

References

- [1] V. Dulio, B. van Bavel, E. Brorström-Lundén, J. Harmsen, J. Hollender, M. Schlabach, J. Slobodnik, K. Thomas, J. Koschorreck, Emerging pollutants in the EU: 10 years of NORMAN in support of environmental policies and regulations, *Environ. Sci. Eur.* 30 (2018). <https://doi.org/10.1186/s12302-018-0135-3>.
- [2] V. Calisto, V.I. Esteves, Psychiatric pharmaceuticals in the environment, *Chemosphere*. 77 (2009) 1257–1274. <https://doi.org/10.1016/j.chemosphere.2009.09.021>.
- [3] S.D. Melvin, Effect of antidepressants on circadian rhythms in fish: Insights and implications regarding the design of behavioural toxicity tests, *Aquat. Toxicol.* 182 (2017) 20–30. <https://doi.org/10.1016/j.aquatox.2016.11.007>.
- [4] O. Malev, M. Lovrić, D. Stipaničev, S. Repec, D. Martinović-Weigelt, D. Zanella, T. Ivanković, V. Sindičić Đuretec, J. Barišić, M. Li, G. Klobučar, Toxicity prediction and effect characterization of 90 pharmaceuticals and illicit drugs measured in plasma of fish from a major European river (Sava, Croatia), *Environ. Pollut.* 266 (2020). <https://doi.org/10.1016/j.envpol.2020.115162>.
- [5] T. Brodin, J. Fick, M. Jonsson, J. Klaminder, Dilute concentrations of a psychiatric drug alter behavior of fish from natural populations, *Science* (80-.). 339 (2013) 814–815. <https://doi.org/10.1126/science.1226850>.
- [6] M. Saaristo, T. Brodin, S. Balshine, M.G. Bertram, B.W. Brooks, S.M. Ehlman, E.S. McCallum, A. Sih, J. Sundin, B.B.M. Wong, K.E. Arnold, Direct and indirect effects of chemical contaminants on the behaviour, ecology and evolution of wildlife, *Proc. R. Soc. B Biol. Sci.* 285 (2018). <https://doi.org/10.1098/rspb.2018.1297>.
- [7] J. Klaminder, M. Jonsson, J. Fick, A. Sundelin, T. Brodin, The conceptual imperfection of aquatic risk assessment tests: Highlighting the need for tests designed to detect therapeutic effects of pharmaceutical contaminants, *Environ. Res. Lett.* 9 (2014). <https://doi.org/10.1088/1748-9326/9/8/084003>.
- [8] A.J. Hernandez-Maldonado, L. Blaney, Contaminants of emerging concern on water and wastewater. Advanced treatment processes, 2020.
- [9] L.M. Gómez-Oliván, *Ecopharmacovigilance Multidisciplinary Approaches to Environmental Safety of Medicines*, 2017.
- [10] L.M. Gómez-Oliván, *Ecopharmacovigilance Multidisciplinary Approaches to Environmental Safety of Medicines*, 2017.
- [11] The European Parliament and the Council of the European Union, Directive 2000/60/EC of the European Parliament and of the Council of 23 October 2000 establishing a framework for Community action in the field of water policy, *Off. J. Eur. Parliam.* L327 (2000) 1–82.

- <https://doi.org/10.1039/ap9842100196>.
- [12] O.F.T.H.E. Council, Water environmental quality standards, *CONCAWE Rev.* 16 (2007) 11–14.
- [13] O.F.T.H.E. Council, Directive 2013/11/EU of the European Parliament and of the Council, *Fundam. Texts Eur. Priv. Law.* 2013 (2020) 1–17.
<https://doi.org/10.5040/9781782258674.0032>.
- [14] European Commission, Commission Implementing Decision (EU) 2015/495 of 20 March 2015 establishing a watch list of substances for Union-wide monitoring in the field of water policy pursuant to Directive 2008/105/EC of the European Parliament and of the Council, *Off. J. Eur. Union.* L78/40 (2015) 20–30. https://doi.org/http://eur-lex.europa.eu/pri/en/oj/dat/2003/l_285/l_28520031101en00330037.pdf.
- [15] European Commission, Commission Implementing Decision (EU) 2018/840 of 5 June 2018 establishing a watch list of substances for Union-wide monitoring in the field of water policy pursuant to Directive 2008/105/EC of the European Parliament and of the Council and repealing Comm, *Off. J. Eur. Parliam.* 141 (2018) 9–12.
- [16] European Parliament, Council, 2001/83/Ec, Dir. (2001) 172. <http://eur-lex.europa.eu/LexUriServ/LexUriServ.do?uri=CELEX:32001L0083:EN:NOT>.
- [17] European Commission, Directive 2001/82/EC of the European Parliament and of the Council of 6 November 2001 on the Community code relating to veterinary medicinal products, *Off. J. Eur. Communities.* (2001).
- [18] European Commission, Directive 2004/27/EC on the Community code relating to medicinal products for human use, 2004.
- [19] P. Bird, The urban waste water treatment directive, *Inst. Water Off. J.* 28 (1992) 14–15.
- [20] European Union 2008, Regulation (EC) No 1333/2008 of the European Parliament and of the Council of 16 December 2008 on food additives, *Off. J. Eur. Union.* 51 (2008) 16–33.
- [21] J. Rivera-Utrilla, M. Sánchez-Polo, M.Á. Ferro-García, G. Prados-Joya, R. Ocampo-Pérez, Pharmaceuticals as emerging contaminants and their removal from water. A review, *Chemosphere.* 93 (2013) 1268–1287. <https://doi.org/10.1016/j.chemosphere.2013.07.059>.
- [22] M. Patel, R. Kumar, K. Kishor, T. Mlsna, C.U. Pittman, D. Mohan, Pharmaceuticals of emerging concern in aquatic systems: Chemistry, occurrence, effects, and removal methods, *Chem. Rev.* 119 (2019) 3510–3673. <https://doi.org/10.1021/acs.chemrev.8b00299>.
- [23] S. Castiglioni, R. Fanelli, D. Calamari, R. Bagnati, E. Zuccato, Methodological approaches for studying pharmaceuticals in the environment by comparing predicted and measured concentrations in River Po, Italy, *Regul. Toxicol. Pharmacol.* 39 (2004) 25–32.
<https://doi.org/10.1016/j.yrtph.2003.10.002>.
- [24] P. Calza, C. Medana, E. Padovano, V. Giancotti, C. Minero, Fate of selected pharmaceuticals in

- river waters, *Environ. Sci. Pollut. Res.* 20 (2013) 2262–2270. <https://doi.org/10.1007/s11356-012-1097-4>.
- [25] C.J. Houtman, J. Kroesbergen, K. Lekkerkerker-Teunissen, J.P. van der Hoek, Human health risk assessment of the mixture of pharmaceuticals in Dutch drinking water and its sources based on frequent monitoring data, *Sci. Total Environ.* 496 (2014) 54–62. <https://doi.org/10.1016/j.scitotenv.2014.07.022>.
- [26] E. Taylor, C.G. Daughton, B.W. Brooks, " Active Pharmaceutical Ingredients and Aquatic Organisms " Chapter in : Bayer N and Meador J . (eds) *Environmental Contaminants in Biota : Interpreting Tissue Concentrations* , 2010.
- [27] L. Patrolecco, S. Capri, N. Ademollo, Occurrence of selected pharmaceuticals in the principal sewage treatment plants in Rome (Italy) and in the receiving surface waters, *Environ. Sci. Pollut. Res.* 22 (2015) 5864–5876. <https://doi.org/10.1007/s11356-014-3765-z>.
- [28] P. Verlicchi, M. Al Aukidy, A. Jelic, M. Petrović, D. Barceló, Comparison of measured and predicted concentrations of selected pharmaceuticals in wastewater and surface water: A case study of a catchment area in the Po Valley (Italy), *Sci. Total Environ.* 470–471 (2014) 844–854. <https://doi.org/10.1016/j.scitotenv.2013.10.026>.
- [29] P. Verlicchi, V. Grillini, Surfacewater and groundwater quality in South Africa and mozambique-analysis of the most critical pollutants for drinking purposes and challenges in water treatment selection, *Water (Switzerland)*. 12 (2020). <https://doi.org/10.3390/w12010305>.
- [30] O.A.H. Jones, N. Voulvoulis, J.N. Lester, Partitioning behavior of five pharmaceutical compounds to activated sludge and river sediment, *Arch. Environ. Contam. Toxicol.* 50 (2006) 297–305. <https://doi.org/10.1007/s00244-005-1095-3>.
- [31] J.R. Romero, I. Kagalou, J. Imberger, D. Hela, M. Kotti, A. Bartzokas, T. Albanis, N. Evmirides, S. Karkabounas, J. Papagiannis, A. Bithava, Seasonal water quality of shallow and eutrophic Lake Pamvotis, Greece: Implications for restoration, *Hydrobiologia*. 474 (2002) 91–105. <https://doi.org/10.1023/A:1016569124312>.
- [32] J.A. Rivera-Jaimes, C. Postigo, R.M. Melgoza-Alemán, J. Aceña, D. Barceló, M. López de Alda, Study of pharmaceuticals in surface and wastewater from Cuernavaca, Morelos, Mexico: Occurrence and environmental risk assessment, *Sci. Total Environ.* 613–614 (2018) 1263–1274. <https://doi.org/10.1016/j.scitotenv.2017.09.134>.
- [33] A.K. Brown, J.K. Challis, C.S. Wong, M.L. Hanson, Selective serotonin reuptake inhibitors and β -blocker transformation products may not pose a significant risk of toxicity to aquatic organisms in wastewater effluent-dominated receiving waters, *Integr. Environ. Assess. Manag.* 11 (2015) 618–639. <https://doi.org/10.1002/ieam.1637>.

- [34] S. Furuhaugen, B. Liewenborg, M. Breitholtz, E. Gorokhova, Feeding activity and xenobiotics modulate oxidative status in daphnia magna: Implications for ecotoxicological testing, *Environ. Sci. Technol.* 48 (2014) 12886–12892. <https://doi.org/10.1021/es5044722>.
- [35] B. Silva, I.C. Neves, SPRINGER BRIEFS IN MOLECULAR SCIENCE Psychiatric Pharmaceuticals as Emerging Contaminants in Wastewater, n.d.
- [36] M.R. Mills, K. Arias-Salazar, A. Baynes, L.Q. Shen, J. Churchley, N. Beresford, C. Gayathri, R.R. Gil, R. Kanda, S. Jobling, T.J. Collins, Removal of ecotoxicity of 17 α -ethinylestradiol using TAML/peroxide water treatment, *Sci. Rep.* 5 (2015) 1–10. <https://doi.org/10.1038/srep10511>.
- [37] R. Maurício, R. Dias, V. Ribeiro, S. Fernandes, A.C. Vicente, M.I. Pinto, J.P. Noronha, L. Amaral, P. Coelho, A.P. Mano, 17 α -Ethinylestradiol and 17 β -estradiol removal from a secondary urban wastewater using an RBC treatment system, *Environ. Monit. Assess.* 190 (2018). <https://doi.org/10.1007/s10661-018-6701-8>.
- [38] R.K. Bhandari, S.L. Deem, D.K. Holliday, C.M. Jandegian, C.D. Kassotis, S.C. Nagel, D.E. Tillitt, F.S. vom Saal, C.S. Rosenfeld, Effects of the environmental estrogenic contaminants bisphenol A and 17 α -ethinyl estradiol on sexual development and adult behaviors in aquatic wildlife species, *Gen. Comp. Endocrinol.* 214 (2015) 195–219. <https://doi.org/10.1016/j.ygcen.2014.09.014>.
- [39] Y. Zhang, J.L. Zhou, Removal of estrone and 17 β -estradiol from water by adsorption, *Water Res.* 39 (2005) 3991–4003. <https://doi.org/10.1016/j.watres.2005.07.019>.
- [40] G.T. Ankley, D. Feifarek, B. Blackwell, J.E. Cavallin, K.M. Jensen, M.D. Kahl, S. Poole, E. Randolph, T. Saari, D.L. Villeneuve, Re-evaluating the Significance of Estrone as an Environmental Estrogen, *Environ. Sci. Technol.* 51 (2017) 4705–4713. <https://doi.org/10.1021/acs.est.7b00606>.
- [41] A. Schoenborn, P. Kunz, M. Koster, Estrogenic activity in drainage water: a field study on a Swiss cattle pasture, *Environ. Sci. Eur.* 27 (2015). <https://doi.org/10.1186/s12302-015-0047-4>.
- [42] J.P. Besse, J. Garric, Progestagens for human use, exposure and hazard assessment for the aquatic environment, *Environ. Pollut.* 157 (2009) 3485–3494. <https://doi.org/10.1016/j.envpol.2009.06.012>.
- [43] N. Sanjuan-Reyes, L.M. Gómez-Oliván, M. Galar-Martínez, P. Vieyra-Reyes, S. García-Medina, H. Islas-Flores, N. Neri-Cruz, Effluent from an NSAID-manufacturing plant in Mexico induces oxidative stress on *Cyprinus Carpio*, *Water. Air. Soil Pollut.* 224 (2013). <https://doi.org/10.1007/s11270-013-1689-8>.
- [44] H. Islas-Flores, L.M. Gómez-Oliván, M. Galar-Martínez, A. Colín-Cruz, N. Neri-Cruz, S. García-Medina, Diclofenac-induced oxidative stress in brain, liver, gill and blood of common carp (*Cyprinus carpio*), *Ecotoxicol. Environ. Saf.* 92 (2013) 32–38.

- <https://doi.org/10.1016/j.ecoenv.2013.01.025>.
- [45] J.D. Cardoso-Vera, H. Islas-Flores, N. SanJuan-Reyes, E.I. Montero-Castro, M. Galar-Martínez, S. García-Medina, A. Elizalde-Velázquez, O. Dublán-García, L.M. Gómez-Oliván, Comparative study of diclofenac-induced embryotoxicity and teratogenesis in *Xenopus laevis* and *Lithobates catesbeianus*, using the frog embryo teratogenesis assay: *Xenopus* (FETAX), *Sci. Total Environ.* 574 (2017) 467–475. <https://doi.org/10.1016/j.scitotenv.2016.09.095>.
- [46] K. Arnold, A.R. Brown, G.T. Ankley, J.P. Sumpter, Assessing risks and impacts of pharmaceuticals in the environment on wildlife and ecosystems, *Philos. Trans. R. Soc. B Biol. Sci.* 369 (2014) 8436.
- [47] J. Harding, Medicare Part D enrollees' use of out-of-plan discounted generic drugs, revisited, 59 (2011) 369–370.
- [48] M.L. Montesinos, Roles for DSCAM and DSCAML1 in central nervous system development and disease., *Adv. Neurobiol.* 8 (2014) 249–270. https://doi.org/10.1007/978-1-4614-8090-7_11.
- [49] W.H. Organization, Pharmaceuticals in drinking water: Public health and environmental water, sanitation, hygiene and health, *J. Am. Pharm. Assoc.* 50 (2010) 600–603.
- [50] M. la Farré, S. Pérez, L. Kantiani, D. Barceló, Fate and toxicity of emerging pollutants, their metabolites and transformation products in the aquatic environment, *TrAC - Trends Anal. Chem.* 27 (2008) 991–1007. <https://doi.org/10.1016/j.trac.2008.09.010>.
- [51] D. Álvarez-Muñoz, S. Rodríguez-Mozaz, A.L. Maulvault, A. Tediosi, M. Fernández-Tejedor, F. Van den Heuvel, M. Kotterman, A. Marques, D. Barceló, Occurrence of pharmaceuticals and endocrine disrupting compounds in macroalgae, bivalves, and fish from coastal areas in Europe, *Environ. Res.* 143 (2015) 56–64. <https://doi.org/10.1016/j.envres.2015.09.018>.
- [52] B.W. Brooks, C.K. Chambliss, J.K. Stanley, A. Ramirez, K.E. Banks, R.D. Johnson, R.J. Lewis, Determination of select antidepressants in fish from an effluent-dominated stream, *Environ. Toxicol. Chem.* 24 (2005) 464–469. <https://doi.org/10.1897/04-081R.1>.
- [53] J. Liu, G. Lu, Z. Xie, Z. Zhang, S. Li, Z. Yan, Occurrence, bioaccumulation and risk assessment of lipophilic pharmaceutically active compounds in the downstream rivers of sewage treatment plants, *Sci. Total Environ.* 511 (2015) 54–62. <https://doi.org/10.1016/j.scitotenv.2014.12.033>.
- [54] J. Liu, X. Dan, G. Lu, J. Shen, D. Wu, Z. Yan, Investigation of pharmaceutically active compounds in an urban receiving water: Occurrence, fate and environmental risk assessment, *Ecotoxicol. Environ. Saf.* 154 (2018) 214–220. <https://doi.org/10.1016/j.ecoenv.2018.02.052>.
- [55] A.B.A. Boxall, M.A. Rudd, B.W. Brooks, D.J. Caldwell, K. Choi, S. Hickmann, E. Innes, K. Ostapyk, J.P. Staveley, T. Verslycke, G.T. Ankley, K.F. Beazley, S.E. Belanger, J.P. Berninger, P. Carriquiriborde, A. Coors, P.C. DeLeo, S.D. Dyer, J.F. Ericson, F. Gagné, J.P. Giesy, T. Gouin, L. Hallstrom, M. V. Karlsson, D.G. Joakim Larsson, J.M. Lazorchak, F. Mastrocco, A. McLaughlin,

- M.E. McMaster, R.D. Meyerhoff, R. Moore, J.L. Parrott, J.R. Snape, R. Murray-Smith, M.R. Servos, P.K. Sibley, J.O. Straub, N.D. Szabo, E. Topp, G.R. Tetreault, V.L. Trudeau, G. Van Der Kraak, Pharmaceuticals and personal care products in the environment: What are the big questions?, *Environ. Health Perspect.* 120 (2012) 1221–1229.
<https://doi.org/10.1289/ehp.1104477>.
- [56] B. Mars, J. Heron, D. Kessler, N.M. Davies, R.M. Martin, K.H. Thomas, D. Gunnell, Influences on antidepressant prescribing trends in the UK: 1995–2011, *Soc. Psychiatry Psychiatr. Epidemiol.* 52 (2017) 193–200. <https://doi.org/10.1007/s00127-016-1306-4>.
- [57] V.L. Borova, N.C. Maragou, P. Gago-Ferrero, C. Pistos, N.S. Thomaidis, Highly sensitive determination of 68 psychoactive pharmaceuticals, illicit drugs, and related human metabolites in wastewater by liquid chromatography-tandem mass spectrometry, *Anal. Bioanal. Chem.* 406 (2014) 4273–4285. <https://doi.org/10.1007/s00216-014-7819-3>.
- [58] L.J.G. Silva, A.M.P.T. Pereira, L.M. Meisel, C.M. Lino, A. Pena, A one-year follow-up analysis of antidepressants in Portuguese wastewaters: Occurrence and fate, seasonal influence, and risk assessment, *Sci. Total Environ.* 490 (2014) 279–287.
<https://doi.org/10.1016/j.scitotenv.2014.04.131>.
- [59] N.S. Thomaidis, P. Gago-Ferrero, C. Ort, N.C. Maragou, N.A. Alygizakis, V.L. Borova, M.E. Dasenaki, Reflection of Socioeconomic Changes in Wastewater: Licit and Illicit Drug Use Patterns, *Environ. Sci. Technol.* 50 (2016) 10065–10072.
<https://doi.org/10.1021/acs.est.6b02417>.
- [60] OCDE, Health at a Glance 2019, OECD, 2019. <https://doi.org/10.1787/4dd50c09-en>.
- [61] B. Puri, I. Treasaden, Textbook of Psychiatry 3rd Edition, Churchill Livingstone 2011, 2011.
- [62] S.K. Khetan, T.J. Collins, Human pharmaceuticals in the aquatic environment: A challenge to green chemistry, *Chem. Rev.* 107 (2007) 2319–2364. <https://doi.org/10.1021/cr020441w>.
- [63] M.M. Schultz, E.T. Furlong, D.W. Kolpin, S.L. Werner, H.L. Schoenfuss, L.B. Barber, V.S. Blazer, D.O. Norris, A.M. Vajda, Antidepressant pharmaceuticals in two U.S. effluent-impacted streams: Occurrence and fate in water and sediment and selective uptake in fish neural tissue, *Environ. Sci. Technol.* 44 (2010) 1918–1925. <https://doi.org/10.1021/es9022706>.
- [64] A. Lajeunesse, S.A. Smyth, K. Barclay, S. Sauvé, C. Gagnon, Distribution of antidepressant residues in wastewater and biosolids following different treatment processes by municipal wastewater treatment plants in Canada, *Water Res.* 46 (2012) 5600–5612.
<https://doi.org/10.1016/j.watres.2012.07.042>.
- [65] S. Matongo, G. Birungi, B. Moodley, P. Ndungu, Occurrence of selected pharmaceuticals in water and sediment of Umgeni River, KwaZulu-Natal, South Africa, *Environ. Sci. Pollut. Res.* 22 (2015) 10298–10308. <https://doi.org/10.1007/s11356-015-4217-0>.

- [66] O. Golovko, V. Kumar, G. Fedorova, T. Randak, R. Grabic, Seasonal changes in antibiotics, antidepressants/psychiatric drugs, antihistamines and lipid regulators in a wastewater treatment plant, *Chemosphere*. 111 (2014) 418–426.
<https://doi.org/10.1016/j.chemosphere.2014.03.132>.
- [67] A.G. Moghadam, M. Rajabi, A. Asghari, Efficient and relatively safe emulsification microextraction using a deep eutectic solvent for influential enrichment of trace main antidepressant drugs from complicated samples, Elsevier B.V., 2018.
<https://doi.org/10.1016/j.jchromb.2017.09.042>.
- [68] R. Jannesar, F. Zare, M. Ghaedi, A. Daneshfar, Dispersion of hydrophobic magnetic nanoparticles using ultrasonic-assisted in combination with coacervative microextraction for the simultaneous preconcentration and determination of tricyclic antidepressant drugs in biological fluids, *Ultrason. Sonochem.* 32 (2016) 380–386.
<https://doi.org/10.1016/j.ultsonch.2016.04.010>.
- [69] M. Safari, M. Shahlaei, Y. Yamini, M. Shakorian, E. Arkan, Magnetic framework composite as sorbent for magnetic solid phase extraction coupled with high performance liquid chromatography for simultaneous extraction and determination of tricyclic antidepressants, Elsevier B.V., 2018. <https://doi.org/10.1016/j.aca.2018.06.023>.
- [70] M. Degreef, A.L.N. van Nuijs, K.E. Maudens, Validation of a simple, fast liquid chromatography-tandem mass spectrometry method for the simultaneous quantification of 40 antidepressant drugs or their metabolites in plasma, *Clin. Chim. Acta.* 485 (2018) 243–257.
<https://doi.org/10.1016/j.cca.2018.06.047>.
- [71] A.R. Breaud, R. Harlan, M. Kozak, W. Clarke, A rapid and reliable method for the quantitation of tricyclic antidepressants in serum using HPLC-MS/MS, *Clin. Biochem.* 42 (2009) 1300–1307.
<https://doi.org/10.1016/j.clinbiochem.2009.05.006>.
- [72] G. Vaghar-Lahijani, M. Saber-Tehrani, P. Aberoomand-Azar, M. Soleimani, Extraction and determination of two antidepressant drugs in human plasma by dispersive liquid–liquid microextraction–HPLC, *J. Anal. Chem.* 73 (2018) 145–151.
<https://doi.org/10.1134/S1061934818020144>.
- [73] A.H. Ide, J.M.F. Nogueira, New-generation bar adsorptive microextraction (BA μ E) devices for a better eco-user-friendly analytical approach–Application for the determination of antidepressant pharmaceuticals in biological fluids, *J. Pharm. Biomed. Anal.* 153 (2018) 126–134. <https://doi.org/10.1016/j.jpba.2018.02.001>.
- [74] G.H. Ragab, E.A. Bahgat, Development of bioanalytical HPLC method for simultaneous determination of the antialzheimer, donepezil hydrochloride and the antidepressant, citalopram hydrobromide in raw materials, spiked human plasma and tablets dosage form,

- Ann. Pharm. Fr. 77 (2019) 112–120. <https://doi.org/10.1016/j.pharma.2018.09.004>.
- [75] M. Kalaboka, C. Chrimatopoulos, C. Jiménez-Holgado, V. Boti, V. Sakkas, T. Albanis, Exploring the efficiency of UHPLC-orbitrap ms for the determination of 20 pharmaceuticals and acesulfame k in hospital and urban wastewaters with the aid of FPSE, *Separations*. 7 (2020) 1–19. <https://doi.org/10.3390/separations7030046>.
- [76] V.A. Boumba, G. Rallis, P. Petrikis, T. Vougiouklakis, V. Mavreas, Determination of clozapine, and five antidepressants in human plasma, serum and whole blood by gas chromatography–mass spectrometry: A simple tool for clinical and postmortem toxicological analysis, *J. Chromatogr. B Anal. Technol. Biomed. Life Sci.* 1038 (2016) 43–48. <https://doi.org/10.1016/j.jchromb.2016.10.023>.
- [77] X. Chen, S. Zheng, J. Le, Z. Qian, R. Zhang, Z. Hong, Y. Chai, Ultrasound-assisted low-density solvent dispersive liquid–liquid microextraction for the simultaneous determination of 12 new antidepressants and 2 antipsychotics in whole blood by gas chromatography–mass spectrometry, *J. Pharm. Biomed. Anal.* 142 (2017) 19–27. <https://doi.org/10.1016/j.jpba.2017.04.032>.
- [78] S. Kamaruzaman, M.M. Sanagi, N. Yahaya, W.A. Wan Ibrahim, S. Endud, W.N. Wan Ibrahim, Magnetic micro-solid-phase extraction based on magnetite-MCM-41 with gas chromatography–mass spectrometry for the determination of antidepressant drugs in biological fluids, *J. Sep. Sci.* 40 (2017) 4222–4233. <https://doi.org/10.1002/jssc.201700549>.
- [79] P.K. Jagtap, K. Tapadia, Pharmacokinetic determination and analysis of nortriptyline based on GC-MS coupled with hollow-fiber drop-to-drop solvent microextraction technique, *Bioanalysis*. 10 (2018) 143–152. <https://doi.org/10.4155/bio-2017-0207>.
- [80] L. Truta, A.L. Castro, S. Tarelho, P. Costa, M.G.F. Sales, H.M. Teixeira, Antidepressants detection and quantification in whole blood samples by GC–MS/MS, for forensic purposes, *J. Pharm. Biomed. Anal.* 128 (2016) 496–503. <https://doi.org/10.1016/j.jpba.2016.06.027>.
- [81] A. Plenis, T. BaCzek, Modern chromatographic and electrophoretic measurements of antidepressants and their metabolites in biofluids, *Biomed. Chromatogr.* 25 (2011) 164–198. <https://doi.org/10.1002/bmc.1558>.
- [82] P. Fernández, V. Taboada, M. Regenjo, L. Morales, I. Alvarez, A.M. Carro, R.A. Lorenzo, Optimization of ultrasound assisted dispersive liquid-liquid microextraction of six antidepressants in human plasma using experimental design, *J. Pharm. Biomed. Anal.* 124 (2016) 189–197. <https://doi.org/10.1016/j.jpba.2016.02.041>.
- [83] S. Rani, A.K. Malik, R. Kaur, R. Kaur, A Review for the Analysis of Antidepressant, Antiepileptic and Quinolone Type Drugs in Pharmaceuticals and Environmental Samples, *Crit. Rev. Anal. Chem.* 46 (2016) 424–442. <https://doi.org/10.1080/10408347.2016.1141670>.

- [84] A. Song, Determination of 13 organic toxicants in human blood by liquid-liquid extraction coupling high-performance liquid chromatography tandem mass spectrometry, *Anal. Sci.* 32 (2016) 645–652. <https://doi.org/10.2116/analsci.32.645>.
- [85] H. Juan, Z. Zhiling, L. Huande, Simultaneous determination of fluoxetine, citalopram, paroxetine, venlafaxine in plasma by high performance liquid chromatography-electrospray ionization mass spectrometry (HPLC-MS/ESI), *J. Chromatogr. B Anal. Technol. Biomed. Life Sci.* 820 (2005) 33–39. <https://doi.org/10.1016/j.jchromb.2005.03.006>.
- [86] A. Kabir, K.G. Furton, Fabric phase sorptive extractors (FPSE), 1 (2014) 1–22. <http://www.google.com/patents/US20140274660>.
- [87] R. Kumar, Gaurav, Heena, A.K. Malik, A. Kabir, K.G. Furton, Efficient analysis of selected estrogens using fabric phase sorptive extraction and high performance liquid chromatography-fluorescence detection, *J. Chromatogr. A.* 1359 (2014) 16–25. <https://doi.org/10.1016/j.chroma.2014.07.013>.
- [88] A. Kabir, K.G. Furton, A. Malik, Innovations in sol-gel microextraction phases for solvent-free sample preparation in analytical chemistry, *TrAC - Trends Anal. Chem.* 45 (2013) 197–218. <https://doi.org/10.1016/j.trac.2012.11.014>.
- [89] I. Racamonde, R. Rodil, J.B. Quintana, B.J. Sieira, A. Kabir, K.G. Furton, R. Cela, Fabric phase sorptive extraction: A new sorptive microextraction technique for the determination of non-steroidal anti-inflammatory drugs from environmental water samples, *Anal. Chim. Acta.* 865 (2015) 22–30. <https://doi.org/10.1016/j.aca.2015.01.036>.
- [90] S.S. Segro, M. Tran, S. Kesani, A. Alhendal, E.B. Turner, A. Malik, Sol-gel microextraction phases for sample preconcentration in chromatographic analysis, *J. Sep. Sci.* 33 (2010) 3075–3096. <https://doi.org/10.1002/jssc.201000316>.
- [91] E. Zilfidou, A. Kabir, K.G. Furton, V. Samanidou, Fabric phase sorptive extraction: Current state of the art and future perspectives, *Separations.* 5 (2018) 1–23. <https://doi.org/10.3390/separations5030040>.
- [92] A. Kabir, K.G. Furton, Fabric phase sorptive extraction: A new generation, green sample preparation approach, Elsevier Inc., 2019. <https://doi.org/10.1016/B978-0-12-816906-3.00013-3>.
- [93] V. Kazantzi, A. Anthemidis, Fabric sol-gel phase sorptive extraction technique: A review, *Separations.* 4 (2017). <https://doi.org/10.3390/separations4020020>.
- [94] A. Kabir, R. Mesa, J. Jurmain, K. Furton, Fabric Phase Sorptive Extraction Explained, *Fabr. Phase Sorptive Extr. Explain.* 4 (2017) 21. <https://doi.org/10.20944/preprints201701.0085.v1>.
- [95] E. Karageorgou, N. Manousi, V. Samanidou, A. Kabir, K.G. Furton, Fabric phase sorptive extraction for the fast isolation of sulfonamides residues from raw milk followed by high

- performance liquid chromatography with ultraviolet detection, *Food Chem.* 196 (2016) 428–436. <https://doi.org/10.1016/j.foodchem.2015.09.060>.
- [96] F.G. Calvo-flores, Detection and Analysis of Chemical Pollutants, *Emerg. Pollut.* (2017) 43–55. <https://doi.org/10.1002/9783527691203.ch3>.
- [97] Waters, How Does High Performance Liquid Chromatography Work?, (n.d.). https://www.waters.com/waters/es_MX/How-Does-High-Performance-Liquid-Chromatography-Work%3F/nav.htm?cid=10049055&locale=es_MX.
- [98] S. Parasuraman, A. Rao, S. Balamurugan, S. Muralidharan, K. Jayaraj Kumar, V. Vijayan, An Overview of Liquid Chromatography-Mass Spectroscopy Instrumentation, *Pharm. Methods.* 5 (n.d.) 47–55. <https://doi.org/10.5530/phm.2014.2.2>.
- [99] M. Čelić, A. Jaén-Gil, S. Briceño-Guevara, S. Rodríguez-Mozaz, M. Gros, M. Petrović, Extended suspect screening to identify contaminants of emerging concern in riverine and coastal ecosystems and assessment of environmental risks, *J. Hazard. Mater.* 404 (2021). <https://doi.org/10.1016/j.jhazmat.2020.124102>.
- [100] Y. Meng, W. Liu, X. Liu, J. Zhang, M. Peng, T. Zhang, A review on analytical methods for pharmaceutical and personal care products and their transformation products, *J. Environ. Sci. (China)*. 101 (2021) 260–281. <https://doi.org/10.1016/j.jes.2020.08.025>.
- [101] W.C.W. Chang, H.Y. Wu, Y. Yeh, P.C. Liao, Untargeted foodomics strategy using high-resolution mass spectrometry reveals potential indicators for fish freshness, *Anal. Chim. Acta.* 1127 (2020) 98–105. <https://doi.org/10.1016/j.aca.2020.06.016>.
- [102] A. Cambrai, E. Marchioni, D. Julien-David, C. Marcic, Discrimination of Cocoa Bean Origin by Chocolate Polyphenol Chromatographic Analysis and Chemometrics, *Food Anal. Methods.* 10 (2017) 1991–2000. <https://doi.org/10.1007/s12161-016-0744-7>.
- [103] C. Applications, www.clinical.proteomics-journal.com Page 1 Proteomics - Clinical Applications, (2015) 1–24. <https://doi.org/10.1002/prca.201800105>.This.
- [104] T. Shi, E. Song, S. Nie, K.D. Rodland, T. Liu, W.J. Qian, R.D. Smith, Advances in targeted proteomics and applications to biomedical research, *Proteomics.* 16 (2016) 2160–2182. <https://doi.org/10.1002/pmic.201500449>.
- [105] I. Mahmud, T.J. Garrett, Mass Spectrometry Techniques in Emerging Pathogens Studies: COVID-19 Perspectives, *J. Am. Soc. Mass Spectrom.* 31 (2020) 2013–2024. <https://doi.org/10.1021/jasms.0c00238>.
- [106] R. Akçan, B. Taştekin, M.Ş. Yildirim, H.C. Aydoğan, N. Sağlam, Omics era in forensic medicine: Towards a new age, *Turkish J. Med. Sci.* 50 (2020) 1480–1490. <https://doi.org/10.3906/sag-1912-197>.
- [107] Y. Xiao, J. Deng, Y. Yao, L. Fang, Y. Yang, T. Luan, Recent advances of ambient mass

- spectrometry imaging for biological tissues: A review, *Anal. Chim. Acta.* 1117 (2020) 74–88. <https://doi.org/10.1016/j.aca.2020.01.052>.
- [108] M. Thevis, T. Kuuranne, H. Geyer, Annual banned-substance review: Analytical approaches in human sports drug testing, *Drug Test. Anal.* 10 (2018) 9–27. <https://doi.org/10.1002/dta.2336>.
- [109] H. Awad, M.M. Khamis, A. El-Aneed, Mass spectrometry, review of the basics: Ionization, *Appl. Spectrosc. Rev.* 50 (2015) 158–175. <https://doi.org/10.1080/05704928.2014.954046>.
- [110] John Roboz, A History of Ion Current Detectors for Mass Spectrometry, *Encycl. Mass Spectrom.* (2016) 183–188. <https://doi.org/10.1016/b978-0-08-043848-1.00023-7>.
- [111] D.W. Koppenaal, C.J. Barinaga, M.B. Denton, R.P. Sperline, G.M. Hieftje, G.D. Schilling, F.J. Andrade, J.H. Barnes IV, MS detectors, *Anal. Chem.* 77 (2005). <https://doi.org/10.1021/ac053495p>.
- [112] J.H. Gross, *Mass Spectrometry*, 1962. <https://doi.org/10.11316/butsuri1946.17.688>.
- [113] W.M.A. Niessen, R.A. Correa C., Interpretation of MS-MS Mass Spectra of Drugs and Pesticides, *Interpret. MS-MS Mass Spectra Drugs Pestic.* (2016) 1–388. <https://doi.org/10.1002/9781119294269>.
- [114] Interfaces for LCMS : SHIMADZU (Shimadzu Corporation), (n.d.).
- [115] G. Hopfgartner, Theory and Instrumentation of Mass Spectrometry, *Mass Spectrom. Drug Metab. Dispos. Basic Princ. Appl.* (2011) 255–290. <https://doi.org/10.1002/9780470929278.ch8>.
- [116] C.I. Kosma, D.A. Lambropoulou, T.A. Albanis, Photochemical transformation and wastewater fate and occurrence of omeprazole: HRMS for elucidation of transformation products and target and suspect screening analysis in wastewaters, *Sci. Total Environ.* 590–591 (2017) 592–601. <https://doi.org/10.1016/j.scitotenv.2017.02.233>.
- [117] P. Calza, C. Jiménez-Holgado, M. Cocha, C. Chrimatopoulos, F. Dal Bello, C. Medana, V. Sakkas, Study of the photoinduced transformations of sertraline in aqueous media, *Sci. Total Environ.* 756 (2021) 143805. <https://doi.org/10.1016/j.scitotenv.2020.143805>.
- [118] M.A.G. Wallace, J.P. Mccord, Chapter 16 - High-resolution mass spectrometry, Elsevier B.V., 2020. <https://doi.org/10.1016/B978-0-12-819967-1.00016-5>.
- [119] A. Agüera, M.J. Martínez Bueno, A.R. Fernández-Alba, New trends in the analytical determination of emerging contaminants and their transformation products in environmental waters, *Environ. Sci. Pollut. Res.* 20 (2013) 3496–3515. <https://doi.org/10.1007/s11356-013-1586-0>.
- [120] H. Richard, R. Perry, G. Cooks, R.J. Noll, Orbitrap MS: instrumentation, ion motion and applications, *WHO Libr. Cat. Data.* (2008) 221–235. <https://doi.org/10.1002/mas.20186>.

- [121] R.A. Zubarev, A. Makarov, Orbitrap mass spectrometry, *Anal. Chem.* 85 (2013) 5288–5296. <https://doi.org/10.1021/ac4001223>.
- [122] M. Smol, C. Adam, M. Preisner, Circular economy model framework in the European water and wastewater sector, *J. Mater. Cycles Waste Manag.* 22 (2020) 682–697. <https://doi.org/10.1007/s10163-019-00960-z>.
- [123] T. Kosjek, E. Heath, A. Krbavčič, Determination of non-steroidal anti-inflammatory drug (NSAIDs) residues in water samples, *Environ. Int.* 31 (2005) 679–685. <https://doi.org/10.1016/j.envint.2004.12.001>.
- [124] R. Nassar, A. Trivella, S. Mokh, M. Al-Iskandarani, H. Budzinski, P. Mazellier, Photodegradation of sulfamethazine, sulfamethoxypyridazine, amitriptyline, and clomipramine drugs in aqueous media, *J. Photochem. Photobiol. A Chem.* 336 (2017) 176–182. <https://doi.org/10.1016/j.jphotochem.2016.12.008>.
- [125] M. Huerta-Fontela, M.T. Galceran, F. Ventura, Occurrence and removal of pharmaceuticals and hormones through drinking water treatment, *Water Res.* 45 (2011) 1432–1442. <https://doi.org/10.1016/j.watres.2010.10.036>.
- [126] A.V. Santos, C.F. Couto, Y.A.R. Lebron, V.R. Moreira, A.F.S. Foureaux, E.O. Reis, L.V. de S. Santos, L.H. de Andrade, M.C.S. Amaral, L.C. Lange, Occurrence and risk assessment of pharmaceutically active compounds in water supply systems in Brazil, *Sci. Total Environ.* 746 (2020) 141011. <https://doi.org/10.1016/j.scitotenv.2020.141011>.
- [127] H. Mestankova, K. Schirmer, B.I. Escher, U. Von Gunten, S. Canonica, Removal of the antiviral agent oseltamivir and its biological activity by oxidative processes, *Environ. Pollut.* 161 (2012) 30–35. <https://doi.org/10.1016/j.envpol.2011.09.018>.
- [128] M. Taheran, S.K. Brar, M. Verma, R.Y. Surampalli, T.C. Zhang, J.R. Valero, Membrane processes for removal of pharmaceutically active compounds (PhACs) from water and wastewaters, *Sci. Total Environ.* 547 (2016) 60–77. <https://doi.org/10.1016/j.scitotenv.2015.12.139>.
- [129] D.B. Miklos, C. Remy, M. Jekel, K.G. Linden, J.E. Drewes, U. Hübner, Evaluation of advanced oxidation processes for water and wastewater treatment – A critical review, *Water Res.* 139 (2018) 118–131. <https://doi.org/10.1016/j.watres.2018.03.042>.
- [130] M. Marjanovic, S. Giannakis, D. Grandjean, L.F. de Alencastro, C. Pulgarin, Effect of MM Fe addition, mild heat and solar UV on sulfate radical-mediated inactivation of bacteria, viruses, and micropollutant degradation in water, *Water Res.* 140 (2018) 220–231. <https://doi.org/10.1016/j.watres.2018.04.054>.
- [131] E. Shabat-Hadas, H. Mamane, V. Gitis, Rhodamine B in dissolved and nano-bound forms: Indicators for light-based advanced oxidation processes, *Chemosphere.* 184 (2017) 1020–1027. <https://doi.org/10.1016/j.chemosphere.2017.06.076>.

- [132] K.G. Linden, M. Mohseni, *Applications of Advanced Oxidation Processes (AOPs) in Drinking Water Treatment*, 2019. <http://link.springer.com/10.1007/978-3-319-76882-3>.
- [133] E.M. Cuerda-correa, M.F. Alexandre-franco, C. Fern, *Advanced Oxidation Processes for the Removal of Antibiotics from Water. An Overview*, *Water*. 12 (2020) 1–50.
- [134] P. Kokkinos, D. Venieri, D. Mantzavinos, *Advanced Oxidation Processes for Water and Wastewater Viral Disinfection. A Systematic Review*, *Food Environ. Virol.* (2021). <https://doi.org/10.1007/s12560-021-09481-1>.
- [135] A. Tufail, W.E. Price, F.I. Hai, *A critical review on advanced oxidation processes for the removal of trace organic contaminants: A voyage from individual to integrated processes*, *Chemosphere*. 260 (2020) 127460. <https://doi.org/10.1016/j.chemosphere.2020.127460>.
- [136] C. Jiménez-Holgado, C. Chrimatopoulos, V. Stathopoulos, V. Sakkas, *Investigating the utility of fabric phase sorptive extraction and hplc-uv-vis/dad to determine antidepressant drugs in environmental aqueous samples*, *Separations*. 7 (2020) 1–14. <https://doi.org/10.3390/separations7030039>.
- [137] S. Chianese, P. Iovino, V. Leone, D. Musmarra, M. Prisciandaro, *Photodegradation of Diclofenac Sodium Salt in Water Solution: Effect of HA, NO₃⁻ and TiO₂ on Photolysis Performance*, *Water. Air. Soil Pollut.* 228 (2017). <https://doi.org/10.1007/s11270-017-3445-y>.
- [138] T. Katagi, *Direct photolysis mechanism of pesticides in water*, *J. Pestic. Sci.* 43 (2018) 57–72. <https://doi.org/10.1584/jpestics.D17-081>.
- [139] I.P. Pozdnyakov, Y.E. Tyutereva, M. V. Parkhats, V.P. Grivin, Y. Fang, L. Liu, D. Wan, F. Luo, Y. Chen, *Mechanistic investigation of humic substances assisted photodegradation of imipramine under simulated sunlight*, *Sci. Total Environ.* 738 (2020) 140298. <https://doi.org/10.1016/j.scitotenv.2020.140298>.
- [140] P.P. Vaughan, N. V. Blough, *Photochemical formation of hydroxyl radical by constituents of natural waters*, *Environ. Sci. Technol.* 32 (1998) 2947–2953. <https://doi.org/10.1021/es9710417>.
- [141] K. Mopper, X. Zhou, *Hydroxyl radical photoproduction in the sea and its potential impact on marine processes*, *Science (80-.)*. 250 (1990) 661–664. <https://doi.org/10.1126/science.250.4981.661>.
- [142] D. Vione, M. Minella, V. Maurino, C. Minero, *Indirect photochemistry in sunlit surface waters: Photoinduced production of reactive transient species*, *Chem. - A Eur. J.* 20 (2014) 10590–10606. <https://doi.org/10.1002/chem.201400413>.
- [143] W.J. Cooper, R.G. Zika, R.G. Petasne, J.M. Plane, *Photochemical formation of hydrogen peroxide in natural waters exposed to sunlight*, *Environ. Sci. Technol.* 22 (1988) 1156–1160.
- [144] R.G. Zepp, P.F. Schlotzhauer, R.M. Sink, *Photosensitized Transformations Involving Electronic*

- Energy Transfer in Natural Waters: Role of Humic Substances, *Environ. Sci. Technol.* 19 (1985) 74–81. <https://doi.org/10.1021/es00131a008>.
- [145] B.M. Peterson, A.M. McNally, R.M. Cory, J.D. Thoemke, J.B. Cotner, K. McNeill, Spatial and temporal distribution of singlet oxygen in Lake Superior, *Environ. Sci. Technol.* 46 (2012) 7222–7229. <https://doi.org/10.1021/es301105e>.
- [146] S. Canonica, U.R.S. Jans, K. Stemmler, J. Hoigne, Transformation Kinetics of Phenols in Water: Photosensitization, *Environ. Sci. Technol.* 29 (1995) 1822–1831.
- [147] Y.M. Kang, M.K. Kim, K.D. Zoh, Effect of nitrate, carbonate/bicarbonate, humic acid, and H₂O₂ on the kinetics and degradation mechanism of Bisphenol-A during UV photolysis, *Chemosphere*. 204 (2018) 148–155. <https://doi.org/10.1016/j.chemosphere.2018.04.015>.
- [148] S. Canonica, T. Kohn, M. Mac, F.J. Real, J. Wirz, U. Von Gunten, Photosensitizer method to determine rate constants for the reaction of carbonate radical with organic compounds, *Environ. Sci. Technol.* 39 (2005) 9182–9188. <https://doi.org/10.1021/es051236b>.
- [149] K. McNeill, S. Canonica, Triplet state dissolved organic matter in aquatic photochemistry: Reaction mechanisms, substrate scope, and photophysical properties, *Environ. Sci. Process. Impacts*. 18 (2016) 1381–1399. <https://doi.org/10.1039/c6em00408c>.
- [150] S. Canonica, M. Freiburghaus, Electron-rich phenols for probing the photochemical reactivity of freshwaters, *Environ. Sci. Technol.* 35 (2001) 690–695. <https://doi.org/10.1021/es0011360>.
- [151] Y. Wang, L. Fan, N. Crosbie, F.A. Roddick, Photodegradation of emerging contaminants in a sunlit wastewater lagoon, seasonal measurements, environmental impacts and modelling, *Environ. Sci. Water Res. Technol.* 6 (2020) 3380–3390. <https://doi.org/10.1039/d0ew00527d>.
- [152] P.K.J. Robertson, D.W. Bahnemann, J.M.C. Robertson, F. Wood, Photocatalytic Detoxification of Water and Air, *Environ. Photochem. Part II*. 2 (2005) 367–423. <https://doi.org/10.1007/b138189>.
- [153] M. Sillanpää, M.C. Ncibi, A. Matilainen, Advanced oxidation processes for the removal of natural organic matter from drinking water sources: A comprehensive review, *J. Environ. Manage.* 208 (2018) 56–76. <https://doi.org/10.1016/j.jenvman.2017.12.009>.
- [154] M. Brienza, C.B. Özkal, G. Li Puma, Photo(Catalytic) oxidation processes for the removal of natural organic matter and contaminants of emerging concern from water, *Handb. Environ. Chem.* 67 (2019) 133–154. https://doi.org/10.1007/698_2017_189.
- [155] A. Fujishima, X. Zhang, D.A. Tryk, TiO₂ photocatalysis and related surface phenomena, *Surf. Sci. Rep.* 63 (2008) 515–582. <https://doi.org/10.1016/j.surfrep.2008.10.001>.
- [156] Q. Xiang, J. Yu, P.K. Wong, Quantitative characterization of hydroxyl radicals produced by various photocatalysts, *J. Colloid Interface Sci.* 357 (2011) 163–167. <https://doi.org/10.1016/j.jcis.2011.01.093>.

Chapter 2. Development of a green analytical microextraction method for the determination of three psychoactive drugs

In this Chapter, a novel and green microextraction technique called Fabric Phase Sorptive Extraction has been developed, optimized and validated for the analysis of three psychoactive drugs used in the treatment of mental diseases.

Part of this work has been carried out during my first secondment at MIRTEC S.A, located in Chalkida, Athens, under the supervision of Dr. Vassilis Stathopoulos. During my period there, we investigated the utility of polylactic acid as a substrate coated with different polymers. This work is already published in *Separations: "Investigating the Utility of Fabric Phase Sorptive Extraction and HPLC-UV-Vis/DAD to Determine Antidepressant Drugs in Environmental Aqueous Samples"* and is described below.

2.1. Abstract

Depression is considered to be one of the most prevalent mental disorders in humans. Antidepressant drugs are released in large concentrations and cause adverse effects on the environment and/or human health. Fabric Phase Sorptive Extraction (FPSE), a contemporary solid

sorbent-handling technique, is a quick, sensitive, and simple analytical process. This paper describes a micro-extraction FPSE procedure coupled with High-Performance Liquid-Chromatography–Photodiode Array Detection (FPSE-HPLC–DAD) for the simultaneous extraction and analysis of five antidepressants, namely citalopram, clozapine, mirtazapine, bupropion and sertraline. Three fabric media (Whatman Cellulose filter, Whatman Microfiber Glass filter and Polylactic acid disks) and two different sol–gel sorbents (polyethylene glycol (PEG 300), alongside poly(ethylene glycol)-block-poly(propylene glycol)-block-poly(ethylene glycol) (PEG-PPG-PEG 5.800)) were tested. The best FPSE device was observed to be the microfiber glass filter coated with PEG 300 sol–gel sorbent. In addition, the parameters that affect the efficiency of the process (FPSE media and sorbents, sample pH, extraction time, elution time, etc.) were optimized. The proposed methodology displays a linear range with absolute recovery values higher than 60%, RSD% of less than 13% and LOQs in the range between 1.9–10.7 $\mu\text{g}\cdot\text{L}^{-1}$. Finally, the method was applied in hospital and urban effluents and lake water samples, but none of the analytes were detected.

2.2.Introduction

Depression (major depressive disorder) is one of the most ordinary and widespread mental diseases caused by various social, psychological, and biological factors interacting and correlating among each other. It negatively affects how someone feels, their way of thinking and how the person acts. Depending on the nature and period of the symptoms, it may cause a severe health disorder that causes restricted psychosocial function, a decreased quality of life and satisfaction, feelings of culpability or low confidence, reduced sleep or hunger, poor performance, and may even result in suicide.

The pharmacological treatment of depression began in the 1950s, with the introduction of the first-generation antidepressant drugs (ADs), such as tricyclic and tetracyclic antidepressants (TCAs), and monoamine oxidase inhibitors (MAOIs). Two decades later, the second-generation agents

were introduced, namely selective serotonin reuptake inhibitors (SSRIs). The newest and most used antidepressants drugs appeared after the 1990s, (serotonin and norepinephrine reuptake inhibitors) [1].

A concerning overconsumption of ADs has been observed in recent years. A big variety of ADs have already been detected in the range of a few $\text{ng}\cdot\text{L}^{-1}$ to several tens of $\mu\text{g}\cdot\text{L}^{-1}$ in surface waters and wastewater [2–5]. Therefore, the identification and quantification of such drugs is now of great importance in natural water, since concentration levels up to $78.3\ \mu\text{g}\cdot\text{L}^{-1}$ have been reported [5].

The literature has documented numerous analytical techniques for the determination of ADs. The most commonly used are high performance liquid chromatography (HPLC) coupled to UV–Vis or a mass spectrometric detector (MS) [6–13]. Gas chromatography (GC) coupled to MS [14–17] or tandem MS [18], and the capillary electrophoretic technique (CE) have also been reported [19]. A significant drawback of GC methods is the restriction of the target compound's volatility [20]. In comparison, HPLC can evaluate both volatile and non-volatile compounds, contributing to an adequately user-friendly separation technique [21].

Pretreatment of the sample is the most important step in the workflow of chromatographic analysis, since most samples are not able to be immediately injected into the chromatographic instrument. Various sample preparation approaches coupled with HPLC for the determination and preconcentration of antidepressant drugs in biological fluids have been reported. The most frequently employed techniques are liquid–liquid extraction (LLE) [22] and solid-phase extraction (SPE) techniques [23]. Fabric-Phase Sorptive Extraction (FPSE) has recently attracted the interest of the scientific community, particularly during its application for the determination of pharmaceutical compounds in biological samples [24,25].

Kabir and Furton first proposed FPSE as a two-step, novel and green sample preparation technique [26]. FPSE utilizes, as an extraction medium, a natural or synthetic fabric substrate, which is chemically coated in the form of an ultra-thin coating with a sol–gel organic–inorganic hybrid

sorbent [27]. This microextraction technique is capable of extracting analytes within a wider polarity range, depending on the sol–gel’s physicochemical properties. The porous network of sol–gel sorbent coating and the permeability of the fabric substratum contribute to the current method, which imitates the extraction of the solid phase. The desorption of analytes from the FPSE media into organic solvents is much more rapid without a significant chance of carryover. This technique overcomes the major drawbacks of other sorptive extraction procedures that exhibit limitations such as sample size and preparation time, system or coating damage, resistance to harsh chemical environments and organic solvents. FPSE has been widely used for the extraction and determination of different analytes from different sample matrices since its invention in 2014 [28–30].

In the present study, an easy, green and fast analytical methodology is proposed for the extraction of five psychoactive drugs that are commonly used in the treatment of mental diseases (citalopram, clozapine, mirtazapine, bupropion and sertraline) by employing FPSE coupled to High Performance Liquid Chromatography–Photodiode Array Detection (HPLC–DAD). The primary parameters affecting extraction efficiency were investigated and optimized using both univariate and multivariate experimental configurations of fractional factorial design followed by Response Surface Methodology. Finally, the applicability of the method was examined by obtaining natural water samples from wastewater treatment plants. To the best of our knowledge, FPSE has been extensively applied to environmental samples [31–34], but the extraction of antidepressants from real water samples has not been explored yet.

2.3. Materials and methods

2.3.1. Reagents

The starting materials to be coated and used as FPSE media were Whatman microfiberglass filters of 110 mm and Whatman cellulose filter papers of 125 mm (Boston, MA, USA). The organic polymers polyethylene glycol (PEG 300) and poly(ethylene glycol)-block-poly(propylene glycol)-block-

poly(ethylene glycol) (PEG-PPG-PEG 5.800) were purchased from Sigma-Aldrich (Athens, Greece). Solvents (dichloromethane, acetonitrile (ACN), acetone, methanol (MeOH) and phosphoric acid) were purchased from Merck (Darmstadt, Germany). Trimethoxymethylsilane (MTMS), trifluoroacetic acid (TFA), sodium hydroxide, and hydrochloric acid were also supplied by Merck (Darmstadt, Germany).

Poly(lactic acid) (PLA) 3D-printed disks of $0.02 \times 0.02 \times 0.0015$ m were prepared using a Prusa i3 3D printer using the fused deposition modeling (FDM) technique [35]. The printing and specimen volume filling parameters for the 3D printing process were modified using slicer software. All the parts were printed (100% filling density) using rectilinear pattern filling, on a heated bed (60 °C) and the nozzle (diameter 4 μm) was maintained at 200 °C during the process [36].

Antidepressants citalopram (CIT), clozapine (CLO), mirtazapine (MIRT), bupropion (BUP) and sertraline (SERT) were purchased from TCI Tokyo Chemical Industry (Tokyo, Japan). All analytes have a purity higher than 98%. By dissolving the compound in methanol, stock solutions containing 1000 $\text{mg}\cdot\text{L}^{-1}$ of each analyte were prepared, and the solutions were stored in glass-stopped bottles at -20 °C in the dark. Standard working solutions were prepared daily. The ultrapure water used was produced by a Milli-Q system (Evoqua, Pittsburg, PA, USA).

STATISTICA 7.0 (StatSoft Inc., Tulsa, OK, USA) was used to produce the experimental matrix and to evaluate the results.

2.3.2. Sample collection

Wastewater samples were collected from the outflow of municipal and university hospital wastewater treatment plants in Ioannina city, located in the Epirus region, NW Greece. In the municipal wastewater treatment plant (WWTP1) the wastewaters of the whole Ioannina city are deposited, with a population of more than 100,000 people. All household and industrial waste and rain waters are collected from the WWTP1, frequently surpassing the WWTP's capacity to handle this

volume. In addition, wastewater from Ioannina hospital's WWTP effluent (WWTP2) was also sampled. Ioannina University Hospital is also the center of learning and applied medical science linked to the School of Medicine and School of Nursing at Ioannina University. About 45,000 patients are treated annually in the Care Clinics of the medical center. Furthermore, the hospital has a Department of Psychiatry, making it interesting to research the occurrence of psychotropic drugs in the hospital's WWTP effluent. The hospital's plant (WWTP2) sheds its treated wastewater into the urban network that eventually goes straight to the municipal WWTP; thus, we have a significant interest in assessing its efficiency in order to determine the presence of ADs in the municipal WWTP.

Moreover, surface water was collected from Pamvotis Lake in Ioannina. Covering an area of 19.4 km², Pamvotis Lake is one of the largest lakes in Greece. The pollution of the lake is due to the illegal dumping of waste from tankers, livestock and industrial plants, pesticide residues, illegal landfills, and the fact that parts of the city have not been connected to the city's wastewater network. All the samples were collected in clean amber glass bottles. Finally, the samples were transported to the laboratory immediately and placed in the refrigerator at 5°C before extraction and analysis.

2.3.3. HPLC analysis

To determine the selected analytes, a Thermo Fisher Scientific UltiMate 3000 HPLC system equipped with a diode array detector and Chromeleon Thermo Fischer software were used. The equipment consists of a Binary Solvent Manager (BSM), a WPS-3000SL autosampler and a column manager, all from Waters Thermo Fisher Scientific (Waltham, MA, USA). The parameters for the detection of the targeted analytes were optimized by using a standard solution of a mixture of all the compounds.

The injection volume into the chromatographic equipment was 20 μL , and the analytical column was a Hypersil GOLD 150 \times 4.6 mm, with a particle size of 5 μm (Thermo Scientific, Waltham, MA, USA), operating at 25 $^{\circ}\text{C}$.

The mobile phase consists of methanol (A) and water with 0.3% phosphoric acid (B), at 1.0 mL/min flow in gradient mode. The gradient started at 15:85 (A:B) (v/v) and increased after 3 min to 50% methanol. The percentage of methanol increased further up to 80% after 7 min and the gradient returned, after 2 min, to its initial state 15:85 (equilibrium time 3 min). The whole chromatographic separation process finished in 15 min. The parameters of the diode array detector (DAD) were chosen for the quantitative analysis of each compound. The UV detector was set at 245 nm for sertraline, clozapine and citalopram, at 230 nm for mirtazapine and at 254 nm for bupropion, with full spectral scanning from 200 to 400 nm.

2.3.4. Preparation of sol-gel sorbent-coated FPSE media

2.3.4.1. Pretreatment of media for sol-gel coatings

All fabrics chosen to produce sol-gel covered sorbents have remaining finishing additives or other contaminants that agglomerated over time on their surface, which required thorough cleaning. Additionally, the surface areas of these fabrics require activation to optimize the sol-gel sorbent loading during the polymer sorbent coating phase.

This was done after we implemented a systematic cleaning procedure. Briefly, a 95 cm^2 (11 cm diameter) circular piece of the Whatman Cellulose filter was soaked with deionized water under constant sonication for 15 min, followed by NaOH treatment (1.0 M, 1 h) and then HCl (0.1 M, 1 h), under sonication, respectively. After each one of these three cleaning steps the fabric media were washed with a profuse amount of deionized water. The media were then left to dry in ambient air at room temperature for 24 h, following the coating step. This procedure was followed to increase the

availability of all the hydroxyl groups of the cellulose chemical structure that lead to more chemical reactions with the sol–gel inorganic–organic network.

Almost the same procedure was adopted for the Whatman Microfiber Glass filter pretreatment to activate the surface silanol groups. The difference with the abovementioned procedure was that the pretreatment time with NaOH (1.0 M) and then HCl (0.1 M) was for 8 h, respectively.

PLA was treated with a mixture of 0.25 M NaOH/EtOH for 4 h to improve its hydrophilicity and cell affinity. To stop any major deterioration of the product, an alkali solution was used. Ethanol has been found to aid the hydroxide nucleophilic effect on ester bonds of PLA. Then, the conditioned PLA was soaked with deionized water and eventually dried overnight under N₂ gas flow in inert conditions.

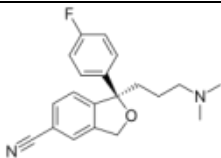
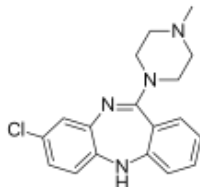
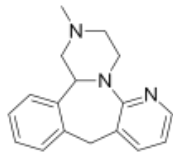
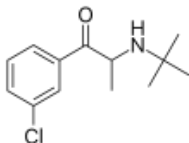
2.3.4.2. Preparation of the sol–gel solutions for coating on the substrate surface

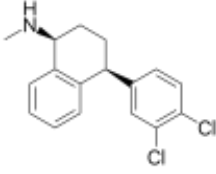
In the sol–gel process, polymer choice is important, depending on the target analytes' polarity/functionality. Taking into account the target analytes' physicochemical characteristics (Table 2.1), two sol–gel sorbents were prepared, including polyethylene glycol 300 (PEG 300) and poly(ethylene glycol)-block-poly(propylene glycol)-block-poly(ethylene glycol) 5.800 (PEG-PPG-PEG 5.800). Sol–gel solutions consist of a solvent system, a sol–gel precursor, an organic polymer, and an aqua solution of the catalyst. In our study, both polymer solutions were developed using methyltrimethoxysilane (MTMS) as the sol–gel precursor, a trifluoroacetic acid (TFA) catalyst containing 5% water, and a combination of acetone and dichloromethane (50/50 v/v) as the organic solvent. The molar ratio between polymer:precursor:organic solvent:catalyst was optimized and maintained at 0.5:0.2:1.0:0.5, respectively.

2.3.4.3. Fabric Phase Sorptive Extraction process

First, the coated materials were soaked for 5 min in 2 mL of methanol:acetonitrile (1:1) solution, and next were treated with 2 mL deionized water for 5 min to remove the previous organic solvents. This step was conducted to clean and activate the coating of the fabric substrate. Afterwards, the FPSE media were immersed in the aquatic sample. Adsorption studies were conducted (spiking level $100 \mu\text{g}\cdot\text{L}^{-1}$, Milli-Q water, continuous stirring at 300 rpm provided by magnetic stir bar) with the appropriate fabrics to choose the one that could be most effective for the target compounds. After this, the target analytes were eluted from the media in a sufficient volume of solvent for an optimal period. The collected solvent was adjusted to 100 μL with a gentle N_2 stream, before HPLC analysis. The schematic procedure of FPSE is shown in Figure S2.

Table 2.1. Structures and respective physico-chemical characteristics of target analytes.

Analyte	Molecular Weight, g/mole	Chemical Structure	pKa	logK _{ow}
Citalopram (CIT)	324.39		9.78	3.76
Clozapine (CLO)	326.82		7.50	3.23
Mirtazapine (MIRT)	265.35		7.70	2.90
Bupropion (BUP)	239.74		8.22	3.85

Sertraline (SERT)	306.20		9.48	5.10
-------------------	--------	--	------	------

2.4. Results and discussion

2.4.1. Selection of FPSE substrate and sol-gel coating

The selectivity of the extraction depends on the hydrophilic/hydrophobic properties of the media and on the polarity of the polymer, which, together, define the extraction performance of the FPSE device. A Milli-Q water solution spiked (at $100 \mu\text{g}\cdot\text{L}^{-1}$) with the five antidepressant drugs was prepared to determine the efficiency of the process ($N = 3$). The concentration of the analytes was measured by HPLC-UV-Vis/DAD before and after the extraction step, as well as after the elution step, in order to determine the adsorption and desorption efficiency, respectively. The performance of extraction was calculated as the ratio of the initial aqueous concentration in the Milli-Q water sample to the final concentration.

During preliminary studies, in which the type and shape of substrate as well as the polymer used in the creation of the sol-gel solution were tested, we decided to assess the following three different substrates: Whatman microfiber glass filter (FG), Whatman cellulose filter (WC), and polylactic acid disks (PLA). Two different sol-gel coatings were developed, high-polarity PEG 300 and medium-polarity PEG-PPG-PEG 5.800, which were finally evaluated. From the results obtained, it was found that the circle-shaped 100% glass microfiber filter (FG) with a diameter of 1 cm coated with PEG300 displayed the greatest adsorption and desorption yields, so this combination was chosen for further optimization.

2.4.2. Optimization of the experimental conditions

2.4.2.1. Preliminary experiments

For the optimization of the FPSE process, both univariate and multivariate analysis approaches were carried out to encourage sound, rational thinking and responsibility instead of 'push-the-button' automated data. There are many variables that may influence FPSE extraction efficiency, among them are sample volume, ionic strength, pH, extraction time and the solvent, as well as the elution solvent, time and volume, etc. Four of them were initially investigated to check their suitability to efficiently recover the target analytes: sample volume (1 and 10 mL), extraction time (10, 20, 30 and 40 min), pH (3, 7, 10 and 12) and ionic strength of the sample (0% and 10% w/v).

The volume of the aqueous sample as well as the final volume of the extract are closely related to the technique's preconcentration ability. Two sample volumes (1 and 10 mL) with a fixed elution volume solvent (1 mL, MeOH) were examined initially under continuous stirring at 300 rpm by a magnetic stir bar. The rate of adsorption for 1 mL was higher than for 10 mL (Figure 2.1a) for a fixed adsorption time of 10 min, so 1 mL was selected to reach faster equilibrium conditions.

The extraction time is directly associated with the distribution parameters that determine the interaction between the FPSE material and the analytes. Four extraction times were investigated: 10, 20, 30 and 40 min. The results revealed that extraction times of 10 and 20 min were marginally worse than longer extraction times of 30 and 40 min (Figure 2.1b). It can be seen that, after 30 min, the equilibrium is established, so 30 min was chosen as the optimum extraction time.

For the 1 mL sample and 30 min extraction time, four separate pH values were measured: pH 3, 7, 10 and 12. At the alkaline pH region (pH 12) the highest extraction efficiency was obtained for all target analytes (Figure 2.1 c). Considering the fact that the analytes act as weak bases (pKas are in the range between 7.5–9.8, Table 2.1), they are positively charged at environmentally relevant pH values, while, at pH values two units higher than their pKa ($pK_a + 2$), they are in neutral form. This explains the higher adsorption yield that is observed at alkaline pH levels (pH 12).

An increased concentration of ions in a solution is advantageous for increasing the recovery of organic contaminants from aqueous solution. The effect of ionic strength on analyte adsorption

was studied, while the remaining parameters were fixed (1 mL sample volume, 30 min of extraction and pH adjusted at 12). For this reason, 10% (w/v) of NaCl was added to the aqueous solution containing analytes (Figure 2.1 d). The results have shown that the adsorption efficiency declines with increasing ionic strength. The decreased adsorption efficiency may be attributed to the increase in the aqueous matrix's viscosity, resulting in a sluggish distribution of analytes to the FPSE media.

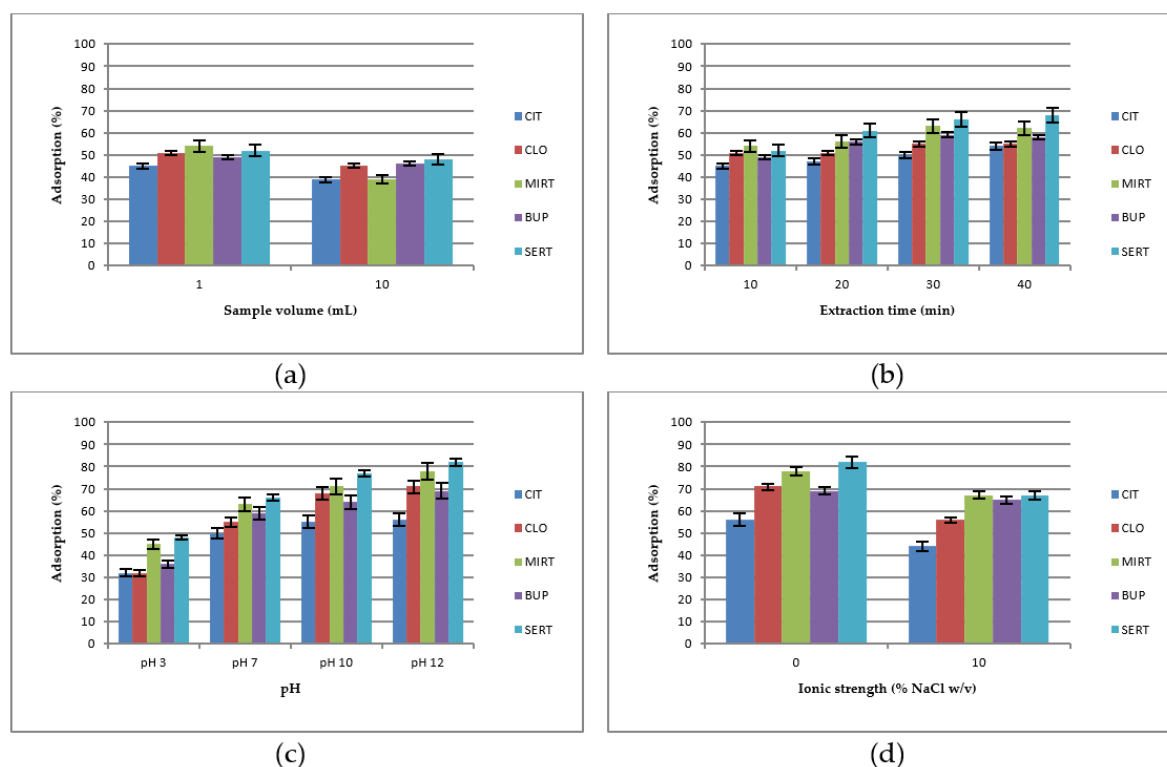


Figure 2.1. Efficiencies of the five antidepressants (ADs) during the adsorption step depending on (a) the volume of the sample, (b) extraction time for 10, 20 30 and 40 min under stirring, (c) different pH values, and (d) ionic strength; citalopram (CIT), clozapine (CLO), mirtazapine (MIRT), bupropion (BUP), sertraline (SERT).

2.4.2.2. Experimental design optimization

In the next step, we decided to select the appropriate elution variables to build a model that best reflected the variation of the microextraction process. The elution procedure was optimized through chemometric tools such as Design of Experiments (DoE) and Response Surface Methodology (RSM) (STATISTICA Software v7). The experimental configuration was initially conducted with four

variables (two levels for each) to define how these affect the extraction performance (elution solvent: MeOH/ACN, elution process: vortex/stirring, elution time: 3/6 min, elution volume 0.1/0.5 mL). Methanol was far more efficient than ACN, followed by stirring at 300 rpm against a vortex as the desorption process, while both a higher elution time and solvent volume had a positive effect on the efficiency of the FPSE process (Figure 2.2).

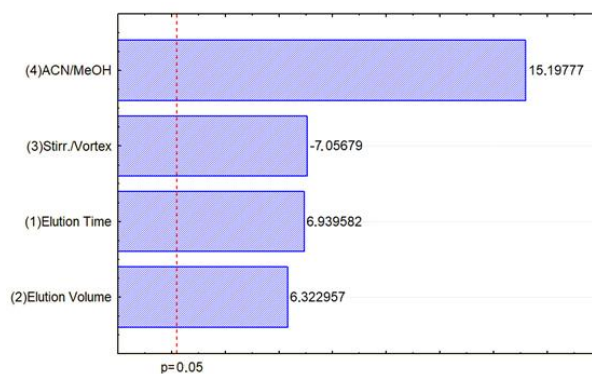


Figure 2.2. Pareto maps of the standardized effects (2^4 experimental configuration).

Having followed the findings of the previous design, the next task was to improve the analytical process further by employing a 3^2 experimental configuration for an elution volume of MeOH (0.75, 1.00 and 1.25 mL) and time (5, 10 and 15 min). The main effects were analyzed, as well as quadratic and interaction effects, by ANOVA (Table 2.2) and proved to be significant. The expressed a 3D correlation between the MeOH volume and the elution time, which is depicted in Figure 2.3. In particular, a higher elution time was needed when a greater amount of MeOH was used. A desirability function was used to determine the optimum extraction conditions (Figure 2.4).

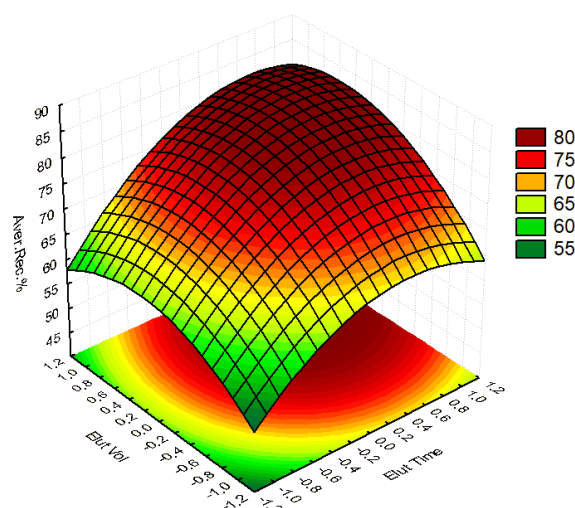


Figure 2.3. 3D Response Surface representation of elution time and solvent volume (coded values).

To conclude, the optimal parameters for the FPSE process in relation to the extraction of the selected antidepressants were as follows: a circle-shaped 100% glass microfiber filter (FG) with a diameter of 1 cm c, with PEG300, as the FPSE device. The extraction of the aqueous sample (1 mL, adjusted to pH 12) was carried out for 30 min and stirred at 300 rpm. Methanol was used as the desorption solvent at 1.0 mL for 10 min under stirring at 300 rpm. The final extract was adjusted to 0.1 mL before analysis to have a preconcentration factor of 10 (from 1 mL to 0.1 mL).

Table 2.2. ANOVA results obtained by 3^2 design.

Factor	SS	df	MS	F	p
(1) Elution Time	741.745	1	747.745	48.1578	0.000025
(2) Elution Volume	615.784	1	615.784	39.9798	0.000057
(3) Stirring/Vortex mixing	767.013	1	767.013	49.7983	0.000021
(4) ACN/MeOH	3557.526	1	3557.526	230.9724	0.000000
Error	169.426	11	15.402		
Total SS	5851.495	15			

2.4.3. Analytical performance

The figures of merit of the proposed method were also assessed. A seven-point curve was developed among the LOQ of each analyte up to $500 \mu\text{g}\cdot\text{L}^{-1}$. The method displays linearity at the specified range with coefficients of determination (R^2) greater than 0.9989. An examination of accuracy and precision was carried out at two concentration levels (LOQ and $10 \times \text{LOQ}$) in Milli-Q water, spiked with the target analytes. The intraday precision of the process was measured through three assessments, while the interday precision was measured over three days by a triplet of measures. As depicted at Table 3, satisfactory absolute recoveries (the % concentration of target analytes recovered from Milli-Q water) in the range of 60–98% were observed. The % RSDs were less than 13% in both cases.

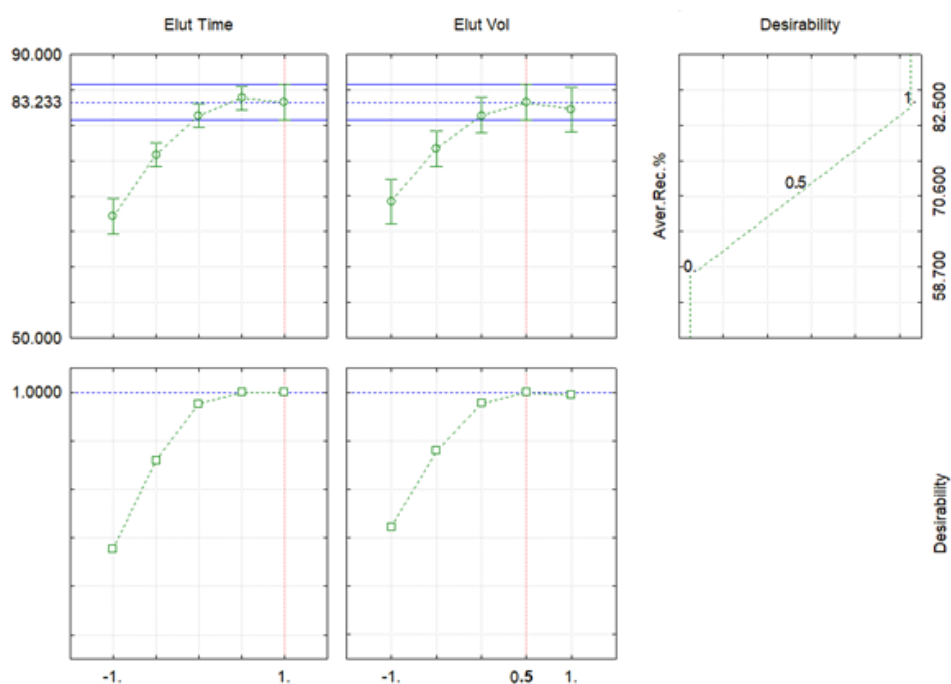


Figure 2.4. Desirability profiles and predict levels (coded values).

The method's LOD and LOQ were determined using a signal-to-noise ratio of three and 10, respectively. LODs ranged between 0.64 to $3.22 \mu\text{g}\cdot\text{L}^{-1}$ (Table 2.3).

2.4.4. Applications in environmental samples

Two wastewater samples from hospital and municipal WWTP effluents and a surface water sample from Pamvotis Lake were investigated to assess the applicability of the proposed method. However, their concentration levels of the target analytes were lower than the established LODs, or antidepressants were absent during this sampling campaign. These water samples were spiked with the selected ADs at $50.0 \mu\text{g}\cdot\text{L}^{-1}$, to confirm the efficiency of the process. A representative chromatogram is shown in Figure 2.5. Relative recoveries in real water samples were estimated from absolute recoveries of the Milli-Q water samples (relative recovery is defined as the % concentration of target analytes recovered from the wastewater and surface water with reference to the concentration found in the spiked Milli-Q water). Depending on the water matrix and the analyte, relative recoveries varied between 69 and 121% (Table 2.4).

Table 2.3. Analytical parameters of Milli-Q water samples (n = 3).

Analyte	LOD $\mu\text{g}\cdot\text{L}^{-1}$	LOQ $\mu\text{g}\cdot\text{L}^{-1}$	Recovery (%)		Intraday		Interday	
					RSD (%)		RSD (%)	
			LOQ	10 × LOQ	LOQ	10 × LOQ	LOQ	10 × LOQ
Citalopram	1.13	3.39	61.94	69.31	2.91	2.40	5.49	3.99
Clozapine	0.64	1.92	70.70	77.50	2.94	2.41	5.40	3.96
Mirtazapine	3.22	10.71	76.34	83.08	6.92	5.87	8.39	12.63
Bupropion	2.05	6.82	71.77	75.70	4.22	4.08	10.79	7.41
Sertraline	1.12	3.36	79.71	98.10	2.38	4.34	4.28	6.76

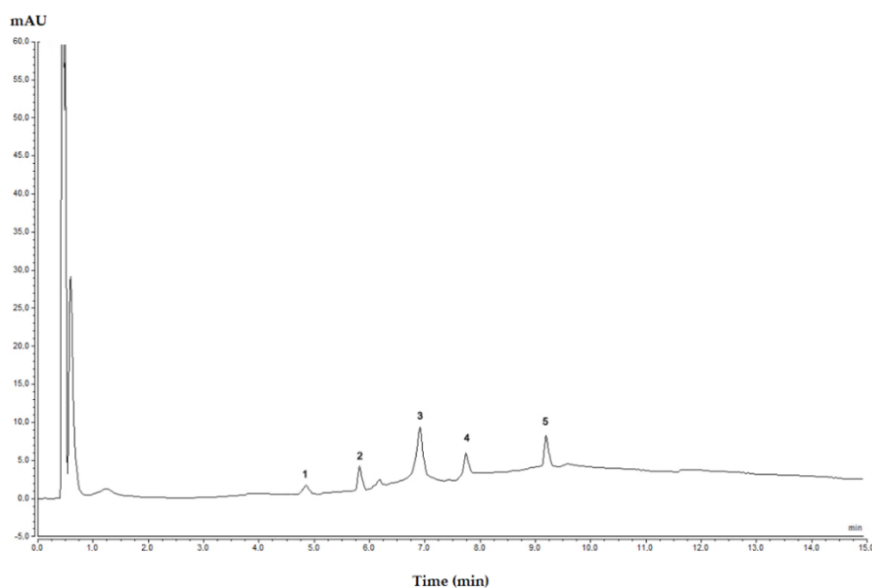


Figure 2.5. A representative chromatogram obtained from Lake water spiked at $50.0 \mu\text{g}\cdot\text{L}^{-1}$, after FPSE procedure coupled with High-Performance Liquid-Chromatography–Photodiode Array Detection (FPSE-HPLC–DAD) (1. MIRT, 2. BUP, 3. CLO, 4. CIT, 5. SERT).

Table 2.4. Analytical parameters of hospital and urban effluents and surface water samples ($n = 3$).

Analyte	Lake Water		Hospital Effluent		Urban Effluent	
	$50.0 \mu\text{g}\cdot\text{L}^{-1}$		$50.0 \mu\text{g}\cdot\text{L}^{-1}$		$50.0 \mu\text{g}\cdot\text{L}^{-1}$	
	Absolute Recovery (%)	Relative Recovery (%)	Absolute Recovery (%)	Relative Recovery (%)	Absolute Recovery (%)	Relative Recovery (%)
Citalopram	65.37	100.57	81.94	116.06	72.92	112.18
Clozapine	74.99	111.36	56.18	86.43	60.04	92.37
Mirtazapine	101.34	104.07	99.01	120.75	107.86	113.34
Bupropion	65.93	93.16	53.46	75.54	49.18	69.49
Sertraline	69.07	107.60	61.22	94.20	56.14	86.38

2.5. Conclusions

The study presented above is the first attempt to introduce the procedure of Fabric Phase Sorptive Extraction to extract and pre-concentrate five ADs contained in aqueous environmental samples. The aim of our study was not to reach the highest sensitivity of the methodology, otherwise different preconcentration factors and more sensitive analytical techniques (ultra-high-performance liquid chromatography coupled to high resolution mass spectrometry, UPLC–HRMS) would have been employed. FPSE proved to be an easy, green and fast analytical method for the determination of the selected psychoactive drugs by employing HPLC-UV-Vis/DAD at concentration levels that may occur in natural aquatic systems ($\mu\text{g}\cdot\text{L}^{-1}$). The most significant variables affecting the efficiency of the process were optimized by employing different experimental configurations. The proposed method is reproducible with good RSDs and acceptable recoveries in Milli-Q and real water samples, respectively. In addition, the method was applied in real water samples (hospital and urban effluents and Pamvotis Lake samples), but no ADs were detected. The future aim of the research team is to investigate different substrate/sorbent combinations in order to produce a FPSE device that would extract a broader number of pharmaceuticals and employ a more sensitive analytical technique (UPLC–HRMS) for their determination.


Acknowledgments

This paper is part of a project that has received funding from the European Union's Horizon 2020 research and innovation programme under the Marie Skłodowska-Curie grant, agreement no. 765860.



Article

Investigating the Utility of Fabric Phase Sorptive Extraction and HPLC-UV-Vis/DAD to Determine Antidepressant Drugs in Environmental Aqueous Samples

Cristina Jiménez-Holgado ¹, Christoforos Chrimatopoulos ¹, Vassilis Stathopoulos ²  and Vasilios Sakkas ^{1,*}

¹ Chemistry Department, University of Ioannina, 45110 Ioannina, Greece; krijimhol@gmail.com (C.J.-H.); xrimatopoulosxris@gmail.com (C.C.)

² General (Core) Department, National and Kapodistrian University of Athens, 34400 Psachna Campus, Evia, Greece; vasta@uoa.gr

* Correspondence: vsakkas@uoi.gr; Tel.: +30-2651008303

Received: 15 May 2020; Accepted: 1 July 2020; Published: 8 July 2020



Supplementary Material

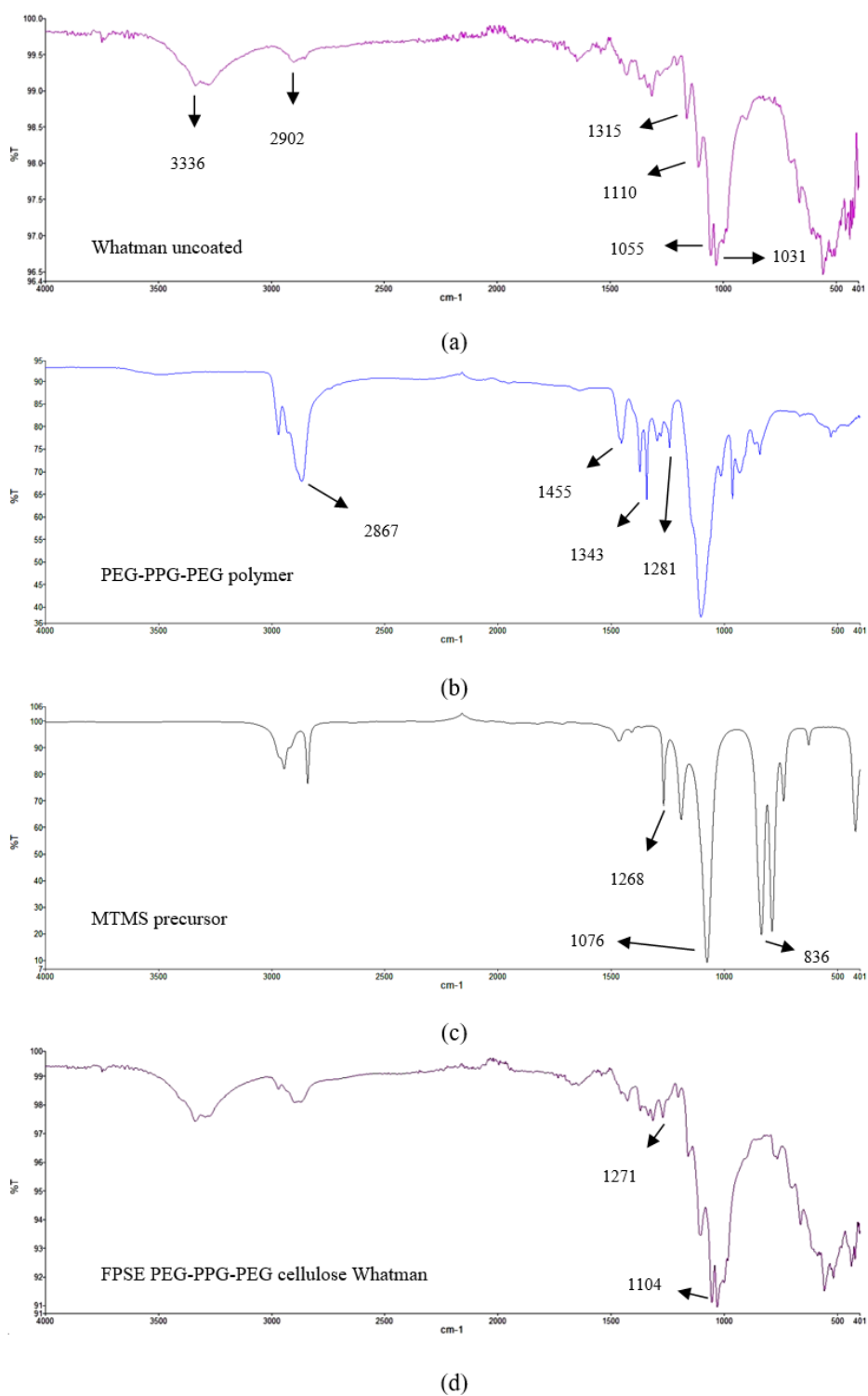


Figure S1. FT-IR spectra of different components in (a) Whatman uncoated material, (b) PEG-PPG-PEG polymer, (c) MTMS precursor and (d) Whatman PEG-PPG-PEG coated media.

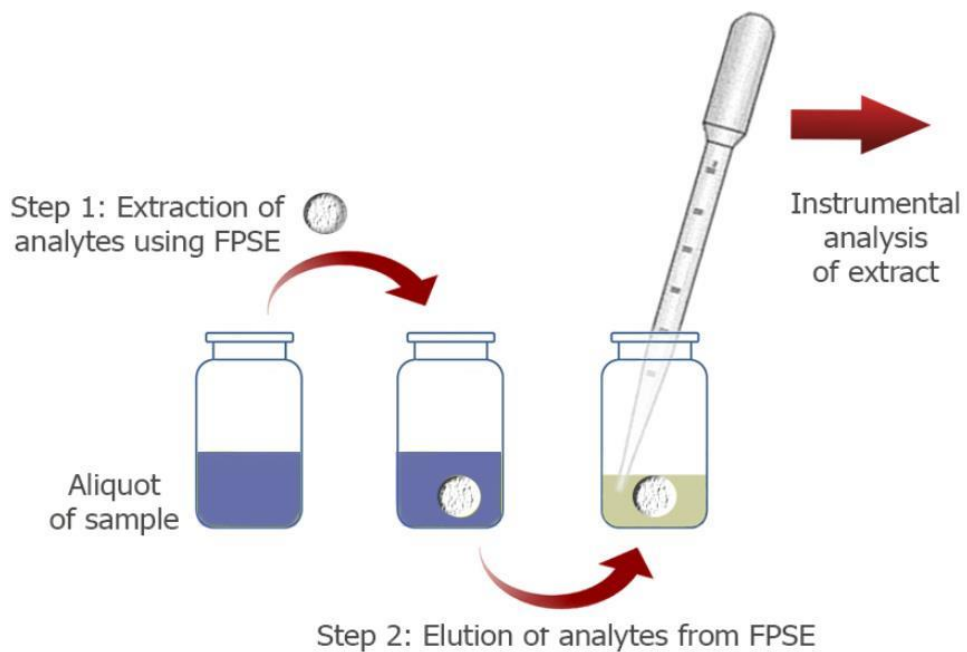


Figure S2. General procedure applied in FPSE extraction.



Figure S3. Different materials in different shapes used in the preliminary experiments for the selection of the optimal FPSE media.

References

1. Vardanyan, R.; Hruby, V.; Vardanyan, R.; Hruby, V. Antidepressants. In *Synthesis of Best-Seller Drugs*, 1st ed.; Academic Press: Tucson, AZ, USA, 2016; pp. 111–143, doi:10.1016/B978-0-12-411492-0.00007-9.
2. Schultz, M.M.; Furlong, E.T.; Kolpin, D.W.; Werner, S.L.; Schoenfuss, H.L.; Barber, L.B.; Blazer, V.S.; Vajda, A.M. Antidepressant pharmaceuticals in two U.S. effluent-impacted streams: Occurrence and fate in water and sediment and selective uptake in fish neural tissue. *Environ. Sci. Technol.* **2010**, *44*, 1918–1925, doi:10.1021/es9022706.
3. Lajeunesse, A.; Smyth, S.A.; Barclay, K.; Sauv e, S.; Gagnon, C. Distribution of antidepressant residues in wastewater and biosolids following different treatment processes by municipal wastewater treatment plants in Canada. *Water Res.* **2012**, *46*, 5600–5612, doi:10.1016/J.WATRES.2012.07.042.
4. Golovko, O.; Kumar, V.; Fedorova, G.; Randak, T.; Grabic, R. Seasonal changes in antibiotics, antidepressants/psychiatric drugs, antihistamines, and lipid regulators in a wastewater treatment plant. *Chemosphere* **2014**, *111*, 418–426, doi:10.1016/J.CHEMOSPHERE.2014.03.132.
5. Matongo, S.; Birungi, G.; Moodley, B.; Ndungu, P.; Occurrence of selected pharmaceuticals in water and sediment of Umgeni River, KwaZulu-Natal, South Africa. *Environ. Sci. Pollut. Res.* **2015**, *22*, 10298–10308, doi:10.1007/s11356-015-4217-0.
6. Moghadam, A.G.; Rajabi, M.; Asghari, A. Efficient and relatively safe emulsification microextraction using a deep eutectic solvent for influential enrichment of trace main antidepressant drugs from complicated samples. *J. Chromatogr. B* **2018**, *1072*, 50–59, doi:10.1016/J.JCHROMB.2017.09.042.
7. Jannesar, R.; Zare, F.; Ghaedi, M.; Daneshfar, A. Dispersion of hydrophobic magnetic nanoparticles using ultrasonic-assisted in combination with coacervative microextraction for the simultaneous preconcentration and determination of tricyclic antidepressant drugs in biological fluids. *UltrasonSonochem* **2016**, *32*, 380–386, doi:10.1016/J.ULTSONCH.2016.04.010.
8. Safari, M.; Shahlaei, M.; Yamini, Y.; Shakorian, M.; Arkan, E. Magnetic framework composite as sorbent for magnetic solid phase extraction coupled with high performance liquid chromatography for simultaneous extraction and determination of tricyclic antidepressants. *Anal. Chim. Acta* **2018**, *1034*, 204–213, doi:10.1016/J.ACA.2018.06.023.
9. Degreef, M.; van Nuijs, A.L.; Maudens, K.E. Validation of a simple, fast liquid chromatography-tandem mass spectrometry method for the simultaneous quantification of

- 40 antidepressant drugs or their metabolites in plasma. *Clin. Chim. Acta* **2018**, *485*, 243–257, doi:10.1016/J.CCA.2018.06.047.
10. Breaud, A.R.; Harlan, R.; Kozak, M.; Clarke, W. A rapid and reliable method for the quantitation of tricyclic antidepressants in serum using HPLC-MS/MS. *Clin. Biochem.* **2009**, *42*, 1300–1307, doi:10.1016/J.CLINBIOCHEM.2009.05.006.
 11. Vaghar-Lahijani, G.; Saber-Tehrani, M.; Aberoomand-Azar, P.; Soleimani, M. Extraction and determination of two antidepressant drugs in human plasma by dispersive liquid–liquid microextraction–HPLC. *J. Anal. Chem.* **2018**, *73*, 145–151, doi:10.1134/S1061934818020144.
 12. Ide, A.H.; Nogueira, J.M.F. New-generation bar adsorptive microextraction (BA μ E) devices for a better eco-user-friendly analytical approach–Application for the determination of antidepressant pharmaceuticals in biological fluids. *J. Pharm. Biomed. Anal.* **2018**, *153*, 126–134, doi:10.1016/J.JPBA.2018.02.001.
 13. Ragab, G.H.; Bahgat, E.A. Development of bioanalytical HPLC method for simultaneous determination of the antialzheimer, donepezil hydrochloride and the antidepressant, citalopram hydrobromide in raw materials, spiked human plasma and tablets dosage form. *Ann. Pharm. Françaises* **2019**, *77*, 112–120, doi:10.1016/J.PHARMA.2018.09.004.
 14. Boumba, V.A.; Rallis, G.; Petrikis, P.; Vougiouklakis, T.; Mavreas, V. Determination of clozapine, and five antidepressants in human plasma, serum and whole blood by gas chromatography–mass spectrometry: A simple tool for clinical and postmortem toxicological analysis. *J. Chromatogr. B* **2016**, *1038*, 43–48, doi:10.1016/J.JCHROMB.2016.10.023.
 15. Chen, X.; Zheng, S.; Le, J.; Qian, Z.; Zhang, R.; Hong, Z.; Chai, Y. Ultrasound-assisted low-density solvent dispersive liquid–liquid microextraction for the simultaneous determination of 12 new antidepressants and 2 antipsychotics in whole blood by gas chromatography–mass spectrometry. *J. Pharm. Biomed. Anal.* **2017**, *142*, 19–27, doi:10.1016/J.JPBA.2017.04.032.
 16. Kamaruzaman, S.; Sanagi, M.M.; Yahaya, N.; Wan Ibrahim, W.A.; Endud, S.; Wan Ibrahim, W.N. Magnetic micro-solid-phase extraction based on magnetite-MCM-41 with gas chromatography–mass spectrometry for the determination of antidepressant drugs in biological fluids. *J. Sep. Sci.* **2017**, *40*, 4222–4233, doi:10.1002/jssc.201700549.
 17. Jagtap, P.K.; Tapadia, K. Pharmacokinetic determination and analysis of nortriptyline based on GC-MS coupled with hollow-fiber drop-to-drop solvent microextraction technique. *Bioanalysis* **2018**, *10*, 143–152, doi:10.4155/bio-2017-0207.
 18. Truta, L.; Castro, A.L.; Tarelho, S.; Costa, P.; Sales, M.G.F.; Teixeira, H.M. Antidepressants detection and quantification in whole blood samples by GC–MS/MS, for forensic purposes. *J. Pharm. Biomed. Anal.* **2016**, *128*, 496–503, doi:10.1016/J.JPBA.2016.06.027.

19. Plenis, A.; BaCzek, T. Modern chromatographic and electrophoretic measurements of antidepressants and their metabolites in biofluids. *Biomed. Chromatogr.* **2011**, *25*, 164–198, doi:10.1002/bmc.1558.
20. Fernández, P.; Taboada, V.; Regenjo, M.; Morales, L.; Alvarez, I.; Carro, A.M.; Lorenzo, R.A. Optimization of ultrasound assisted dispersive liquid-liquid microextraction of six antidepressants in human plasma using experimental design. *J. Pharm. Biomed. Anal.* **2016**, *124*, 189–197, doi:10.1016/J.JPBA.2016.02.041.
21. Rani, S.; Malik, A.K.; Kaur, R.; Kaur, R. A Review for the Analysis of Antidepressant, Antiepileptic and Quinolone Type Drugs in Pharmaceuticals and Environmental Samples. *Crit. Rev. Anal. Chem.* **2016**, *46*, 424–442, doi:10.1080/10408347.2016.1141670.
22. Song, A. Determination of 13 organic toxicants in human blood by liquid-liquid extraction coupling high-performance liquid chromatography tandem mass spectrometry. *Anal. Sci.* **2016**, *32*, 645–652, doi:10.2116/analsci.32.645.
23. Juan, H.; Zhiling, Z.; Huande, L. Simultaneous determination of fluoxetine, citalopram, paroxetine, venlafaxine in plasma by high performance liquid chromatography–electrospray ionization mass spectrometry (HPLC–MS/ESI). *J. Chromatogr. B* **2005**, *820*, 33–39, doi:10.1016/J.JCHROMB.2005.03.006.
24. Zilfidou, E.; Kabir, A.; Furton, K.G.; Samanidou, V. An improved fabric phase sorptive extraction method for the determination of five selected antidepressant drug residues in human blood serum prior to high performance liquid chromatography with diode array detection. *J. Chromatogr. B* **2019**, *1125*, 121720, doi:10.1016/J.JCHROMB.2019.121720.
25. Lioupi, A.; Kabir, A.; Furton, K.G.; Samanidou, V. Fabric phase sorptive extraction for the isolation of five common antidepressants from human urine prior to HPLC-DAD analysis. *J. Chromatogr. B* **2019**, *1118*, 171–179, doi:10.1016/J.JCHROMB.2019.04.045.
26. Kabir, A.; Furton, K.G. Fabric Phase Sorptive Extractors (FPSE). U.S. Patent No. 9,283,544, 15 March 2016.
27. Kabir, A.; Furton, K.G.; Malik, A. Innovations in sol-gel microextraction phases for solvent-free sample preparation in analytical chemistry. *Trends Anal. Chem.* **2013**, *45*, 197–218, doi:10.1016/j.trac.2012.11.014.
28. Aznar, M.; Alfaro, P.; Nerin, C.; Kabir, A.; Furton, K.G. Fabric phase sorptive extraction: An innovative sample preparation approach applied to the analysis of specific migration from food packaging. *Anal. Chim. Acta* **2016**, *936*, 97–107, doi:10.1016/j.aca.2016.06.049.
29. Karageorgou, E.; Manousi, N.; Samanidou, V.; Kabir, A.; Furton, K.G. Fabric phase sorptive extraction for the fast isolation of sulfonamides residues from raw milk followed by high

- performance liquid chromatography with ultraviolet detection. *Food Chem.* **2016**, *196*, 428–436, doi:10.1016/j.foodchem.2015.09.060.
30. Santana-Viera, S.; Guedes-Alonso, R.; Sosa-Ferrera, Z.; Santana-Rodríguez, J.J.; Kabir, A.; Furton, K.G. Optimization and application of fabric phase sorptive extraction coupled to ultra-high performance liquid chromatography tandem mass spectrometry for the determination of cytostatic drug residues in environmental waters. *J. Chromatogr. A* **2017**, *1529*, 39–49, doi:10.1016/j.chroma.2017.10.070.
 31. Kumar, R.; Gaurav; Kabir, A.; Furton, K.G.; Malik, A.K. Development of a fabric phase sorptive extraction with high-performance liquid chromatography and ultraviolet detection method for the analysis of alkyl phenols in environmental samples. *J. Sep. Sci.* **2015**, *38*, 3228–3238, doi:10.1002/jssc.201500464.
 32. Montesdeoca-Esponda, S.; Sosa-Ferrera, Z.; Kabir, A.; Furton, K.G.; Santana-Rodríguez, J.J. Fabric phase sorptive extraction followed by UHPLC-MS/MS for the analysis of benzotriazole UV stabilizers in sewage samples. *Anal. Bioanal. Chem.* **2015**, *407*, 8137–8150, doi:10.1007/s00216-015-8990-x.
 33. Lakade, S.S.; Borrull, F.; Furton, K.G.; Kabir, A.; Marcé, R.M.; Fontanals, N. Dynamic fabric phase sorptive extraction for a group of pharmaceuticals and personal care products from environmental waters. *J. Chromatogr. A* **2016**, *1456*, 19–26, doi:10.1016/J.CHROMA.2016.05.097.
 34. Lakade, S.S.; Borrull, F.; Furton, K.G.; Kabir, A.; Fontanals, N.; Marcé, R.M. Comparative study of different fabric phase sorptive extraction sorbents to determine emerging contaminants from environmental water using liquid chromatography–tandem mass spectrometry. *Talanta* **2015**, *144*, 1342–1351, doi:10.1016/J.TALANTA.2015.08.009.
 35. Luzanin, O.; Movrin, D.; Stathopoulos, V.; Pandis, P.; Radusin, T.; Guduric, V. Impact of processing parameters on tensile strength, in-process crystallinity and mesostructure in FDM-fabricated PLA specimens. *Rapid Prototyp. J.* **2019**, *25*, 1398–1410, doi.org/10.1108/RPJ-12-2018-0316.
 36. Pandis, P.K.; Papaioannou, S.; Koukou, M.K.; Vrachopoulos, M.G.; Stathopoulos, V.N. Differential scanning calorimetry based evaluation of 3D printed PLA for phase change materials encapsulation or as container material of heat storage tanks. *Energy Procedia* **2019**, *161*, 429–437, doi.org/10.1016/j.egypro.2019.02.088.
 37. Kumar, R.; Malik, A.K.; Kabir, A.; Furton, K.G. Efficient analysis of selected estrogens using fabric phase sorptive extraction and high-performance liquid chromatography-fluorescence detection. *J. Chromatogr. A* **2014**, *1359*, 16–25, doi:10.1016/J.CHROMA.2014.07.013.

Chapter 3. Phototransformation of three psychoactive drugs in presence of sedimental water extractable organic matter

In this Chapter, the direct photolytic behaviour of the three target drugs has been studied in three different matrices: in MQ and lake waters and WW samples. For this, samples have been irradiated under natural and artificial solar light. As well, during my secondment at CNRS in France, under the supervision of Prof. Claire Richard, organic matter was isolated from sediments from lake Pamvotis and in the presence of the target analytes were irradiated and the effect on the kinetics of the three compounds was studied. This last part has been already published in *Molecules: "Phototransformation of Three Psychoactive Drugs in Presence of Sedimental Water Extractable Organic Matter"*. It is described below.

3.1. Abstract

Psychoactive drugs are classified as contaminants of emerging concern but there is limited information on their fate in surface waters. Here, we studied the photodegradation of three psychoactive drugs (sertraline, clozapine and citalopram) in the presence of organic matter (WEOM) extracted under mild conditions from sediment of Lake Pamvotis, Greece. Spectral characterization

of WEOM confirmed its humic-like nature. Preliminary experiments using chemical probes showed that WEOM was able to produce oxidant triplet excited state ($^3\text{WEOM}^*$), singlet oxygen ($^1\text{O}_2$) and hydroxyl radicals under irradiation with simulated solar light. Then, WEOM at 5 mgC.L⁻¹ was irradiated in the presence of the three drugs. It enhanced their phototransformation by a factor of 2, 4.2 and 16 for sertraline, clozapine and citalopram, respectively. The drastic inhibiting effect of 2-propanol (5×10^{-3} M) on the reactions demonstrated that hydroxyl radical was the key intermediate responsible for drugs photodegradation. A series of photoproducts were identified by ultra-high-performance liquid chromatography (UHPLC) coupled to high resolution mass spectrometry (HR-MS). The photodegradation of the three drugs proceeded through several pathways, in particular oxidations of the rings with or without O atom inclusion, N elimination, and substitution of the halogen by OH. Formation of halogenated aromatics was observed for sertraline. To conclude, sedimental natural organic matter can significantly phototransform the studied antidepressant drugs and these reactions need to be more investigated. Finally, ecotoxicity was estimated for the three target analytes and their photoproducts, using the Ecological Structure Activity Relationships (ECOSAR) computer program.

3.2. Introduction

Psychoactive drugs are widely used to treat diseases such as depressive symptoms and social anxiety disorder. This is due to the lack of regulation, together with the ignorance of their fate and the absence of effective methods of elimination, these drugs have been classified as contaminants of emerging concern (CECs). The increasing consumption of these compounds in developed countries enhances in fact the risk of environmental contamination and adverse effects on human health and habitats [1]. They enter the aquatic environment mainly through hospital effluents and wastewater treatment plants and, being poorly degradable by traditional biological processes, they are present in relative high amounts in water bodies and sediments. The psychoactive drug sertraline (SER),

citalopram (CIT), and clozapine (CLO) were detected between 13.2 ng L⁻¹ to 15.0 µg L⁻¹ in wastewater treatment plants effluents, 8.9 ng L⁻¹ to 30.0 µg L⁻¹ in fresh waters, and 14.4 to 71.9 ngg⁻¹ in river sediments [2–4]. Once released in the aquatic environment, these compounds can undergo chemical reactions and generate new chemicals, that might also be harmful and therefore need to be identified. Although there is no consistent literature data on the ecotoxicity of these compounds, it has been found that acute and chronic exposure of SER and CIT show effects on algae [5], crustaceans [6–8], bivalves [9,10] and fish [11]. As well, Villain et al. classified these 3 drugs as class 1 toxicity, where metabolites should be analyzed in priority and the ecotoxicity can be estimated with QSAR models [12]. Calza et al. has found that after 20 min of solar light irradiation, SER and its photoproducts, in the presence of TiO₂ display higher acute toxicity potential (based on ECOSAR software) [13]).

The degradation of these psychoactive drugs can be induced by solar light because they absorb solar radiations between 295 and 450 nm (Figure 3.1A). According to the literature data, irradiation with simulated solar light in pure water yielded a half-life of 65 d for CIT [14], 8 h for CLO [4] and between 6 min at pH 12 and > 1 h at pH 5 for SER [15]. The phototransformation of SER and CIT were also reported to be sensitized by the natural organic matter, NOM, present in surface water [13–16]. Indeed, NOM that contains humified light-absorbing compounds can photoinduce the degradation of chemicals through the generation of reactive species such as hydrogen peroxide (H₂O₂) and superoxide radical anion (O₂⁻) [17], ¹O₂ [18,19], oxidant triplet excited state (³NOM*) [20], and hydroxyl radical (HO·) [21–23].

Part of NOM present in the water column of lakes and rivers comes from sediment resolubilization. Sediments are formed by accumulation of deposited particulate organic matter, that undergoes biochemical transformations [24]. Sediment organic matter generally contains a high proportion of humified compounds and can potentially sensitize the photodegradation of aquatic contaminants. The water-soluble sediment organic matter can be

recovered by sampling the sedimental pore water [25], or by extraction from sediment using neutral or slightly alkaline water as described for soils [26].

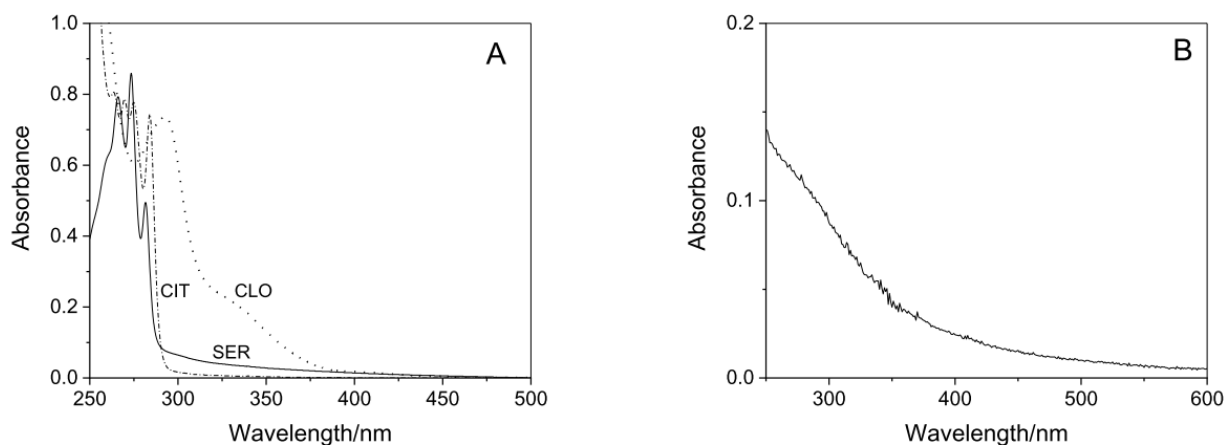


Figure 3.1. UV-vis absorption of sertraline (SER), clozapine (CLO) and citalopram (CIT) at 5 ppm in water at pH 7 (A) and WEOM (18 mgC L⁻¹) at pH 9.2 (B).

In this work, we aimed to better understand the fate of SER, CLO and CIT psychoactive drugs when irradiated in the presence of natural organic matter extracted from the Lake Pamvotis (Ioannina, NW Greece) sediment. The water soluble sedimental organic matter (WEOM), beforehand extracted with water under mild conditions, was first characterized by spectral techniques to confirm its humic-like nature. Then, using the scavenging technique, we investigated its capacity to generate reactive species ($^3\text{WEOM}^*$, $^1\text{O}_2$ and $\text{HO}\cdot$) to finally demonstrate the important role of $\text{HO}\cdot$ in the photodegradation of the three drugs. The drugs photoproducts were identified by means of UHPLC-HR-MS and photodegradation pathways were proposed. A toxicity assessment was followed based on the ECOSAR computer model for the parent molecules and their by-products.

3.3. Materials and methods

3.3.1. Sediment sampling and analysis

Sediment was collected in Lake Pamvotis in Ioannina (Epirus Region, Greece). Lake Pamvotis is a shallow Mediterranean urban lake and it occupies an area of 22.8 km² with a mean depth of 5 m, and is classified among the few European lakes that are sufficiently old to feature native faunas and floras. It is considered as one of the European biodiversity hot spot and is used for different activities such as recreation, tourism, fishing and irrigation. The regional capital Ioannina to the west and the town of Perama to the north are urban settlements fringing the lake, the remaining of its periphery is composed of farmland. In the form of ditches, two major inflows of surface runoff water occur. One of them drains an agricultural watershed mainly, while the second drains a mixed of urban, rural, agricultural and industrial land use watershed. An outflow to the north-west controls the water level for flood prevention. The climate in the region is continental, with cold, wet winters (<0 °C) and hot, dry summers (>30 °C). Annual precipitation (1.1–1.2 m) approximates the evaporation of the lake surface. Sediments were collected in September 2019 close to the lake bank (depth 3–7 cm) using an Eckman type sampler [48] and were air-dried. The samples were then stainless-steel sieved over 2 mm to remove large detritus and benthic organisms. The average particle size of sediment was measured in wet dispersions using a laser diffraction particle size analyzer Malvern Mastersizer 3000 and the percentage of organic matter was obtained by loss-on-ignition (dry combustion between 400 and 500 °C) during 8 h using a high temperature furnace.

3.3.2. Chemicals and preparation of solutions

Clozapine (8-Chloro-11-(4-methyl-1-piperazinyl)-5H-dibenzo[b,e][1,4]-diazepine) was purchased from Sigma-Aldrich (quality level 300). Citalopram (1-[3-(dimethylamino)propyl]-1-(4-fluorophenyl)-3H-2-benzofuran-5-carbonitrile, hydrobromide) and sertraline (1S,4S-4-(3,4-dichlorophenyl)-N-methyl-1,2,3,4-tetrahydronaphthalen-1-amine, hydrochloride) were purchased from TCI Tokyo Chemical Industry (Tokyo, Japan). All these drugs had a purity higher than 98%. 2,4,6-Trimethylphenol (certified reference material), furfuryl alcohol (analytical grade), terephthalic acid

(98%) and hydroxyterephthalate disodium (97%) were purchased from Sigma-Aldrich and used as received. Acetonitrile and methanol for HPLC were from Carlo-Erba and VWR, respectively. The other reagents were of the highest grade available. Water was purified using a reverse osmosis RIOS 5 and Synergy (Millipore) device (resistivity 18 M Ω .cm, DOC < 0.1 mg L⁻¹).

Stock solutions of sertraline (1×10^{-3} M) and citalopram (5×10^{-3} M) were prepared in purified water while those of clozapine (10^{-3} M) in water-acetonitrile (95-5, v/v). Solubilization was achieved after 24 h stirring at 400 rpm. Stock solutions of 2,4,6-trimethylphenol (6.2×10^{-4} M), furfuryl alcohol (10^{-2} M), 2-propanol (2 M), terephthalic acid (10^{-2} M), and hydroxyterephthalate (10^{-3} M) were prepared in purified water and stored in the refrigerator in amber glass bottles before use. When necessary, solutions were buffered at pH 7 using a mixture of KH₂PO₄ and Na₂HPO₄.

3.3.3. Water extractable organic matter extraction

Extraction of WEOM was performed by adding 12 g of sediment in 100 mL of purified water adjusted at pH 9.0–9.5 using NaOH and containing Na₂HPO₄ (6.6×10^{-3} M). Suspensions were placed in 200 mL amber glass screw-capped bottles, degassed in a stream of N₂ during 10 min, closed and stirred during 5 d at 500 rpm at room temperature. After that, the suspensions were filtered using a vacuum filtering flask (Millipore system), first with filters of 5 μ m (5VPP, Durapore membrane filters, Millipore) and then with filters of 0.45 μ m (HA, Nitrocellulose, Millipore). The obtained WEOM aqueous solutions were characterized in terms of dissolved organic carbon (DOC), UV-Vis absorption, and fluorescence. The procedure was repeated 3 times and all the WEOM solutions were pooled.

3.3.4. DOC analyses

A Shimadzu 5050 TOC analyser was used to measure the DOC content of solutions. Measurements were made in triplicate.

3.3.5. Optical analyses

UV-visible analyses of WEOM solutions were conducted on a Varian Cary 3 spectrophotometer in a 1-cm cuvette with purified water as a reference. The absorbances were measured from 250 to 600 nm. The spectral slope (S in nm^{-1}) was calculated between 275 and 295 nm using Equation (1):

$$A_{\lambda} = A_{\lambda_0} \times e^{-S(\lambda-\lambda_0)} \quad (1)$$

where A_{λ} and A_{λ_0} are the absorbances at 295 and 275 nm, respectively [48]. The specific absorption coefficient at 254 nm (SUVA_{254} in $\text{L mg}^{-1} \text{m}^{-1}$) was calculated by dividing the absorbance at 254 nm by the DOC concentration in mg L^{-1} . The ratio $E2/E3$ was calculated by dividing the absorbance at 250 nm by the absorbance at 365 nm, where $E2$ and $E3$ are the absorbance at 250 and 365 nm, respectively. The percentage of aromaticity [49] and the average molecular weight (M_w) of WEOM [50] were estimated following Equations (2) and (3), respectively:

$$\text{percent aromaticity} = 6.52 \times \text{SUVA}_{254} + 3.63 \quad \text{Eq}(2)$$

$$M_w = 0.315 \times e^{(4.96/(-1.72 + E2/E3))} \quad \text{Eq}(3)$$

The three-dimensional fluorescence spectrum was recorded using a Perkin Elmer LS 55 Luminescence Spectrometer fitted with a 1-cm quartz cuvette. The bandwidths were set to 10 nm for excitation and 10 nm for emission. A series of emission scans between 250 and 600 nm were collected over excitation wavelengths between 240 and 450 nm at 10 nm increments. The fluorescence index (FI) was obtained by dividing the emission intensity at 450 nm by the emission intensity at 500 nm for excitation at 370 nm [51] and the biological index (BIX) was calculated as the ratio of emission intensity at 380 nm to 430 nm with excitation at 310 nm [52].

3.3.6. Irradiations

Irradiations were carried out in a device equipped with six fluorescent tubes (Sylvania, F15 W/350BL) emitting polychromatic light between 300 and 500 nm with a maximum at 365 nm (Supplementary Figure S5). Ten mL of solutions were irradiated in a Pyrex glass reactor (14 mm i.d.)

let open to air. Drugs (5×10^{-6} M) were irradiated alone in purified water buffered to pH 7, or in presence of WEOM (5 mgC L^{-1}). Dark control experiments were also performed in order to determine whether adsorption of drugs on WEOM takes place. For this, starting solutions of each drug and WEOM (5 mgC L^{-1}) covered with aluminum foil were kept in the dark and aliquots (5 mL) were withdrawn from the bottles after 1, 2 and 3 h to determine the drug concentration. Probe molecules (2,4,6-trimethylphenol at 5×10^{-6} M, furfuryl alcohol at 10^{-4} and 5×10^{-5} M, or terephthalic acid at 10^{-5} M) were also irradiated alone in pH 7 buffered purified water, or in presence of WEOM (5 mgC L^{-1}). When drugs, or probe molecules were irradiated in the presence of WEOM, the reactants were mixed with vortex during 3 min, poured in the reactor and immediately after lamps were turned on. At given irradiation times, small aliquots were taken for HPLC analyses. These data were used to determine the initial rates of phototransformation. The number of photons received by the 10 mL of solutions in the cylindrical reactor was measured using a radiometer QE65000 from Ocean Optics coupled to chemical actinometry using metamitron [53]. The rate of light absorption of WEOM (5 mgC L^{-1}), R_a^{WEOM} was equal to $(7.2 \pm 0.7) \times 10^{-6} \text{ E s}^{-1}$ (Supplementary Figure S1).

The screen effect of WEOM on drugs was calculated as described in SI-Text 1. All the rates of photodegradation obeyed an apparent first order kinetics, and the apparent first order reaction rate constants (k in s^{-1}) were calculated according to Equation (4):

$$\ln C_t/C_0 = -k \times t \quad (4)$$

where C_t is the concentration of the chemical at the irradiation time t and C_0 is the initial concentration. Irradiations were duplicated.

3.3.7. HPLC Analyses

HPLC analyses were carried out at $25 \text{ }^\circ\text{C}$ on an Alliance (Waters, Milford, MA, USA) apparatus equipped with a photodiode array detector (model 2998), fluorescence detector (model 2475) and

two pumps (Waters 2695). Separation was achieved on a reverse phase Nucleodur, Macherey-Nagel C₈ column (5 μm, 150 mm × 4.6 mm) equipped with a 4/3 pre-column made of the same material. The binary solvent system used was posed of solvent A (100% MeOH) and solvent B (water acidified by 0.03% of H₃PO₄). The best separation of psychoactive drugs was obtained with the following gradient: from 0–20 min, 20% A, then from 20–27 min, 80% A and return to 20% A. The solvent flow was 0.75 mL.min⁻¹ and the volume injection was 25 μL. The eluent was a mixture of 20% MeOH and 80% water acidified with orthophosphoric acid (0.1%) for the experiments with terephthalic acid and furfuryl alcohol while a mobile phase of 50% acetonitrile and 50% acidified water was used for the experiments with 2,4,6-trimethylphenol. Hydroxyterephthalate concentration was measured by fluorescence ($\lambda_{exc} = 320$ nm and $\lambda_{em} = 430$ nm) using a calibration curve (Supplementary Figure S3). Analyses were duplicated.

Psychoactive drugs photoproducts were identified by HRMS performed on an Orbitrap Q-Exactive (Thermo Scientific, Waltham, MA, USA) coupled to an UHPLC Ultimate 3000 RSLC (Thermo Scientific, Waltham, MA, USA) equipped with an Acquity Phenomenex (2.1 mm × 100 mm, 1.7 μm particle size) analytical column (Waters, Milford, MA, USA). The aqueous solvent (A) consisted of a mixture of 0.1% formic acid and the organic phase (B) was acetonitrile. The separation was achieved with a gradient program consisting of 0–7.5 min 5%, 7.5–8.5 min 99% of the mobile phase B. After 8.5 min the gradient was returned to the initial conditions and analytical column was reconditioned for 3.5 min. The flow rate was set to 0.45 mL.min⁻¹. The injection volume was 20 μL. The mass spectrometer operated in the positive and negative (ESI) electrospray ionization mode. The system was controlled by Xcalibur 2.2 (Thermo Fisher Scientific software, Waltham, MA, USA). The spray voltage was 3 kV for the positive and negative mode. For all proposed elemental formula, the error between the measured mass and the exact mass was less than 5 ppm.

3.3.8. Ecotoxicity assessment

The ecotoxicity of the 3 target analytes and their by-products were predicted using ECOSAR program (v 2.0). ECOSAR uses a quantitative structure-activity relationship approach to predict the toxicity of a molecule based on its structure. The relevant endpoints are the acute toxicity, LC50 (concentration of tested compound that is lethal to half of fish and daphnia population after 96 h and 48 h of exposure, respectively) and EC50 (concentration of tested compound that inhibits the growth % of green algae after 96 h of exposure). The chronic toxicity values (ChV) of the drugs and their by-products also were predicted using the same program, for freshwater fish, daphnid and algae as well. Concerning accuracy, a compound is considered more toxic than another if the expected values vary by at least an order of magnitude [54]. The program (v 2.0) is freely available at the website: <https://www.epa.gov/tsca-screening-tools/ecological-structure-activity-relationships-ecosar-predictive-model> (accessed on 1 March 2021).

3.4. Results and discussion

3.4.1. Main characteristics of the sediments

Sediment was analyzed prior to drugs adsorption measurements. The sediment particle size was found to be equal to $100 \pm 10 \mu\text{m}$ and the percentage of organic matter to $1.91 \pm 0.02\%$ of the dry matter. In the literature, the averaged grain size and organic matter content in lake, river and sea sediments vary between silt ($2\text{--}500 \mu\text{m}$) and clay ($<2 \mu\text{m}$) composition, and contain between 0.37–8.0% of organic matter [27]. Lake Pamvotis is a shallow, closed and eutrophic Mediterranean Lake with ecological significance [28,29]. This lake has been shown to exist since the Pleistocene period [30]. In a previous work, the organic matter content in Lake Pamvotis sediments was found to vary between 4.8% and 15.3%, where the lowest content was found in the coarser sandy sediments and the highest in the silt-clay portion [31]. Our sediments showed a grain size larger than that of previous studies, and the organic matter content obtained was therefore lower, in agreement with previous publications [32,33].

3.4.2. Extraction and characterization of WEOM from sediments

By stirring sediment (120 g L^{-1}) in pH 9.2 water during 5 d, we could recover WEOM. The DOC content of the WEOM solution was of 18 mgC/L . WEOM showed the typical UV-visible absorption spectrum of humic-like substances with an exponentially decreasing absorption extending up to 600 nm with a shoulder around 280 nm (Figure 3.1B). SUVA_{254} was equal to 0.44 L./mg m , $\text{S}_{275-295}$ to 0.0105 nm^{-1} and E2/E3 to 3.41. From the SUVA_{254} and E2/E3 values, we could estimate that the percentage of aromaticity was equal to 6.5% and the average Mw to 1.7 kDa. These data that characterize an organic matter moderately aromatic with an overall small molecular weight are in line with those of other sediment organic matters [25,34]. Among main ions detected in Lake Pamvotis, nitrate was the highest concentrated. UHPLC-MS analysis revealed that nitrate ($m/z = 61.9873$ at $\pm 5 \text{ ppm}$) was present in WEOM at a concentration $< 5 \times 10^{-5} \text{ M}$, therefore too low for a significant photochemical effect.

The three-dimensional fluorescence spectrum of WEOM contained peaks A and C, assigned as UVC and UVA humic-like fluorophores, respectively, and peaks T assigned as protein tryptophan-like fluorophores (Figure 3.2) [35]. All these spectral characteristics confirmed the humic-like nature of WEOM. The values of fluorescence indices FI (1.47) and BIX (0.79) that represent the relative contribution of terrestrial and microbial DOM sources and the relative contribution of autochthonous natural organic matter, respectively, indicated that sediments from Lake Pamvotis had a terrestrial contribution, as supported by previous publications [36].

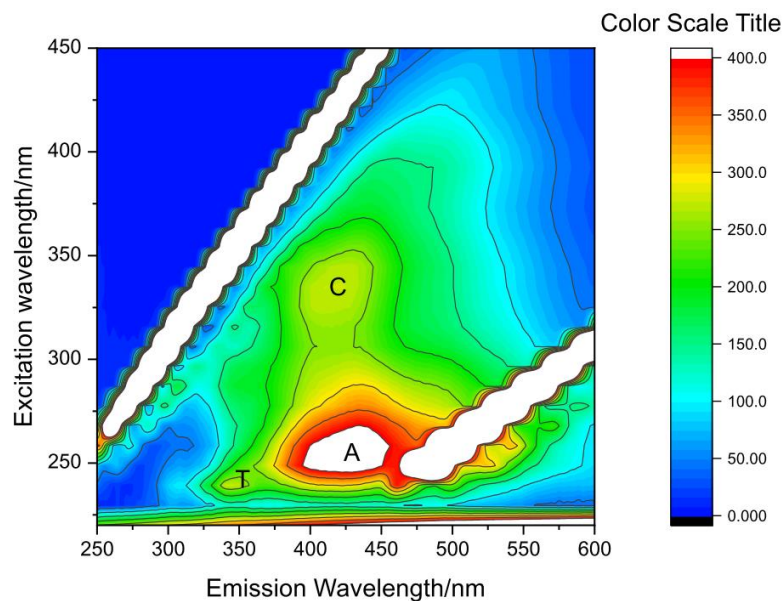


Figure 3.2. Three-dimensional fluorescence spectrum of WEOM (18 mgC L⁻¹) at pH 9.2.

3.4.3. Photoproduction of reactive species upon WEOM irradiation

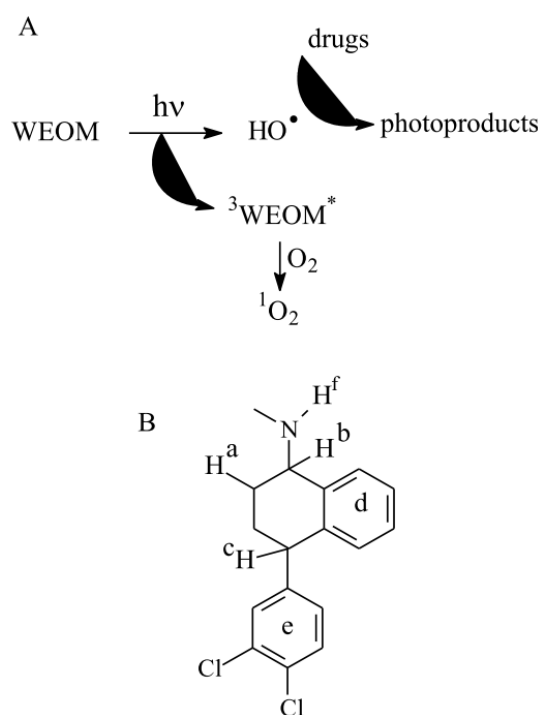
Three chemical probes (2,4,6-trimethylphenol, furfuryl alcohol and terephthalic acid) were used to evidence the production of photooxidants ³WEOM*, ¹O₂ and HO·, respectively [37]. While it is photostable when irradiated alone, 2,4,6-trimethylphenol (5 × 10⁻⁶ M) disappeared in the presence of WEOM (5 mgC L⁻¹) at circumneutral pH in accordance with the formation of ³WEOM* (Supplementary Figure S3). The apparent first order rate constant of reaction *k* was equal to 0.020 ± 0.002 min⁻¹ (Supplementary Figure S1). The quantum yield coefficient of the phenol photodegradation *f*_{TMP} was equal to *k*/*R*_a WEOM, where *R*_a WEOM was the rate of light absorption by WEOM in the reactor. One found *f*_{TMP} = 46 ± 5 M⁻¹, a value falling in the range of those reported for other NOMs [38].

WEOM was also expected to generate ¹O₂ because this species is produced from the deactivation of ³WEOM* by oxygen. The loss of furfuryl alcohol (5 × 10⁻⁵ and 10⁻⁴ M) upon irradiation in the presence of WEOM (5 mgC L⁻¹) confirmed this hypothesis (Supplementary Figure S2). From the *k* value (0.0011 ± 0.0002 min⁻¹), one could estimate the quantum yield of ¹O₂ formation, Φ_{SO}, using

the simplified relationship: $\Phi_{SO} = \alpha_{FFA} \times k \times (\text{Furfuryl alcohol})/R_a^{\text{WEOM}}$, where α_{FFA} is the fraction of $^1\text{O}_2$ scavenged by furfuryl alcohol. Considering that $^1\text{O}_2$ reacts with furfuryl alcohol with a bimolecular rate constant of $1.2 \times 10^8 \text{ M}^{-1}\text{s}^{-1}$ [39] and is deactivated in water with a monomolecular rate constant of $2.5 \times 10^5 \text{ s}^{-1}$ [40], it comes that α_{FFA} was equal to 2.3% and 4.6% by furfuryl alcohol at 5×10^{-5} and 10^{-4} M , respectively. This gives $\Phi_{SO} = 0.055 \pm 0.010$, a value in the upper limit of those reported for aquatic NOMs [19].

We also irradiated terephthalate (10^{-5} M) in the presence of WEOM (5 mgC L^{-1}) at $\text{pH} = 7$. As expected, we observed the formation of the fluorescent hydroxylated photoproduct resulting from the reaction between terephthalic acid and $\text{HO}\cdot$ radicals ($4.4 \times 10^9 \text{ M}^{-1}\text{s}^{-1}$ [41]) (Supplementary Figure S3). Using a calibration curve (Supplementary Figure S3), one could determine that the hydroxylated photoproduct was formed at a rate of $(5.9 \pm 0.6) \times 10^{-11} \text{ M s}^{-1}$ during the first 40 min of the reaction.

Therefore, as for other NOMs of water and soils, WEOM of Lake Pamvotis sediment was able to generate photooxidants under simulated solar light irradiation (Scheme 3.1A).



Scheme 3.1. Reactive species production from WEOM (A) and chemical structure of SER (B).

3.4.4. Irradiation of drugs in the presence of WEOM

The drugs (5×10^{-6} M) were first irradiated in pH 7 buffered purified water to measure their rate of direct photolysis. Plots of $\ln C/C_0$ vs. irradiation time are presented in Figure 3.3A–C. The rate constants deduced from these linear plots ($k_{\text{direct photolysis}}$) were of $(1.6 \pm 0.2) \times 10^{-5}$, $(0.60 \pm 0.03) \times 10^{-5}$ and $(1.3 \pm 0.1) \times 10^{-6} \text{ s}^{-1}$ for SER, CLO and CIT, respectively (Figure 3.3D and Supplementary Table S1). This order of photoreactivity is consistent with the literature data, where SER was reported to be faster photolyzed than the two other drugs [4,14,15].

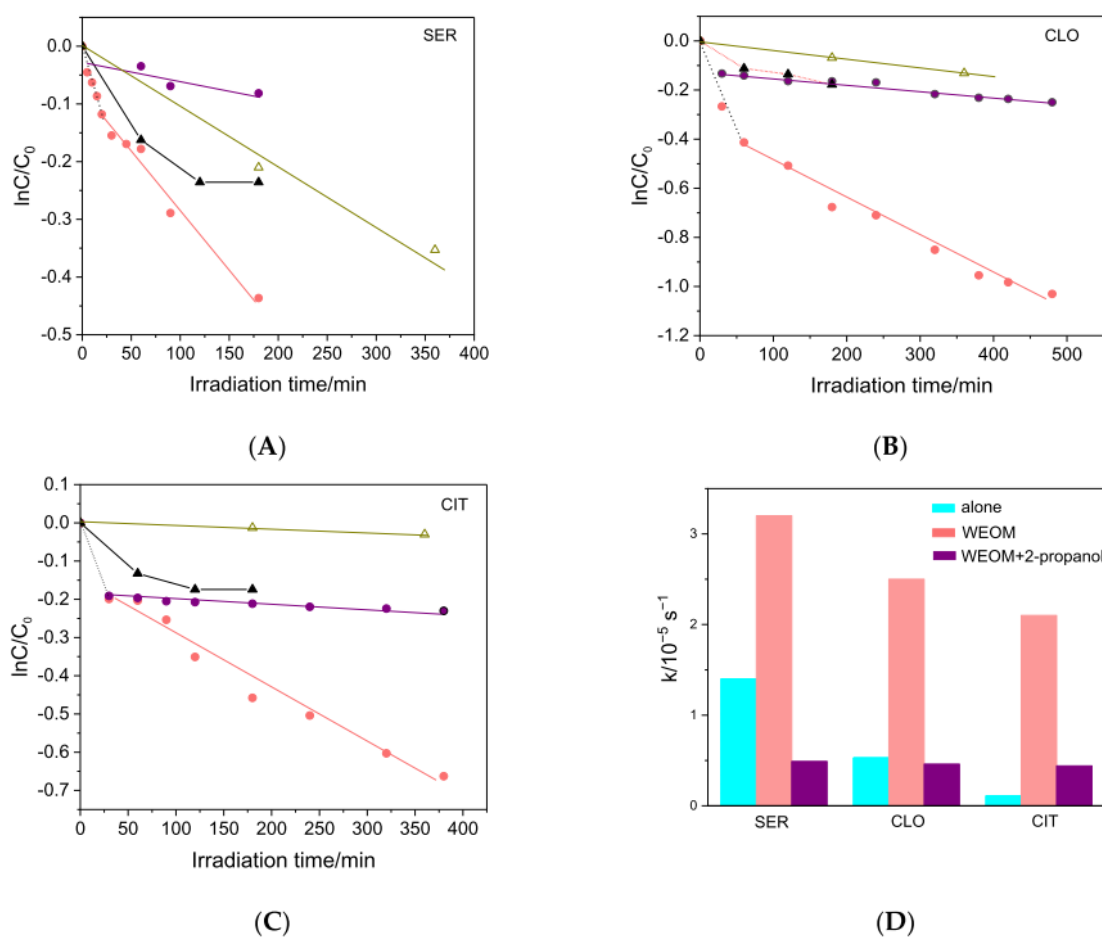


Figure 3.3. Photodegradation of SER (A), CLO (B) and CIT (C) (5×10^{-6} M) in purified water buffered at pH 7 (Δ), in the presence of WEOM (5 mgC L^{-1}) (\bullet) and in the presence of WEOM (5 mgC L^{-1}) and 2-propanol (5×10^{-3} M) (\blacklozenge). Dark control experiments (\blacktriangle). Apparent first order of disappearance of drugs in different conditions (D).

Then, drugs were irradiated in the presence of WEOM (5 mgC L⁻¹) (Figure 3.3A–C). For all of them, the plot of $\ln C/C_0$ vs. irradiation time presented two parts. The slope of the first linear part (between 0 and 20 to 50 min) was higher than that of the second linear part. Such a two-part photodegradation curve was neither observed with 2,4,6-trimethylphenol (Supplementary Figure S1) nor with furfuryl alcohol (Supplementary Figure S2). Dark control experiments revealed that drugs disappeared even in the absence of light—likely by adsorption on the small particles < 0.45 μm present in WEOM solutions filtrated with 0.45 μm filters. Accordingly, the three drugs showed significant adsorption on the sediment (Supplementary Figure S4). Therefore, the first part of the plots was not taken into account for the kinetic study and the rate constants k were extracted from the second part of the plots exclusively.

The k values in the presence of WEOM varied between 2.1 and $3.5 \times 10^{-5} \text{ s}^{-1}$ (Figure 3.3D). In the presence of WEOM, drugs were supposed to disappear by direct photolysis and by WEOM-mediated photodegradation and k was thus equal to:

$$k = k_{\text{direct photolysis}^*} + k_{\text{WEOM}}$$

where $k_{\text{direct photolysis}^*}$ was $k_{\text{direct photolysis}}$ after correction for the screen effect of WEOM (SI, Text 1), and k_{WEOM} is the rate constant due to the sole contribution of WEOM. Values of k_{WEOM} were obtained by subtracting $k_{\text{direct photolysis}^*}$ from k . Values of k_{WEOM} varied within a very narrow range ($1.8\text{--}2.0 \times 10^{-5} \text{ s}^{-1}$) (Supplementary Table S1) in line with an important contribution of HO \cdot radical in the reactions because these radicals show poor specificity and were expected to oxidize the three drugs at the same rate.

To confirm the involvement of HO \cdot radical, drugs were irradiated in the presence of WEOM (5 mgC L⁻¹) and 2-propanol ($5 \times 10^{-3} \text{ M}$) used as an HO \cdot radical quencher ($k_{\text{HO}} = 1.9 \times 10^9 \text{ M}^{-1} \text{ s}^{-1}$ [42]). All the rates of disappearance were drastically reduced (Figure 3.3 A–C) and for each drug the rate constant obtained in the presence of WEOM and 2-propanol ($k_{2\text{-propanol}}$) approached $k_{\text{direct photolysis}^*}$ indicating the very high contribution of HO \cdot radical in the WEOM photosensitized reaction (Figure 3.3D, Supplementary Table S1). In the case of SER, $k_{2\text{-propanol}}$ was even lower than $k_{\text{direct photolysis}^*}$.

3.4.5. Drugs photoproducts

Photoproduct analysis was performed on neutral solutions of drugs (5×10^{-6} M) and WEOM (5 mgC L^{-1}) irradiated for 8 h until drugs conversion between 33% and 69%. UHPLC-MS data are compiled in Tables 3.1–3.3 while main pathways deduced from MS data are given in Figure 3.4.

Table 3.1. HRMS data of the main photoproducts of SER after 8 h of irradiation in the presence of WEOM. Percentage of conversion = 69%

Peak Code	Elemental formula of $[M+H]^+$	m/z	TIC Peak Area	Chemical Modifications vs. SER
SER	$C_{17}H_{18}Cl_2N$	306.0803 308.0771 310.0734		
SER-1 Several peaks	$C_{17}H_{18}Cl_2NO$	322.0753 324.0722 326.0687	3.2×10^8	SER + O fragment M- H_2O
SER-1bis Several peaks	$C_{17}H_{18}Cl_2NO$	322.0753 324.0722 326.0687		
SER-2 Several peaks	$C_{17}H_{18}Cl_2NO_2$	338.0699 340.0670 342.0641	1.7×10^7	SER + 2O FragmentM- H_2O for some of the peaks
SER-3 2 peaks	$C_{17}H_{16}Cl_2N$	304.0647 306.0615 308.0581	4.3×10^7	SER - 2H
SER-4	$C_{16}H_{13}Cl_2O$	291.0330 293.0300 295.0266	9.8×10^7	SER - CH_3NH_2 + O
SER-5 2 peaks	$C_{17}H_{19}ClNO$	288.1146 290.1110	3.7×10^7	SER - Cl + OH
SER-6	$C_{17}H_{20}NO_2$	270.1481	1.8×10^6	SER - 2Cl + OH + OH
SER-7	$C_{16}H_{14}ClO$	257.0721 259.0690	1.8×10^7	SER - CH_3NH_2 + O - Cl+H
SER-8	$C_6H_3Cl_2O$	160.9553 162.9524 164.9495	5.7×10^6	3,4-dichlorophenol
SER-9	$C_7H_3Cl_2O_2$	188.9507 190.9275 192.9279	2.6×10^6	3,4-dichlorobenzoic acid

Table 3.2. HR-MS data of the main photoproducts of CLO after 8 h of irradiation in the presence of WEOM. Percentage of conversion = 44%.

Peak Code	Elemental Formula of [M+H] ⁺	m/z	TIC Peak Area	Chemical Modifications vs. SER
CLO	C ₁₈ H ₂₀ Cl ₂ N ₄	306.0803 308.0771 310.0734	327.1375 329.1341	
CLO-1 Several peaks	C ₁₈ H ₂₀ Cl ₂ N ₄ O	322.0753 324.0722 326.0687	343.1323 345.1291	CLO + O
CLO -2 Several peaks	C ₁₈ H ₂₀ Cl ₂ N ₄ O ₂	338.0699 340.0670 342.0641	359.1273 361.1238	CLO + 2O
CLO -3 2 peaks	C ₁₈ H ₂₀ Cl ₂ N ₄ O ₃	304.0647 306.0615 308.0581	375.1226 377.1193	CLO + 3O
CLO-4	C ₁₇ H ₁₈ ClN ₄	291.0330 293.0300 295.0266	313.1218 315.1186	CLO – CH ₂
CLO-5	C ₁₆ H ₁₈ ClN ₄	288.1146 290.1110	301.1216	CLO – C ₂ H ₂
CLO-6	C ₁₈ H ₂₁ N ₄ O	270.1481	309.1716	CLO – Cl + OH
CLO -7	C ₁₇ H ₁₈ ClN ₄ O	257.0721 259.0690	329.1166 331.1136	CLO– Cl + H - CH ₂
CLO -8	C ₁₇ H ₁₉ N ₄ O ₃	160.9553 162.9524 164.9495	327.1455	CLO – CH ₂ – Cl + OH + 2O
CLO -9	C ₁₈ H ₁₉ N ₄ O ₂	188.9507 190.9275 192.9279	323.1504	CLO – Cl + OH -2H + O

Table 3.3. HR-MS data of the main photoproducts of CIT after 8 h of irradiation in the presence of WEOM. Percentage of conversion = 33%.

Peak Code	Elemental Formula of [M+H] ⁺	m/z	TIC Peak Area	Chemical Modifications vs. SER
CIT	C ₂₀ H ₂₂ ON ₂ F	325.1714		
CIT -1 Several peaks	C ₂₀ H ₂₂ O ₂ N ₂ F	341.1658	1.3 × 10 ⁹	CIT + O Fragment M – H ₂ O
CLO -1 bis Several peaks	C ₂₀ H ₂₂ O ₂ N ₂ F	341.1658		CIT + O
CIT -2	C ₂₀ H ₂₀ O ₂ N ₂ F	339.1506	7.2 × 10 ⁸	CIT – 2H + O
CIT -3	C ₂₀ H ₂₀ O ₃ N ₂ F	355.1456	1.3 × 10 ⁷	CIT – 2H + 2O
CIT -4	C ₁₉ H ₂₀ ON ₂ F	311.1560	2 × 10 ⁷	CIT – CH ₂
CIT -5	C ₂₀ H ₂₃ O ₂ N ₂	323.1757	2.5 × 10 ⁸	CIT – F + OH
CIT -6	C ₂₁₄ H ₁₉₉ ON ₂	231.1492	1 × 10 ⁷	CIT–aromatic ring
CIT -7 Several peaks	C ₁₄ H ₁₇ O ₂ N ₂	245.1287	2.2 × 10 ⁸	CIT – aromatic ring – 2H + O
CIT -8	C ₁₉ H ₂₀ O ₂ N ₂ F	327.1509	2 × 10 ⁸	CIT – CH ₂ + O
CIT -9	C ₁₉ H ₂₀ O ₃ N ₂ F	343.1456	1 × 10 ⁷	CIT – CH ₂ + 2O
CIT -10	C ₁₉ H ₁₉ O ₂ N ₂ F	325.1350	1.2 × 10 ⁸	CIT – CH ₂ – 2H + O
CIT -11	C ₂₀ H ₂₁ O ₄ N ₂	353.1495	8.3 × 10 ⁶	CIT – F – 2H + OH + 2O
CIT -12	C ₂₀ H ₂₁ O ₃ N ₂	337.1546	1.1 × 10 ⁷	CIT – F + OH – 2H
CIT -13	C ₂₀ H ₂₃ O ₃ N ₂	339.1703	1.2 × 10 ⁷	CIT – F + OH + O
CIT -14 Several peaks	C ₁₉ H ₂₁ O ₄ N ₂	341.1491	1 × 10 ⁷	CIT – CH ₂ – F + OH + 2O
CIT -15	C ₁₀ H ₁₉ O ₃ N ₂	323.1393	1.3 × 10 ⁶	CIT – CH ₂ – F + OH – 2H + O

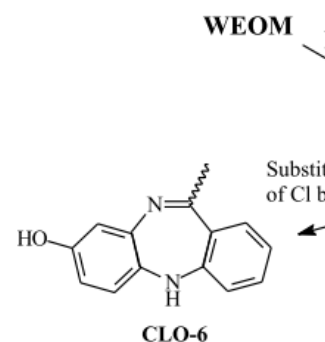
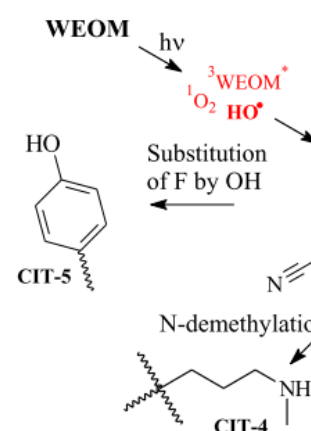
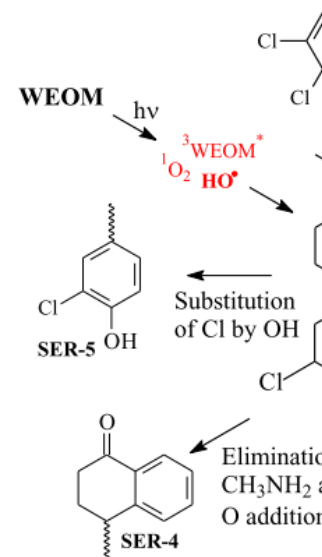


Figure 3.4. Photodegradation pathways.

Most of the peaks were detected in positive mode. Molecular ion clusters at $m/z = 322.0753$, 324.0722 , 326.0687 (SER- and SER-1bis), $m/z = 343.1323$, 345.1291 (CLO-1) and peak at $m/z = 341.1658$ (CIT-1) corresponded all to $[M+O+H]^+$. Double O atom addition was also detected for SER and CLO (SER-2, CLO-2) and even triple O atom addition for CLO (CLO-3).

Molecular ion clusters at $m/z = 304.0647$, 306.0615 , 308.0581 (SER-3) corresponded to $[M-2H+H]^+$ and to the formation of a double bond $C = C$ or $C = N$. Formation of an imine was already proposed [15,16]. In acidic aqueous solution, the imine is expected to be hydrolyzed into the corresponding carbonyl [43]. SER-4 with $m/z=291.0330$, 293.0300 , 295.0266 corresponding to $SER-CH_3NH_2+O$, could therefore be formed in two steps, first oxidation with the imine $RR'C = N-CH_3$ formation, then imine hydrolysis into the carbonyl $RR'C = O$. In the case of CIT, the elimination of 2 H atoms and addition of O was observed (CIT-2) in accordance with a carbonyl formation [44].

Substitution of the halogen atoms, F or Cl, by OH was observed for the three drugs: SER-5 with $m/z = 288.1146$ and 290.1110 , SER-6 with $m/z = 270.1481$ [16], CLO-6 with $m/z = 309.1716$ and CIT-5 with $m/z = 323.1757$. Such nucleophilic substitution was often reported in the photolysis of halogenoaromatics and was already observed for the studied drugs [4,44,45].

Interestingly, analysis in negative mode yielded molecular ion clusters at $m/z = 160.9553$, 162.9524 , 164.9495 (SER-8) and $m/z = 188.9507$, 190.9275 , 192.9279 (SER-9) corresponding to 3,4-dichlorophenol and 3,4-dichlorobenzoic acid, respectively. This result demonstrated that ring detachment took place. The formation of these compounds that show potential toxicity as halogenophenols in general was never reported in the literature to the best of our knowledge. For CIT, the peak at $m/z = 231.1492$ (CIT-6) may also result from the cleavage of the aromatic ring.

CLO and CIT both underwent N-demethylation as demonstrated by the detection of $[M-CH_2+H]^+$ ions (CLO-4 and CIT-4), not observed in the case of SER. This reaction was reported by several authors [2,4,14,44] under various oxidation conditions (UV photolysis, photocatalysis, simulated sunlight irradiation in river water).

Last, in the case of CLO, piperazine ring opening probably took place as shown by the detection of molecular ions cluster at $m/z = 301.1216$ and 303.1184 (CLO-5) corresponding to $[M-C_2H_2+H]^+$. The same compound was observed in the photocatalysis transformation of CLO [4].

Several other photoproducts were found, arising from the combination of the above described pathways, for instance: SER-7 formed after CH_3NH_2 and Cl elimination, CLO-7 after demethylation and dechlorination, and CIT-10 after demethylation and oxidation.

Given the complexity of the drugs structure and the very oxidant properties of $HO\cdot$ radicals, it is highly probable that the attack of drugs by $HO\cdot$ took place on several sites (Scheme 3.1. B). Some of M+O compounds (SER-1 and CIT-1) loose H_2O easily. It is in line with the presence of $CH(OH)-CH_2$ functionalities in the molecule and with the abstraction of H^a , H^b or H^c , leading to the aliphatic ring oxidation. N-demethylation observed for CLO and CIT were likely due to abstraction of methyl H atoms. $HO\cdot$ radicals could also add to the aromatic rings (d and e in Scheme 3.1B) to form phenolic structures at the end [2,15,16]. Lastly, the oxidation of the N atom into N-oxide after abstraction of H^f seems possible [14,44]. The carbon radical produced after H abstraction can either loose a second H atom and yield a double bond or add O_2 to generate a peroxy radical, then an hydroperoxide and further a carbonyl or an alcohol. On the other hand, the addition of $HO\cdot$ on the aromatic ring leads to a ring- $HO\cdot$ adduct and finally to a phenolic compound after abstraction of a ring H-atom elimination. Ring eliminations required the cleavage of a C-C bond and probably involved a complex sequence of processes, the first step of which might have been the abstraction of H^c by $HO\cdot$. (Scheme 3.1B).

3.4.6. Prediction of ecotoxicity assessment

The potential acute (LC50 and EC50) and chronic toxicity (ChV) of the 3 target analytes and their photoproducts were predicted using ECOSAR computer program (version 2.0). Based on the predicted ecotoxicity values, SER, CLO, CIT, and their transformation products (TPs), could be

classified according to the system established by the Globally Harmonized System of Classification and Labelling of Chemicals (GHS) [46] (Table 3.4).

Table 3.4. Toxicity classification according to the Globally Harmonized System of Classification and Labelling of Chemicals (GHS). (United Nations, 2011).

Toxicity range [mg/L]	Class
$LC_{50}/EC_{50}/ChV \leq 1$	Very toxic
$1 > LC_{50}/EC_{50}/ChV \leq 10$	Toxic
$10 > LC_{50}/EC_{50}/ChV \leq 100$	Harmful
$LC_{50}/EC_{50}/ChV > 100$	Not harmful

SER has been found as a moderately toxic compound ($EC = 20 \text{ mg L}^{-1}$) [13]. ECOSAR program predicted that SER and its by-products were very toxic to fish, daphnia and algae, except by-product SER-6, which shows an acute toxicity LC_{50} for fish up to 10.8 mg/L , and is classified as a harmful compound (Table 3.5). SER-3 in particular was even more toxic than SER. This finding supports the previously reported observation that treatment of drugs by irradiation can generate products of greater toxicity than the parent compound [47].

CLO is considered to be a harmful compound, and most of its TPs formed during the degradation process are much less toxic (Table 3.6). No standardized acute or chronic assay was found in the literature for CLO.

In the case of CIT, data at Table 3.7 show that the obtained for the parent molecule for fish was about 4.47 mg L^{-1} , while LC_{50} and EC_{50} were much lower for daphnia and green algae (about 0.652 and 0.360 mg L^{-1} respectively). The same behavior has been observed for SER and CLO (Tables 3.5 and 3.6). In the three cases, the values for chronic toxicity estimated by ECOSAR are lower than those for acute toxicity, suggesting that invertebrates are likely the most sensitive species to these TPs. Based on the predicted ecotoxicity values, SER and its TPs are toxic or very toxic. CIT is

considered as a toxic compound and most of the TPs formed are harmful or not harmful. By contrast, CLO is classified as harmful and most of its by-products formed are not harmful.

Table 3.5. Toxicity predictions for SER and its transformation products using ECOSAR software.

	Acute toxicity [mg/L]			Chronic toxicity (ChV) [mg/L]		
	Fish (LC ₅₀)	Daphnid (LC ₅₀)	Algae (EC ₅₀)	Fish (LC ₅₀)	Daphnid (LC ₅₀)	Algae (EC ₅₀)
SER	0.408	0.071	0.028	0.0074	0.0085	0.012
SER-1	0.887	0.147	0.063	0.019	0.017	0.027
SER-2	1.93	0.301	0.154	0.049	0.032	0.059
SER-3	0.078	0.132	0.00072	0.0018	0.021	0.019
SER-4	0.477	0.357	0.839	0.065	0.075	0.408
SER-5	2.10	0.322	0.162	0.0057	0.034	0.064
SER-6	10.8	1.45	0.942	0.435	0.134	0.341
SER-7	1.59	1.13	2.07	0.201	0.201	0.879
SER-8	6.24	3.88	0.566	0.671	0.489	1.46
SER-9	5.96	3.92	5.31	0.692	0.572	1.92

Table 3.6. Toxicity predictions for CLO and its transformation products using ECOSAR software.

	Acute toxicity [mg/L]			Chronic toxicity (ChV) [mg/L]		
	Fish (LC ₅₀)	Daphnid (LC ₅₀)	Algae (EC ₅₀)	Fish (LC ₅₀)	Daphnid (LC ₅₀)	Algae (EC ₅₀)
CLO	17.7	2.32	1.58	0.764	0.210	0.563
CLO-1	65.2	20.1	6.40	4.58	2.20	8.65
CLO-2	141	15.9	14.6	9.71	1.24	4.67
CLO-3	518	53.1	59.1	47.9	3.76	17.6
CLO-4	23.3	2.98	2.13	1.09	0.263	0.746
CLO-5	26.0	3.29	2.41	1.25	0.287	0.835
CLO-6	155	17.2	16.4	11.3	1.31	5.17
CLO-7	86.0	10.0	8.66	5.38	0.804	2.83
CLO-8	1.65E+3	153	207	206	9.82	57.3
CLO-9	683	67.7	80.5	69.8	4.65	23.4

Table 3.7. Toxicity predictions for CIT and its transformation products using ECOSAR software.

	Acute toxicity [mg/L]			Chronic toxicity (ChV) [mg/L]		
	Fish (LC ₅₀)	Daphnid (LC ₅₀)	Algae (EC ₅₀)	Fish (LC ₅₀)	Daphnid (LC ₅₀)	Algae (EC ₅₀)
CIT	4.47	0.652	0.360	0.140	0.065	0.138
CIT-1	48.0	5.86	4.62	2.60	0.493	1.56
CIT-2	21.3	2.77	1.93	0.954	0.247	0.680
CIT-3	249	26.9	27.0	19.7	2.01	8.35
CIT-4	5.88	0.838	0.486	0.199	0.082	0.183
CIT-5	61.6	7.35	6.06	3.58	0.604	2.01
CIT-6	37.2	4.50	3.62	2.08	0.374	1.21
CIT-7	260	27.2	29.1	22.7	1.97	8.80
CIT-8	56.7	6.81	5.54	3.23	0.564	1.85
CIT-9	330	34.7	36.6	28.0	2.53	11.1
CIT-10	28.1	3.56	2.60	1.36	0.310	0.903
CIT-11	636	63.8	74.1	62.6	4.44	21.7
CIT-12	294	31.2	32.	24.4	2.29	9.88
CIT-13	134	15.1	13.9	9.22	1.17	4.43
CIT-14	918	89.3	110	99.2	6.02	31.6
CIT-15	176	19.4	18.8	13.1	1.48	5.88

3.5. Conclusions

We showed that the water-soluble organic constituents of sediments are able to induce the oxidation of drugs under simulated solar light. The scavenging techniques revealed that hydroxyl radicals were the major contributors of these oxidations even though irradiation of WEOM led to other oxidant species. Thirty-five photoproducts were detected and identified by means of high-resolution mass spectrometry. Some of the proposed degradation pathways are found to be in common with all three drugs (oxidation through O addition or substitution of the halogen by OH), some are shared by only two of them (ring detachment or N-demethylation), while others are specific to a particular drug (de-hydrogenation, N-elimination or ring opening). This study demonstrates that the fate of sertraline, clozapine and citalopram in lakes can be affected by sedimental organic constituents through photodegradation and that many by-products potentially toxic can be formed. Based on ECOSAR software, ecotoxicity assessments showed that toxic and very toxic by-products can be produced for sertraline, while harmful and not harmful TPs could be formed after WEOM mediated photodegradation of citalopram and clozapine.

Acknowledgments: The authors would like to thank Martin Lereboure (Engineer CNRS) and Frédéric Emmenegger (Tech CNRS) for UHPLC-MS analyses and Guillaume Voyard (Engineer CNRS) for assistance in HPLC.



Article

Phototransformation of Three Psychoactive Drugs in Presence of Sedimental Water Extractable Organic Matter

Cristina Jiménez-Holgado ^{1,2}, Vasilios Sakkas ¹ and Claire Richard ^{2,*}

¹ Laboratory of Analytical Chemistry, Department of Chemistry, School of Sciences, University of Ioannina, 45110 Ioannina, Greece; crjimhol@gmail.com (C.J.-H.); vsakkas@uoi.gr (V.S.)

² Institute of Chemistry of Clermont-Ferrand, Université Clermont Auvergne, CNRS, SIGMA-Clermont, ICCF, F-63000 Clermont-Ferrand, France

* Correspondence: claire.richard@uca.fr

Abstract: Psychoactive drugs are classified as contaminants of emerging concern but there is limited information on their fate in surface waters. Here, we studied the photodegradation of three psychoactive drugs (sertraline, clozapine, and citalopram) in the presence of organic matter (WEOM) extracted under mild conditions from sediment of Lake Pamvotis, Greece. Spectral characterization of WEOM confirmed its humic-like nature. Preliminary experiments using chemical probes showed that WEOM was able to produce oxidant triplet excited state (³WEOM*), singlet oxygen (¹O₂), and hydroxyl radicals under irradiation with simulated solar light. Then, WEOM at 5 mgC L⁻¹ was irradiated in the presence of the three drugs. It enhanced their phototransformation by a factor of 2, 4.2, and 16 for sertraline, clozapine, and citalopram, respectively. The drastic inhibiting effect of 2-propanol (5 × 10⁻³ M) on the reactions demonstrated that hydroxyl radical was the key intermediate responsible for drugs photodegradation. A series of photoproducts were identified by ultra-high performance liquid chromatography (UHPLC) coupled to high resolution mass spectrometry (HR-MS). The photodegradation of the three drugs proceeded through several pathways, in particular oxidations of the rings with or without O atom inclusion, N elimination, and substitution of the halogen by OH. The formation of halogenated aromatics was observed for sertraline. To conclude, sedimental natural organic matter can significantly phototransform the studied antidepressant drugs and these reactions need to be more investigated. Finally, ecotoxicity was estimated for the three target analytes and their photoproducts, using the Ecological Structure Activity Relationships (ECOSAR) computer program.

Citation: Jiménez-Holgado, C.; Sakkas, V.; Richard, C. Phototransformation of Three Psychoactive Drugs in Presence of Sedimental Water Extractable Organic Matter. *Molecules* **2021**, *26*, x. <https://doi.org/10.3390/xxxxx>

Academic Editor: Wanhong Ma

Received: 25 March 2021

Accepted: 16 April 2021

Published: date

Keywords: antidepressants; sediment; photodegradation; water extractable organic matter; photoproducts

Supplementary material
Table SI-1. Physicochemical properties of Lake Pamvotis water taken from Kosma et al. (2017).

Parameter	Value
pH	8.5
Conductivity ($\mu\text{S}\cdot\text{cm}^{-1}$)	242
TDS ($\text{mg}\cdot\text{L}^{-1}$)	273
DOC ($\text{mg}\cdot\text{L}^{-1}$)	10.0
NO_3^- ($\text{mg}\cdot\text{L}^{-1}$)	9.50
Br^- ($\text{mg}\cdot\text{L}^{-1}$)	0.483
NO_2^- ($\text{mg}\cdot\text{L}^{-1}$)	0.012
Cl^- ($\text{mg}\cdot\text{L}^{-1}$)	100
HPO_4^{2-} ($\text{mg}\cdot\text{L}^{-1}$)	0.04
NH_4^+ ($\text{mg}\cdot\text{L}^{-1}$)	0.261

TDS: Total Dissolved Solids; DOC: Dissolved Organic Carbon

Kosma, C.I., Lambropoulou, D.A., Albanis, T.A., 2017. Photochemical transformation and wastewater fate and occurrence of omeprazole: HRMS for elucidation of transformation products and target and suspect screening analysis in wastewaters. *Sci. Tot. Environ.*, 590-591, 592-601.

Table SI-2. Rate constants of photodegradation of SER, CLO and CIT in water ($k_{\text{direct photolysis}}$), in the presence of WEOM (k), and in the presence of WEOM+2-propanol ($k_{2\text{-propanol}}$). $k_{\text{direct photolysis}}^*$ corresponds to $k_{\text{direct photolysis}}$ after correction for the screen effect of WEOM.

$k(\text{s}^{-1})$	Sertraline	Clozapine	Citalopram
$k_{\text{direct photolysis}}$	1.6×10^{-5}	0.60×10^{-5}	0.13×10^{-5}
$k_{\text{direct photolysis}}^*$	1.4×10^{-5}	0.53×10^{-5}	0.11×10^{-5}
$k = k_{\text{direct photolysis}} + k_{\text{WEOM}}$	3.2×10^{-5}	2.5×10^{-5}	2.1×10^{-5}
k_{WEOM}	1.8×10^{-5}	2.0×10^{-5}	2.0×10^{-5}
$k_{2\text{-propanol}}$	0.49×10^{-5}	0.46×10^{-5}	0.44×10^{-5}

Text 1. Screen effect calculation

The rate of light absorption by drugs (R_a^d) are calculated using the following Eq. SI-1 when they are alone:

$$R_a^d = \sum_{\lambda=290}^{\lambda=500} I_0^\lambda (1 - 10^{-A^\lambda d}) \quad (\text{SI-1})$$

where I_0^λ is the amount of photons received by the samples for the wavelength range $\lambda - \lambda + 5$ nm and $A^\lambda d$ is the absorbance of the drug solution averaged for the same wavelength range. The rate of light absorption by WEOM (R_a^{WEOM}) is also calculated using Eq. SI-1 by replacing $A^\lambda d$ by $A^\lambda \text{WEOM}$.

In the presence of WEOM, the rate of light absorption by the drugs, R_a^d becomes:

$$R_a^d = \sum_{\lambda=290}^{\lambda=500} \frac{A^\lambda d}{A^\lambda d + A^\lambda \text{WEOM}} I_0^\lambda (1 - 10^{-(A^\lambda d + A^\lambda \text{WEOM})}) \quad (\text{SI-2})$$

The apparent first order reaction rate constants $k_{\text{direct photolysis}^*}$ of drug disappearance in presence of WEOM are therefore equal to:

$$k_{\text{direct photolysis}^*} = k_{\text{direct photolysis}} \times \frac{R_a^d}{I_a^d} \quad (\text{SI-3})$$

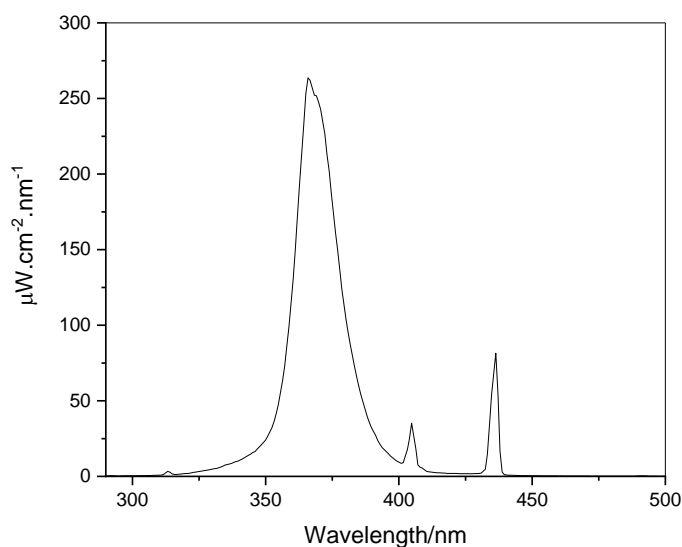


Figure SI-1. Irradiance of the fluorescent tubes.

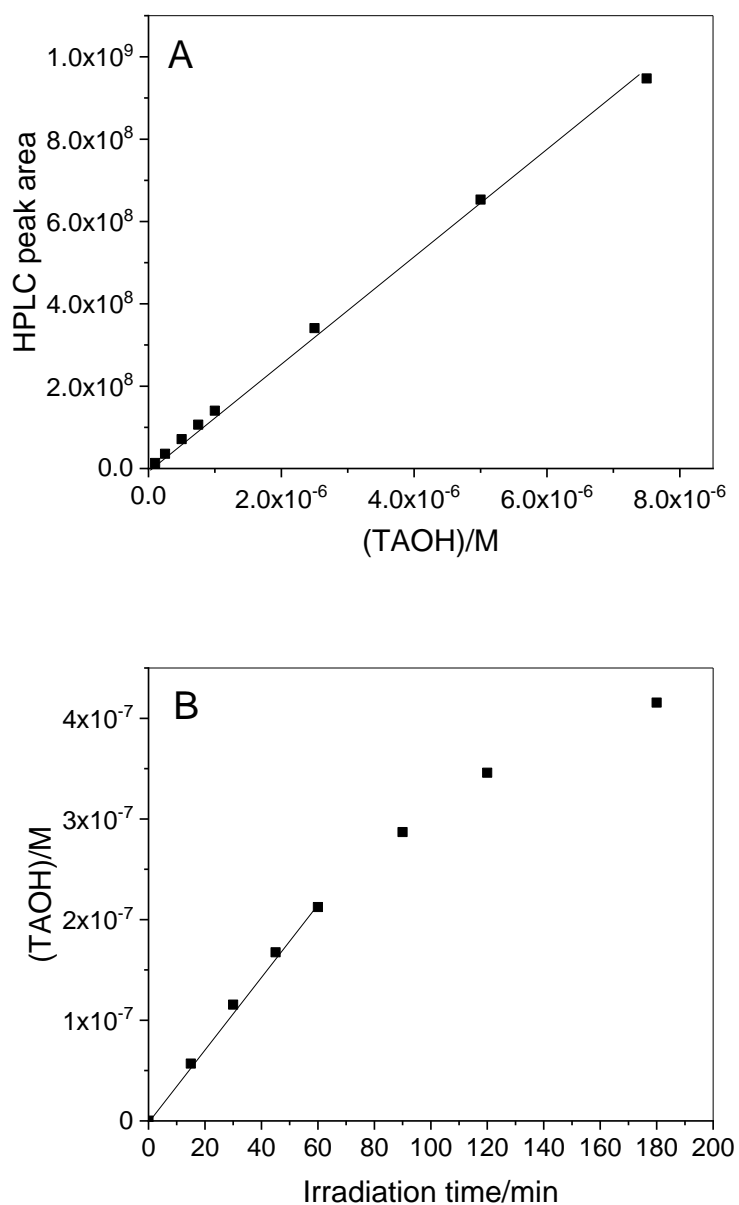


Figure SI-2. Calibration curve of hydroxyterephthalic acid (TAOH) obtained by UHPLC-HRPS analyses (A) and formation profile of TAOH upon irradiation of terephthalate (10^{-5} M) in the presence of WEOM ($5 \text{ mg}\cdot\text{L}^{-1}$) at pH=7 (B). TAOH is formed by reaction of terephthalate with $\text{HO}\cdot$ radicals.

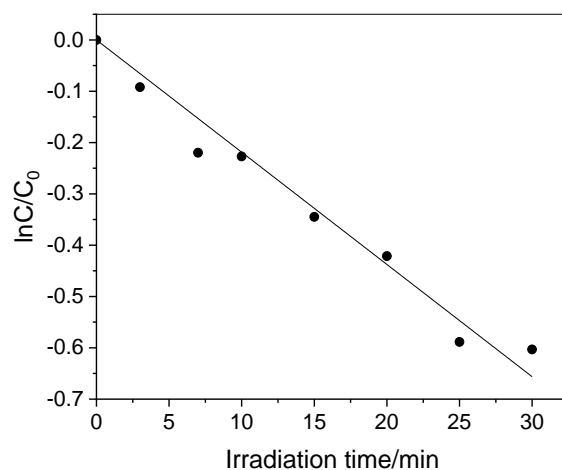


Figure SI-3. Photodegradation of 2,4,6-trimethylphenol (5×10^{-6} M) irradiation in the presence of WEOM ($5 \text{ mg} \cdot \text{L}^{-1}$) at pH=7. The slope corresponding to the apparent first order reaction rate constant is equal to $k=0.020 \pm 0.002 \text{ min}^{-1}$.

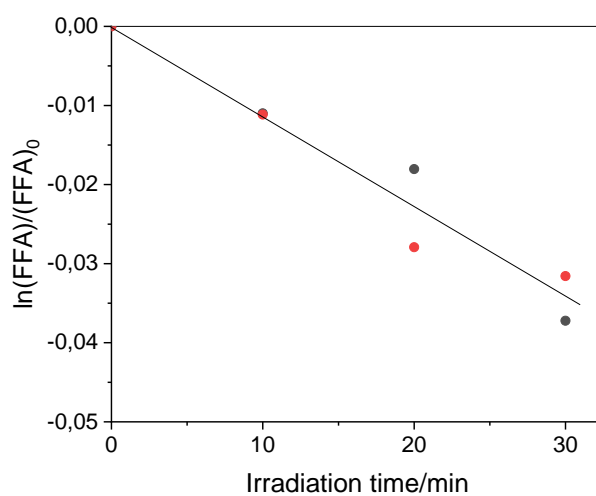
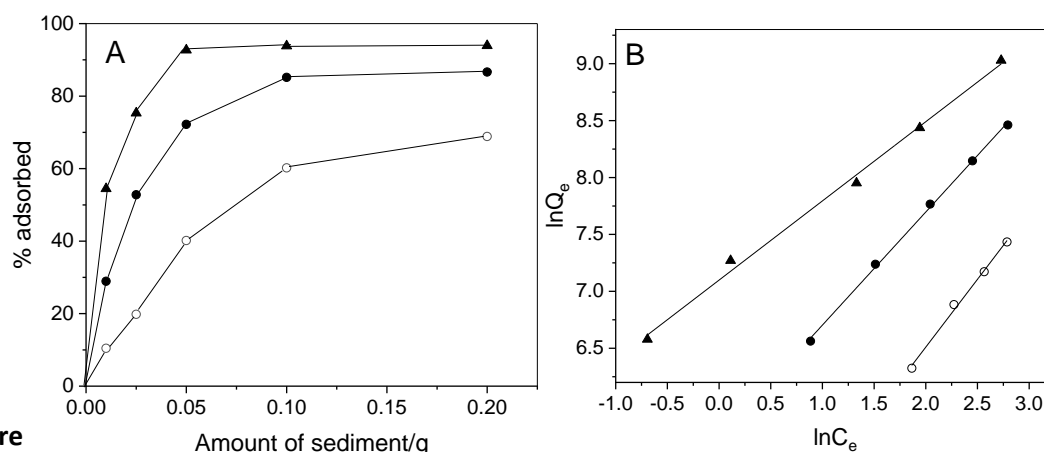


Figure SI-4 Photodegradation of furfuryl alcohol (10^{-4} M and 5×10^{-5} M) upon irradiation in the presence of WEOM ($5 \text{ mg} \cdot \text{L}^{-1}$) at pH=7. The slope corresponding to the apparent first rate constant is equal to $k= -0.0011 \pm 0.002 \text{ min}^{-1}$.


Figure

SI-5: Adsorption of SER (▲), CLO (●), and CIT (○) (0.27-0.29 mg) to sediment. Percentage of adsorbed drug against the amount of sediment in suspension (A) and logarithmic representation of Freundlich equation (B). $K_F = 1210, 302$ and 62 for SER, CLO and CIT, respectively.

Adsorption experiments were performed by adding 2.5, 5, 10, 25, 50, 100 and 500 mg of sediments to 16 ml of purified water and 2 ml of phosphate buffer at pH 7 in 50 ml amber glass screw-capped bottles. The suspensions were stirred at 400 rpm for 30 min. After this equilibrium period, drugs at 10^{-4} or 5×10^{-5} M were added and suspensions were stirred again for 24 h. Then, 1.5 ml of suspensions were sampled, centrifuged during 10 min at 13400 rpm and analyzed by high pressure liquid chromatography (HPLC) to determinate the drug concentrations in water at the equilibrium.

References

- [1] Calisto, V.; Esteves, V. Psychiatric pharmaceuticals in the environment. *Chemosphere* 2009, 77, 1257–1274.
- [2] Skibiński, R.; Trawiński, J.; Komsta, Ł.; Bajda, K. Characterization of forced degradation products of clozapine by LC-DAD/ESI-Q-TOF. *J. Pharm. Biomed. Anal.* 2016, 131, 272–280.
- [3] Trawiński, J.; Skibiński, R. Studies on photodegradation process of psychotropic drugs: A review. *Environ. Sci. Pollut. Res.* 2017, 24, 1152–1199.
- [4] Trawiński, J.; Skibiński, R. Rapid degradation of clozapine by heterogeneous photocatalysis. Comparison with direct photolysis, kinetics, identification of transformation products and scavenger study. *Sci. Total. Environ.* 2019, 665, 557–567.
- [5] Delorenzo, M.; Fleming, J. Individual and mixture effects of selected pharmaceuticals and personal care products on the marine phytoplankton species *Dunaliella tertiolecta*. *Arch. Environ. Contam. Toxicol.* 2008, 54, 203–210.
- [6] Dietrich, S.; Ploessl, F.; Bracher, F.; Laforsch, C. Single and combined toxicity of pharmaceuticals at environmentally relevant concentrations in *Daphnia magna*—A multigenerational study. *Chemosphere*. 2010, 79, 60–66.
- [7] Godoy, A.; de Oliveira, A.; Silva, J.; Azevedo, C.; Domingues, I.; Nogueira, A.; Kummrow, F. Single and mixture toxicity of four pharmaceuticals of environmental concern to aquatic organisms, including a behavioral assessment. *Chemosphere* 2019, 235, 373–382.
- [8] Hossain, M.; Kubec, J.; Guo, W.; Roje, S.; Ložek, F.; Grabicová, K.; Randák, T.; Kouba, A.; Buřič, M. A combination of six psychoactive pharmaceuticals at environmental concentrations alter the locomotory behaviour of clonal marbled crayfish. *Sci. Total. Environ.* 2021, 751, 141383.
- [9] Gonzales-Rey, M.; Mattos, J.; Piazza, C.; Bairy, A.; Bebianno, M. Effects of active pharmaceutical ingredients mixtures in mussel *Mytilus galloprovincialis*. *Aquat. Toxicol.* 2014, 153, 12–26.
- [10] Franzellitti, S.; Buratti, S.; Bowen, D.; Haddad, S.; Chambliss, C.; Brooks, B. A multibiomarker approach to explore interactive effects of propranolol and fluoxetine in marine mussels. *Environ. Pollut.* 2015, 205, 60–69.
- [11] Ding, J.; Lu, G.; Li, Y. Interactive effects of selected pharmaceutical mixtures on bioaccumulation and biochemical status in crucian carp (*Carassius auratus*). *Chemosphere* 2016, 148, 21–31.
- [12] Villain, J.; Minguez, L.; Halm-Lemeille, M.; Durrieu, G.; Bureau, R. Acute toxicities of pharmaceuticals toward green algae. mode of action, biopharmaceutical drug disposition classification system and quantile regression models. *Ecotoxicol. Environ. Saf.* 2016, 124, 337–343.
- [13] Calza, P.; Jiménez-Holgado, C.; Coha, M.; Chrimatopoulos, C.; dal Bello, F.; Medana, C.; Sakkas, V.

- Study of the Photoinduced Transformations of Sertraline in Aqueous Media. *Sci. Tot. Environ.* 2021, 756, 143805.
- [14] Kwon, J.W.; Armbrust, K.L. Degradation of citalopram by simulated sunlight. *Environ. Toxicol. Chem.* 2005, 24, 1618–1623.
- [15] Gornik, T.; Vozic, A.; Heath, E.; Trontelj, J.; Roskar, R.; Zigon, D.; Vione, D.; Kosjek, T. Determination and photodegradation of sertraline residues in aqueous environment. *Environ. Pollut.* 2020, 256, 113431.
- [16] Jakimska, A.; Śliwka Kaszyńska, M.; Nagórski, P.; Kot Wasik, A.; Namieśnik, J. Environmental Fate of Two Psychiatric Drugs, Diazepam and Sertraline: Phototransformation and Investigation of their Photoproducts in Natural Waters. *J. Chromatogr. Sep. Tech.* 2014, 5, 1000253/1–1000253/12.
- [17] Cooper, W.J.; Zika, R.G.; Petasne, R.G.; Plane, J.M. Photochemical formation of hydrogen peroxide in natural waters exposed to sunlight. *Environ. Sci. Technol.* 1988, 22, 1156–1160.
- [18] Zepp, R.G.; Schlotzhauer, P.F.; Sink, R.M. Photosensitized Transformations Involving Electronic Energy Transfer in Natural Waters: Role of Humic Substances. *Environ. Sci. Technol.* 1985, 19, 74–81.
- [19] Peterson, B.M.; McNally, A.M.; Cory, R.M.; Thoemke, J.D.; Cotner, J.B.; McNeill, K. Spatial and temporal distribution of singlet oxygen in Lake Superior. *Environ. Sci. Technol.* 2012, 46, 7222–7229.
- [20] Canonica, S.; Urs, J.; Stemmler, K.; Hoigné, J. Transformation Kinetics of Phenols in Water: Photosensitization. *Environ. Sci. Technol.* 1995, 29, 1822–1831.
- [21] Vaughan, P.P.; Blough, N.V. Photochemical formation of hydroxyl radical by constituents of natural waters. *Environ. Sci. Technol.* 1998, 32, 2947–2953.
- [22] Mopper, K.; Zhou, X. Hydroxyl radical photoproduction in the sea and its potential impact on marine processes. *Science* 1990, 250, 661–664.
- [23] Vione, D.; Minella, M.; Maurino, V.; Minero, C. Indirect photochemistry in sunlit surface waters: Photoinduced production of reactive transient species. *Chem. A Eur. J.* 2014, 20, 10590–10606.
- [24] Koelmans, A.A.; Prevo, L. Production of dissolved organic carbon in aquatic sediment suspensions. *Water Res.* 2003, 37, 2217–2222.
- [25] Chen, M.; Hur, J. Pre-treatments, characteristics, and biogeochemical dynamics of dissolved organic matter in sediments: A review. *Water Res.* 2015, 79, 10–25.
- [26] Nkhili, E.; Boguta, P.; Bejger, R.; Guyot, G.; Sokołowska, Z.; Richard, C. Photosensitizing properties of water-extractable organic matter from soils. *Chemosphere* 2014, 95, 317–323.
- [27] Ritchie, J.C. Organic Matter Content in Sediments of Three Navigation Pools along the Upper

- Mississippi River. *J. Freshw. Ecol.* 1988, 4, 343–349.
- [28] Romero, J.; Kagalou, I.; Imberger, J.; Hela, D.; Kotti, M.; Bartzokas, A.; Albanis, T.; Evmirides, N.; Karkabounas, S.; Papagiannis, J.; et al. Seasonal water quality of shallow and eutrophic Lake Pamvotis, Greece: Implications for restoration. *Hydrobiologia* 2002, 474, 91–105.
- [29] Touka, A.; Vareli, K.; Igglezou, M.; Monokrousos, N.; Alivertis, D.; Halley, J.; Hadjikakou, S.; Frillingos, S.; Sainis, I. Ancient European Lakes: Reservoirs of Hidden Microbial Diversity? The Case of Lake Pamvotis (NW Greece). *Open J. Ecol.* 2008, 8, 537–578.
- [30] Frogley, M.R.; Huw, I.G.; Heaton, T.H.E. Historical Biogeography and Late Quaternary Environmental Change of Lake Pamvotis, Ioannina (North-Western Greece): Evidence from Ostracods. *J. Biogeogr.* 2001, 28, 745–756.
- [31] Daskalou, V.; Polona, V.; Gregor, M.; Constantine, S. Recent Environmental Changes in the Shallow Lake Pamvotis (NW Greece): Evidence from Sedimentary Organic Matter, Hydrocarbons, and Stable Isotopes. *Arch. Environ. Contam. Toxicol.* 2009, 57, 21–31.
- [32] Cole, R.A.; Weigmann, D.L. Relationships among Zoobenthos, Sediments, and Organic Matter in Littoral Zones of Western Lake Erie and Saginaw Bay. *J. Great Lakes Res.* 1983, 9, 568–581.
- [33] Lara, R.J.; Gomez, E.A.; Pucci, A.E. Organic Matter, Sediment Particle Size and Nutrient Distributions in a Sewage Affected Shallow Channel. *Mar. Pollut. Bull.* 1985, 16, 360–364.
- [34] Fu, P.; Wu, F.; Liu, C.Q.; Wei, Z.; Bai, Y.; Liao, H. Spectroscopic characterization and molecular weight distribution of dissolved organic matter in sediment porewaters from Lake Erhai, Southwest China. *Biogeochemistry* 2006, 81, 179–189.
- [35] Coble, P.G. Marine optical biogeochemistry: The chemistry of ocean color. *Chem. Rev.* 2007, 107, 402–418. [CrossRef] 36. Xu, H.; Zou, L.; Guan, D.; Li, W.; Jiang, H. Molecular Weight-Dependent Spectral and Metal Binding Properties of Sediment Dissolved Organic Matter from Different Origins. *Sci. Tot. Environ.* 2019, 665, 828–835.
- [37] Rosario-Ortiz, F.L.; Canonica, S. Probe Compounds to Assess the Photochemical Activity of Dissolved Organic Matter. *Environ. Sci. Technol.* 2016, 50, 12532–12547.
- [38] McKay, G.; Huang, W.; Romera-Castillo, C.; Crouch, J.E.; Rosario-Ortiz, F.L.; Jaffé, R. Predicting Reactive Intermediate Quantum Yields from Dissolved Organic Matter Photolysis Using Optical Properties and Antioxidant Capacity. *Environ. Sci. Technol.* 2017, 51, 5404–5413.
- [39] Haag, W.R.; Hoigné, J.R.; Gassman, E.; Braun, A.M. Singlet oxygen in surface waters Part I: Furfuryl alcohol as a trapping agent. *Chemosphere* 1984, 13, 631–640.
- [40] Wilkinson, F.; Helman, W.P.; Ross, A.B. Rate constants for the decay and reactions of the lowest electronically excited singlet state of molecular oxygen in solution. An expanded and revised compilation. *J. Phys. Chem. Ref. Data* 1995, 24, 663–677.
- [41] Page, S.E.; Arnold, W.A.; McNeill, K. Terephthalate as a probe for photochemically generated

- hydroxyl radical. *J. Environ. Monit.* 2010, 12, 1658–1665.
- [42] Buxton, G.V.; Greenstock, C.L.; Helman, W.P.; Ross, A.B. Critical review of rate constants for reactions of hydrated electrons, hydrogen atoms and hydroxyl radicals in aqueous solution. *J. Phys. Chem. Ref. Data* 1988, 17, 513–886.
- [43] Shen, L.Q.; Beach, E.S.; Xiang, Y.; Tshudy, D.J.; Khanina, N.; Horwitz, C.P.; Bier, M.E.; Collins, T.J. Rapid Biomimetic Degradation in Water of the Persistent Drug Sertraline by TAML Catalysts and Hydrogen Peroxide. *Environ. Sci. Technol.* 2011, 45, 7882–7887.
- [44] Osawa, R.A.; Carvalho, A.P.; Monteiro, O.C.; Oliveira, M.C.; Florêncio, M.H. Transformation products of citalopram: Identification, wastewater analysis and in silico toxicological assessment. *Chemosphere* 2019, 217, 858–868.
- [45] Hörsing, M.; Kosjek, T.; Andersen, H.R.; Heath, E.; Ledin, A. Fate of Citalopram during Water Treatment with O₃, ClO₂, UV and Fenton Oxidation. *Chemosphere* 2012, 89, 129–135.
- [46] United Nations. Globally Harmonized System of Classification and Labelling of Chemical (GHS), 4th ed.; United Nations Publications: New York, NY, USA, 2011.
- [47] Brown, A.; Challis, J.; Wong, C.; Hanson, M. Selective serotonin reuptake inhibitors and β -blocker transformation products may not pose a significant risk of toxicity to aquatic organisms in wastewater effluent-dominated receiving waters. *Integr. Environ. Assess. Manag.* 2015, 11, 618–639.
- [48] Dimitra, G.H.; Lambropoulou, D.A.; Konstantinou, I.K.; Albanis, T.A. Environmental Monitoring and Ecological Risk Assessment for Pesticide Contamination and Effects. in Lake Pamvotis, northwestern Greece. *Environ. Toxicol. Chem.* 2005, 24, 1548–1556.
- [49] Weishaar, J.L.; Aiken, G.R.; Bergamaschi, B.A.; Fram, M.S.; Fujii, R.; Mopper, K. Evaluation of Specific Ultraviolet Absorbance as an Indicator of the Chemical Composition and Reactivity of Dissolved Organic Carbon. *Environ. Sci. Technol.* 2003, 37, 4702–4708.
- [50] Lou, T.; Xie, H. Photochemical Alteration of the Molecular Weight of Dissolved Organic Matter. *Chemosphere* 2006, 65, 2333–2342.
- [51] McKnight, D.M.; Boyer, E.W.; Westerhoff, P.K.; Doran, P.T.; Kulbe, T.; Andersen, D.T. Spectrofluorometric Characterization of Dissolved Organic Matter for Indication of Precursor Organic Material and Aromaticity. *Limnol. Oceanogr.* 2001, 46, 38–48.
- [52] Huguet, A.; Vacher, L.; Relexans, S.; Saubusse, S.; Froidefond, J.M.; Parlanti, E. Properties of Fluorescent Dissolved Organic Matter in the Gironde Estuary. *Org. Geochem.* 2009, 40, 706–719.
- [53] Kouras-Hadef, S.; de Sainte Claire, P.; ter Halle, A.; Amine-Khodja, A.; Richard, C. The Role of Triplet State Keto-Enol Tautomerism in the Photodeamination of Metamitron. *J. Phys. Chem. A* 2011, 115, 14397–14406.

- [54] Mayo-Bean, K.; Moran, K.; Meylan, B. Methodology Document for the ECOlogical Structure-Activity Relationship Model (ECOSAR) Class Program; US-EPA: Washington, DC, USA, 2012

Chapter 4. Exploring the photolytic and photocatalytic transformation of Sertraline: kinetics, degradation mechanism and toxicity assessment

This Chapter describes the photolytic fate of sertraline in different aqueous matrices via direct and indirect pathways. As it was mentioned, although the compounds were degraded faster in environmental waters, still they are stable in the environment, so advance oxidation processes were applied for the abatement of pollution caused by the presence of residual sertraline in waters. This work is already published in Science of the Total Environment: *“Study of the Photoinduced Transformations of Sertraline in Aqueous Media”* and it is described below.

In the same way, Chapters 4 and 5 develop the same concepts but for citalopram and clozapine, respectively. The work on citalopram has been accepted in Molecules: *“Exploring the photolytic and photocatalytic transformation of the antidepressant Citalopram: kinetics, degradation mechanism and toxicity assessment”*. For clozapine, the corresponding publication is now in progress.

4.1. Abstract

In the present study, the photoinduced degradation of the antidepressant drug sertraline under artificial solar radiation was examined. Photolysis was studied under different experimental conditions to explore its photolytic fate in the aqueous environment. Photolytic degradation kinetics were carried out in ultrapure water, wastewater effluent, as well as in the presence of dissolved organic matter (humic acids), bicarbonate and nitrate ions which enabled their assessment on sertraline photo-transformation. The reaction of sertraline with photoactive compounds accelerated sertraline transformation in comparison with direct photolysis. Moreover, TiO₂-mediated photocatalytic degradation of sertraline was investigated, and focus was placed on the identification of by-products. As expected, photocatalysis was extremely effective for sertraline degradation. Photocatalytic degradation proceeded through the formation of forty-four transformation products identified by HPLC-HRMS and after 240 min of irradiation total mineralization was achieved. Microtox bioassay (*Vibrio fischeri*) was employed to assess the ecotoxicity of the photocatalysis-treated solutions and results have indicated that sertraline photo-transformation proceeds through the formation of toxic compounds.

4.2. Introduction

Antidepressants are medications that can help relieve symptoms of depression, social anxiety disorder, anxiety disorders, seasonal affective disorder, and dysthymia, or mild chronic depression, as well as other conditions. As with other emerging pollutants, these compounds enter the aquatic environment mainly through effluents from wastewater treatment plants (WWTPs) and hospitals [1]. The presence and fate of these chemicals in wastewater and receiving waters has attracted the attention from the scientific community.

There is a growing public and scientific concern about the effects on ecosystem and human

health posed by the presence of pharmaceuticals in the environment. Over the last few decades, the fate and occurrence and effects of pharmaceutical compounds, including psychiatric drugs, in the aquatic environment (i.e. drinking water, groundwater, surface water and treated water) was assessed [2-8]. Psychiatric drugs in surface water and waste water have been reported in a wide range of concentration levels from ppt to several ppb over the world [6-8].

Once released in the surface water, they can be subjected to several attenuation processes such as hydrolysis, biodegradation, adsorption and photolysis [9,10]. Photochemical reactions occurring in surface waters, that comprises direct and indirect photolysis, play a key role in their environmental attenuation. In the case of direct photolysis, sunlight absorption by the pollutant triggers its transformation [11]. As far as indirect photochemistry is concerned, sunlight is absorbed by photoactive compounds called photosensitizers [12]. Upon sunlight absorption, these compounds produce reactive transients such as the hydroxyl radical ($\bullet\text{OH}$), singlet oxygen ($^1\text{O}_2$) and CDOM triplet states ($^3\text{CDOM}^*$), which can induce pollutant transformation [13]. Natural water constituents such as nitrates, bicarbonate and especially dissolved organic matter play an important role in the photolytic degradation of organic compounds since they can participate in the production of the above-mentioned reactive species [14]. Therefore, indirect photolysis has been found as an environmentally important elimination way of organic pollutants, including pharmaceutical compounds and personal care products. Accordingly, identifying their effect on sertraline photo-transformation was of interest.

Sertraline occurrence in waste water and surface waters has been reported at concentration levels from 2 ng/L up to few $\mu\text{g/L}$ [15-17].

Low to moderate removal rates (25–48%) of sertraline from WWTPs [18] implicates search for alternative and more effective methods. The exploitation of Advanced Oxidation Processes is among the possible ways for increasing the treatment efficiency. In particular, the use of photocatalysis could be a powerful solution for environmental remediation, and TiO_2 is among the most commonly used and effective metal oxides [19,20].

Considering the fact that sertraline residues have been detected in environmental aquatic systems, firstly the aim of this work was to perform experiments under simulated solar radiation in ultrapure water as a reference (without matrix components) and in an effluent of WWTP to investigate its photolytic fate; to simulate a natural process that occurs in the environment. The effects of natural organic matter, nitrate and bicarbonate ions were also studied. Moreover, AOPs were applied for the abatement of pollution caused by the presence of residual sertraline in waters. Special attention has been given to the assessment of the photocatalytic transformation of sertraline, using mild experimental conditions to identify possible transformation by products evolved and suggest possible degradation pathways. Finally, toxicity assessment was followed based on the bioluminescent bacterium, *Vibrio fischeri* and US EPA ECOSAR computer model.

4.3. Experimental details

4.3.1. Reagents

Antidepressant sertraline (SERT) was purchased from TCI Tokyo Chemical Industry (Tokyo, Japan). The analyte has purity higher than 98%. For analytical purposes sertraline was dissolved in methanol to provide a stock solution containing 1000 mg/L of analyte. The solution was stored in glass-stopped bottles at $-20\text{ }^{\circ}\text{C}$ in the dark. Standard working solutions were prepared, daily. Ultrapure water used was produced by a Milli-Qsystem (Evoqua, Pittsburg, USA). Photosensitizers: humic acid, NaNO_3 and NaHCO_3 were purchased from Sigma-Aldrich (Athens, Greece). Irradiation procedures of sertraline were carried out by experimental solutions that were prepared by dissolving sertraline directly in ultrapure water, ultrapure water+sensitizers, WWTP effluent. The latter was collected from the WWTP of the city of Ioannina in amber glass bottles prerinsed with deionized water. Up on their arrival in the laboratory, were centrifuged (4000 rpm, $25\text{ }^{\circ}\text{C}$, 10 min) and filtered with 0.2- μm polypropylene (PP) filters to eliminate the particulate matter. Wastewater

characterization parameters are given at Table S1.

4.3.2. Irradiation procedures

4.3.2.1. Direct and indirect photolysis

Aqueous solutions of sertraline (1 mg/L, 50 mL) were irradiated under simulated solar conditions using a Suntest CPS+ apparatus from Heraeus (Hanau, Germany) equipped with a Xenon arc lamp (1500 W). The runs were performed adjusting the lamp power to 750 W m^{-2} with a simulated solar emission within 300 to 800 nm. The lamp was equipped with a glass filter that inhibits the transmission of wavelengths under 290 nm. Solutions were irradiated in a 100 mL Pyrex glass UV-reactor with a flat flange lid with three necks. Samples were irradiated under magnetic stirring. A tap-water cooling system was used, for samples to not exceed $25 \text{ }^\circ\text{C}$. Aliquots (0.5mL) were drawn from the photoreactor at specific time intervals.

In order to examine the effect of humic acids (2.5, 5.0, 10 mg/L), nitrate (2.5, 5.0, 10 mg/L) and bicarbonate ions (2.5, 5.0, 10 mg/L), aqueous sertraline solutions (1 mg/L) in ultrapure water (50 mL), were exposed to artificial solar light (Suntest).

The kinetics of reaction is analysed directly from the concentration versus time curves. The first-order equation $C_t = C_0 e^{-kt}$ was applied to determine the rate constant (C_t is sertraline concentration at time t , C_0 is the initial concentration and k is the rate constant).

4.3.2.2. Photocatalytic procedures

Sertraline photocatalytic degradation in ultrapure water was carried out in Pyrex glass cells (2.3 cm height \times 4.0 cm diameter), filled with 5 mL of sertraline (20 mg/L) and TiO_2 (400 mg/L) suspension kept under magnetic stirring. Samples were irradiated for different times using a PHILIPS Cleo 6 \times 15WTL-D Actinic BL with maximum emission wavelength at 365 nm. The UV integrated irradiance on the cells in the 290–400 nm range wavelengths was $90 \pm 2 \text{ Wm}^{-2}$ (measured with a

CO.FO.MEGRA. (Milan, Italy) power-meter). After irradiation, samples were filtered through a 0.45 μm filter and analysed with the proper analytical technique. In all studied photoinduced processes, the decomposition rate of sertraline fitted a pseudo-first kinetics model.

4.3.3. Analytical procedures

Kinetics from direct and indirect photolysis were followed by a Thermo Scientific UltiMate 3000 HPLC system equipped with a diode array detector and Chromeleon Thermo Scientific software. The equipment consists of a Binary Solvent Manager (BSM), a WPS-3000SL autosampler and a column manager all from Waters Thermo Scientific (Waltham, Massachusetts, USA). The injection volume into the chromatographic equipment was 20 μL , and the analytical column was a Hypersil GOLD 150 \times 4.6 mm, with a particle size of 5 μm (Thermo Scientific, Waltham, Massachusetts, USA) operating at 25 $^{\circ}\text{C}$. The mobile phase consists of methanol (A) and water with 0.3% phosphoric acid (B), at 1.0 mL/min flow in gradient mode. The gradient starts at 15:85 (A:B) (v/v) and is increasing in 3 min to 50% methanol. The percentage of methanol further increased up to 80% in 7 min and the gradient returned in 2 min to the first state 15:85 (equilibrium time 3 min). The whole chromatographic separation process finished in 15 min. The UV detector was set at 245nm.

The degradation of sertraline and the identification of its transformation products (TPs) in ultrapure water was followed using an Ultimate 3000 High Pressure Liquid Chromatography coupled through an ESI source to an LTQ-orbitrap mass spectrometer (Thermo Scientific, Bremen, Germany). The chromatographic separation was achieved with a reverse phase C18 column (Gemini NX C18, 150 \times 2 mm, 3 μm , 110 \AA ; Phenomenex, Castel Maggiore, BO, Italy) using 5 mM aqueous heptafluorobutanoic acid (eluent A) and acetonitrile (eluent B). Gradient separation ramp started with 5% B, increased up to 40% B in 18 min and to 100% in 5 min; then the column came back to the initial conditions.

The LC mobile phase was delivered to ESI ion source using nitrogen both as sheath and

auxiliary gas. Source parameters were set as followed: sheath gas 30 arbitrary unit (arb), auxiliary gas 25 arb, capillary voltage 4.0 kV and capillary temperature 275 °C. Full mass spectra were acquired in positive ion mode in the m/z range between 50 and 500, with a resolution of 30 k. MSn spectra were acquired in the range between ion trap cut-off and precursor ion m/z values. Precursor ions were focused in a window of 3 Da width, for supposed chlorinated species the width was extended to 5 Da. Mass accuracy of recorded ions (versus calculated) was ± 0.001 u (without internal calibration).

As described by Zhu et al. (2006) the photocatalysis degradation processes that characterize the photodegradation operation brought to a customized list of the main unknown m/z values of the hypothetical transformation products derived from sertraline [21]. The customized list of suspected TPs was prepared using Xcalibur software (Xcalibur 4.1). In particular we searched for the following “known-unknowns” derivatives: mono-hydroxylated (322 m/z), di-hydroxylated (338 m/z), tri-hydroxylated (354 m/z), oxidized (304 m/z), oxidized/mono-hydroxylated (320 m/z), oxidized/di-hydroxylated (336 m/z), oxidized/tri-hydroxylated (352 m/z), dechlorinated (272 m/z), dechlorinated/mono-hydroxylated (288 m/z). By Xcalibur software additional non-target analytes were identified after manual inspection of the chromatograms (“unknown unknowns” based on signal/noise value). Three technical replicates for each time point was performed. Isotope ratio was manually checked in the case of supposed chlorinated species, using isotopic pattern simulator of Xcalibur software. $M+2$ and $M+4$ ion intensity of the hypothesized molecules was confirmed within $\pm 10\%$ of relative values.

Total organic carbon (TOC) was measured using a Shimadzu TOC-5000 analyzer (catalytic oxidation on Pt at 680 °C). The calibration was performed using standards of potassium phthalate.

Inorganic ions formed during sertraline degradation were identified by ion chromatography analysis using a Dionex chromatograph equipped with a Dionex 40 ED pump and Dionex 40 ED conductimetric detector. For chloride, nitrate and nitrite anions, a Dionex Ion Pac AS9- HC 4 × 250 mm column, and Ion Pac ASRS-ULTRA 4 mm conductivity suppressor was applied. Ammonium was analyzed using a Dionex Ion Pac CS12A 4 × 250mm column, and Ion Pac CSRS-ULTRA 4mm

conductivity suppressor, using 9 mM Na₂CO₃ as eluent at 1 mL/min.

4.3.4. Toxicity

The acute toxicity of sertraline and its transformation products in ultrapure water in the presence of TiO₂ (400mg/ L) was evaluated using a Microtox Model 500 toxicity analyzer (Milan, Italy). The analysis was performed evaluating the bioluminescence inhibition assay in the marine bacterium *Vibrio fischeri* by monitoring changes in the natural emission of the luminescent bacteria. Freeze-dried bacteria, reconstitution solution, diluent (2% NaCl) and an adjustment solution (non-toxic 22% sodium chloride) were obtained from Azur (Milan, Italy). Samples were tested in a medium containing 2% sodium chloride, and the luminescence was recorded after 5, 15 and 30min of incubation at 15 °C. The luminescence inhibition percentage was determined by comparing with a non-toxic control. Moreover, the acute toxicity of SER and its transformation products to three aquatic organisms was assessed employing the ECOSAR model v2.0. The chronic toxicity concentrations for these organisms were also calculated using ECOSAR [22,23].

4.4. Results and discussion

4.4.1. Photolytic degradation

Direct photolysis of sertraline in ultrapure water and in WWTP effluent under artificial solar irradiation, followed a first order kinetics (Figure 4.1). Sertraline photolysis at the effluent of WWTP is greater than ultrapure water showing a strong dependence on the constitution of the irradiated media. To be more specific, when sertraline was irradiated in ultrapure water, a half-life ($t_{1/2}$) of 57h was found. However, when sertraline was irradiated at different aqueous matrix (effluent of WWTP) the rate constant increased almost 40%, ($t_{1/2}$ decreased to 34 h, Table 4.1). There are several parameters that may affect the photodegradation process: radiation source, presence of organic and inorganic substances, pH etc. Jakimska et al. (n.d.) have conducted photolytic degradation

experiments of sertraline at the same concentration level (1mg/L) in a variety of experimental conditions employing natural solar irradiation as well as xenon lamp [24]. Pseudo-first order degradation kinetics were followed, and sertraline photolysis was faster in natural waters in comparison to ultrapure water attributed to autocatalytic reactions [24]. However, there were no solid conclusions with regards to the effects of different water matrices. It is well documented in the literature that natural water constituents such as dissolved organic matter, nitrates, and bicarbonates are significant participants in the photochemical degradation of organic microcontaminants in surface waters. Studies have shown that DOM can promote or inhibit the photolysis of organic pollutants [13]. The promotion mechanism is mainly through indirect photolysis processes such as photosensitized oxidation reaction. This behaviour has been reported also for other antidepressants such as clozapine [25]. Inhibition mechanism is mainly embodied in the abundant conjugated chromophore structure in DOM, which may be related to the photo-shielding effect of organic pollutants competing to absorb light and the quenching effect of DOM on the excited state of pollutants. In addition, the presence of bicarbonate or nitrate ions hastens the photoinduced reactions thanks to the production of reactive oxygen species (ROS) [14]. Therefore, in our study to investigate their reactivity on the photodegradation of sertraline, experiments were carried out in ultrapure water and different environmentally realistic concentrations of humic acids, nitrate, and bicarbonate ions.

Figure 4.1 depicts the degradation curves of the antidepressant in different irradiation conditions specified at Table 4.1. Our data clearly demonstrate that humic acids (HA) greatly increase the rate of sertraline photo-transformation ($t_{1/2} = 7$ h, when HA = 10 mg/L). HA can promote sertraline photolysis, by acting as a photosensitizer through the generation of $\bullet\text{OH}$ and O_2 [26,27], suggesting that natural organic matter (NOM) would affect the photolytic process, particularly at high concentrations. Recently, Gornik et al. (2019), investigated the phototransformation of sertraline (at 0.01 and 1mg/L, 125 W medium pressure mercury lamp) under laboratory scale measurements in different matrices chosen based on the requirements of the modelling software APEX (Aqueous

Photochemistry of Environmentally-occurring Xenobiotics) [28]. Results have shown that photodegradation is pH dependent, resulting in fastest degradation at the alkaline pH, as observed in our study (ultrapure water vs WWT effluent). Moreover, in agreement with our findings, the presence of photosensitizers such as dissolved organic matter, nitrate and carbonate/bicarbonate ions accelerated the photolysis reaction rate in comparison to ultrapure water [28].

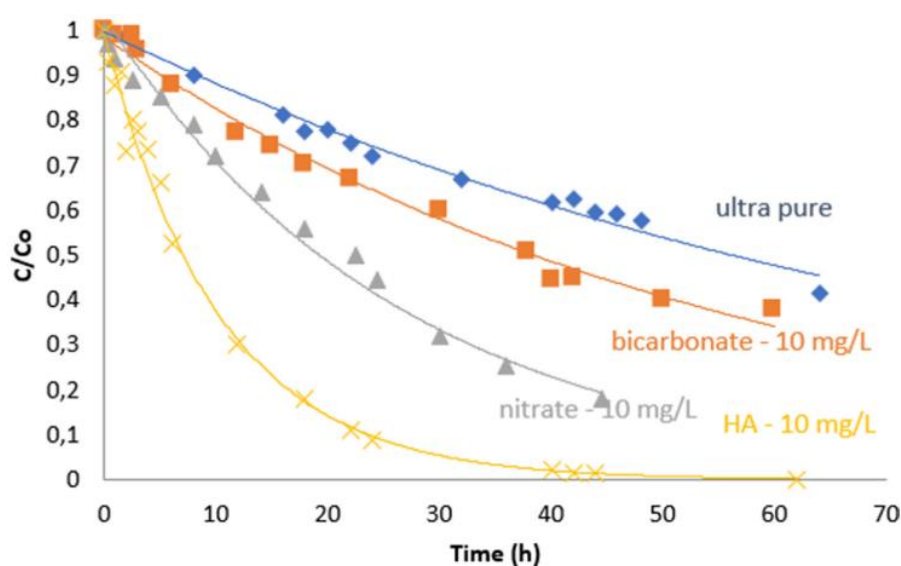


Figure 4.1. Kinetics of sertraline in direct and indirect photolysis.

The degradation rates in the presence of OH radicals produced by nitrate photolysis, was higher compared to ultrapure water (Table 4.1). Increased concentrations of NO_3^- from 2.5 to 10 mg/L have a positive effect on the photodegradation rate, with $t_{1/2}$ comprising between 35 and 18 h. Considering the effect of carbonate radicals that were produced in the presence of different bicarbonate concentrations (2.5–10 mg/L, and 1 mg/L of nitrate), results have demonstrated that carbonate radicals enhance the degradation of sertraline although to a much lesser extent compared to organic matter and nitrate. Even if studies have shown that sertraline is affected by irradiation, and undergoes direct/indirect degradation, it does not mean that the contamination problem is solved since photo-transformation products formed can be more toxic than the parent molecules

[27]. The effectiveness of the photodegradation efficiency could be dramatically increased by employing AOPs [29-32].

Table 4.1. Degradation kinetic parameters of sertraline in different aqueous media under artificial solar irradiation.

		R^2	k (h^{-1})	$t_{1/2}$ (h)
Ultrapure water		0.9767	0.012	58
WWTP		0.9968	0.0203	34
HA(mg/L)	2.5	0.9889	0.0193	36
	5	0.9855	0.0313	22
	10	0.9984	0.0978	7
NaNO ₃ (mg/L)	2.5	0.9762	0.0198	35
	5	0.9907	0.0242	29
	10	0.9823	0.0380	18
NaHCO ₃ ^a (mg/L)	2.5	0.9867	0.0126	55
	5	0.9735	0.0141	49
	10	0.9850	0.0180	39

^a Nitrate 1 mg/L was present to assist on CO₃^{·-} production

4.4.2. Photocatalytic performance

The introduction of the TiO₂ as photocatalyst [29-31] strongly enhanced the process, and after 1 h of irradiation, both parent molecule and its TPs were mineralized.

As regards the mineralization process, after only 1 h of irradiation, the TOC was <5% of the initial organic carbon (Figure4.2). Chlorine atoms are released faster than nitrogen and they reach the stoichiometric amount within 1 h of irradiation. Nitrogen is mainly released as ammonium [30,32] and it reaches the stoichiometric amount after 1 h of irradiation, when ammonium accounts for almost 75% and nitrate 25% of the stoichiometric amount. Although pharmaceuticals found in the outlet of municipal WWTPs may not require immediate attention regarding their removal, treatment-at- source may still be a plausible option replacing conventional chlorination by an AOP

induced disinfection/oxidation technique [32].

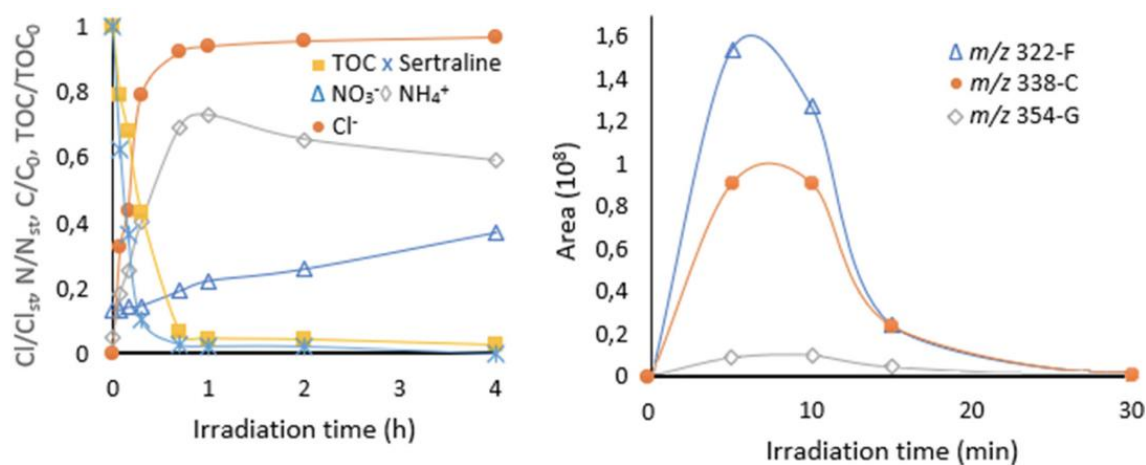


Figure 4.2. Sertraline disappearance, TOC decrease and ammonium, nitrate, and chloride ions release (left) and some TPs (right) in the presence of TiO_2 .

Our findings suggest that consideration of advanced treatment strategies like photocatalysis may overcome the limitations of primary and secondary treatment processes to eliminate sertraline residues in wastewater. Moreover, the attention should also be given to the potential that removal of these drugs following AOPs could lead to the evolution of by-products that would need to be identified, quantified and evaluated for their biological activity [18]. For this reason, all samples were analyzed via HPLC coupled with high-resolution mass spectrometry (Orbitrap) with an electrospray ionization source in positive ion mode for the identification of sertraline transformation products. The photocatalytic process used for the abatement of sertraline leads to the formation of forty-four transformation products, as can be observed all of them are completely abated in 40–60 min. Figure 4.3 depicts a representative LC-HRMS chromatogram showing main TPs formation at 5 min of photocatalytic degradation.

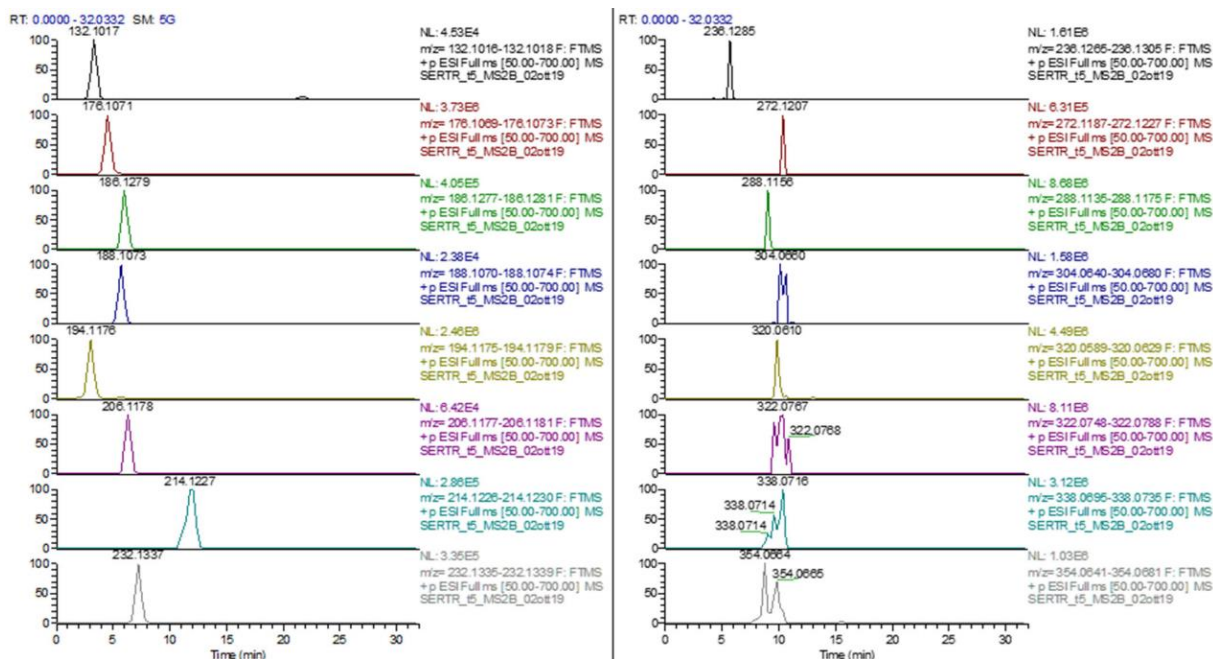


Figure 4.3. LC-HRMS chromatogram showing main TPs formation at 5 min of photocatalytic degradation. On peaks top, m/z values are displayed.

4.4.3. Structural elucidation of the transformation products

The accurate mass for all transformation products (TP) was established, so allowing to obtain their empirical formulae and are collected in Table 4.2. MS^2 and MS^3 spectra analysis permits to assign a tentative structure for most of the transformation products; all MS^n fragments are reported in Tables S2-S10 as Supplementary Information, while MS^2 spectra and the proposed fragmentation pathways are shown in Figs. S1–S23.

A level of confidence recommended by Schymanski et al. (2014) was assigned to each TP and is reported in Table 4.2 as well. Aiming at TPs structural elucidation, the sertraline fragmentation pathway was firstly investigated by MS^n experiments, ascertaining the most likely losses from the protonated molecule ($[M+H]^+$ 306.0820). MS^2 spectrum presents the structural diagnostic ion at 275.0395 m/z that involves the detachment of methylamine from the tetrahydronaphthalene moiety (Table S2 and Figure S1). MS^3 shows two peculiar fragments at 129.0697 m/z, due to the detachment

of dichlorobenzene with the formation of the protonated dihydronaphtalene and 158.9756 m/z, resulting from the formation of the very stable dichlorotropylium cation, in agreement in literature data [17].

Among the identified TPs, many of them are in the form of several isobaric species and their formation involves mono and polihydroxylation, oxidation, dehydration, dechlorination, cleavage of the molecule with the partial or total release of the dichlorophenyl moiety; their structural elucidation is presented below because of the reaction involved in their formation. All the identified TPs are collected in Fig 4.4 and, based on the evolution profiles shown in Figs. S24 and S25, tentative transformation routes are proposed.

Table 4.2. Sertraline and its transformation products formed during the photocatalytic process.

[M + H ⁺]	Empirical formula	Δm_{mu}	DBE	RT (min)	Confidence level
306.0820 (sertraline)	C ₁₇ H ₁₈ NCl ₂		9	13.10	L1
132.1017	C ₆ H ₁₄ O ₂ N	-0.205	1	2.89	L3
176.1071	C ₁₁ H ₁₄ ON	0.109	6	3.55	L2b
186.1279	C ₁₃ H ₁₆ N	0.174	7	5.59	L2b
188.1072	C ₁₂ H ₁₄ ON	0.209	7	13.58	L2b
194.1177	C ₁₁ H ₁₆ O ₂ N	0.145	5	2.89	L2b
206.1179	C ₁₂ H ₁₆ O ₂ N	0.345	6	5.97	L3
214.1228	C ₁₄ H ₁₆ ON	0.159	8	13.98	L3
232.1337	C ₁₄ H ₁₈ O ₂ N	0.495	7	7.42	L2b
236.1285	C ₁₃ H ₁₈ O ₃ N	0.380	6	5.14	L3
272.1207 (A, B)	C ₁₇ H ₁₉ NCl	0.646	9	12.20	L2b
288.1155 (A, B)	C ₁₇ H ₁₉ ONCl	0.532	9	10.34–10.84	L2b
304.0660	C ₁₇ H ₁₆ NCl ₂	0.010	10	11.88	L2b
320.0609 (A, B)	C ₁₇ H ₁₆ ONCl ₂	0.554	10	11.47	L2b, L2b
322.0768 (A, B, C, D, E, F)	C ¹⁷ H ¹⁸ ONCl ₂	0.255	9	11.00 - 11.25 - 11.80- 12.03 - 12.44 - 12.99	L3-L3-L2b-L2b- L2b-L3
338.0715 (A, B, C, D, E)	C ₁₇ H ₁₈ O ₂ NCl ₂	0,589	9	10.28 - 10.56 - 11.14- 11.68 - 12.39	L3-L3-L3-L2b-L3
352.0507	C ₁₇ H ₁₆ O ₃ NCl ₂	0.525	10	11.79	L2
354.0661 (A, B, C, D, E, F, G, H, I, L)	C ₁₇ H ₁₈ O ₃ NCl ₂	0,275	9	9.12 - 9.90 - 10.32- 10.50 - 10.89 - 11.19- 11.52 - 11.93 - 12.25 - 16.67	L3-L-L3-L3-L3-L3- L3-L3-L3-L2b

4.4.3.1. Hydroxylated compounds

We detected six species at m/z 322.0768, five at m/z 338.0715 and ten at m/z 354.0661, matched with formulae corresponding to the monohydroxy, dihydroxy and trihydroxysertraline, respectively. They are among the most abundant TPs, are quickly formed, reached the maxima amount after 5 min, and then completely disappear in 20 min of irradiation (see Figure S24). Monohydroxylation was already recognized to occur via biodegradation [17] and phototransformation [24] with the formation of two isomers, while we identified several bihydroxy and trihydroxysertraline isomers for the first time. The loss of unmodified methylamine was detected in their MS^2 spectra; therefore, a hydroxylation on the methylamine moiety can be excluded for all of them. No additional data useful to assign the OH position was available (see Tables S2–S4).

Analyzing monohydroxysertraline, isomers C, D and E share the fragment at m/z 129.0697 implying the detachment of the hydroxydichlorophenyl group; thus, based on their retention times, the three isomers bear the hydroxyl group on C2 (E), C5 (C) and C6 (D) of the phenyl ring (see Figs. S2 and S3-top). Conversely, isomers A, B and F display two product ions at m/z 145.0646 and 158.9756 in MS^3 spectrum, well-matched with the hydroxylation on the tetrahydronaphthyl moiety. Even if it was not possible to definitely elucidate their structures, for isomer B the loss of a molecule of water in MS^2 spectrum allows to place the OH group in the tetrahydro ring, while for isomers A and F hydroxylation occurs on the aromatic ring (see Figure S3, bottom).

Considering dihydroxy sertraline, isomer B bears both hydroxylations on the dichlorophenyl moiety as assessed by the formation of the ion at m/z 129.0697 in MS^3 spectrum, while isomer A produced the ions at m/z 145.0646 and 174.9712, consistent with one hydroxylation on the dichlorophenyl moiety and the other one on tetrahydronaphthalene.

Isomers C, D and E produce the ion at m/z 158.9756, coherent with the presence of both OH groups on the tetrahydronaphthalene unit; the formation of the complementary ion at m/z 161.0597 further supports this assumption (see Figure S4). For isomer D the structural diagnostic loss of hydrogen peroxide (34.0062 Da) in MS^2 spectrum allows to locate the two OH groups on C2 and C3

(see Figure S5). Isomer E bears the loss of a molecule of water MS^2 spectrum, thus signifying the presence of a hydroxy group in the tetrahydro ring. The fragment at m/z 158.9756 in MS^3 spectrum evidenced that the dichlorophenyl ring was not subjected to hydroxylation and, being the less polar isomer, we can tentatively postulate a hydroxylation on C2 prone to form a hydrogen bond with the amino group. In the case of isomer C, the absence of water losses suggests the presence of both OH groups on the aromatic moiety.

Regarding the trihydroxylated species, for isomer L the structural diagnostic ion at m/z 129.0697 permits to postulate that tri-hydroxylation took place on the free positions on the dichlorophenyl ring. For the other isobaric species, the available information is not enough for a definite structure elucidation but allows some considerations (see Figure S6 and S7). The absence of water losses for isomers A–D, F and G permits to state that the hydroxylation occurring on tetrahydronaphthalene involved the aromatic portion. Additionally, for isomers C, D and F the ion at m/z 161.0597 is well-matched with the presence of two of the three OH groups on the dichlorophenyl moiety, while for isomers A, B and G the formation of the ion at 145.0646 m/z in MS^3 lets to place there only one OH group.

Conversely, isomers E, H and I hold the tri-hydroxylation on the tetrahydronaphthalene moiety as assessed by the formation of the ion at m/z 177.0546; the loss of a molecule of water in MS^2 spectrum advises that one of them is on the tetrahydro moiety and the other two on the aromatic portion.

Four TPs involved the formation of double bond(s) and are collected in Table S5 and Figs. S9–12. TP with $[M+H]^+$ 304.0660 and empirical formula $C_{17}H_{16}NCl_2$ is attributed to sertraline with a double bond; the loss of methylenamine (29.0266 Da) allows to place it on the methylamine moiety, in agreement with literature data [24]).

Two TPs at m/z 320.0609 were detected and derived from one of the aforementioned monohydroxylated species. They practically coeluted and are distinguishable only by MS^n . Because of different fragmentation pathways these species are not the same of 320 m/z species identified by

Gornik et al. (2020). Isomer B holds the double bond in the methyl- amine moiety, as assessed by the loss of methylenamine, and the hydroxyl group on the dichlorophenyl moiety, justified by the formation of the ions at m/z 129.0697 and 174.9712 in MS^3 spectrum; it reasonably comes from the reduction of 322 (C, D or E). Isomer 320 A produces in MS^2 spectrum the neutral loss of 47.0372 Da attributed to methanolamine (see Figure S11), reliable with the hydroxylation on the methylamine and a double bond formed in the tetrahydro ring.

TP at m/z 352.0507 was detected for the first time; it yields the double bond on the methylamine moiety owing to the loss of methylenamine. The formation of the ion at m/z 158.9756 allows locating the three hydroxyl groups on the tetrahydronaphthalene moiety; the loss of hydrogen peroxide in MS^3 spectrum (ions at m/z 289.0182) attested that the two OH groups are on C2 and C3 and the third one on the aromatic moiety (Figure S12).

4.4.3.2. Dechlorinated compounds

We detected four de-chlorinated TPs quickly formed with a maximum evolution achieved in 5 min and a complete disappearance after 30 min of irradiation (see Figure S24) collected in Table S6. Two of them involved a reductive dechlorination with the removal of one chlorine atom and the formation of two isobaric species at m/z 272.1207 (see Figure S13), in agreement with literature data [14]. We also detected two TPs at m/z 288.1155 formed through the replacement of a chlorine atom by an OH group. The formation of the cation chlorohydroxytropolium at m/z 141.0100 confirms the proposed structure (see Figure S14).

4.4.3.3. Compounds at lower molecular weight

We identified nine TPs at lower molecular weight, whose formation involved the molecule breakage and occurred slower (maximum at 10 min of irradiation, see Figure S24).

TPs with $[M + H]^+$ 176.1071 and 194.1177 are formed via the detachment of the dichlorophenyl ring followed by mono (or di)hydroxylation. TP at m/z 176 is one of the main TPs, already recognized via biotransformation [14]. Its MS^2 spectrum evidenced the loss of methylamine and of a molecule of water, suggesting a hydroxylation on the tetrahydro ring (see Table S7 and Figure S15). TP at m/z 194.1177 was detected for the first time and, again, the loss of hydrogen peroxide with the formation of the fragment at m/z 160.1121 argues in favor of the two OH groups on C2 and C3 and to link its formation to the rupture of TP 338-D (Figure S16).

Finally, we detected for the first time six TPs at $[M+ H]^+$ 186.1279, 188.1072, 236.1285, 206.117, 214.1228 and 232.1337 that involved a partial detachment of dichlorophenyl ring (see Tables S8–S10 for their MS^n ions). TPs 214 and 232 are abundant and easily formed, while TPs 186, 188, 236 and 206 are among the less abundant by-products and their formation is delayed.

TPs with $[M+ H]^+$ 236.1285 and 206.1179 and empirical formula $C_{13}H_{18}O_3N$ and $C_{12}H_{16}O_2N$ hold a carboxylic group. The former exhibits the loss of two molecules of water (fragments at m/z 218.1179 and 200.1073), the joint losses of water and methylamine (m/z 187.0756) and of methylamine and formic acid (m/z 159.0804) (Figure S17), while the latter involved the loss of methylamine (ion at m/z 175.0755) and formic acid as well (m/z 129.0697) (Figure S18).

The species with $[M + H]^+$ 214.1228 and 232.1337 result from a partially oxidized chain. The proposed structures are shown in Figs. S19–20 and are justified by the joint loss of CO and methylamine, with the formation of the ion at m/z 155.0855. The absence of other losses could be the result of the highly stable ion formed. Furthermore, for TP at m/z 232.1337 the loss of a molecule of water is consistent with the hydroxylation on the tetrahydro ring.

A species at $[M+H]^+188.1072$ is formed from TP 232 through a demethylation and the detachment of CO. It forms the fragment at m/z 160.0757 via the loss of a molecule of ethylene and at m/z 131.0583 through the ring opening via the loss of C_2H_3NO and ethylene (see Figure S21). Considering m/z 186.1279, it comes from TP 214 via CO loss. MS^2 spectrum shows the loss of ethylene (ion at m/z 158.0695), so we can postulate the structure shown in Figure 4.4.

Lastly, TP at m/z 132.1017 exhibits a linear structure, is one of the most abundant TPs and its formation is delayed, as assessed in Figure S25. MS² spectrum forms the ion at m/z 86.0960 through the loss of formic acid, well matched with the proposed structure (see Figures 4.4 and S23).

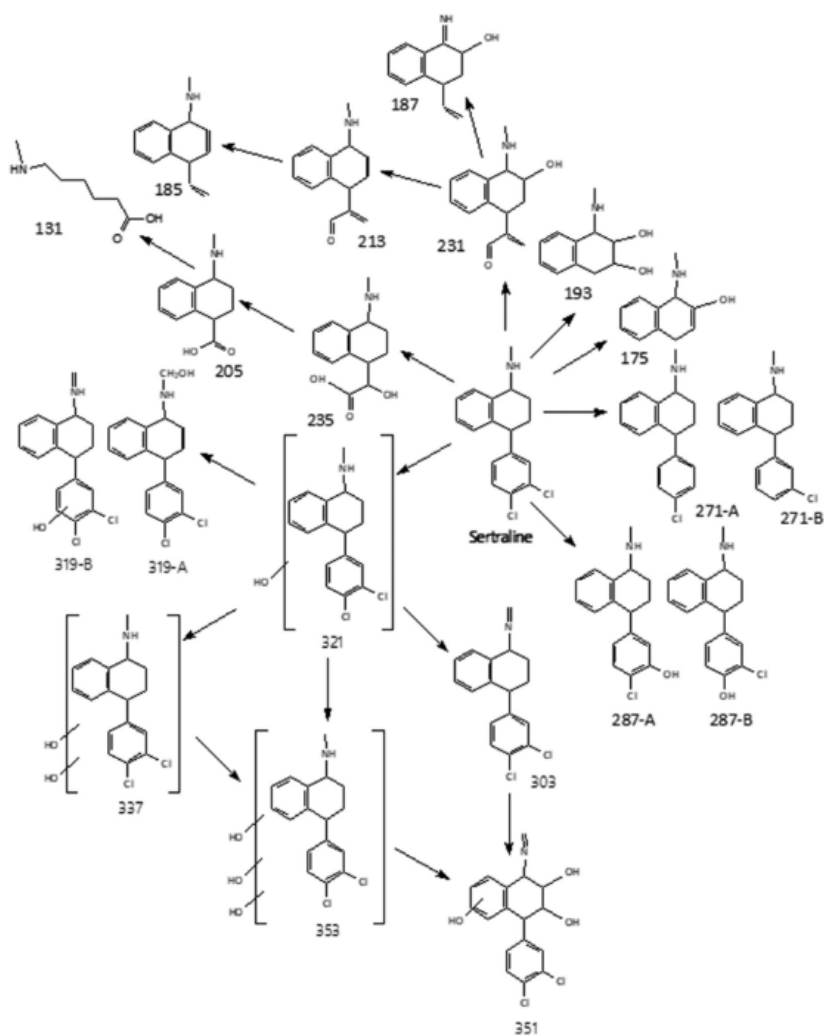


Figure 4.4. Main transformation products formed during the photocatalytic process.

4.4.4. Toxicity of sertraline and its TPs

The potential acute toxicity of sertraline and its formed TPs was assessed via the *Vibrio fischeri* bioassays by assessing the inhibition on the luminescent bacteria emission. The samples resulting

from the photo-catalytic degradation as a function of irradiation time are plotted (Figure 4.5). Sertraline is a moderately toxic compound ($EC_{50} = 20 \text{ mg/L}$) and its transformation in the first steps proceeded through the formation of toxic compounds. The percentage of inhibition increased up to 70%, at irradiation times when the larger part of TPs was formed. Then after 20 min of irradiation, the toxicity of the irradiated solution decreased to levels around 10%. The samples from 40 min present a significantly lower inhibition in agreement with the complete removal of the observed identified TPs and the significant mineralization observed, as shown in Figure 4.5.

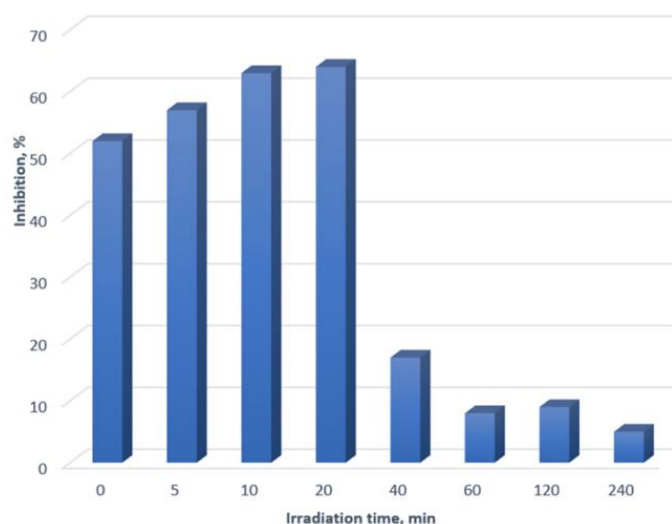


Figure 4.5. Toxicity assessed for sertraline as a function of the irradiation times.

Since the identified TPs of SER are not commercially available, ECOSAR program was employed as a good alternative to derive toxicity data for fish, daphnia, and algae and to link the toxicity results obtained by luminescent bacterium test. This program can screen and predict the aquatic toxicity of chemicals based on the similarity of structure to chemicals for which the aquatic toxicity has been previously reported, and therefore is widely used to predict acute and chronic toxicity of compounds observed during water treatment processes [23]. Data at Table 4.3 show that the LC_{50} obtained for SER for fish was about 0.408 mg/L , whilst LC_{50} and EC_{50} were much lower for daphnid and green

algae (about 0.071 and 0.028 mg/L respectively). Considering the ranking of these toxicity values, almost all the TPs produced during the photocatalytic treatment of SERT exhibited higher toxicity than the parent molecule in contrast to photolytic experiments where the ECOSAR toxicity prediction software showed that transformation products will either have comparable or lower toxicity than their parent compound [28]. Probably, the employment of multispecies is crucial for evaluating the toxicity during such treatments. Nevertheless, it should be also noted that other TPs, which were not identified under the given experimental conditions, might also contribute to the increased toxicity in the early stages of the photocatalytic treatment.

4.5. Conclusions

The photolytic and photocatalytic behaviour of antidepressant drug sertraline was investigated under simulated solar irradiation. Results have shown that first-order kinetics were followed, and that indirect photolysis demonstrate a significant contribution to the environmental fate of sertraline in aquatic systems. Introduction of titania as a catalyst dramatically accelerated the process even at mild conditions (400 mg/L) and after 1 h of irradiation, both parent molecule and its TPs were totally removed. Forty-four transformation products were identified by means of high-resolution mass spectrometry, seventeen of them are reported for the first time. Our findings demonstrate that identification of transformation byproducts although a very challenging analytical process could bring some substantial knowledge with regards to the “targeted” determination of potential transformation products in environmental aquatic systems considering the fact that thirty four of these chemicals display higher acute toxicity potential (based on ECOSAR software).

Table 4.3. Toxicity predictions for sertraline (SERT) and its transformation products using ECOSAR.

[M+H ⁺]	Empirical formula	Acute toxicity [mg/L]			Chronic toxicity (ChV) [mg/L]		
		Fish (LC ₅₀)	Daphnid (LC ₅₀)	Algae (EC ₅₀)	Fish (LC ₅₀)	Daphnid (LC ₅₀)	Algae (EC ₅₀)
306.0803 (SERT)	C ₁₇ H ₁₈ NCl ₂	0.408	0.071	0.028	0.0074	0.0085	0.012
132.1017	C ₆ H ₁₄ O ₂ N	1.02×10 ³	91.8	133	142	5.71	35.9
176.1071	C ₁₁ H ₁₄ ON	126	13.6	13.7	10.0	1.01	4.24
186.1279	C ₁₃ H ₁₆ N	3.33	0.476	0.274	0.111	0.047	0.104
188.1072	C ₁₂ H ₁₄ ON	5.96	3.92	5.31	0.692	0.572	1.92
194.1177	C ₁₁ H ₁₆ O ₂ N	558	54.0	67.0	61.3	3.62	19.2
206.1179	C ₁₂ H ₁₆ O ₂ N	7.94×10 ⁴	6.29×10 ³	1.16×10 ⁴	1.60×10 ⁴	348	2.88×10 ³
214.1228	C ₁₄ H ₁₆ ON	19.4	2.45	1.80	0.949	0.213	0.624
232.1337	C ₁₄ H ₁₈ O ₂ N	156	16.9	16.8	12.2	1.26	5.22
236.1285	C ₁₃ H ₁₈ O ₃ N	1.59×10 ⁵	1.21×10 ⁴	2.43×10 ⁴	3.66×10 ⁴	641	5.84×10 ³
272.1207 (A, B)	C ₁₇ H ₁₉ NCl	0.960	0.156	0.070	0.022	0.017	0.029
288.1155 (A, B)	C ₁₇ H ₁₉ ONCl	2.10	0.132	0.162	0.057	0.034	0.064
304.0660	C ₁₇ H ₁₆ NCl ₂	0.078	0.322	0.00072	0.0018	0.021	0.019
320.0609 (A, B)	C ₁₇ H ₁₆ ONCl ₂	0.053	0.155	0.0054	0.0080	0.036	0.032
322.0768 (A, B, C, D, E, F)	C ₁₇ H ₁₈ ONCl ₂	0.887	0.147	0.063	0.019	0.017	0.027
338.0715 (A, B, C, D, E)	C ₁₇ H ₁₈ O ₂ NCl ₂	1.93	0.301	0.154	0.049	0.032	0.059
352.0507	C ₁₇ H ₁₆ O ₃ NCl ₂	3.96	3.50	0.371	0.461	0.504	1.14
354.0661 (A, B, C, D, E, F, G, H, I, L)	C ₁₇ H ₁₈ O ₃ NCl ₂	4.17	0.616	0.332	0.126	0.062	0.129

Acknowledgements This work is part of a project that has received funding from the European Union's Horizon 2020 research and innovation programme under the Marie Skłodowska-Curie Grant Agreement No 765860 (AQUALity).

Science of the Total Environment 756 (2021) 143805



Contents lists available at ScienceDirect

Science of the Total Environment

journal homepage: www.elsevier.com/locate/scitotenv

Study of the photoinduced transformations of sertraline in aqueous media



Paola Calza^a, Cristina Jiménez-Holgado^b, Marco Coha^a, Christoforos Chrimatopoulos^b, Federica Dal Bello^c, Claudio Medana^c, Vasilios Sakkas^{b,*}

^a Department of Chemistry, Via Giuria 5, 10125, Università degli Studi di Torino, Torino, Italy

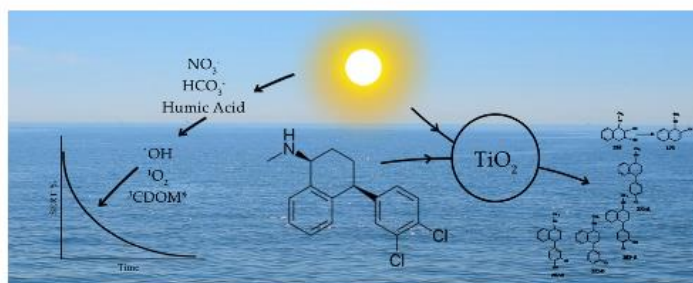
^b Department of Chemistry, University of Ioannina, Laboratory of Analytical Chemistry, Ioannina 45 110, Greece

^c Department of Molecular Biotechnology and Health Sciences, Via Giuria 5, 10125 Torino, Italy

HIGHLIGHTS

- $T_{1/2}$ of sertraline decreased from 57 h in ultrapure water to 7 h in aqueous solution of 10 mg/L HA.
- Sertraline showed high degradation rate in photocatalysis with TiO_2 .
- Forty-four transformation products were identified.
- More toxic compounds were produced in the first stages of photocatalysis.

GRAPHICAL ABSTRACT



ARTICLE INFO

Article history:

Received 15 July 2020

Received in revised form 25 October 2020

Accepted 25 October 2020

Available online 27 November 2020

Editor: Dimitra A Lambropoulou

Keywords:

Antidepressants

Photodegradation

Photosensitizers

Photocatalysis

Toxicity

Transformation products

ABSTRACT

In the present study, the photoinduced degradation of the antidepressant drug sertraline under artificial solar radiation was examined. Photolysis was studied under different experimental conditions to explore its photolytic fate in the aqueous environment. Photolytic degradation kinetics were carried out in ultrapure water, wastewater effluent, as well as in the presence of dissolved organic matter (humic acids), bicarbonate and nitrate ions which enabled their assessment on sertraline photo-transformation. The reaction of sertraline with photoactive compounds accelerated sertraline transformation in comparison with direct photolysis. Moreover, TiO_2 -mediated photocatalytic degradation of sertraline was investigated, and focus was placed on the identification of by-products. As expected, photocatalysis was extremely effective for sertraline degradation. Photocatalytic degradation proceeded through the formation of forty-four transformation products identified by HPLC-HRMS and after 240 min of irradiation total mineralization was achieved. Microtox bioassay (*Vibrio fischeri*) was employed to assess the ecotoxicity of the photocatalysis-treated solutions and results have indicated that sertraline photo-transformation proceeds through the formation of toxic compounds.

© 2020 The Authors. Published by Elsevier B.V. This is an open access article under the CC BY license (<http://creativecommons.org/licenses/by/4.0/>).

Supplementary material
Table S1: Physicochemical characteristics of WWTP effluent aqueous sample.

Effluent of WWTP	
pH	7.3
DOC ^a (mg/L)	27.5
NO ₃ ⁻ (mg/L)	96.4
P total (mg/L)	1.0
N total (mg/L)	15.5

^aDOC: Dissolved Organic Carbon

Table S2: List of MSⁿ for sertraline and monohydroxyderivatives.

[M + H] ⁺ and empirical formula	Δ mmu	MS ²	Δ mmu	MS ³	Δ mmu
306.0820 C ₁₇ H ₁₈ NC ₂	0.908	275.0395 [100] C ₁₆ H ₁₃ Cl ₂ (-CH ₅ N)	0.578	129.0697 [70] C ₁₀ H ₉ (-C ₆ H ₄ Cl ₂)	-0.207
				158.9756 [100] C ₇ H ₅ Cl ₂ (-C ₉ H ₈)	-0.712
322.0768-A, F C ₁₇ H ₁₈ ONCl ₂	0.255	291.0345 [100] C ₁₆ H ₁₃ OCl ₂ (-CH ₅ N)	0.703	145.0646 [97] C ₁₀ H ₉ O (-C ₆ H ₄ Cl ₂)	-0.191
				158.9756 [100] C ₇ H ₅ Cl ₂ (-C ₉ H ₈ O)	-0.682
322.0768-B C ₁₇ H ₁₈ ONCl ₂	0.255	291.0345 [58] C ₁₆ H ₁₃ OCl ₂ (-CH ₅ N)	0.703	145.0646 [36] C ₁₀ H ₉ O (-C ₆ H ₄ Cl ₂)	-0.191
				158.9756 [100] C ₇ H ₅ Cl ₂ (-C ₉ H ₈ O)	-0.682
		304.0662 [100] C ₁₇ H ₁₆ NC ₂ (-H ₂ O)	0.769	-	-
322.0768-C, D, E C ₁₇ H ₁₈ ONCl ₂	0.255	291.0345 [100] C ₁₆ H ₁₃ OCl ₂ (-CH ₅ N)	0.703	129.0697 [30] C ₁₀ H ₉ (-C ₆ H ₄ OCl ₂)	-0.177
				174.9712 [100] C ₇ H ₅ OCl ₂ (-C ₉ H ₈)	0.003

Table S3. Species at m/z 338 (dihydroxyderivatives) and their MS^n ions.

$[M + H]^+$ and empirical formula	Δ mmu	MS^2	Δ mmu	MS^3	Δ mmu
338.0715-A $C_{17}H_{18}O_2NCl_2$	0.589	307.0293 [100] $C_{16}H_{13}O_2Cl_2$ (- CH_5N)	0.588	145.0646 [100] $C_{10}H_9O$ (- $C_6H_4OCl_2$)	-0.191
				174.9712 [53] $C_7H_5OCl_2$ (- C_9H_8O)	0.003
338.0715-B $C_{17}H_{18}O_2NCl_2$	0.589	307.0293 [100] $C_{16}H_{13}O_2Cl_2$ (- CH_5N)	0.588	129.0697 [19] $C_{10}H_9$ (- $C_6H_4O_2Cl_2$)	-0.177
				190.9691 [100] $C_7H_5O_2Cl_2$ (- C_9H_8)	2.989
338.0715-C $C_{17}H_{18}O_2NCl_2$	0.589	307.0293 [100] $C_{16}H_{13}O_2Cl_2$ (- CH_5N)	0.588	161.0597 [100] $C_{10}H_9O_2$ (- $C_6H_4Cl_2$)	-0.006
				158.9756 [62] $C_7H_5Cl_2$ (- $C_9H_8O_2$)	-0.682
338.0715-D $C_{17}H_{18}O_2NCl_2$	0.589	307.0293 [100] $C_{16}H_{13}O_2Cl_2$ (- CH_5N)	0.588	161.0597 [100] $C_{10}H_9O_2$ (- $C_6H_4Cl_2$)	-0.006
				158.9756 [62] $C_7H_5Cl_2$ (- $C_9H_8O_2$)	-0.682
				320.0609 [30] $C_{17}H_{16}ONCl_2$ (- H_2O)	0.554
		304.0653 [45] $C_{17}H_{16}NCl_2$ (- H_2O_2)	-0.131	-	-
338.0715-E $C_{17}H_{18}O_2NCl_2$	0.589	307.0293 [100] $C_{16}H_{13}O_2Cl_2$ (- CH_5N)	0.588	161.0597 [100] $C_{10}H_9O_2$ (- $C_6H_4Cl_2$)	-0.006
				158.9756 [62] $C_7H_5Cl_2$ (- $C_9H_8O_2$)	-0.682
				320.0609 [12] $C_{17}H_{16}ONCl_2$ (- H_2O)	0.554

Table S4. Species at m/z 354 (dihydroxyderivatives) and their MS^n ions.

$[M + H]^+$ and empirical formula	Δ mmu	MS^2	Δ mmu	MS^3	Δ mmu
354.0661- A, B, G $C_{17}H_{18}O_3NCl_2$	0,275	323.0239 [100] $C_{16}H_{13}O_3Cl_2 (-CH_5N)$	0.474	145.0646 [100] $C_{10}H_9O(-C_6H_4O_2Cl_2)$	-0.191
				190.9691 [55] $C_7H_5O_2Cl_2 (-C_9H_8O)$	2.989
354.0661- C, D, F $C_{17}H_{18}O_3NCl_2$	0.275	323.0239 [100] $C_{16}H_{13}O_3Cl_2 (-CH_5N)$	0.474	161.0597 [100] $C_{10}H_9O_2 (-C_6H_4OCl_2)$	-0.006
				174.9712 [34] $C_7H_5OCl_2 (-C_9H_8O_2)$	0.003
354.0661- E, H, I $C_{17}H_{18}O_3NCl_2$	0.275	323.0239 [100] $C_{16}H_{13}O_3Cl_2 (-CH_5N)$	0.474	177.0546 [41] $C_{10}H_9O_3(-C_6H_4Cl_2)$	-0.021
				158.9756 [8] $C_7H_5Cl_2(-C_9H_8O_3)$	-0.682
				305.0135 [100] $C_{16}H_{11}O_2Cl_2(-H_2O)$	0.438
		336.0555 [28] $C_{17}H_{16}O_2NCl_2 (-H_2O)$	0.239	305.0135 [100] $C_{16}H_{11}O_2Cl_2 (-H_2O)$	0.438
354.0661-L $C_{17}H_{18}O_3NCl_2$	0.275	323.0239 [100] $C_{16}H_{13}O_3Cl_2 (-CH_5N)$	0.474	129.0697 [32] $C_{10}H_9$ $(-C_6H_4O_3Cl_2)$	-0.177
				206.9611 [100] $C_7H_5O_3Cl_2 (-C_9H_8)$	0.074

Table S5: species at m/z 304 (oxidized derivatives), 320 (oxidized monohydroxyderivatives) and 352 (oxidized trihydroxyderivatives) and their MS^n ions.

[M + H]⁺ and empirical formula	Δ mmu	MS²	Δ mmu	MS³	Δ mmu
304.0660 C ₁₇ H ₁₆ NCl ₂	0.010	275.0394 [100] C ₁₆ H ₁₃ Cl ₂ (-CH ₃ N)	0.041	129.0697 [40] C ₁₀ H ₉ (-C ₆ H ₄ Cl ₂)	-0.177
				158.9756 [100] C ₇ H ₅ Cl ₂ (-C ₉ H ₈)	-0.682
320.0609-A C ₁₇ H ₁₆ ONCl ₂	0.554	273.0237 [100] C ₁₆ H ₁₁ Cl ₂ (-CH ₅ ON)	0.468	158.9756 [5] C ₇ H ₅ Cl ₂ (-C ₉ H ₈)	-0.177
320.0609-B C ₁₇ H ₁₆ ONCl ₂	0.554	291.0345 [100] C ₁₆ H ₁₃ OCl ₂ (-CH ₃ N)	0.703	129.0697 [30] C ₁₀ H ₉ (-C ₆ H ₄ OCl ₂)	-0.177
				174.9712 [100] C ₇ H ₅ OCl ₂ (-C ₉ H ₈)	0.003
352.0507 C ₁₇ H ₁₆ O ₃ NCl ₂	0.525	323.0241 [100] C ₁₆ H ₁₃ O ₃ Cl ₂ (-CH ₃ N)	0.474	305.0135 [23] C ₁₆ H ₁₁ O ₂ Cl ₂ (-H ₂ O)	0.438
				289.0181 [100] C ₁₆ H ₁₁ OCl ₂ (-H ₂ O ₂)	-0.047
				177.0546 [10] C ₁₀ H ₉ O ₃ (-C ₆ H ₄ Cl ₂)	-0.021
				158.9756 [10] C ₇ H ₅ Cl ₂ (-C ₉ H ₈ O ₃)	-0.682

Table S6: species at m/z 272 (dechlorinated derivatives) and 288 (dechlorinated monohydroxyderivatives) and their MS^n ions.

[M + H]⁺ and empirical formula	Δ mmu	MS²	Δ mmu	MS³	Δ mmu
272.1207-A, B C ₁₇ H ₁₉ NCl	0.646	241.0784 [100] C ₁₆ H ₁₄ Cl (-CH ₅ N)	0.545	129.0697 [58] C ₁₀ H ₉ (-C ₆ H ₅ Cl)	-0.177
				125.0150 [100] C ₇ H ₆ Cl (-C ₉ H ₈)	-0.254
288.1155-A, B C ₁₇ H ₁₉ ONCl	0.532	257.0733 [100] C ₁₆ H ₁₄ OCl (-CH ₅ N)	0.531	129.0697 [100] C ₁₀ H ₉ (-C ₆ H ₅ OCl)	-0.177
				141.0100 [92] C ₇ H ₆ OCl (-C ₉ H ₈)	-0.169

Table S7. Species at m/z 176 and 194 and their MS^n ions.

$[M + H]^+$ and empirical formula	Δ mmu	MS^2	Δ mmu	MS^3	Δ mmu
176.1071 $C_{11}H_{14}ON$	0.109	145.0648 [100] $C_{10}H_9O$ (- CH_5N)	0.009	-	-
		158.0965 [30] $C_{11}H_{12}N$ (- H_2O)	0.074	-	-
194.1177 $C_{11}H_{16}O_2N$	0.145	176.1071 [50] $C_{11}H_{14}ON$ (- H_2O)	0.109	145.0647 [20] $C_{10}H_9O$ (- CH_5N)	-0.091
		163.0754 [12] $C_{10}H_{11}O_2$ (- CH_5N)	0.044	145.0647 [11] $C_{10}H_9O$ (- H_2O)	-0.091
				129.0697 [100] $C_{10}H_9$ (- H_2O_2)	-0.177
		160.1120 [87] $C_{11}H_{14}N$ (- H_2O_2)	-0.076	129.0697 [40] $C_{10}H_9$ (- CH_5N)	-0.177
		145.0647 [82] $C_{10}H_9O$ (- CH_7ON)	-0.091	-	-
		129.0697 [100] $C_{10}H_9$ (- CH_7O_2N)	-0.177	-	-

Table S8: species at m/z 206 and 236 and their MS^n ions

$[M + H]^+$ and empirical formula	Δ mmu	MS^2	Δ mmu	MS^3	Δ mmu
206.1179 $C_{12}H_{16}O_2N$	0.345	175.0755 [100] $C_{11}H_{11}O_2$ (- CH_5N)	0.144	129.0697 [100] $C_{10}H_9$ (- CH_2O_2)	-0.177
		129.0697 [35] $C_{10}H_9$ (- $C_2H_7O_2N$)	-0.177	-	-
236.1285 $C_{13}H_{18}O_3N$	0.380	218.1179 [51] $C_{13}H_{16}O_2N$ (- H_2O)	0.345	200.1073 [15] $C_{13}H_{14}ON$ (- H_2O)	0.309
				187.0756 [28] $C_{12}H_{11}O_2$ (- CH_5N)	0.244
				159.0804 [100] $C_{11}H_{11}O$ (- C_2H_5ON)	-0.042
		200.1073 [33] $C_{13}H_{14}ON$ (-2 H_2O)	0.309	-	-
		187.0756 [39] $C_{12}H_{11}O_2$ (- CH_7ON)	0.244	159.0804 [100] $C_{11}H_{11}O$ (- CO)	-0.042
		159.0804 [100] $C_{11}H_{11}O$ (- $C_2H_7O_2N$)	-0.042	129.0697 [100] $C_{10}H_9$ (- CH_2O)	-0.177

Table S9: species at m/z 132, 214 and 232 and their MS^n ions

$[M + H]^+$ and empirical formula	Δ mmu	MS^2 (%)	Δ mmu	MS^3 (%)	Δ mmu
214.1228 $C_{14}H_{16}ON$	0.159	183.0806 [100] $C_{13}H_{11}O$ (- CH_5N)	0.158	155.0855 [20] $C_{12}H_{11}$ (- CO)	-0.027
		155.0855 [72] $C_{12}H_{11}$ (- C_2H_5ON)	0.027	-	-
232.1337 $C_{14}H_{18}O_2N$	0.495	201.0913 [100] $C_{13}H_{13}O_2$ (- CH_5N)	0.294	183.0806 [100] $C_{13}H_{11}O$ (- H_2O)	0.158
				155.0855 [50] $C_{12}H_{11}$ (- CH_2O_2)	-0.027
		183.0806 [32] $C_{13}H_{11}O$ (- CH_7ON)	0.158	155.0855 [100] $C_{12}H_{11}$ (-CO)	-0.027

Table S10: species at m/z 186 and 188 and their MS^n ions.

$[M + H]^+$ and empirical formula	Δ mmu	MS^2	Δ mmu	MS^3	Δ mmu
132.1017 $C_6H_{14}O_2N$	-0.205	86.0961 [100] $C_5H_{12}N$ (- CH_2O_2)	- 0.326	-	-
186.1279 $C_{13}H_{16}N$	0.174	158.0965 [100] $C_{11}H_{12}N$ (- C_2H_4)	0.074	-	-
188.1072 $C_{12}H_{14}ON$	0.209	160.0757 [100] $C_{10}H_{10}ON$ (- C_2H_4)	0.010	-	-
		131.0853 [91] $C_{10}H_{11}$ (- C_2H_3ON)	- 0.227	-	-
		129.0697 [45] $C_{10}H_9$ (- C_2H_5ON)	- 0.177	-	-

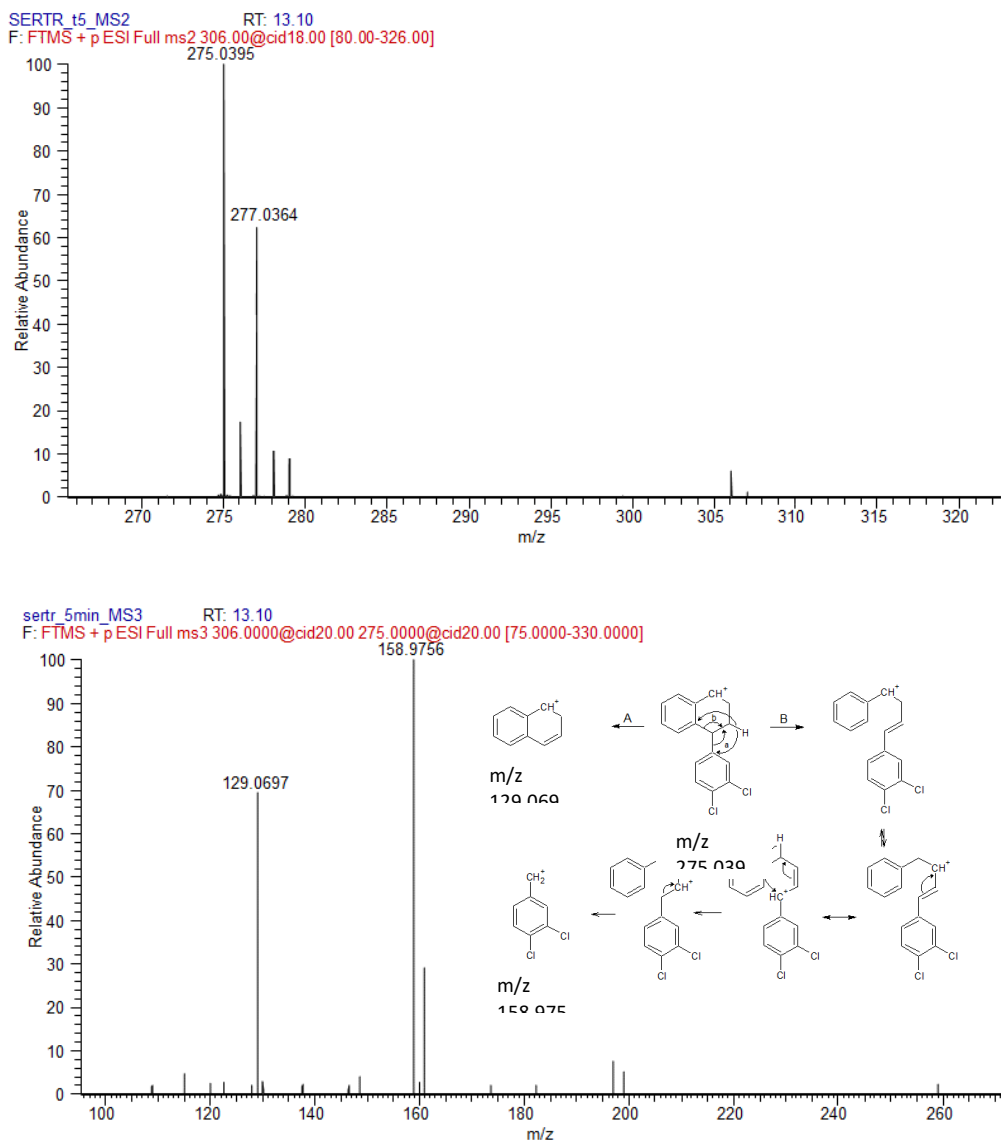


Figure S1. MS² spectrum (top) and MS³ spectrum (bottom) for sertraline.

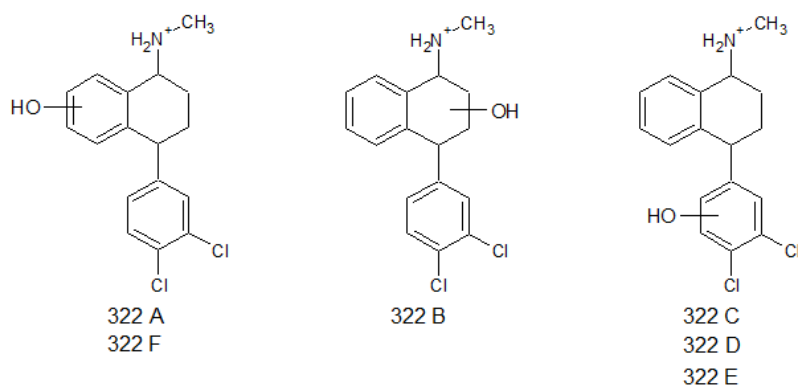


Figure S2. Proposed structures for species at m/z 322.0718.

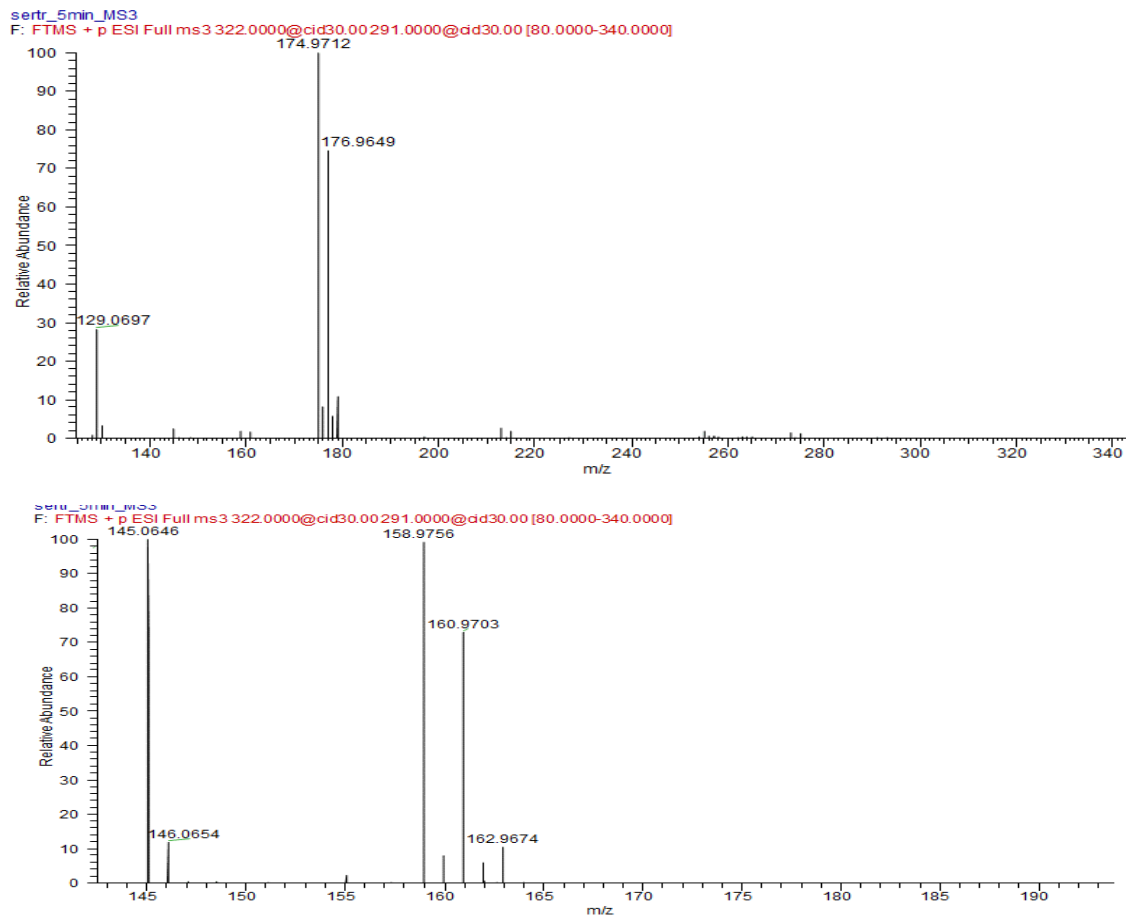


Figure S3: MS³ spectra for isomers C, D and E (top) and isomers 322 A, B and F (bottom).

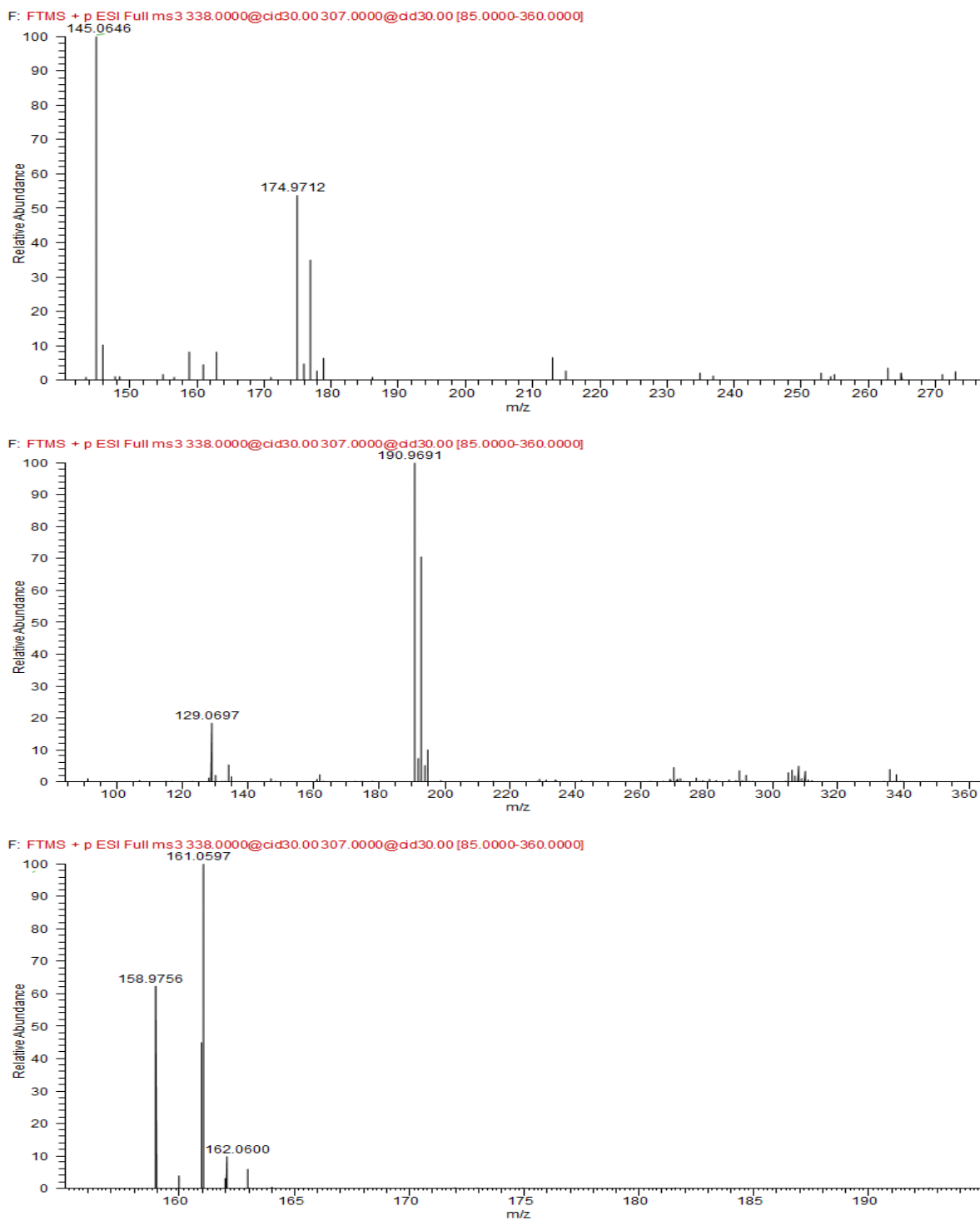
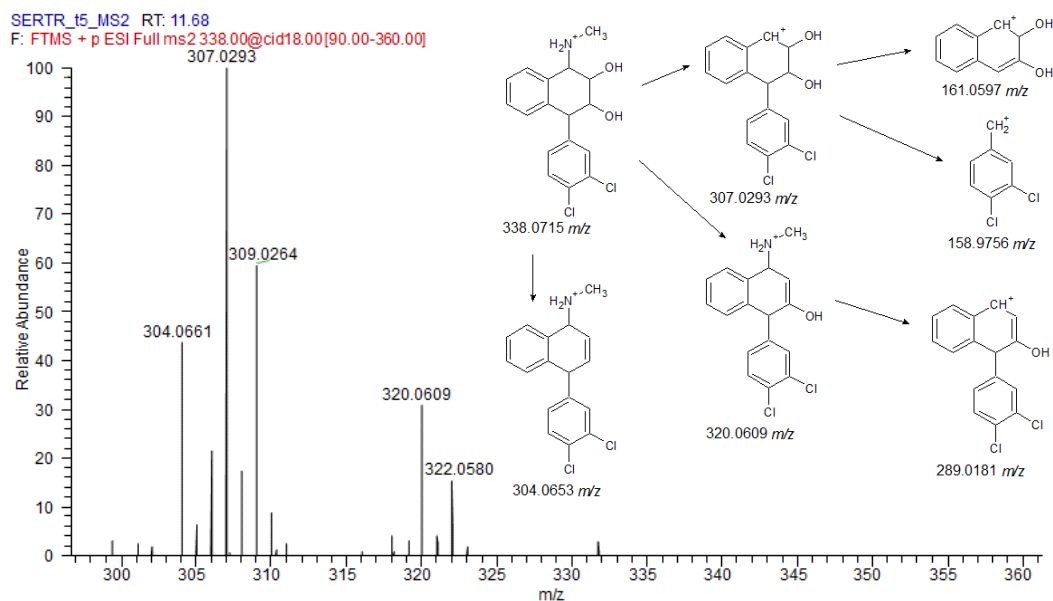
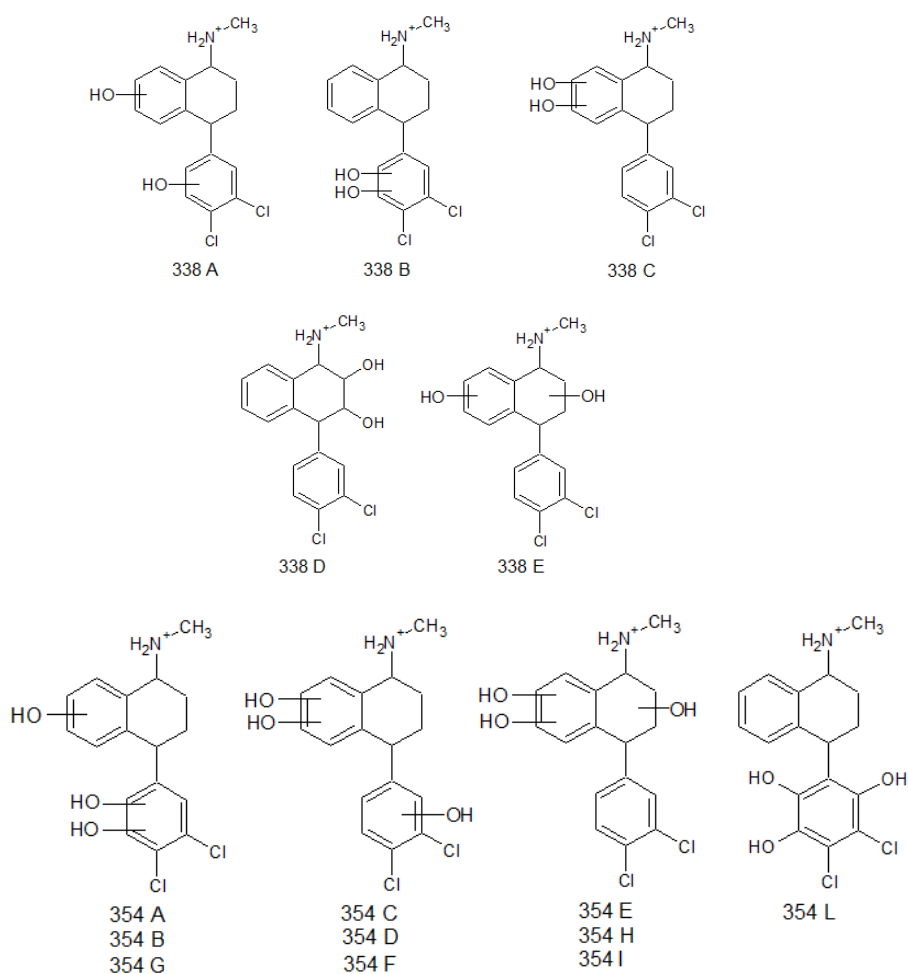


Figure S4: MS³ spectra for 338 A (top), B (middle) and C (bottom).

Figure S5: Spectrum MS² for 338 D.Figure S6: Proposed structures for species at m/z 338.0715 and 354.0661.

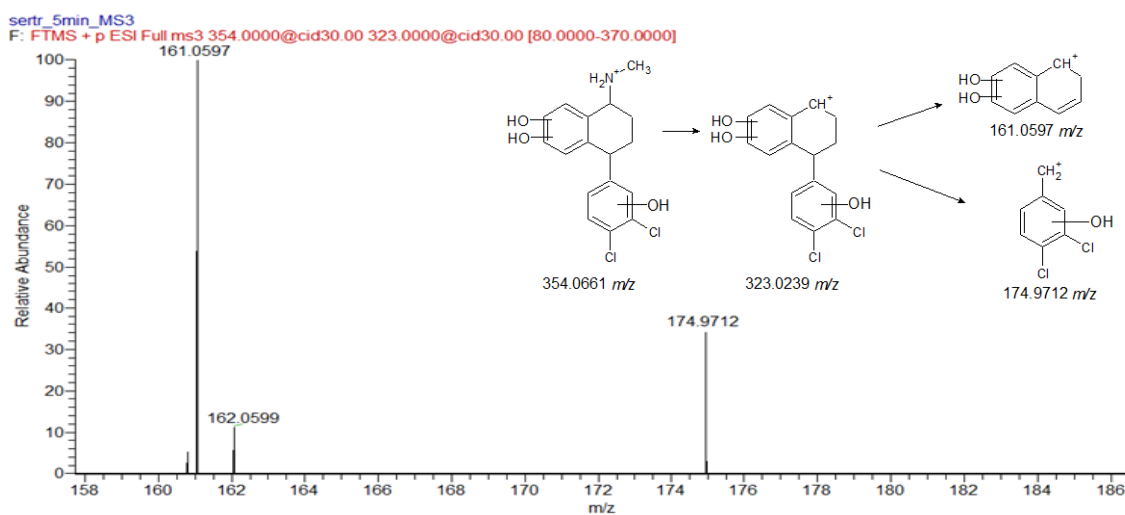
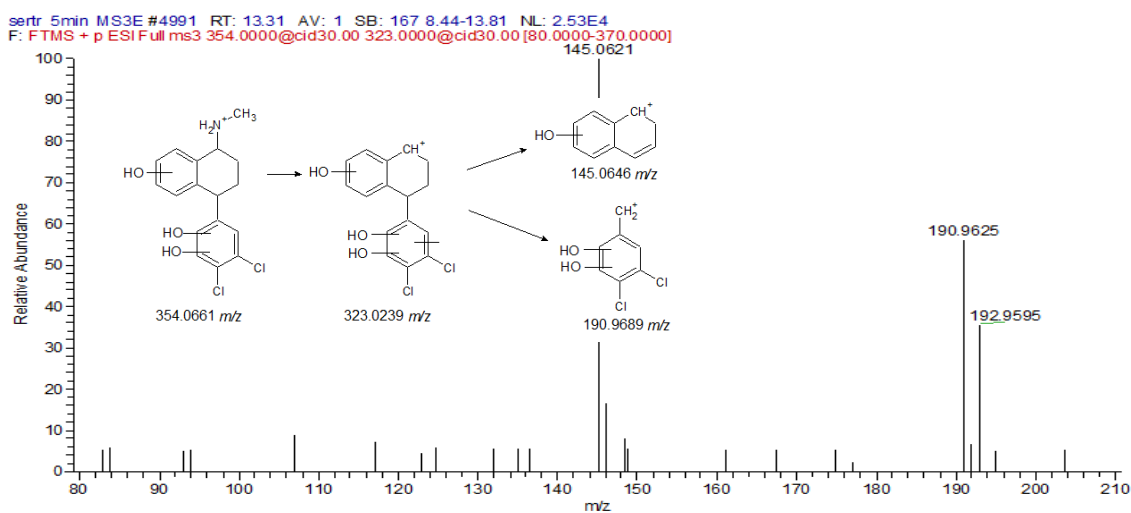
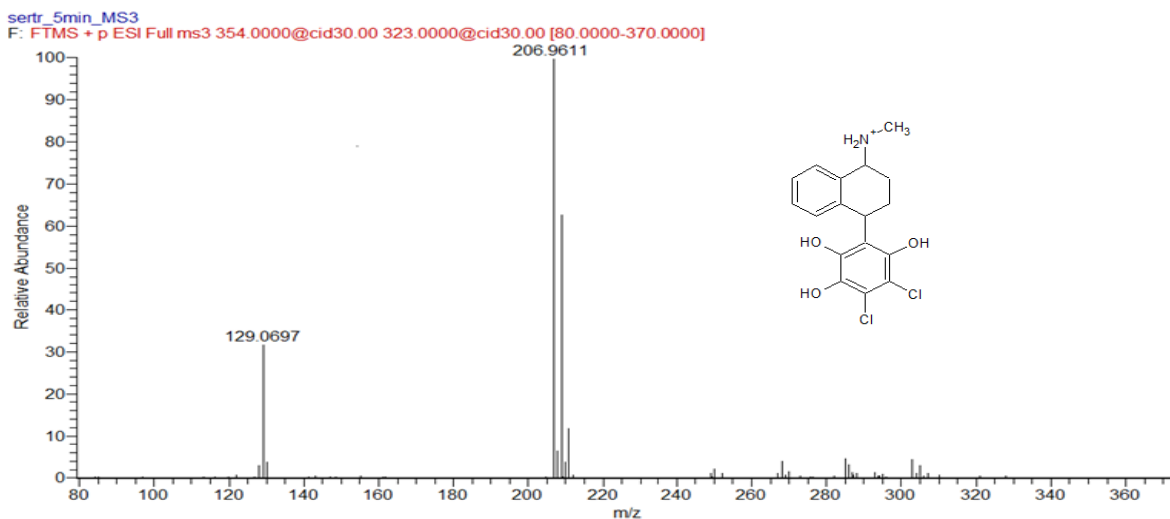


Figure S7: MS³ spectra for 354-L (top) A, B and G (middle) and isomers C, D and F (bottom).

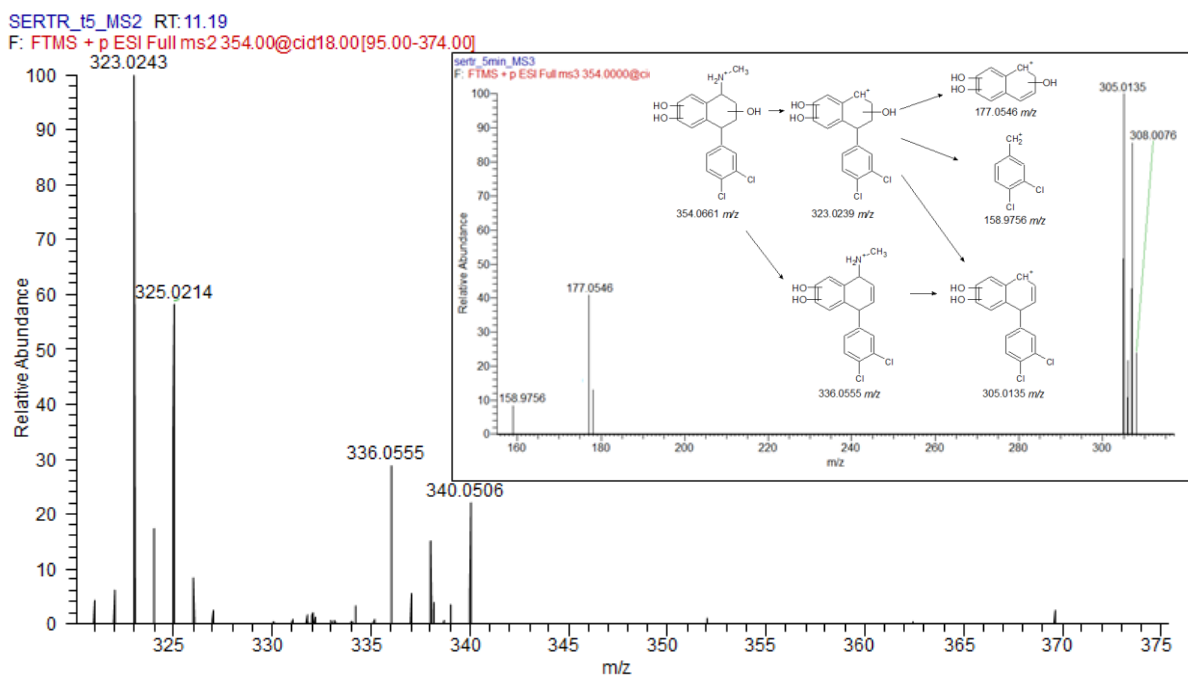


Figure S8: MS² and MS³ spectra for 354 E, H and I.

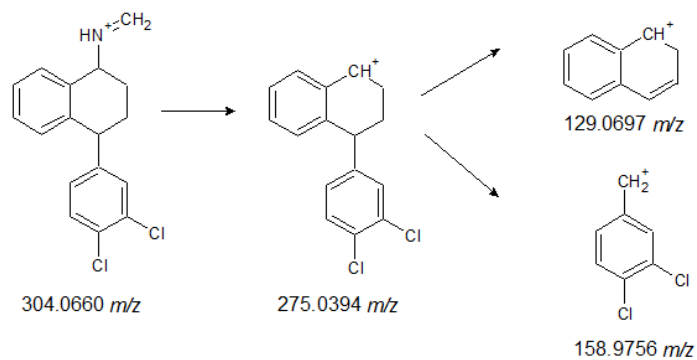


Figure S9: fragmentation pathway for m/z 304.0660.

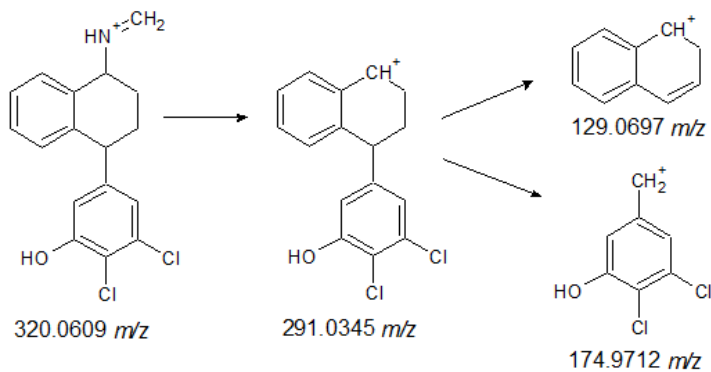


Figure S10: fragmentation pathway for m/z 320.0609 B.

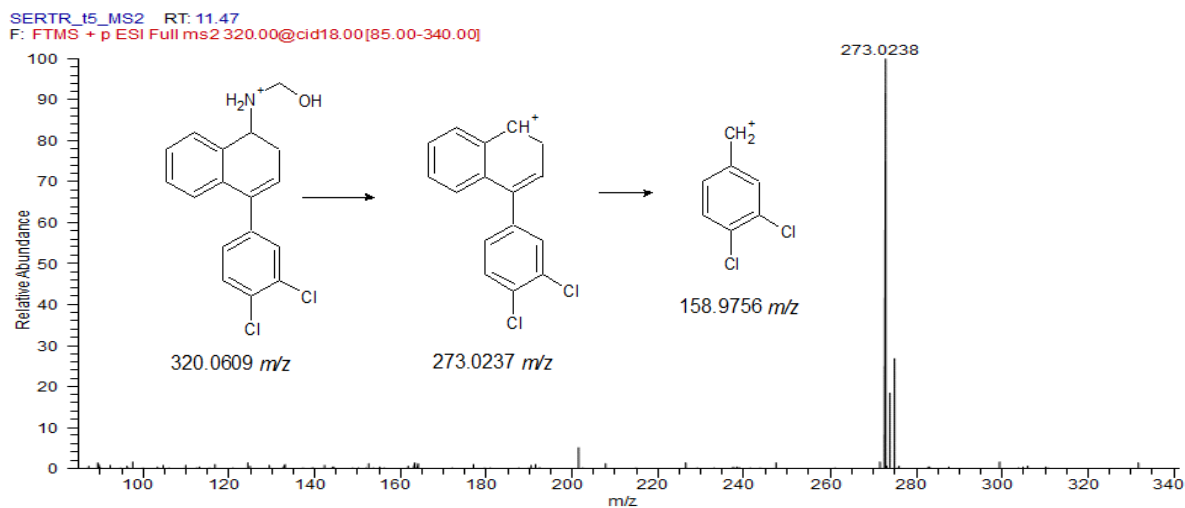


Figure S11: MS² spectrum for m/z 320.0609 A.

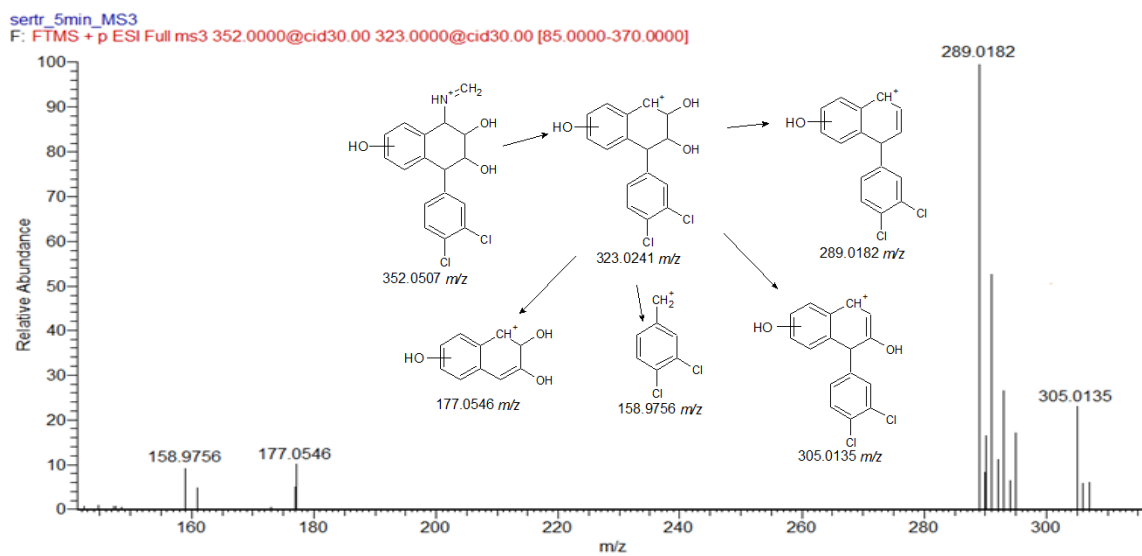


Figure S12: MS² spectrum for m/z 352.0507.

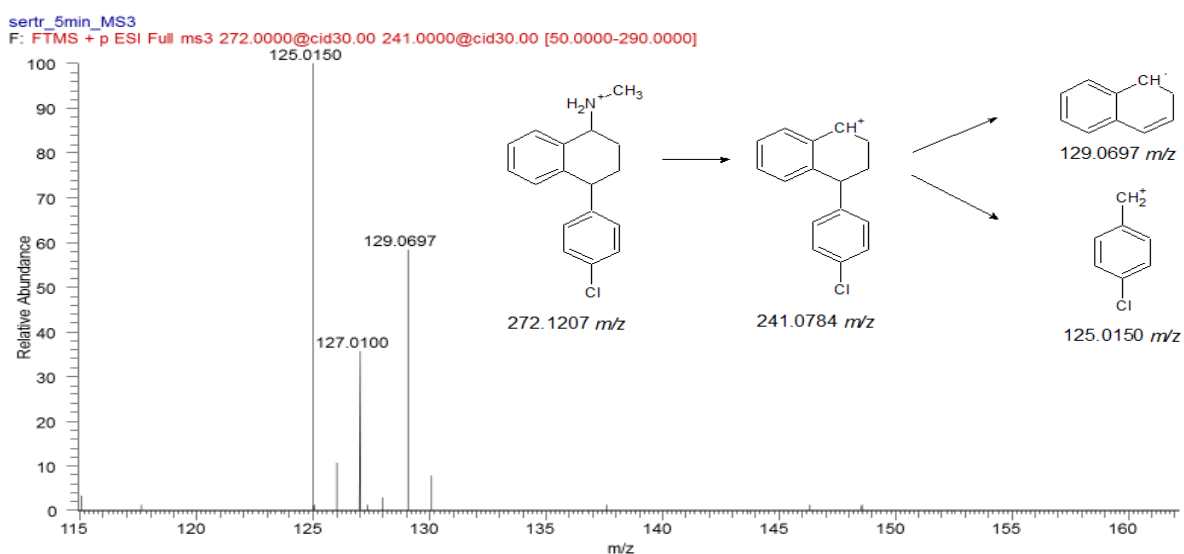


Figure S13: MS² spectrum for m/z 272.1207 A.

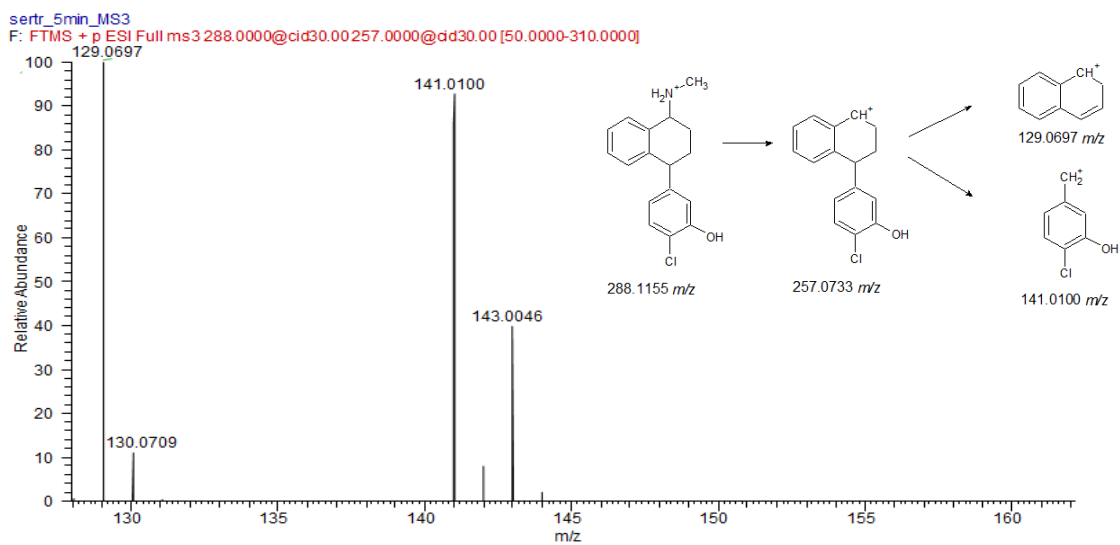
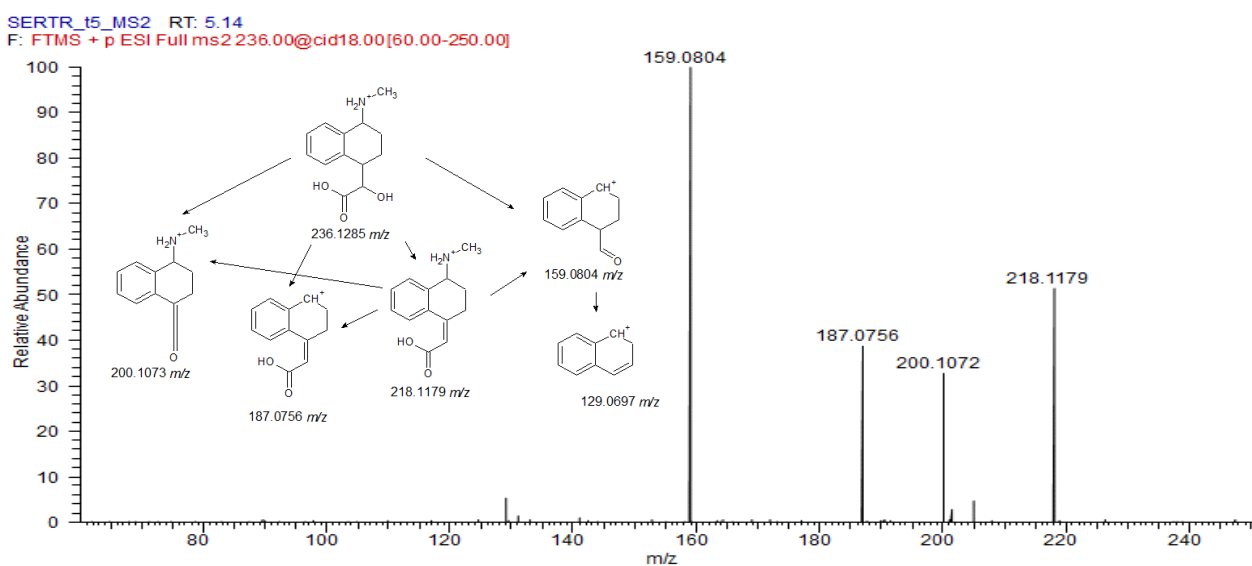
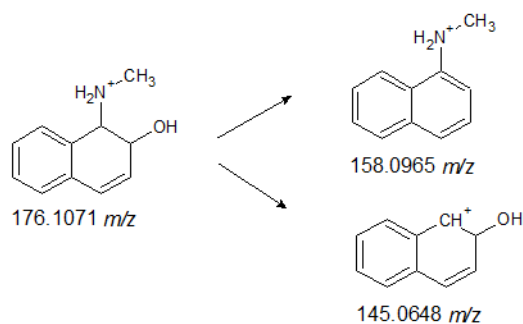
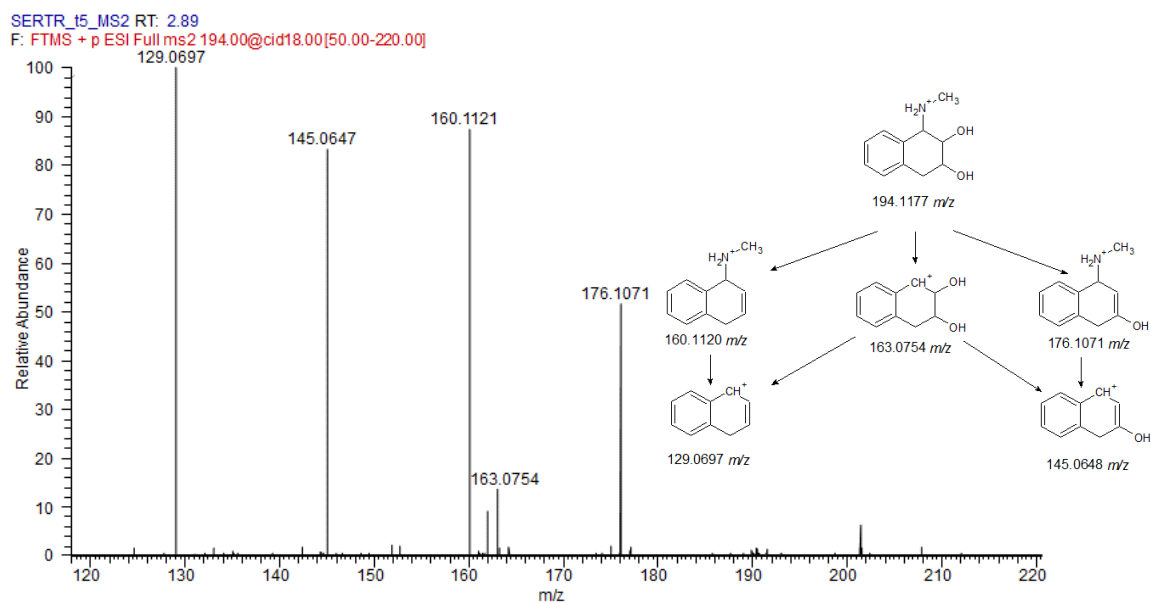
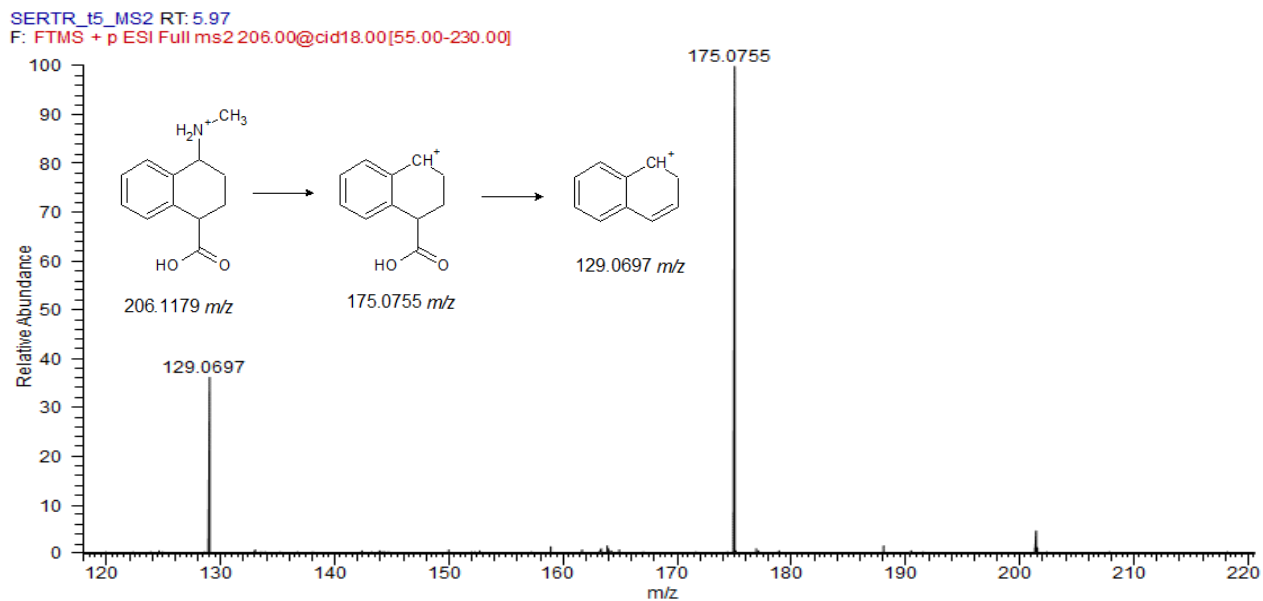
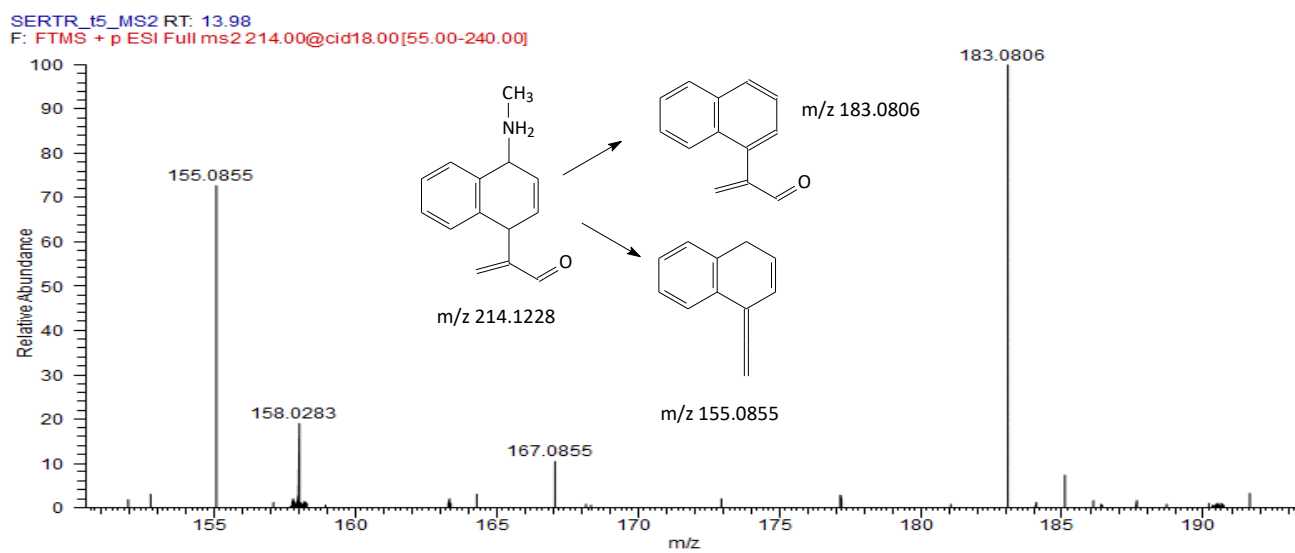


Figure S14: MS² spectrum for m/z 288.1155 A.



Figure S18. MS² spectrum for m/z 206.1179.Figure S19. MS² spectrum for m/z 214.1228.

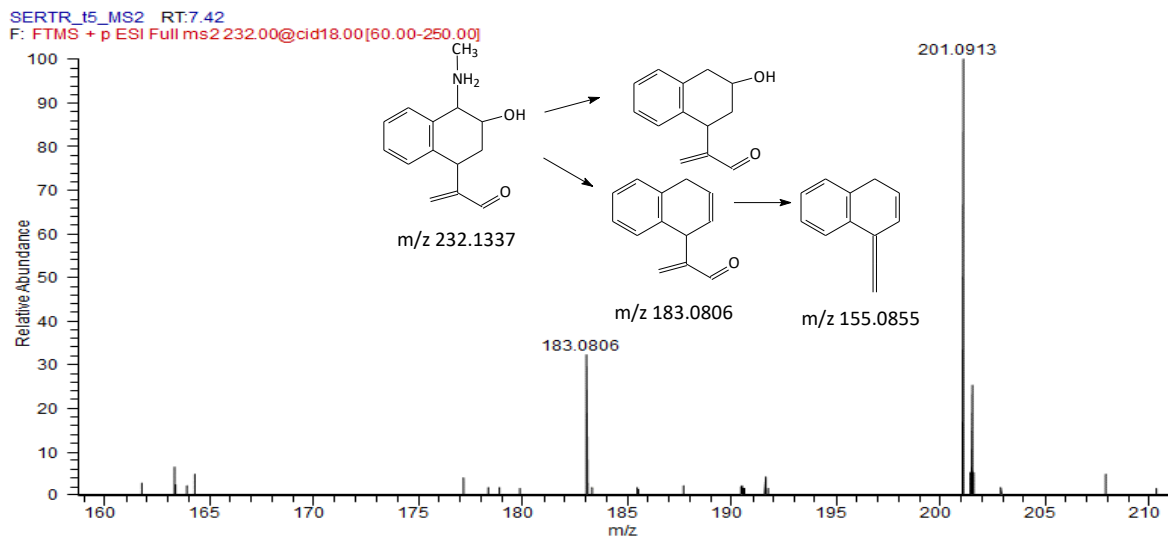


Figure S20: MS² spectrum for m/z 232.1337.

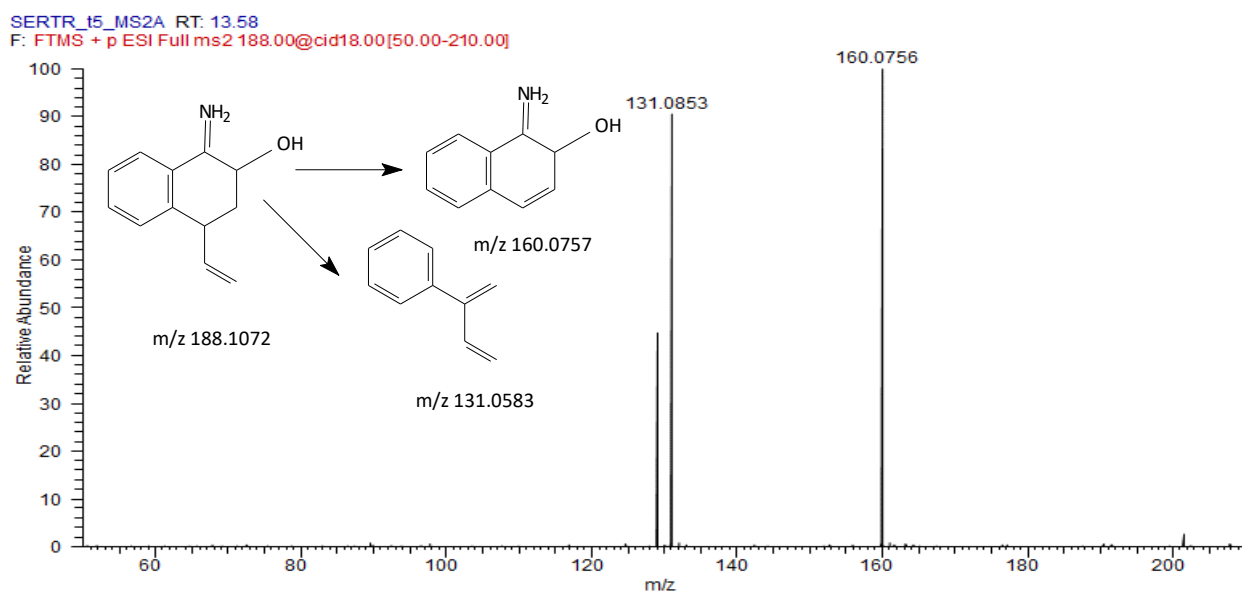
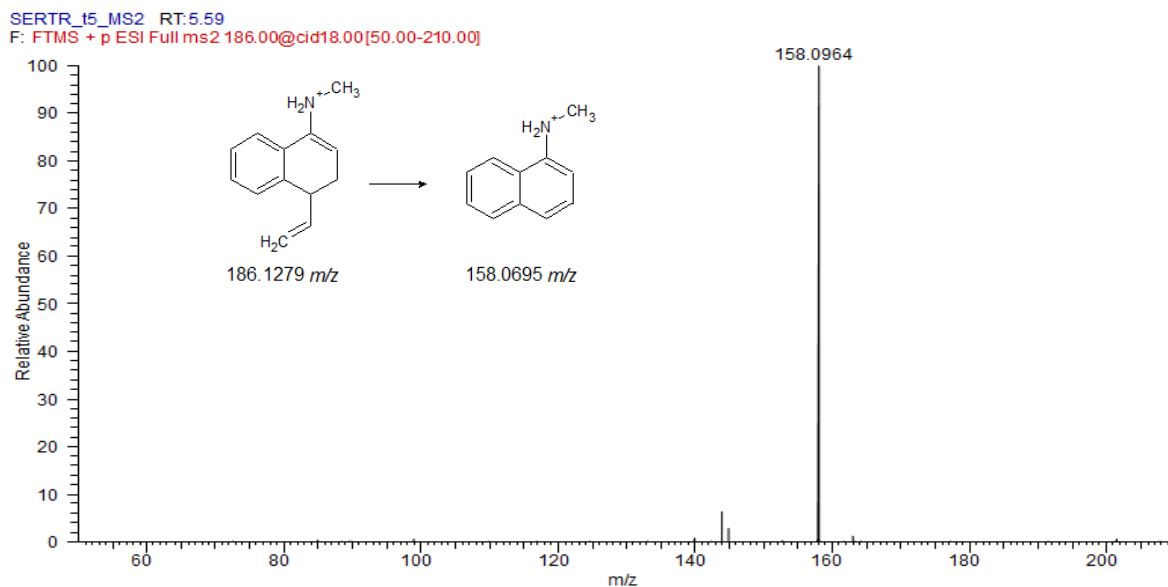
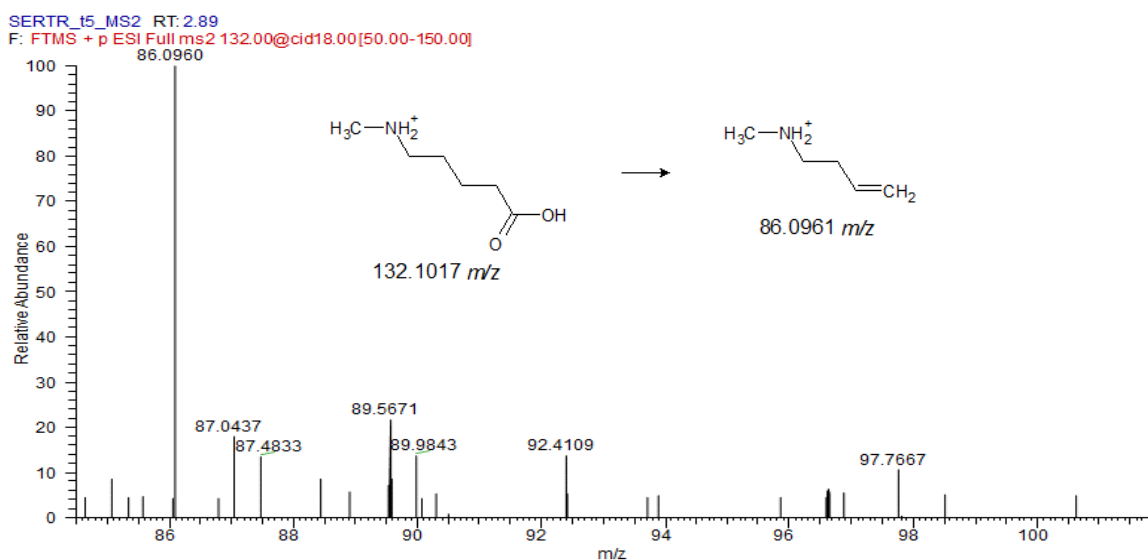


Figure S21: MS² spectrum for m/z 188.1072.

Figure S22: MS² spectrum for m/z 186.1279.Figure S23: MS² spectrum for m/z 132.1017.

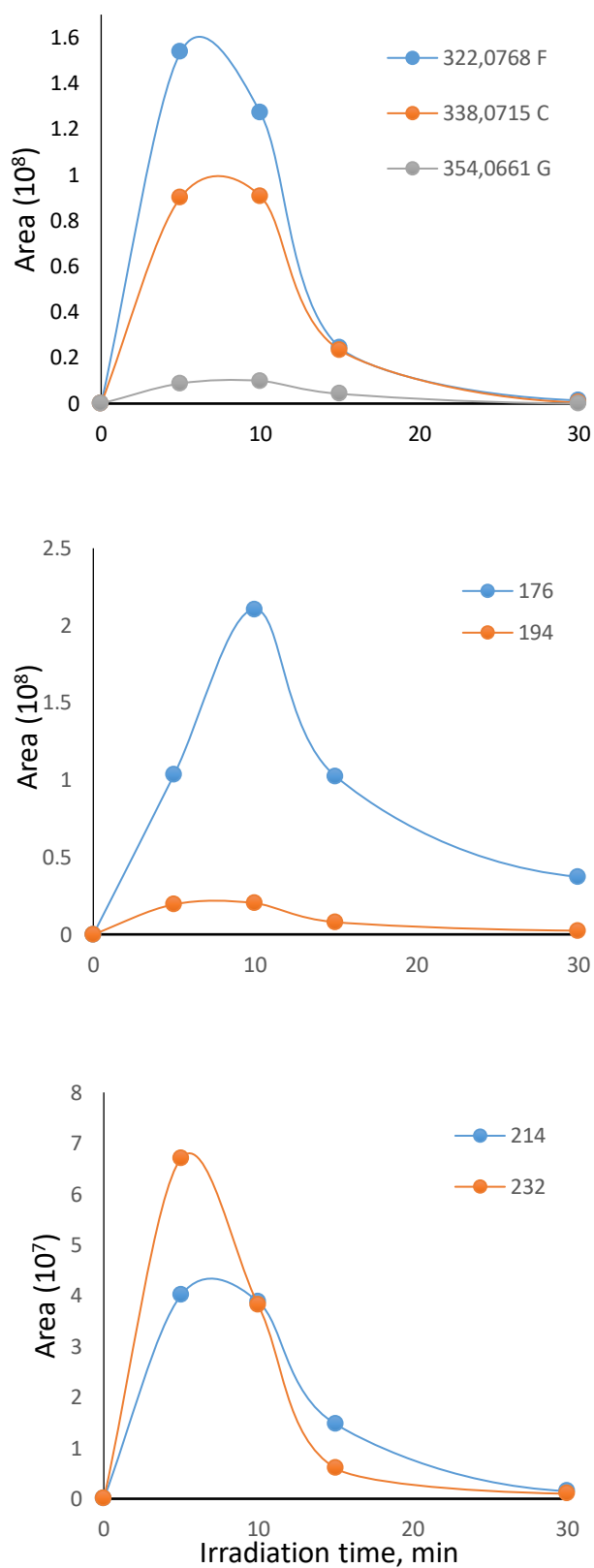


Figure S24: Evolution profiles over time in the presence of TiO_2 for the most abundant TPs.

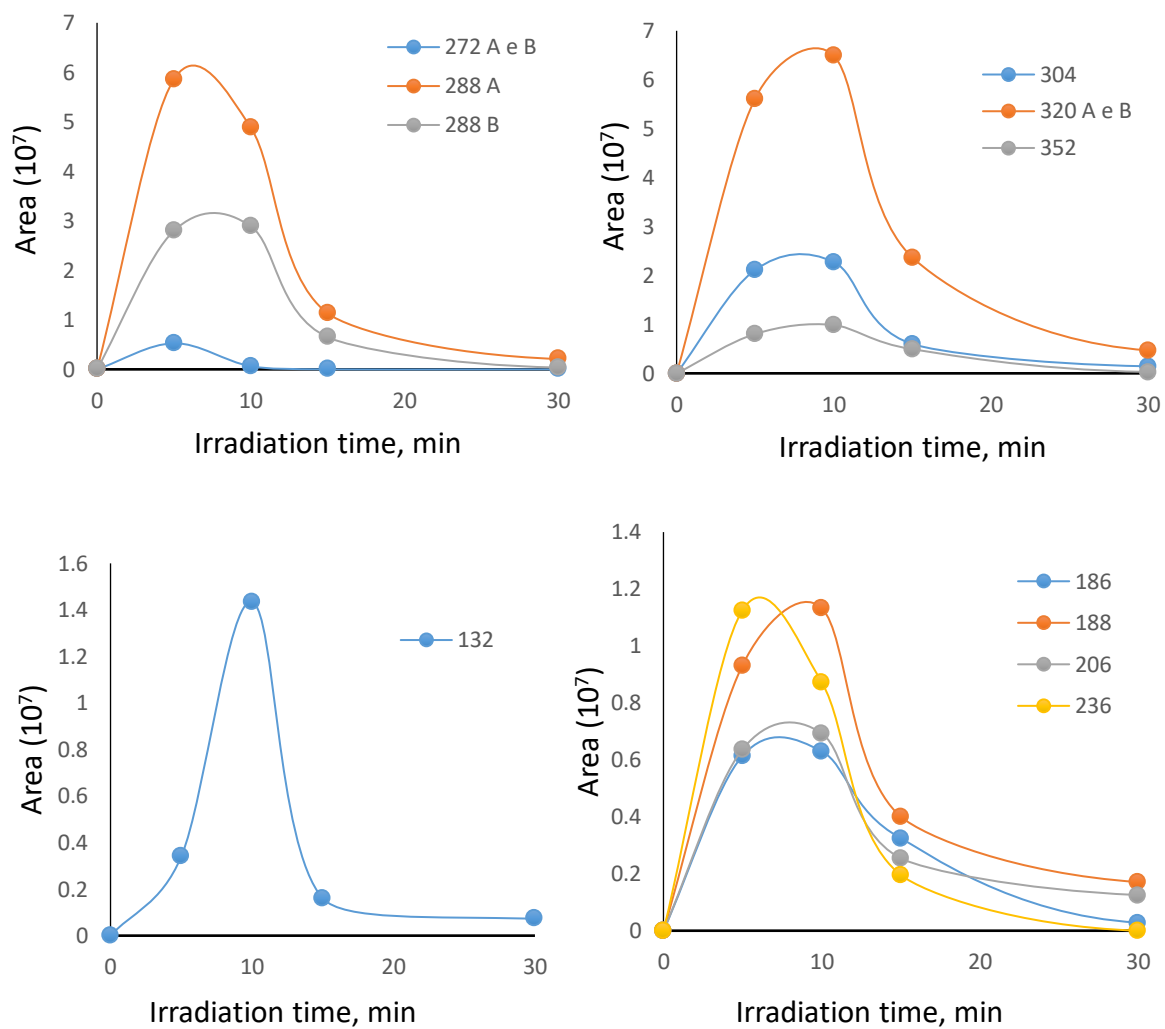


Figure S25: Evolution profiles over time in the presence of TiO₂ for less abundant TPs.

References

1. Baker, D.R., Kasprzyk-Hordern, B., 2011. Multi-residue analysis of drugs of abuse in wastewater and surface water by solid-phase extraction and liquid chromatography- positive electrospray ionisation tandem mass spectrometry. *J. Chromatogr. A* 1218 (12), 1620–1631. <https://doi.org/10.1016/j.chroma.2011.01.060>.
2. Calza, P., Sakkas, V.A., Medana, C., et al., 2006. Photocatalytic degradation study of diclofenac over aqueous TiO₂ suspensions. *Appl. Catal. B Environ.* 67 (3–4), 197–205. <https://doi.org/10.1016/j.apcatb.2006.04.021>.
3. El Mouchtari, E.M., Daou, C., Rafqah, S., et al., 2020. TiO₂ and activated carbon of Argania Spinosa tree nutshells composites for the adsorption photocatalysis removal of pharmaceuticals from aqueous solution. *J. Photochem. Photobiol. A Chem.* 388 (October), 112183. <https://doi.org/10.1016/j.jphotochem.2019.112183>.
4. Gornik, T., Vozic, A., Heath, E., Trontelj, J., Roskar, R., Zigon, D., Vione, D., Kosjek, T., 2019. Determination and photodegradation of sertraline residues in aqueous environment. *Environ. Pollut.* 256, 113431. <https://doi.org/10.1016/j.envpol.2019.113431>.
5. Gornik, T., Kovacic, A., Heath, E., Hollender, J., Kosjek, T., 2020. Biotransformation study of antidepressant sertraline and its removal during biological wastewater treatment. *Water Res.* 181, 115864. <https://doi.org/10.1016/j.watres.2020.115864>.
6. Hernando, M.D., Mezcuá, M., Fernández-Alba, A.R., Barceló, D., 2006. Environmental risk assessment of pharmaceutical residues in wastewater effluents, surface waters and sediments. *Talanta* 69 (2 SPEC. ISS), 334–342. <https://doi.org/10.1016/j.talanta.2005.09.037>.
7. Hörsing, M., Kosjek, T., Andersen, H.R., Heath, E., Ledin, A., 2012. Fate of citalopram during water treatment with O₃, ClO₂, UV and Fenton oxidation. *Chemosphere* 89 (2), 129–135. <https://doi.org/10.1016/j.chemosphere.2012.05.024>.
8. A. Jakimska, M. Śliwka Kaszyńska, P. Nagórski, A. Kot Wasik and J. Namieśnik, Environmental fate of two psychiatric drugs, diazepam and sertraline: photo-transformation and

- investigation of their photoproducts in natural waters. *J. Chromatogr. Sep. Tech.* 5: 253, <https://doi.org/10.4172/2157-7064.1000253>.
9. Kang, Y.M., Kim, M.K., Zoh, K.D., 2018. Effect of nitrate, carbonate/bicarbonate, humic acid, and H₂O₂ on the kinetics and degradation mechanism of Bisphenol-A during UV photolysis. *Chemosphere* 204, 148–155. <https://doi.org/10.1016/j.chemosphere.2018.04.015>.
 10. Katagi, T., 2018. Direct photolysis mechanism of pesticides in water. *J. Pestic. Sci.* 43 (2), 57–72. <https://doi.org/10.1584/jpestics.D17-081>.
 11. Klavarioti, M., Mantzavinos, D., Kassinos, D., 2009. Removal of residual pharmaceuticals from aqueous systems by advanced oxidation processes. *Environ. Int.* 35 (2), 402–417. <https://doi.org/10.1016/j.envint.2008.07.009>.
 12. Kosjek, T., Heath, E., 2008. Applications of mass spectrometry to identifying pharmaceutical transformation products in water treatment. *TrAC Trends Anal. Chem.* 27 (10), 807–820. <https://doi.org/10.1016/j.trac.2008.08.014>.
 13. Kosjek, T., Heath, E., 2010. Tools for evaluating selective serotonin re-uptake inhibitor residues as environmental contaminants. *TrAC Trends Anal. Chem.* 29 (8), 832–847. <https://doi.org/10.1016/j.trac.2010.04.012>.
 14. Kosjek, T., Heath, E., Krbavčič, A., 2005. Determination of non-steroidal anti-inflammatory drug (NSAIDs) residues in water samples. *Environ. Int.* 31 (5), 679–685. <https://doi.org/10.1016/j.envint.2004.12.001>.
 15. Kuang, J., Huang, J., Wang, B., Cao, Q., Deng, S., Yu, G., 2013. Ozonation of trimethoprim in aqueous solution: identification of reaction products and their toxicity. *Water Res.* 47 (8), 2863–2872. <https://doi.org/10.1016/j.watres.2013.02.048>.
 16. Lajeunesse, A., Smyth, S.A., Barclay, K., Sauvé, S., Gagnon, C., 2012. Distribution of antidepressant residues in wastewater and biosolids following different treatment processes by municipal wastewater treatment plants in Canada. *Water Res.* 46 (17), 5600–5612. <https://doi.org/10.1016/j.watres.2012.07.042>.

17. Minero, C., Pelizzetti, E., Sega, M., Friberg, S.E., Sjöblom, J., 1999. The role of humic substances in the photocatalytic degradation of water contaminants. *J. Dispers. Sci. Technol.* 20 (1–2), 643–661. <https://doi.org/10.1080/01932699908943812>.
18. Mole, R.A., Brooks, B.W., 2019. Global scanning of selective serotonin reuptake inhibitors: occurrence, wastewater treatment and hazards in aquatic systems. *Environ. Pollut.* 250, 1019–1031. <https://doi.org/10.1016/j.envpol.2019.04.118>.
19. Nassar, R., Trivella, A., Mokh, S., Al-Iskandarani, M., Budzinski, H., Mazellier, P., 2017. Photodegradation of sulfamethazine, sulfamethoxypyridazine, amitriptyline, and clobipramine drugs in aqueous media. *J. Photochem. Photobiol. A Chem.* 336, 176–182. <https://doi.org/10.1016/j.jphotochem.2016.12.008>.
20. Niu, J., Li, Y., Wang, W., 2013. Light-source-dependent role of nitrate and humic acid in tetracycline photolysis: kinetics and mechanism. *Chemosphere* 92 (11), 1423–1429. <https://doi.org/10.1016/j.chemosphere.2013.03.049>.
21. Ofoegbu, P.U., Lourenço, J., Mendo, S., Soares, A.M.V.M., Pestana, J.L.T., 2019. Effects of low concentrations of psychiatric drugs (carbamazepine and fluoxetine) on the freshwater planarian, *Schmidtea mediterranea*. *Chemosphere* 217, 542–549. <https://doi.org/10.1016/j.chemosphere.2018.10.198>.
22. Pozdnyakov, I.P., Tyutereva, Y.E., Parkhats, M.V., et al., 2020. Mechanistic investigation of humic substances assisted photodegradation of imipramine under simulated sunlight. *Sci. Total Environ.* 738, 140298. <https://doi.org/10.1016/j.scitotenv.2020.140298>.
23. Schymanski, E.L., Jeon, J., Gulde, R., et al., 2014. Identifying small molecules via high resolution mass spectrometry: communicating confidence. *Environ. Sci. Technol.* 48 (4), 2097–2098. <https://doi.org/10.1021/es5002105>.
24. Sugihara, M.N., Moeller, D., Paul, T., Strathmann, T.J., 2013. TiO₂-photocatalyzed transformation of the recalcitrant X-ray contrast agent diatrizoate. *Appl. Catal. B Environ.* 129, 114–122. <https://doi.org/10.1016/j.apcatb.2012.09.013>.

25. Talwar, S., Sangal, V.K., Verma, A., 2018. Feasibility of using combined TiO₂ photocatalysis and RBC process for the treatment of real pharmaceutical wastewater. *J. Photochem. Photobiol. A Chem.* 353, 263–270. <https://doi.org/10.1016/j.jphotochem.2017.11.013>.
26. Tay, K.S., Madehi, N., 2015. Ozonation of ofloxacin in water: by-products, degradation pathway and ecotoxicity assessment. *Sci. Total Environ.* 520, 23–31. <https://doi.org/10.1016/j.scitotenv.2015.03.033>.
27. Trawiński, J., Skibiński, R., 2017. Studies on photodegradation process of psychotropic drugs: a review. *Environ. Sci. Pollut. Res. Int.* 24 (2), 1152–1199. <https://doi.org/10.1007/s11356-016-7727-5>.
28. Trawiński, J., Skibiński, R., 2019. Rapid degradation of clozapine by heterogeneous photocatalysis. Comparison with direct photolysis, kinetics, identification of transformation products and scavenger study. *Sci. Total Environ.* 665, 557–567. <https://doi.org/10.1016/j.scitotenv.2019.02.124>.
29. *Science of the Total Environment* 756 (2021) 143805
30. Vione, D., Minella, M., Maurino, V., Minero, C., 2014. Indirect photochemistry in sunlit surface waters: Photoinduced production of reactive transient species. *Chem. Eur. J.* 20 (34), 10590–10606. <https://doi.org/10.1002/chem.201400413>.
31. Wu, M., Xiang, J., Que, C., Chen, F., Xu, G., 2015. Occurrence and fate of psychiatric pharmaceuticals in the urban water system of Shanghai, China. *Chemosphere* 138, 486–493. <https://doi.org/10.1016/j.chemosphere.2015.07.002>.
32. Xiang, J., Wu, M., Lei, J., Fu, C., Gu, J., Xu, G., 2018. The fate and risk assessment of psychiatric pharmaceuticals from psychiatric hospital effluent. *Ecotoxicol. Environ. Saf.* 150 (December 2017), 289–296. <https://doi.org/10.1016/j.ecoenv.2017.12.049>.
33. Xie, Z., Lu, G., 2019. Interactive effects of sertraline and diphenhydramine on biochemical and behavioural responses in crucian carp (*Carassius auratus*). *Int. J. Environ. Res. Public Health* 16 (17). <https://doi.org/10.3390/ijerph16173137>.

34. Zhu, M., Ma, L., Zhang, D., Ray, K., Zhao, W., Humphreys, W.-G., Skiles, G., Sanders, M., Zhang, H., 2006. Detection and characterization of metabolites in biological matrices using mass defect filtering of liquid chromatography/high resolution mass spectrometry data. *Drug Metab. Dispos.* 34 (10), 1722–1733. <https://doi.org/10.1124/dmd.106.009241>.

Chapter 5. Exploring the photolytic and photocatalytic transformation of Citalopram: kinetics, degradation mechanism and toxicity assessment

5.1. Abstract

This study investigated the direct and indirect photochemical degradation of citalopram (CIT), a selective serotonin reuptake inhibitor (SSRI), under natural and artificial solar radiation. Experiments were conducted in a variety of different operating conditions including Milli-Q (MQ) water and natural waters (lake water and municipal WWT effluent), as well as in the presence of natural water constituents (organic matter, nitrate and bicarbonate). Results showed that indirect photolysis can be an important degradation process in the aquatic environment since citalopram photo-transformation in natural waters was accelerated in comparison to MQ water both under natural and simulated solar irradiation. In addition, to investigate the decontamination of water from citalopram, TiO₂-mediated photocatalytic degradation was carried out, and attention was given to mineralization and toxicity evaluation together with the identification of by-products. The photocatalytic process gave rise to the formation of transformation products, eleven of them were identified by HPLC-HRMS, whereas the complete mineralization was almost achieved after 5 hours of

irradiation. The assessment of toxicity of the treated solutions was performed by Microtox bioassay (*Vibrio fischeri*) and in silico tests showing that citalopram photo-transformation involved the formation of harmful compounds.

5.2. Introduction

In the 2030 Agenda for Sustainable Development, adopted by UN Member States in 2015, one important goal is devoted to ensuring the availability and the sustainable management of water [1]. In this framework, the study concerning the fate of organic pollutants in the aquatic environment has the aim to assess if their release and the formation of by-products in the aqueous matrices can represent a potential health hazard. These aspects should be taken into consideration in order to implement the most suitable strategies to abate pollutants or to restrict their discharge in environment. Among the xenobiotic compounds that can have negative impacts on human health and aqueous ecosystems, the pharmaceuticals represent a class of greatest environmental concern due to their low degradability and their continuous inlet in the environmental waters [2,3].

Citalopram (CIT) is a selective serotonin reuptake inhibitor (SSRIs) widely used in Northern Europe as antidepressant drug and it has been detected in influent, effluent, downstream and hospital wastewater treatment plants (WWTPs) at concentration levels up to about 300-800 ngL⁻¹ [4,5]. There is a high range of half-lives on the literature for CIT depending on the pH of the sample, the matrices, the concentration of the pollutant and many other variables[6–9]. For example, J. Kwon et al. found a half-life of 65 days for citalopram in ultrapure water buffered at pH 9, 14 and 43 days in two different lakes and 24 days in a WWTP sample under a fluorescent lamp [7]. R. Osawa et al. reported that citalopram was 100% degraded after 4 hours under a UV lamp in a lake water sample[6]. The photodegradation of CIT was also reported to be induced by the natural organic matter, NOM, present in surface water [7]. Indeed, NOM that contains humified light-absorbing

compounds can photo-induce the degradation of chemicals through the generation of reactive species such as excited triplet states ($^3\text{DOM}^*$) [10], hydroxyl radical ($\cdot\text{OH}$) [11–13], singlet oxygen ($^1\text{O}_2$) [14,15], superoxide radical anion ($\text{O}_2^{\cdot-}$) and hydrogen peroxide (H_2O_2) [16].

CIT was classed as harmful substance with a value of EC50 equal to 30.14 mg L⁻¹ on *Daphnia magna* (48 h-exposure) without excluding possible chronic toxicity at lower exposure concentrations [17]. Recently, investigations about the effects of this antidepressant on the behavior of two different life stages of fish revealed that this drug poses potential risks for the aquatic environment and therefore its presence in water matrices has to be monitored carefully [18]. Previous studies showed that photolysis and hydrolysis do not significantly remove the molecule [19] and two of TPs identified during the photolytic process were found also as human metabolites [7]. Taking into account that CIT was moderately removed by the aerobic and anoxic biodegradation [20], some advanced water treatment technologies (e.g. O₃, ClO₂ oxidation, UV irradiation and Fenton oxidation) have been applied to abate CIT [4] with a particular focus on the transformation products formed during the processes. In the case of ozonization, the complete mineralization was not achieved in 90 min and the identified intermediates matched with those observed during the ClO₂ oxidation, even if with different abundances.

Considering that, once released in the aqueous environment, pollutants can undergo biotic and abiotic degradation [5,21,22], this work aimed to investigate the photoinduced fate of CIT under simulated and solar irradiation in MilliQ water and in the presence of dissolved organic matter (humic acids), bicarbonate and nitrate ions, as well in two real matrices (lake water and municipal WWT effluent). Moreover, in order to assess the possible application of heterogeneous photocatalysis to remove CIT in water, we performed irradiation experiments in presence of titanium dioxide, one of the most widely exploited semiconductors to abate several classes of water pollutants [22–24]. Particular attention was focused on the identification of transformation by-products formed during

the process using HRMS and on the evaluation of toxicity, performed by bioluminescent test (*Vibrio fischeri* bacterium) and *in silico* approach (US EPA ECOSAR computer model).

5.3. Materials and methods

5.3.1. Reagents and materials

Citalopram (1-[3-(dimethylamino)propyl]-1-(4-fluorophenyl)-3H-2-benzofuran-5-carbonitrile, hydrobromide), purity grade >95%, was purchased from LGC Promochem (Molsheim, France). For analytical purposes, citalopram (CIT) was dissolved in methanol to provide a stock solution containing 1000 mg L⁻¹ of analyte. The solution was stored in glass-stopped bottles at -20 °C in the dark. Standard working solutions were prepared daily. Ultrapure water used was produced by a Milli-Q system (Evoqua, Pittsburgh, USA). Photosensitizers: freeze-dried Suwannee River natural organic matter (NOM) was obtained from International Humic Substances Society (Denver, CO), NaNO₃ and NaHCO₃ were purchased from Sigma-Aldrich (Athens, Greece). Irradiation procedures of CIT were carried out by experimental solutions that were prepared by dissolving CIT directly in Milli-Q water (MQ), MQ water+sensitizers, WWTP effluent and lake water. Acetonitrile (≥99.9%) was purchased from Merck Life Science S.r.l. (Milan, Italy). TiO₂ P25 (Evonik Industries, Italy) was used as photocatalyst.

5.3.2. Sample collection

Effluent and lake water samples of 2.5 L were collected from the municipal WWTP of Ioannina city, and Pamvotis Lake, respectively, located in NW Greece, in the region of Epirus. After collection, the samples were transported to the lab and were immediately filtered with 0.45 µm polyamide filters. The filtered samples were then kept in the dark at -5 °C till the irradiation experiments. The most relevant physicochemical characteristics of the aqueous samples are provided in Table S1.

5.3.3. Irradiation procedures

5.3.3.1. Natural sunlight irradiation

Experiments were carried out in the roof terrace of the Department of Chemistry of Ioannina University (2018) in MQ water as well as natural waters (WWTP effluent and lake water) at 10 mg L⁻¹ of CIT. The solutions (1 L) were put into capped Pyrex glass bottles and were homogenized by magnetic stirring. Irradiation of the samples was conducted on platform with an inclination of 30° from the horizon, facing due south, following the recommendations of Environmental Protection Agency. Dark control experiments were also performed by exposing amber glass bottles at the same concentration and covered with aluminum foil in the same environmental conditions in order to calculate for other degradation processes like hydrolysis and biodegradation. Aliquots (1.0 mL) were withdrawn from the bottles at specific time intervals. The average total daily short-wave radiation was 286 and 273 W/m² for July and August, respectively, while the sunshine duration from sunrise to sunset was 10 and 11 h, for the two months, respectively. The mean daily air temperature was 23 and 26 °C, with minimum air temperature at 17 and 18 °C and maximum air temperature at 26 and 32 °C, for July and August, respectively. Experiments were carried out in duplicate.

5.3.3.2. Simulated solar irradiation

Photodegradation experiments were also carried out at the same aqueous matrices and CIT concentration in a sunlight simulator (Solarbox, CO.FO.Me.Gra, Milan) equipped with a xenon lamp (1500 W) with a cut-off filter at below 340 nm. On top of the solutions the irradiance was 18 W m⁻² in the 295–400 nm range (like the natural sunlight UV irradiance at middle European latitude in sunny days) [40]. Irradiation was carried out in magnetically stirred cylindrical closed cells (Pyrex glass, 40 mm i.d. 25 mm), on 5 mL aqueous solutions containing 10 mgL⁻¹ of CIT and were subjected to different irradiation times.

To test whether DOM, nitrate and bicarbonate ions (10 mgL⁻¹ each), affect the photodegradation rate of CIT solutions (1 mgL⁻¹), MQ water containing the above sensitizers were exposed to the same irradiation conditions. All experiments were carried out in triplicate including dark controls that were performed under the same conditions.

The rate constants were calculated by linear regression analysis of the plot of the first-order equation $C_t = C_0 e^{-kt}$, where C_0 is the initial concentration, C_t is the concentration at a certain time and k is the rate constant. The half-life is calculated by $t_{1/2} = \ln 2/k$.

5.3.3.3. Photocatalytic experiments

Photocatalytic experiments were performed in the same cylindrical closed cells on 5 mL aqueous solutions containing 20 mgL⁻¹ of CIT and 400 mgL⁻¹ TiO₂. Samples were subjected to different irradiation times (ranging from 5 min to 3 h), using the 40 W Philips TL K05 lamp. After illumination, the samples were filtered through 0.45 μm Millex LCR hydrophilic PTFE membranes (Millipore) before the analysis. The lamp irradiance over the irradiated solutions was around 30 Wm⁻² in the wavelength range of 290–400 nm (measured with a power meter from CO.FO.ME.GRA., Milan, Italy).

5.3.4. Analytical procedures

Concentrations of CIT under all irradiation conditions was monitored with a Merck-Hitachi chromatograph equipped with Rheodyne injector (20 μL sample loop), L-6200 and L-6200A pumps for high-pressure gradients, L-4200 UV-vis detector, and RP-C18 column (Lichrospher, 4mm i.d.× 125 mm length, from Merck). Isocratic elution (1 mL/min flow rate) was carried out with 80% of 0.01 M phosphoric acid solution at pH 2.8 and 20 % acetonitrile. The detector wavelength was 239 nm.

The formation of ionic products in samples irradiated with simulated solar light, was followed by a suppressed ion chromatography, employing a Dionex DX 500 instrument (Thermo Scientific) equipped with a conductometer detector (ED 40, Dionex). The anions (nitrate and nitrite) were

separated by an AS9HC anionic column (200 mm long × 4 mm i.d.) using an aqueous solution of K₂CO₃ (9 mM) as mobile phase; the elution was performed at 30 °C, at a flow rate of 1mL/min. The determination of ammonium ions was performed by employing a CS12A column, using 25mM methanesulfonic acid as eluent, at a flow rate of 1mL/min.

The evolution of the dissolved organic carbon (DOC) during the photocatalytic runs was followed using a Shimadzu TOC-V CSH (catalytic oxidation on Pt at 680 °C) equipped with a Shimadzu ASI-V autosampler. Calibration was achieved by injection of known amounts of potassium phthalate.

5.3.5. Identification of by-products

HPLC-HRMS was used to determine and elucidate CIT and its by-products under photocatalytic conditions. The chromatographic separations, monitored using an MS analyzer, were carried out with a Phenomenex Gemini NX C18 150 × 2.1 mm × 3 μm particle size (Phenomenex, Bologna, Italy), using an Ultimate 3000 HPLC instrument (Dionex, Thermo Scientific, Milan, Italy). Injection volume was 20 μL and flow rate 200 μLmin⁻¹. The following gradient mobile phase composition was adopted: A/B was varied from 5/95 to 50/50 in 30 min, followed by second step to reach 100/0 in 5 min where A = formic acid 0.05% v/v in acetonitrile and B = formic acid 0.05% v/v in water. A LTQ Orbitrap mass spectrometer (Thermo Scientific, Milan, Italy) equipped with an ESI ion source was used. The LC column effluent was delivered into the ion source using nitrogen as both sheath and auxiliary gas. The capillary voltage and tube lens voltage in the ESI source were maintained at 28 V and 70 V, respectively. The source voltage was set to 4.5 kV (in positive ion mode). The capillary temperature was maintained at 270°C. The acquisition method used was optimized beforehand in the tuning sections for the parent compound (capillary, magnetic lenses and collimating octapole voltages) to achieve maximum sensitivity. Mass accuracy of recorded ions (vs calculated) was ± 5 ppm, without internal calibration. Analyses were run using full scan MS (50–1000

m/z range), MS² acquisition in the positive ion mode, with a resolution of 30,000 (500 m/z FWHM) in FTMS (full transmission) mode. The ions submitted to MS² acquisition were chosen on the base of full MS spectra abundance without using automatic dependent scan. Collision energy was set to 30% for all the MS² acquisition methods. MS² acquisition range was between the values of ion trap cut-off and m/z of the [M+H]⁺ ion. Xcalibur (Thermo Scientific, Milan, Italy) software was used both for acquisition and data analysis.

5.3.6. Toxicity measurements

The toxicity samples collected at different irradiation times was evaluated with a Microtox Model 500 Toxicity Analyzer (Milan, Italy). Acute toxicity was determined with a bioluminescence inhibition assay using the marine bacterium *Vibrio fischeri* by monitoring changes in the natural emission of the luminescent bacteria when challenged with toxic compounds. Freeze-dried bacteria, reconstitution solution, diluent (2% NaCl) and an adjustment solution (non-toxic 22% sodium chloride) were obtained from Azur (Milan, Italy). Samples were tested in a medium containing 2% sodium chloride, in five dilutions, and luminescence was recorded after 5, 15, and 30 min of incubation at 15 °C. Since no substantial change in luminescence was observed between 5 and 30 min, the results related to 15 min of contact are reported below. Inhibition of luminescence, compared with a toxic-free control to give the percentage inhibition, was calculated following the established protocol using the Microtox calculation program.

Moreover, since the identified TPs of CIT are not commercially available, three different software were employed ECOSAR (v. 2.0), Toxicity Estimation Software Tool T.E.S.T. (v. 5.1.1) and Vega (v. 1.1.5).

5.4. Results and discussion

5.4.1. Irradiation experiments

5.4.1.1. Natural sunlight experiments

Experiments were carried out in MQ water as well as natural waters (lake and WWTP samples) at 10 mgL⁻¹ of CIT. The quality parameters for the collected lake and WWTP samples are presented in Table S1 and S2. All the studied samples were characterized by a medium-to-high abundance of organic matter [25], with a DOM values of 23.2 and 11.7 mgL⁻¹ for WWTP effluent and lake water, respectively. Nitrate in these waters was significantly higher in WWTP than in lake samples (86.1 and 10.5 mgL⁻¹, respectively).

Dark controls were found to be stable for all treatments, as less than 10% was degradation over the course of the exposure period. This hydrolytically stable behavior has been observed also by Kwon and Armbrust [7]. Considering the UV/Vis absorption spectrum of CIT, reported in a previous work [26], and the low absorbance above 290 nm, direct photolysis rate in MQ water seems to be low with a half-life of 144 days (Figure 5.1 and Table 5.1) under the investigated conditions, revealing that CIT is a highly photostable molecule under these conditions.

On the other hand, the photodegradation rates of CIT in wastewater and lake water were significantly higher than in MQ water, thus showing that the aqueous matrix played a significant role in promoting the photolysis of CIT. When exposed to natural sunlight in wastewater, CIT photodegradation rate was 2.8-fold faster compared to MQ water. This sensitization effect was also observed for lake water as well. The CIT photodegradation rate was almost 2.4 times higher in lake water compared to MQ, indicating a photosensitization effect in the respective aqueous matrices. In order to confirm this relationship and to assess the contribution of different natural aqueous constituents, experiments at the same water matrices and as well in the presence of NOM, nitrate and bicarbonate ions were carried out in laboratory-simulated irradiations.

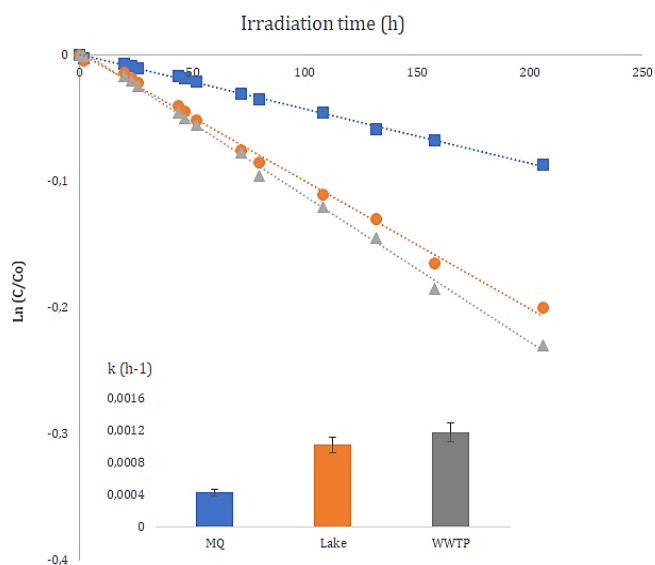


Figure 5.1. Kinetics and rate constant (h^{-1}) of citalopram in different matrices under natural solar light.

Table 5.1. Kinetics of the photolysis of citalopram in different aqueous media under solar and simulated solar irradiation.

Photolysis	$t_{1/2}$ (hrs)	k (hrs^{-1})	R^2
<i>Solar irradiation (outdoor)</i>			
MQ water	3465.74	0.0002	0.9461
Lake Pamvotis	693.15	0.0010	0.9805
WWTP water	462.10	0.0015	0.9821
<i>Simulated solar irradiation (solar box)</i>			
MQ water	61.89	0.0112	0.9486
Lake Pamvotis	25.77	0.0269	0.9940
WWTP water	23.42	0.0296	0.9811
HA^- 10 mg L^{-1}	14.03	0.0494	0.9783
NO_3^- 10 mg L^{-1}	45.60	0.0152	0.9409
HCO_3^- 10 mg L^{-1}	27.08	0.0256	0.9604

5.4.1.2. Simulated solar irradiation experiments.

Figure 5.2 depicts the experimental degradation profiles of CIT among the photolysis rate constants for the three matrices. All degradation curves matched well a pseudo-first order kinetic model with r^2 generally above 0.94. The half-lives $t_{1/2}$ ranged between 62 h in MQ water to 23 h in WWTP effluent (Table 5.1).

At the same conditions, no degradation has been observed in dark controls in either MQ water or lake/WWTP samples, indicating that the compound under investigation was hardly susceptible to hydrolysis. Photolysis rates followed the same order as the natural sunlight experiments: WWTP > lake > MQ water, indicating that constituents of natural waters affect CIT's decomposition [26]. According to Table S1 and S2, natural organic matter (NOM) concentration is higher in WWTP, followed by the lake, showing that as the NOM concentration increases in natural waters, the rate of photolysis increases.

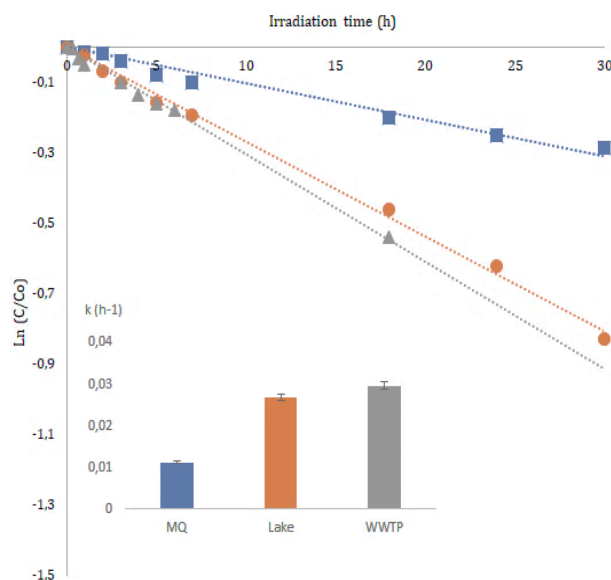


Figure 5.2. Kinetics and rate constant (h^{-1}) of citalopram in different matrices under artificial solar irradiation.

Hence, in order to further elucidate the role of organic matter on the performance of the photolytic process, Suwannee River natural organic matter was used as representative of NOM at a concentration level of 10 mgL^{-1} in MQ water. A significant acceleration effect of the photolytic rate was observed. In a previous study we have shown that Water Extractable Organic Matter (WEOM) was able to produce oxidant triplet excited state ($^3\text{WEOM}^*$), singlet oxygen ($^1\text{O}_2$), and hydroxyl radicals under irradiation with simulated solar light [11]. Apart from NOM, the effect of nitrate and carbonate ions on the photolytic rate were also investigated (Table 5.1). The results demonstrated that nitrate at 10 mgL^{-1} enhanced the photolytic rate of CIT, as well as carbonate (in the presence of 1 mgL^{-1} of nitrate), but to lesser extent in agreement with Kwon and Armbrust, 2005 [7].

The results showed that degradation order in artificial-laboratory irradiation experiments are in good agreement with experiments under natural sunlight, suggesting that laboratory-scale experiments using artificial irradiation can help predicting the behavior of CIT in natural waters [27]. However, the photodegradation rate of each case cannot be compared directly due to differences in the irradiation spectrum and daily light variation (night-day circle) [27,28]. Both of these experimental approaches should be viewed as complementary and proxies for the processes that occur in real waters by providing a better understanding of the photodegradation actually occurring in natural environment [29,30].

Nevertheless, the time needed for the total elimination of the antidepressant in the natural environment, seemed to be far from effective, therefore heterogeneous photocatalysis was assessed as an effective method of decontamination.

5.4.1.3. Photocatalytic experiments

As expected, the presence of semiconductor accelerated the degradation of the pollutant. Under the adopted experimental conditions, the complete abatement of CIT by heterogeneous photocatalysis occurred in around half hour (see Figure 5.3), whereas the organic carbon

mineralization processed much slower than the primary process. About 50% of initial TOC content was mineralized within 1 h of irradiation, but only after 5 hours TOC residual percentage reached a value <10%. The delay between the primary process and TOC evolution was attributed to the formation of TPs.

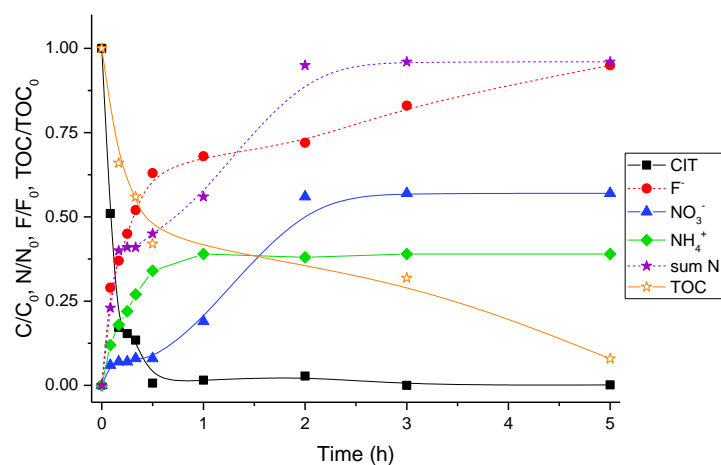


Figure 5.3. Time evolution of primary process, end-inorganic products (nitrate, ammonium, and fluoride) and organic carbon during the photocatalytic degradation of CIT (CIT 20 mgL⁻¹, TiO₂ 200 mgL⁻¹).

Nitrogen was released over time as nitrate and ammonium ions and the stoichiometric amount was achieved within 2h. Ammonium was more easily released and reached a plateau value at 60 min, while nitrate ions exhibited a sharp increase later between 1 and 2 h. Taking into account that the cyano group is mainly transformed into nitrate [31], the evolution of this ion suggested that the oxidative process occurred on this part of molecule only at longer times of irradiation. The identification of several transformation products (see below) that still bear a carbonitrile substituent agreed with this hypothesis. No traces of nitrite ions were detected under the employed

experimental conditions. During the photocatalytic degradation, we also followed the evolution of fluoride arising from the breaking of bond C-F present in the molecular structure. Like nitrogen trend, the fluoride concentration reached the 50% of stoichiometric concentration within half hour and then achieved the maximum after 5 h.

5.4.2. Identification and evolution of TPs

The HRMS analysis allowed us to identify and characterize eleven transformation products of CIT formed during the first steps of photocatalytic process, and they are collected in Table 5.2 and Table S3. A level of confidence recommended by Schymanski et al. [32] was assigned to each TP and is reported in Table 2 as well. Although already present in the literature [6], the MS² spectrum of CIT (m/z 325.1718) is reported in Figure S1 for the sake of clarity. Therein, it can be observed the fragment at m/z 307.1612 arising from the loss of water (H₂O), together with the rearrangement of furan ring and the fragment at m/z 280.1139 due to the loss of dimethylamine. The detachment of both groups justifies the base peak at m/z 262.1032, whereas the fragment at m/z 109.0445 is consistent to the fluorotropylium ion formation.

Two signals at m/z 341.1669 and chemical formula C₂₀H₂₂O₂N₂F were detected and attributed to monohydroxylated products (TP341A, B), where the OH attack was supposed to occur on the lateral chain.

The MS² spectrum of TP341A (see Figure S2) suggests that the hydroxylation involved the lateral chain giving an intermediate already identified in the presence of organic matter [26] and during the UV and hydrolysis processes [6]. Indeed, the base peak at m/z 323.1554 shows that the loss of the first molecule of H₂O is more favorable than that observed for CIT, as not entailing the rearrangement of furan ring that conversely can be involved to justify the second H₂O loss (m/z 305.1455).

Table 2. CIT and its TPs observed during the photocatalytic process.

Name, [M+H] ⁺	Empirical formula	Δ ppm	RT (min)	Confidence level
Citalopram-325.1718	C ₂₀ H ₂₂ ON ₂ F	2.251	19.92	L1
T245A-245.1292	C ₁₄ H ₁₇ O ₂ N ₂	3.042	6.54	L2b
T245B- 245.1292	C ₁₄ H ₁₇ O ₂ N ₂	3.042	8.41	L2a
T247-247.1446	C ₁₄ H ₁₉ O ₂ N ₂	2.005	5.79	L3
T261-261.1241	C ₁₄ H ₁₇ O ₃ N ₂	2.800	8.13	L2a
T323-323.1762	C ₂₀ H ₂₃ O ₂ N ₂	2.462	14.16	L2a
T337-337.1554	C ₂₀ H ₂₁ O ₃ N ₂	2.168	13.93	L3
T339-339.1512	C ₂₀ H ₂₀ O ₂ N ₂ F	2.558	18.92	L2a
T341A-341.1669	C ₂₀ H ₂₂ O ₂ N ₂ F	2.689	17.40	L3
T341B-341.1669	C ₂₀ H ₂₂ O ₂ N ₂ F	2.689	18.70	L2b
T355-355.1457	C ₂₀ H ₂₀ O ₃ N ₂ F	1.275	17.84	L3
T357-357.1618	C ₂₀ H ₂₂ O ₃ N ₂ F	2.528	16.42	L3

Regarding the TP341B, detected in this work for the first time, the MS² spectrum reported in Figure S3 shows some peculiar differences. The abundance of the fragment at m/z 323.1560 and the absence of m/z 305.1449 are still consistent with the presence of a hydroxyl group on the chain, but in a position close to the furan ring, thus hindering the loss of a second molecule of H₂O. The detachment of NH(CH₃)₂ and the further loss of H₂O lead to the formation of the fragments at m/z 296.1088 and m/z 278.0981, respectively. The presence in the MS² spectrum of a fragment corresponding to fluorotropylium (m/z 109.0444), also detected for CIT, excludes the hydroxylation involved the fluorophenyl moiety. However, the formation of TP339 (*vedi infra*) may suggest an OH attack on the furan ring, although in this case, the loss of a molecule of H₂O should be less favored.

The intermediate TP357 at $[M + H]^+$ 357.1618 and empirical formula $C_{20}H_{22}O_3N_2F$ indicated the formation of a dihydroxylated product. This TP was identified here for the first time; it presents in its MS² spectrum two main peaks only, attributable to the loss of two H₂O molecules (see Figure S4), likely from the furan ring and the alkyl chain. Considering the overall degradation pathway, it was reasonable to assume that the hydroxylation involved both the furan ring and alkyl chain.

Concerning the TP323 (m/z 323.1762), the elemental composition $C_{20}H_{23}O_2N_2$ has been proposed, consistent with the substitution of the fluorine atom by an OH group on the benzene ring bearing to the formation of a phenol structure. To support this statement and in agreement with the literature [4,26], the MS² fragmentation pathway appears similar to that observed for CIT with the formation however of hydroxytropylium ion (m/z 107.04888) as reported in Figure S5.

The TP339 (m/z 339.1512 and chemical formula $C_{20}H_{20}O_2N_2F$) can be assigned to an oxidized product. The MS² spectrum (Figure S6) matches well with the data reported in the literature [6,26]; the key fragment with m/z 248.0876 can be explained by the loss of a CO group, thus supporting the formation of a carbonyl group on the furan ring.

A transformation product with m/z 355.1457 and chemical formula $C_{20}H_{20}O_3N_2F$ was detected (TP 355) and is consistent with the hydroxylation of TP339 [26]. The RDB for this intermediate was higher than that of CIT, also suggesting the formation of a carbonyl group for this by-product. The MS² spectrum (see Figure S7) reports a fragment at m/z 337.1353 resulting from the loss of a molecule of H₂O and the base peak at m/z 292.0775 arising by the joint loss of $NH(CH_3)_2$ and H₂O. Considering the abundance of m/z 337.1353 (60%), we can hypothesize the presence of an OH on the alkyl chain that promotes this fragmentation. A further loss of the CO group involving the furan ring generates the signal at m/z 264.0825, thus confirming the presence of a carbonyl group. Finally, the fragment at m/z 274.0668 arises from the joint loss of two molecules of H₂O, one of which entailed the furan ring, and of the dimethylamine group.

The analysis of MS² spectrum of TP337 (Figure S8) suggested a dehalogenated structure bearing an OH group and a carbonyl group, as reported in the literature [6]. However, the fragment at m/z 319.1447 (-18 Da) is not very intense, indicating that, in this case, the loss of H₂O involves the rearrangement of furan ring in the CIT spectrum and not from an OH group present on the chain. Furthermore, the peak base at m/z 274.0868 corresponds to the contemporaneous loss of one molecule of H₂O and NH(CH₃)₂ group, whereas a further loss of H₂O molecule is observed at very low intensity as it occurs on the fluorobenzene ring (m/z 256.1762). For the above-mentioned reasons, differently from the hypothesis of Osawa and co-workers [6], it may be assumed that the hydroxylation occurred on the benzene ring alongside the detachment of the fluorine atom, as already reported for the photocatalytic degradation of similar structures [33].

TP247 (m/z 247.1446 and chemical formula C₁₄H₁₉O₂N₂) is involved in the detachment of the fluorophenyl ring together with mono-hydroxylation. Unfortunately, the MS² shows only one abundant fragment at m/z 229.1339 due to the loss of H₂O (Figure S9), which is not useful to determinate the exact position of an OH attack. Taking into account the main mechanisms occurring in the photocatalytic degradation, it can be hypothesized that a substitution by an OH radical on the quaternary carbon that loses the aromatic ring, supported by the formation of unsaturated system in the fragment m/z 184.0757, which can prevent the rearrangement of furan ring and the loss of a second molecule of water.

Two isomers were detected with m/z 245.1292 corresponding to the chemical formula C₁₄H₁₇N₂O₂. They can be attributed to the formation of TPs resulting from the detachment of fluorophenyl group, analogously to the TP247, with the presence of a carbonyl group (Figure 10S and 11S). As observed for CIT and reported in literature [6], the MS² spectrum of TP245B exhibits a fragment at m/z 227.1183 that can be explained by the loss of H₂O and the most intense peak at m/z 200.0708 arising from the loss of dimethylamine group. The signal at m/z 182.0602 is ascribable to the loss of both H₂O and NH(CH₃)₂ molecules, whereas the fragment at m/z 158.0236 with chemical

formula $C_9H_4O_2N$ can be explained by the presence of the carbonyl group on the furan ring. As regards the TP245A, it can be hypothesized by a different position of the carbonyl group, as the MS² spectrum shows only a fragment at m/z 200.0708. The absence of signals arising from the H₂O loss can be justified by the involvement of the carbon in the chain in the α position in respect to the furan ring that prevented the rearrangement of molecule favoring only the loss of NH(CH₃)₂.

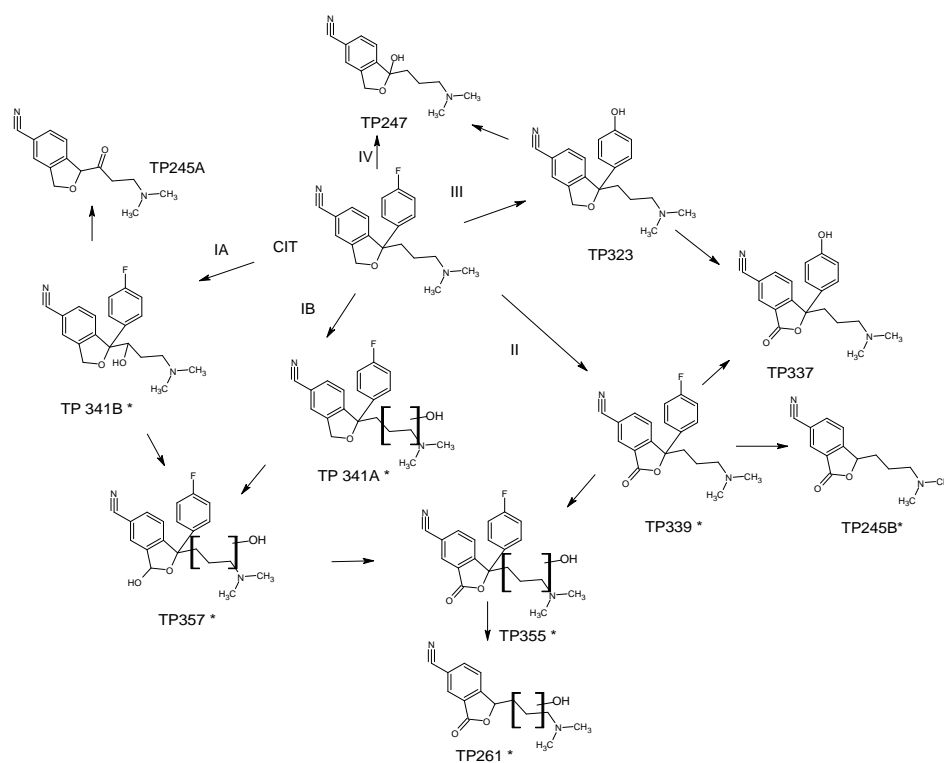
The TP261 with m/z 261.1241 and chemical formula $C_{14}H_{17}O_3N_2$ involves a further hydroxylation of TP245 (see Figure S12). The fragmentation pattern in MS² suggests the formation of an intermediate similar to TP245B but with a further hydroxylation on the alkyl chain in agreement with the literature [6]. The high abundance of the fragment at m/z 243.1132 corresponding to the loss of H₂O suggests that the hydroxylation did not occur on the aromatic moiety, whereas the signal at m/z 216.659 is consistent with the detachment of NH(CH₃)₂. The concomitant loss of H₂O and dimethylamine agreed with the fragment observed at m/z 198.0552 for which the chemical formula $C_{12}H_8O_2N$ was proposed. In contrast with photolytic process, no *N*-oxygenation and *N*-demethylation derivatives were detected during the photocatalytic treatment in the adopted experimental conditions.

Based on MS data and the time evolution of TPs reported in Figure S13, a possible pathway for the early steps of CIT degradation is proposed in Scheme 5.1.

The photocatalytic degradation of CIT proceeds through the formation of mono- and di-hydroxylated intermediates (route IA and IB), where the OH attack involves primarily the alkyl chain and the furan ring producing the TP341A, B and T357.

Furthermore, the heterocycle structure can undergo oxidation to give the TP339 following the route II with the formation of a carbonyl group on the structure. The oxidized and hydroxylated intermediate TP355 can be yielded by pathways I and II, as it can be generated by hydroxylation of TP339 or oxidation of TP357.

The subsequent steps of degradation result in the detachment of the fluorophenyl group with the formation of TP261 and TP245B, the former arising from TP355, and the second from TP339 and TP337. The TP245A also shares a similar structure but it can be supposed to be produced from TP341B by a further oxidation of alcoholic group on the alkyl chain to a carbonyl group. The route III provides for the substitution reaction leading to the formation TP323 where the fluorine atom in the phenyl moiety is replaced by an OH group. Successively, the oxidation of this intermediate on the furan ring produces TP337 that can also be obtained through the route II via the dehalogenation/hydroxylation of TP339. Finally, the TP247 can be formed through the path IV or from TP323 by the substitution of the fluorophenyl moiety by the OH group.



Scheme 5.1. Pathway proposed for CIT

Four of the identified intermediates in photocatalytic treatment were also detected during the direct photolysis in MQ and they have been marked in the Scheme 5.1. with an asterisk.

In photocatalytic experiment, TP341 A, B and TP339 were the most abundant and they achieved the maximum concentrations during the first few minutes of treatment. Then all transformation products of photocatalysis were totally degraded after 60 min, and the evolution profiles of TPs are shown in Figure S13.

5.4.3. Toxicity assessment

The acute toxicity trend during the treatment was also assessed using the *Vibrio fischeri* assay (Figure 5.4). An increased percentage of inhibition was observed within the first stages of photocatalytic degradation reaching the maximum value of ca. 30 % after 20 min, justified by the formation of transformation products moderate harmful toward bacteria. However, afterwards, the toxicity slowed down, settling at negligible value (~5%) at the end of treatment in agreement with the organic carbon content reduction described in Figure 5.3.

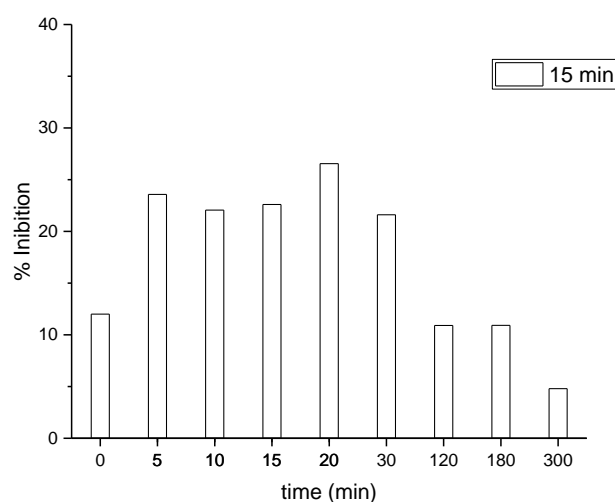


Figure 5.4. Acute toxicity of CIT as a function of the irradiation time, in the presence of TiO₂.

In a previous study, the toxicity evaluated *in silico* reported for some of identified TPs during AOPs treatments a higher toxicity towards *T. Pyriformis* in respect to CIT and mutagenic and carcinogenic effects [6]. However, these previous results depend on type of text employed and do not consider the simultaneous presence of several TPs, so synergistic, antagonistic and additive effects cannot be excluded.

Furthermore, the latest versions of TEST and Vega software were employed along with ECOSAR to compare the aquatic toxicity results obtained by luminous bacterium test. The evaluation of toxicity was estimated with the use of several models (Table 5.3), and therefore, principal component analysis(PCA) was applied to facilitate the interpretation of the information obtained graphically (Figure 5.5).

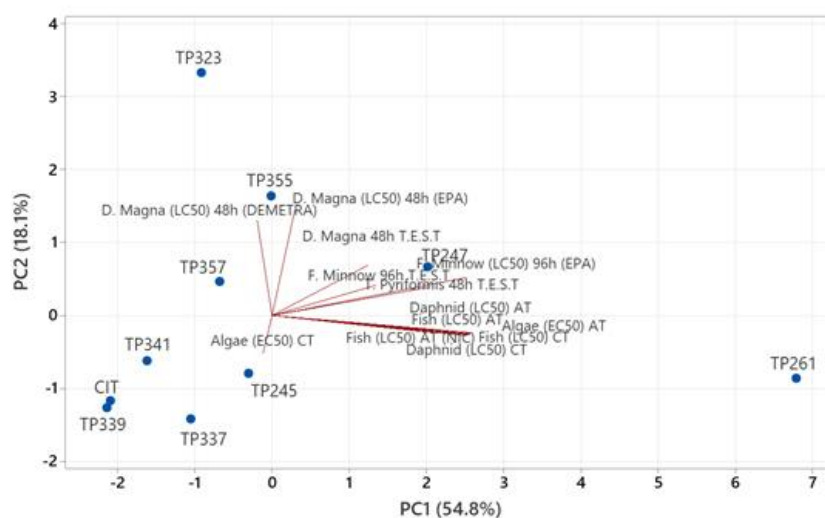


Figure 5.5. Comparison of aquatic toxicity of CIT TPs by PCA.

In total, 13 models were applied, namely, acute for Daphnid LC50 48 h, Fish LC50 96 h and Green Algae EC50 96 h, and chronic for Daphnid LC50, Fish LC50 Green Algae EC50, (by ECOSAR), *D. magna* LC50 48 h, *F. minnow* LC50 96 h, *T. pyriformis* IGC50 48 h (by T.E.S.T.), *D. magna* LC50 48 h

DEMETRA, Fish Acute NIC model and *F. minnow* LC50 96 h EPA model (Vega software). Raw data concerning aquatic toxicity are presented in Table 5.3. Based on the PCA calculations (Figure 5.5), the applied models were not strongly correlated (PC1 and PC2 explained 54.8% and 18.1% of the total data variance, respectively). The ECOSAR, T.E.S.T. and *F. minnow* LC50 96 h EPA models provided rather similar results in the same direction. The other models predicted a zero correlation since the angle between vectors was close to 90°. Thus, *D. magna* LC50 48 h EPA and LC50 48 h DEMETRA, or -90° Algae (EC50) CT. TP339, TP341 A-B, TP245 A-B, TP337 and TP357, were grouped along with the parent compound in a cluster. TP339 was more toxic than the parent molecule in 9 of the 13 models, while TP261 was found to be the less toxic compound (Table 5.3). Our findings support that irradiation treatment of pharmaceuticals can result in compounds that are more harmful than the parent substance [34].

5.5. Conclusions

The photolytic behavior of the antidepressant drug CIT was investigated under both natural and simulated solar irradiation conditions, and its removal from water exploiting heterogeneous photocatalysis was evaluated. Direct photolysis of CIT proceeds very slowly; however, indirect photolytic process plays a significant role on its environmental attenuation in the aqueous matrices. As expected, the use of TiO₂ greatly increased the degradation rate of CIT and brought about the formation of several TPs. Eleven transformation products were identified and characterized by means of high-resolution mass spectrometry. The complete abatement of CIT occurred at around 30 min, whereas the organic carbon mineralization proceeded in a much slower rate. Toxicity studies have shown that a few transformation products (mainly TP339) are more toxic than the parent molecule; however, the TiO₂-based photocatalysis has been demonstrated to have a good efficiency to remove them completely.




Funding: This paper is part of a project that has received funding from the European Union's Horizon 2020 research and innovation programme under the Marie Skłodowska-Curie grant, agreement no. 765860 (AQUALity).

	Fish (LC ₅₀) AT	Daphnid (LC ₅₀) AT	Algae (EC ₅₀) AT	Fish (LC ₅₀) CT	Daphnid (LC ₅₀) CT	Algae (EC ₅₀) CT	F. Minnow 96h T.E.S.T	D. Magna 48h T.E.S.T	T. Pyriformis 48h T.E.S.T	Fish (LC ₅₀) AT (NIC)	F. Minnow (LC ₅₀) 96h (EPA)	D. Magna (LC ₅₀) 48h (EPA)	D. Magna (LC ₅₀) 48h (DEMETRA)
CIT	4.47	0.652	0.36	0.14	0.065	0.14	1.2	0.34	7.99	1.06	2.92	0.0084	2.26
TP245A,B	260	27.2	29.1	22.7	1.97	8.8	4.2	1.26	27.1	62.9	12.38	0.0593	1.41
TP247	589	57.8	70	61.9	3.94	20.2	16.75	1.58	90.1	63.4	29.23	0.1288	11.44
TP261	2840	248	379	427	15.1	101	5.62	3.36	66.57	67.03	48.58	0.1326	5.54
TP337	294	31.2	32	24.2	2.29	988	2.29	2.57	12.31	0.4955	7.35	0.0187	2.33
TP323	61.6	7.35	6.06	3.58	0.604	2.01	3.24	2.65	20.76	1.06	23.93	0.4744	80.03
TP339	21.3	2.77	1.93	0.954	0.247	0.68	0.59	0.36	5.54	0.0835	1.63	0.0068	1.04
TP341A,B	48	5.86	4.62	2.6	0.493	1.56	2.29	1.75	16.64	0.5014	5.73	0.0195	6.49
TP355	249	26.9	27	19.7	2.01	8.35	5.25	4.7	42.33	0.0879	20.07	0.336	10.1
TP357	279	29.8	30.5	22.5	2.21	9.36	3.01	0.94	43.23	0.0879	13.44	0.2764	12.09

Table 5.3. Aquatic toxicity of CIT and its TPs (mg L⁻¹).

Article

Investigation of the Aquatic Photolytic and Photocatalytic Degradation of Citalopram

Cristina Jiménez-Holgado ¹, Paola Calza ², Debora Fabbri ^{2,*} , Federica Dal Bello ³ , Claudio Medana ³ 
and Vasiliios Sakkas ¹

¹ Laboratory of Analytical Chemistry, Department of Chemistry, University of Ioannina, 45110 Ioannina, Greece; krijimhol@gmail.com (C.J.-H.); vsakkas@uoi.gr (V.S.)

² Department of Chemistry, University of Torino, Via Giuria 5, 10125 Torino, Italy; paola.calza@unito.it

³ Department of Molecular Biotechnology and Health Sciences, University of Torino, Via Giuria 5, 10125 Torino, Italy; federica.dalbello@unito.it (F.D.B.); claudio.medana@unito.it (C.M.)

* Correspondence: debora.fabbri@unito.it; Tel.: +39-0116705278

Abstract: This study investigated the direct and indirect photochemical degradation of citalopram (CIT), a selective serotonin reuptake inhibitor (SSRI), under natural and artificial solar radiation. Experiments were conducted in a variety of different operating conditions including Milli-Q (MQ) water and natural waters (lake water and municipal WWT effluent), as well as in the presence of natural water constituents (organic matter, nitrate and bicarbonate). Results showed that indirect photolysis can be an important degradation process in the aquatic environment since citalopram photo-transformation in the natural waters was accelerated in comparison to MQ water both under natural and simulated solar irradiation. In addition, to investigate the decontamination of water from citalopram, TiO₂-mediated photocatalytic degradation was carried out and the attention was given to mineralization and toxicity evaluation together with the identification of by-products. The photocatalytic process gave rise to the formation of transformation products, and 11 of them were identified by HPLC-HRMS, whereas the complete mineralization was almost achieved after 5 h of irradiation. The assessment of toxicity of the treated solutions was performed by Microtox bioassay (*Vibrio fischeri*) and in silico tests showing that citalopram photo-transformation involved the formation of harmful compounds.

Keywords: citalopram; photocatalytic degradation; transformation products; high-resolution mass spectrometry; toxicity; photodegradation



Citation: Jiménez-Holgado, C.; Calza, P.; Fabbri, D.; Dal Bello, F.; Medana, C.; Sakkas, V. Investigation of the Aquatic Photolytic and Photocatalytic Degradation of Citalopram. *Molecules* **2021**, *26*, 5331. <https://doi.org/10.3390/molecules26175331>

Academic Editor: Polonca Trebse

Received: 22 July 2021

Supplementary Materials

Table S1. Physicochemical properties of Lake Pamvotis.

Parameter	Value
pH	8.3
Conductivity ($\mu\text{S cm}^{-1}$)	262
TDS (mg L^{-1})	2213
NOM (mg L^{-1})	11.7
NO_3^- (mg L^{-1})	10.5
Br^- (mg L^{-1})	0.38
NO_2^- (mg L^{-1})	0.010
Cl^- (mg L^{-1})	88.0
HPO_4^{2-} (mg L^{-1})	0.03
NH_4^+ (mg L^{-1})	0.21

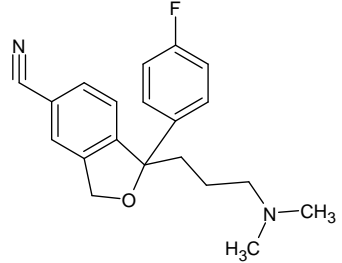
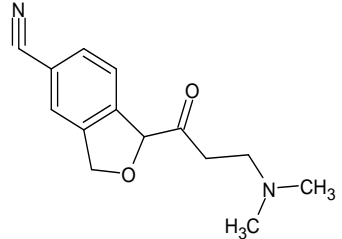
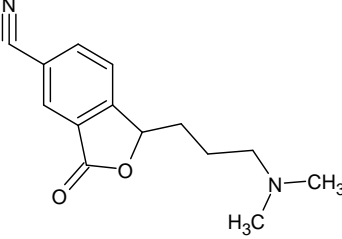
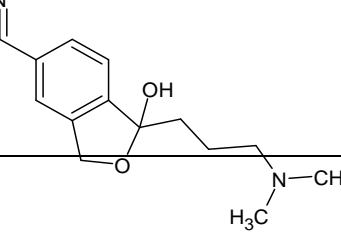
TDS: Total Dissolved Solids; NOM: Natural Organic Matter

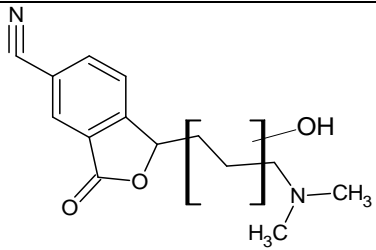
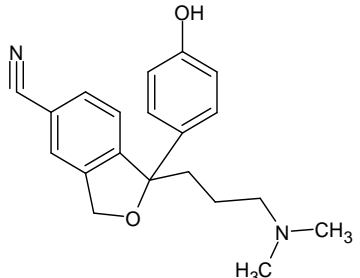
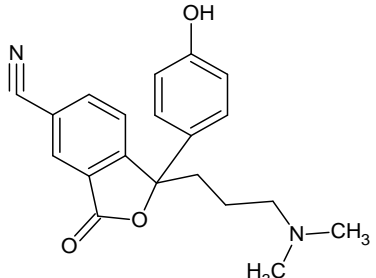
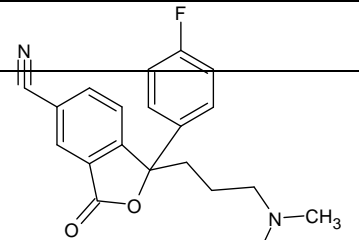
Table S2. Physicochemical characteristics of WWTP effluent aqueous sample

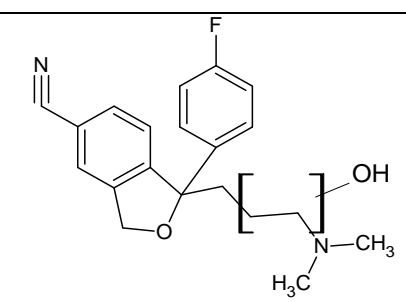
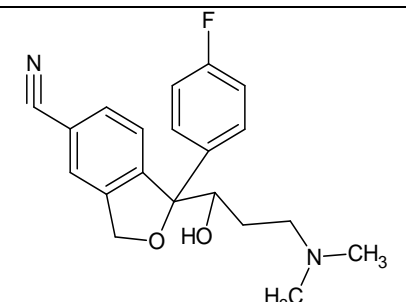
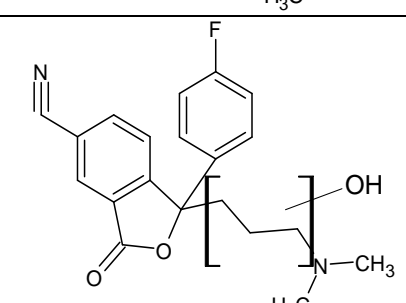
Parameter	Effluent of WWTP
pH	7.4
NOM ^a (mg L^{-1})	23.2
NO_3^- (mg L^{-1})	86.1
P total (mg L^{-1})	1.0
N total (mg L^{-1})	13.5

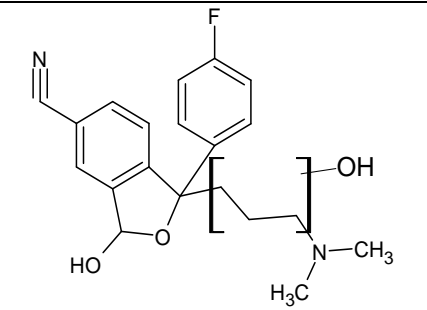
^a NOM: natural Organic Matter

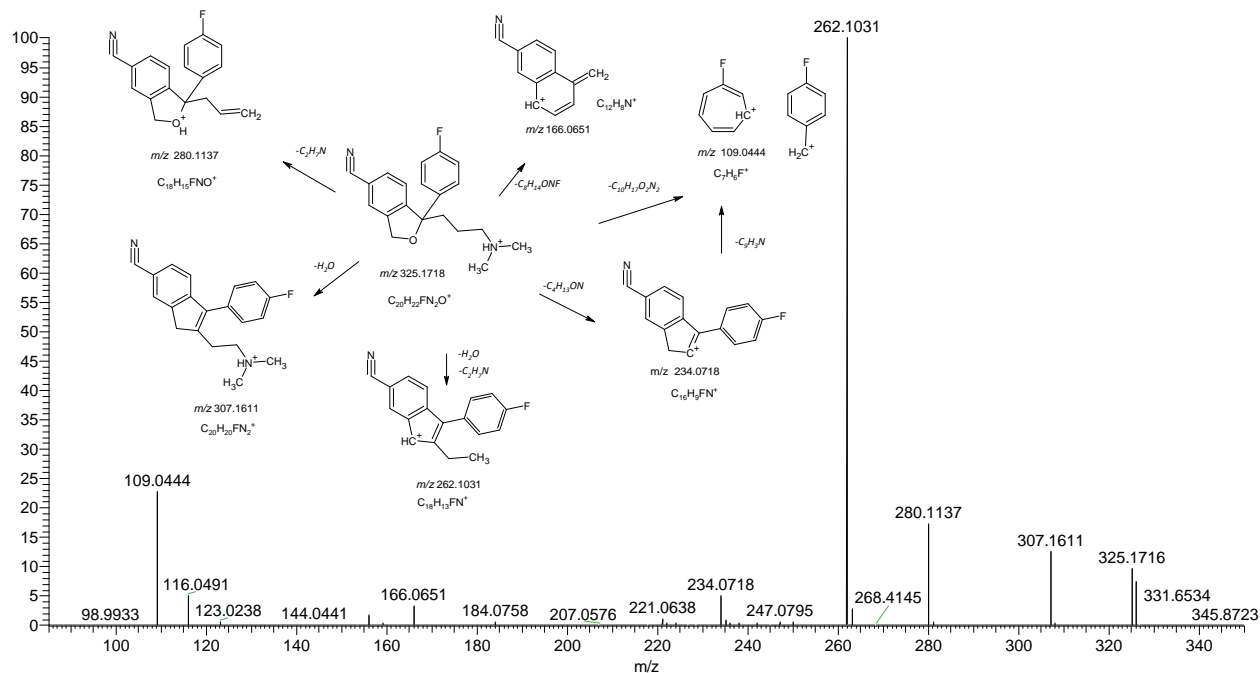
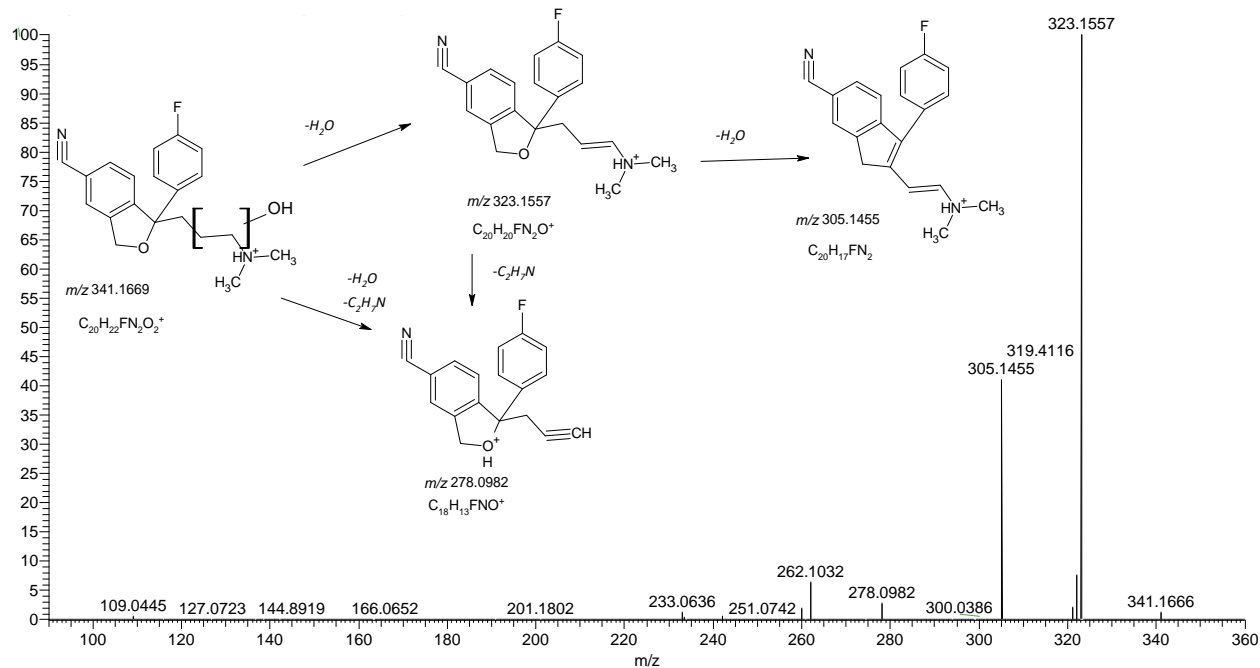
Table S3. MS² product ions formed from CIT and its transformation products.

[M+H] ⁺ and empirical formula	Δppm	RDB	RT (min)	MS ²	Relative intensity	Δppm	Ref.	
Citalopram 325.1718 C ₂₀ H ₂₂ ON ₂ F	2.251	11	19.92	307.1611 C ₂₀ H ₂₀ N ₂ F	13	1.942	[1]	
				280.1137 C ₁₈ H ₁₅ ONF	17	1.718		
				262.1031 C ₁₈ H ₁₃ NF	100	1.701		
				234.0718 C ₁₆ H ₉ NF	5	1.905		
				166.0651 C ₁₂ H ₈ N	3	-0.156		
				109.0444 C ₇ H ₆ F	23	3.714		
T245-A 245.1292 C ₁₄ H ₁₇ O ₂ N ₂	3.042	8	6.54	200.0708 C ₁₂ H ₁₀ O ₂ N	100	0.974	In this work	
T245-B 245.1292 C ₁₄ H ₁₇ O ₂ N ₂	3.042	8	8.41	227.1183 C ₁₄ H ₁₅ ON ₂	20	1.807	[1]	
				200.0708 C ₁₂ H ₁₀ O ₂ N	50	0.974		
				182.0602 C ₁₂ H ₈ ON	16	0.876		
				158.0236 C ₉ H ₄ O ₂ N	20	-0.348		
T247 247.1446 C ₁₄ H ₁₉ O ₂ N ₂	2.005	7	5.79	229.1339 C ₁₄ H ₁₇ ON ₂	100	1.572	In this work	
				202.0865 C ₁₂ H ₁₂ O ₂ N	2	1.212		

				184.0758 C ₁₂ H ₁₀ ON	3	0.595		
T261 261.1241 C ₁₄ H ₁₇ O ₃ N ₂	2.800	8	8.13	243.1132 C ₁₄ H ₁₅ O ₂ N ₂	90	1.628	[1]	
				216.0659 C ₁₂ H ₁₀ O ₃ N	100	1.760		
				198.0552 C ₁₂ H ₈ O ₂ N	30	1.237		
T323 323.1762 C ₂₀ H ₂₃ O ₂ N ₂	2.462	11	14.16	305.1655 C ₂₀ H ₂₁ ON ₂	10	2.163	[2][3]	
				278.1182 C ₁₈ H ₁₆ O ₂ N	20	2.318		
				260.1075 C ₁₈ H ₁₄ ON	100	1.958		
				242.0970 C ₁₈ H ₁₂ N	2	2.371		
				232.0762 C ₁₆ H ₁₀ ON	4	2.195		
				166.0652 C ₇ H ₇ N ₄ F	3	0.447		
				107.0488 C ₇ H ₇ O	15	- 3.189		
T337 337.1554 C ₂₀ H ₂₁ O ₃ N ₂	2.168	12	13.93	319.1447 C ₂₀ H ₁₉ O ₂ N ₂	15	1.866	In this work	
				292.0974 C ₁₈ H ₁₄ O ₃ N	15	1.986		
				274.0868 C ₁₈ H ₁₂ O ₂ N	100	1.988		
				256.0762 C ₁₈ H ₁₀ ON	15	1.990		
				172.0394 C ₁₀ H ₆ O ₂ N	10	0.552		
T339	2.558	12	18.92	321.1406 C ₂₀ H ₁₈ ON ₂ F	5	2.591	[1][2][3]	

339.1512 C ₂₀ H ₂₀ O ₂ N ₂ F				294.0932 C ₁₈ H ₁₃ O ₂ NF	5	2.437		
				276.0825 C ₁₈ H ₁₁ ONF	40	2.105		
				258.0719 C ₁₈ H ₉ NF	5	2.115		
T341 A 341.1669 C ₂₀ H ₂₂ O ₂ N ₂ F	2.689	11	17.40	323.1557 C ₂₀ H ₂₀ ON ₂ F	100	0.870	[1][3]	
				305.1455 C ₂₀ H ₁₈ N ₂ F	42	2.119		
				278.0982 C ₁₈ H ₁₃ ONF	3	2.270		
				262.1032 C ₁₈ H ₁₃ NF	7	2.082		
T341 B 341.1669 C ₂₀ H ₂₂ O ₂ N ₂ F	2.689	11	18.70	323.1560 C ₂₀ H ₂₀ ON ₂ F	100	1.801	In this work	
				296.1088 C ₁₈ H ₁₅ O ₂ NF	20	2.251		
				278.0981 C ₁₈ H ₁₃ ONF	70	1.910		
				240.0824 C ₁₅ H ₁₁ ONF	10	2.005		
				109.0444 C ₇ H ₆ F	6	-3.714		
T355 355.1457 C ₂₀ H ₂₀ O ₃ N ₂ F	1.275	12	17.84	337.1353 C ₂₀ H ₁₈ O ₂ N ₂ F	50	1.861	[3]	
				292.0775 C ₁₈ H ₁₁ O ₂ NF	100	2.283		
				274.0668 C ₁₈ H ₉ ONF	13	1.939		

T357 357.1618 $C_{20}H_{22}O_3N_2F$	2.528	10.5	16.42	339.1509 $C_{20}H_{20}O_2N_2F$	100	1.673	In this work	
				321.1404 $C_{20}H_{18}ON_2F$	17	1.968		


 Figure S1. MS² spectrum of Citalopram.

 Figure S2. MS² spectrum of TP341A.

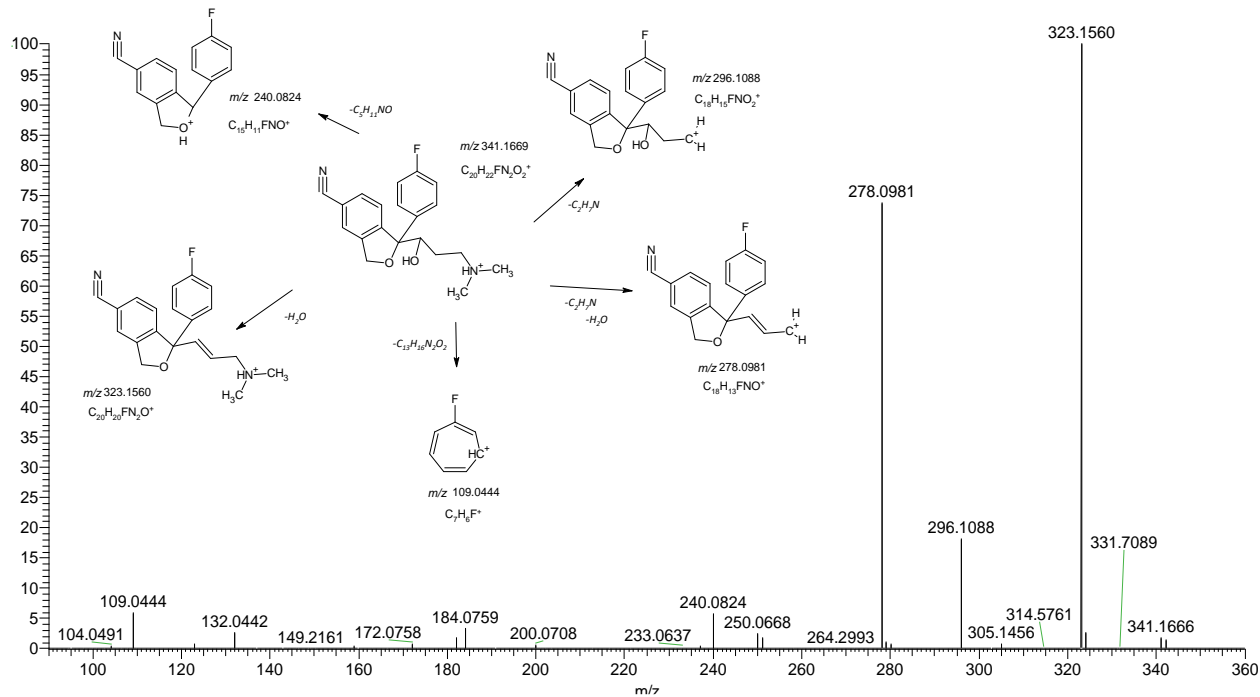


Figure S3 MS² spectrum of TP341B.

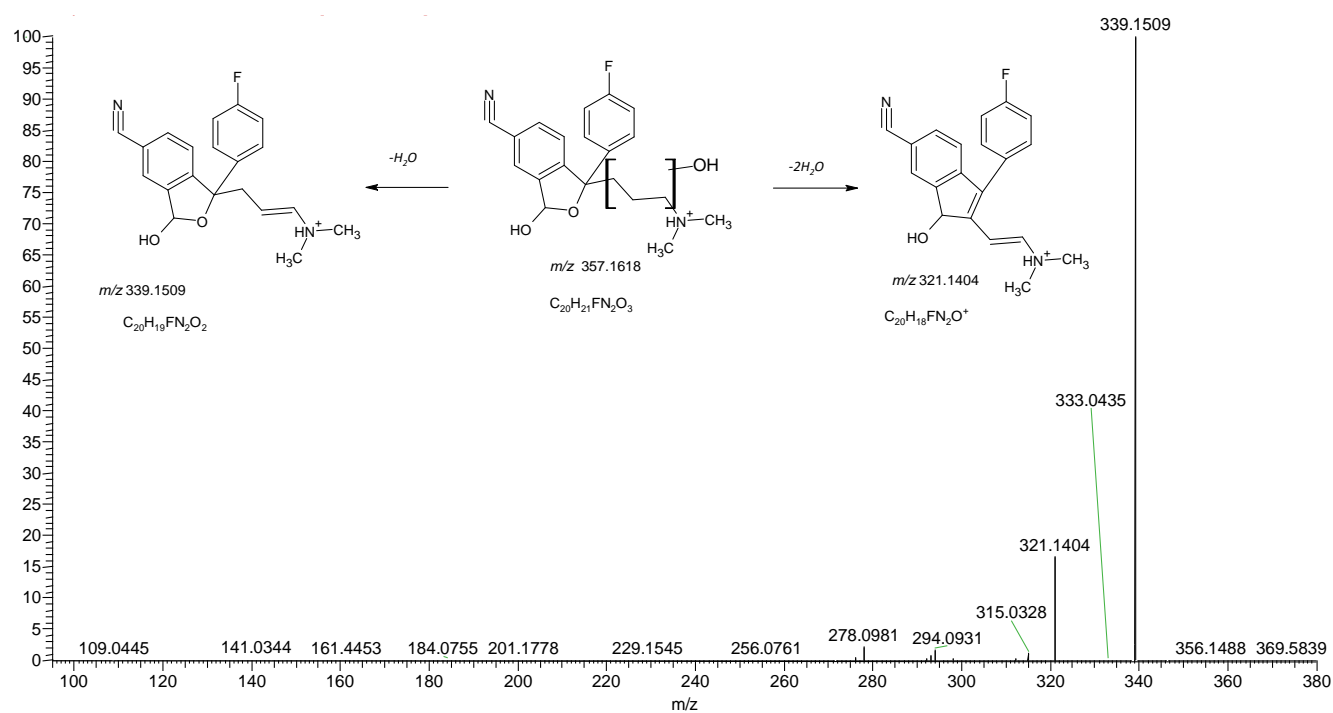
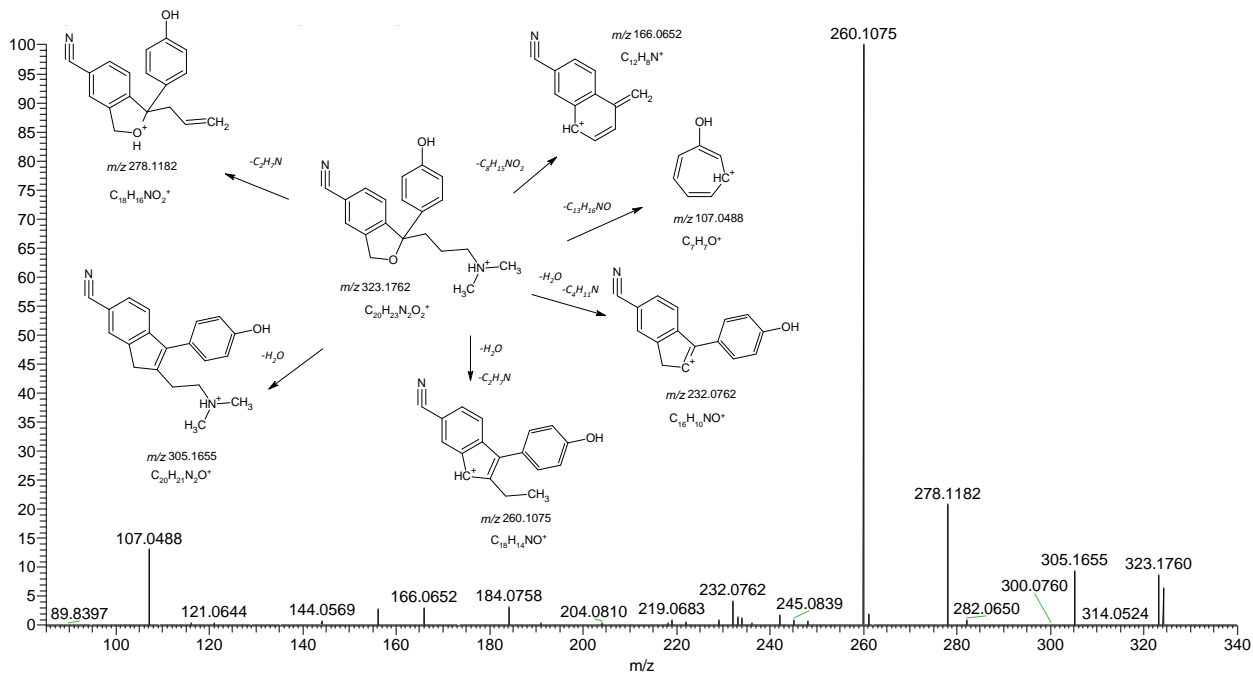
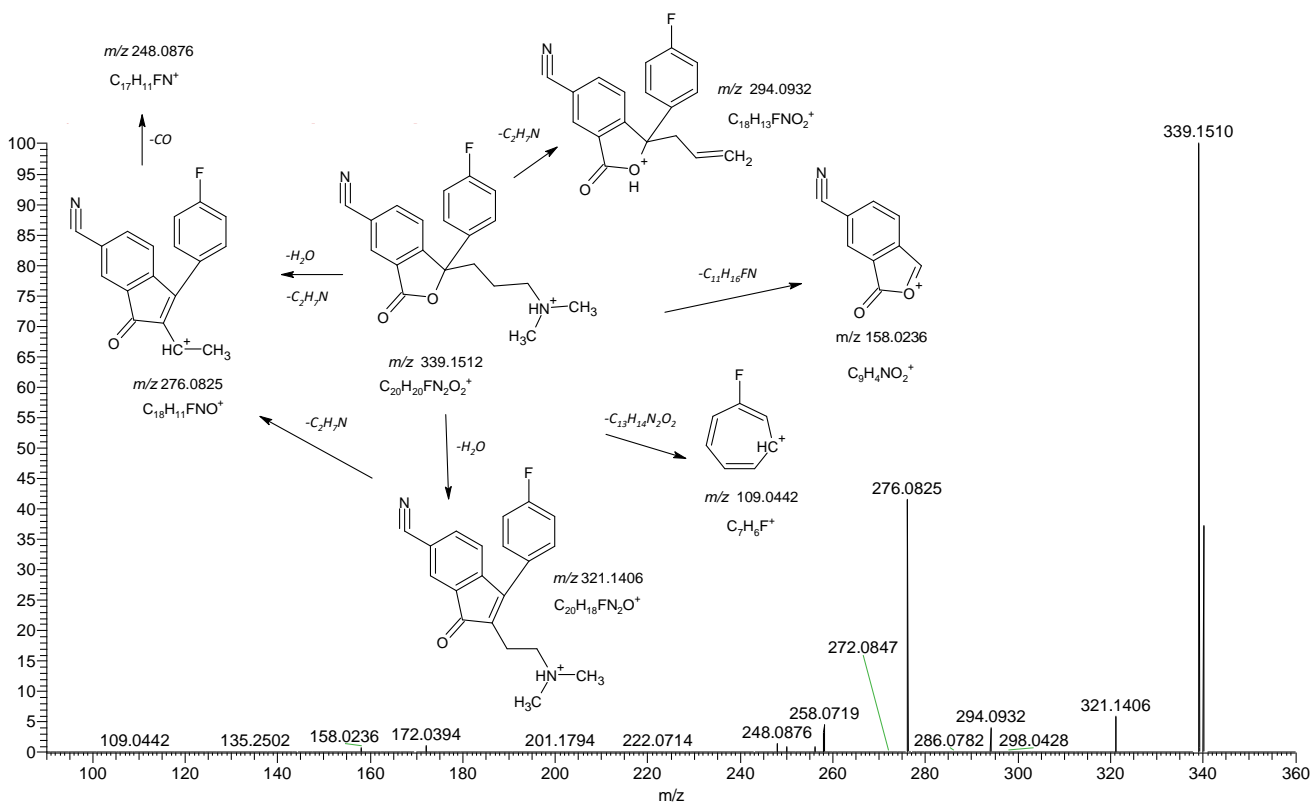
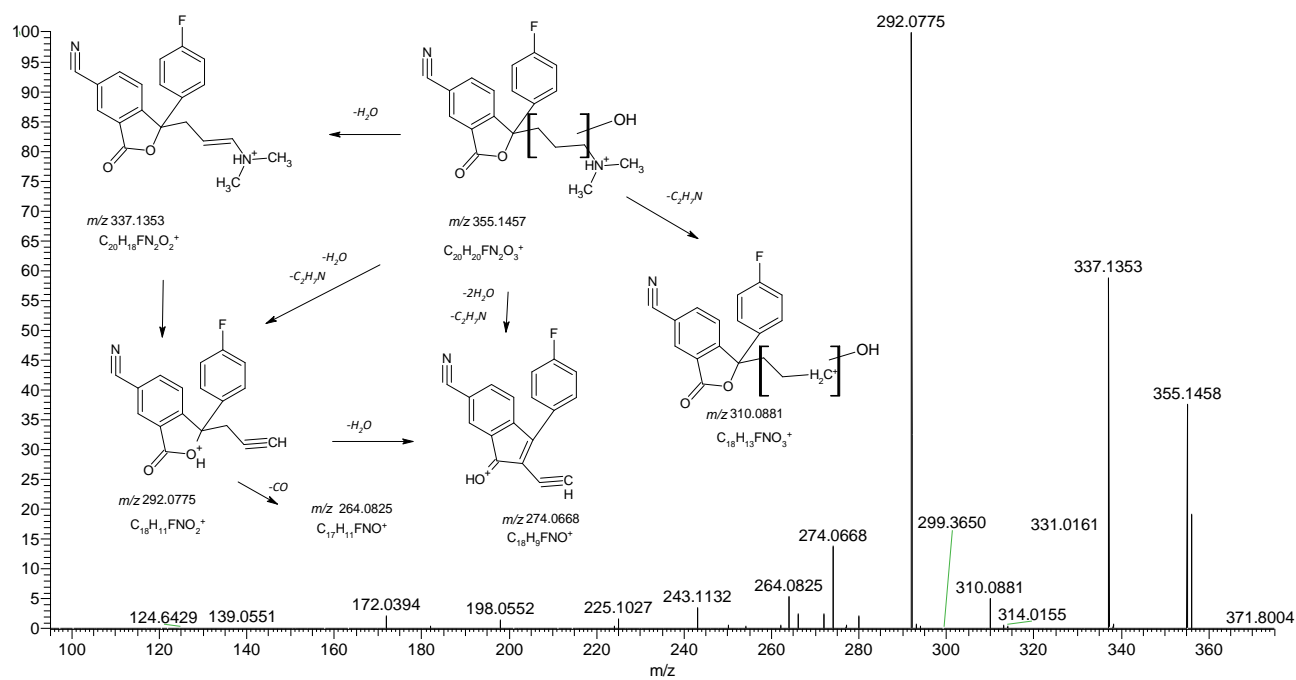
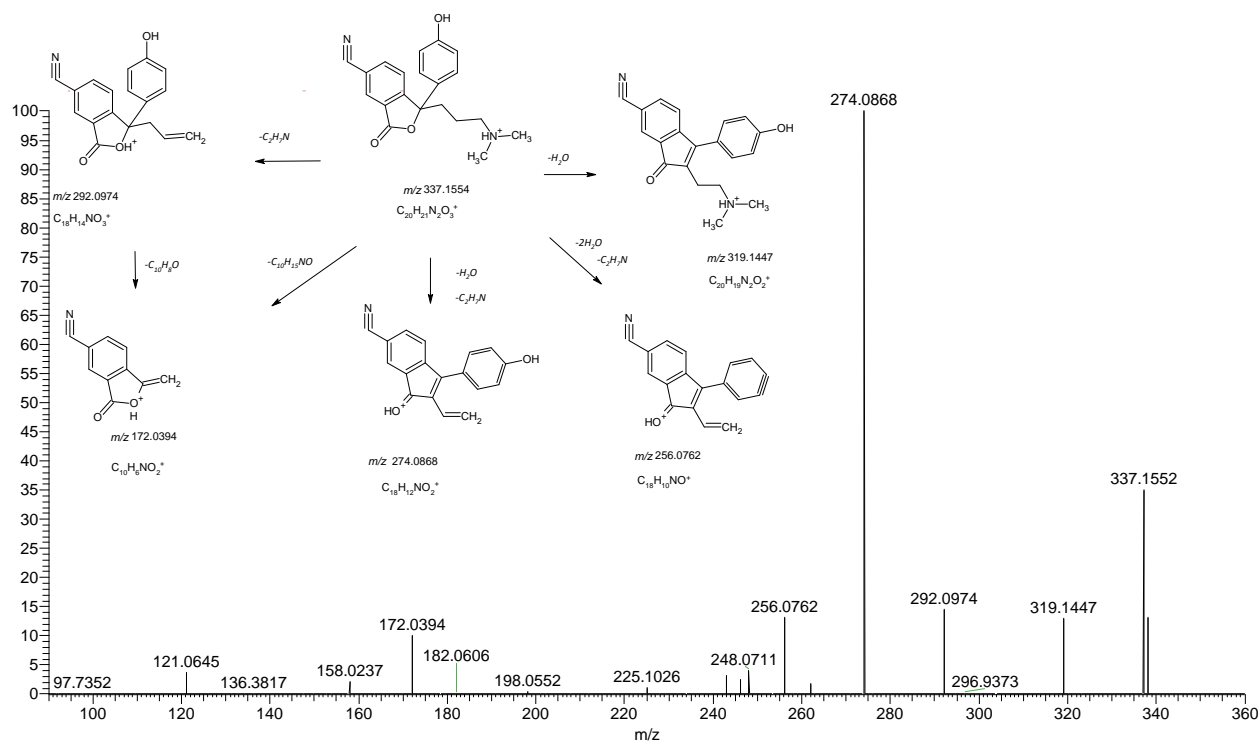


Figure S4 MS² spectrum of TP357.


 Figure S5 MS² spectrum of TP323.

 Figure S6 MS² spectrum of TP339.

Figure S7 MS² spectrum of TP355.Figure S8 MS² spectrum of TP337.

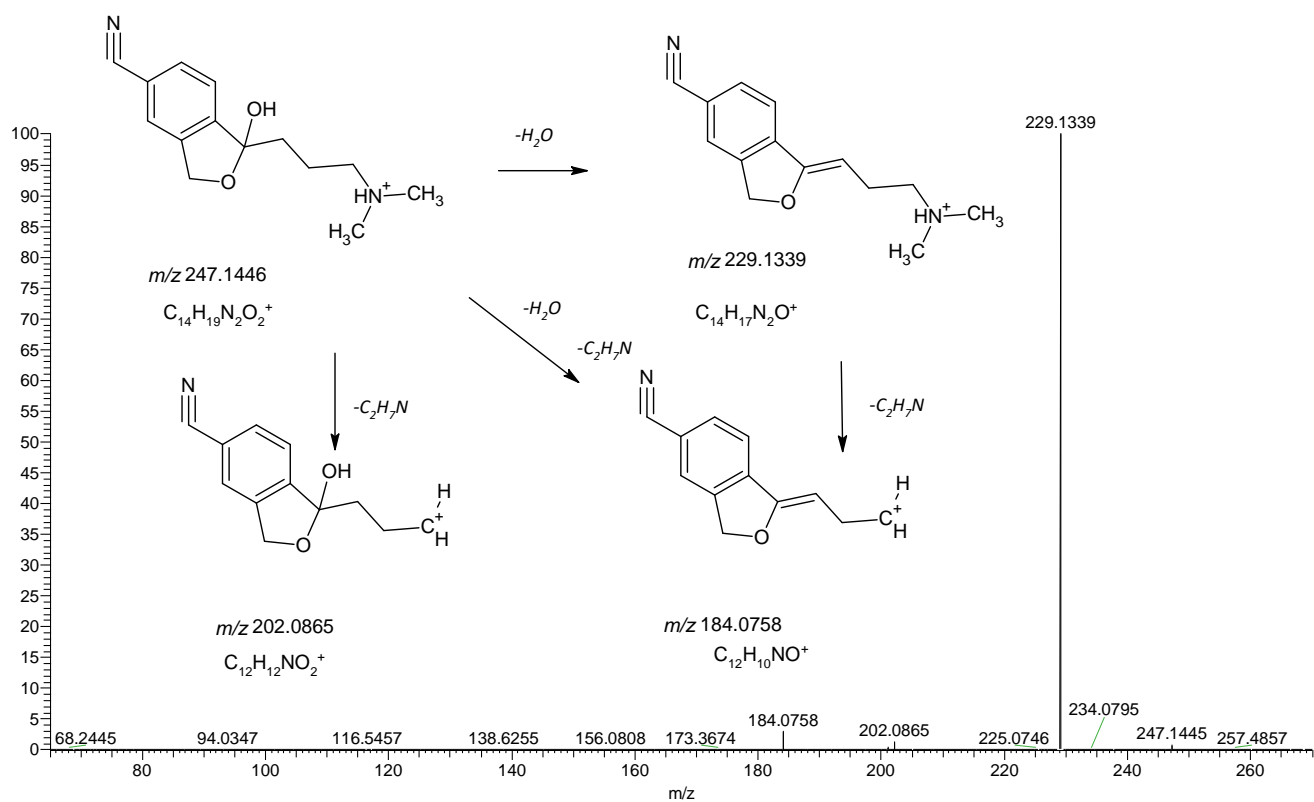


Figure S9 MS² spectrum of TP247.

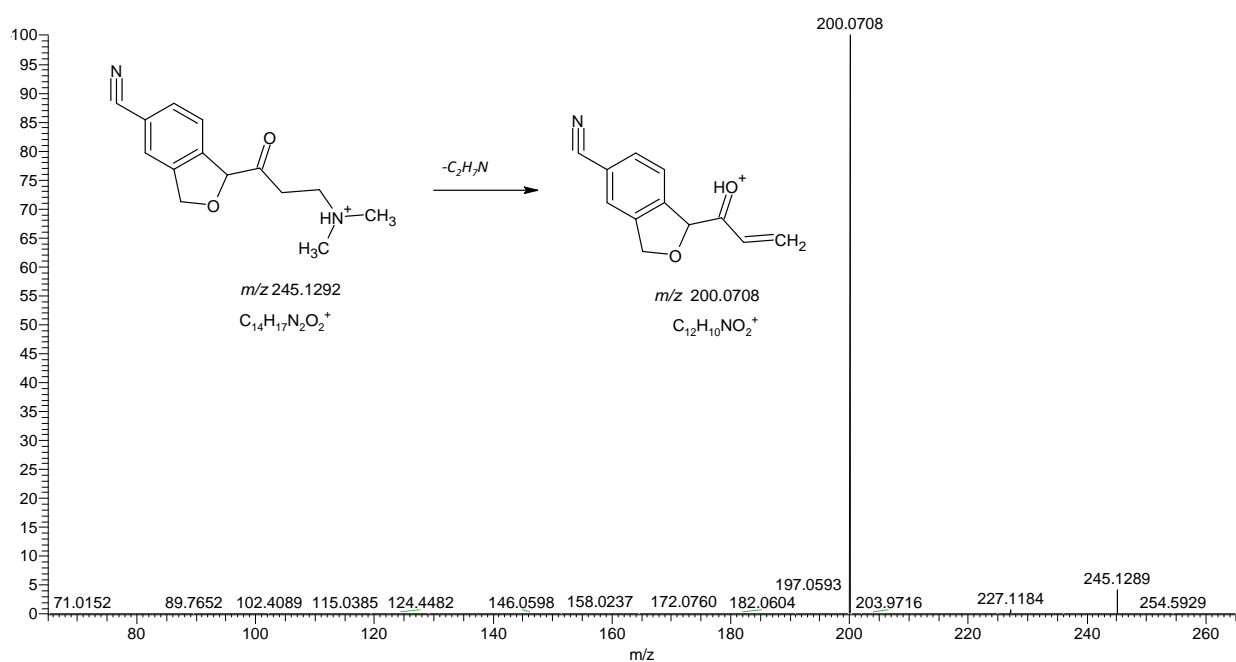
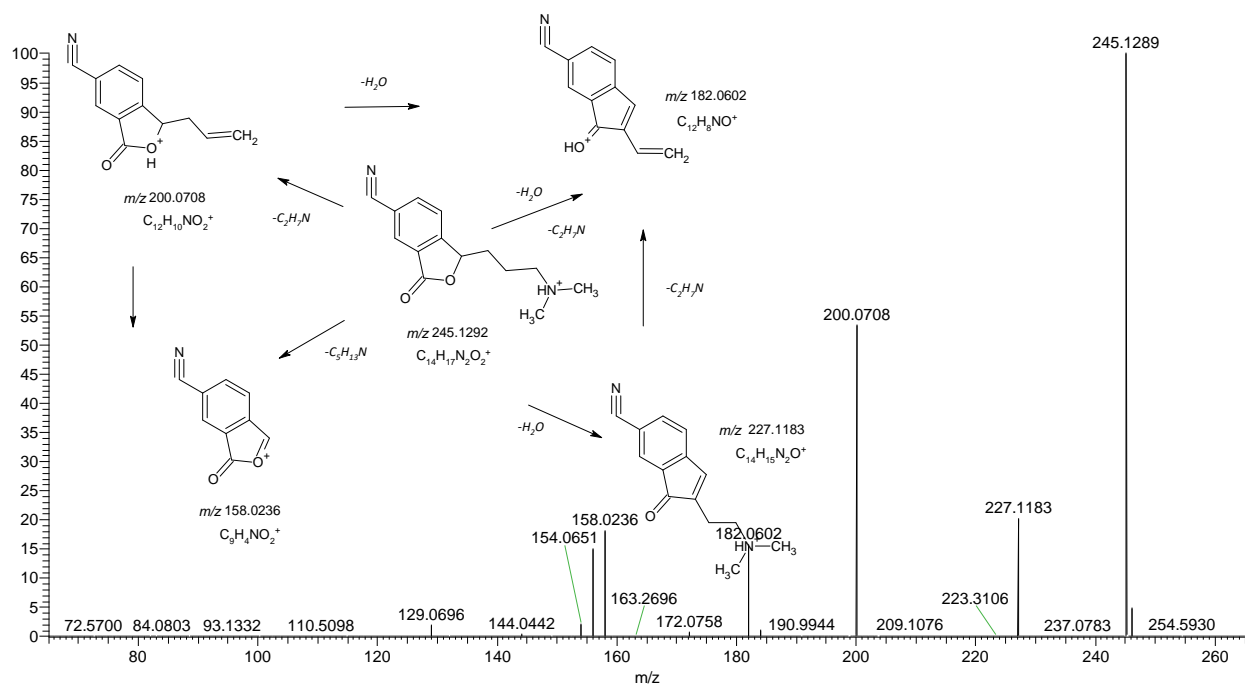
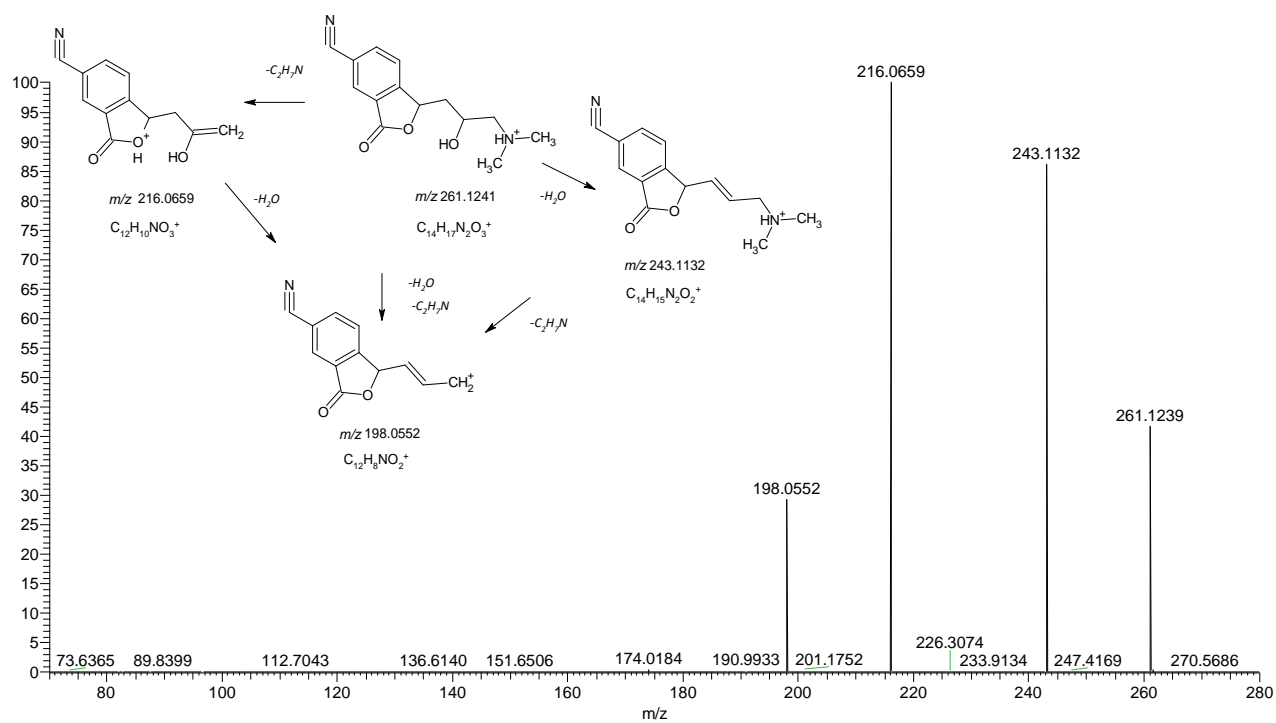


Figure S10. MS² spectrum of TP245A.

Figure S11. MS² spectrum of TP245B.Figure S12. MS² spectrum of TP261.

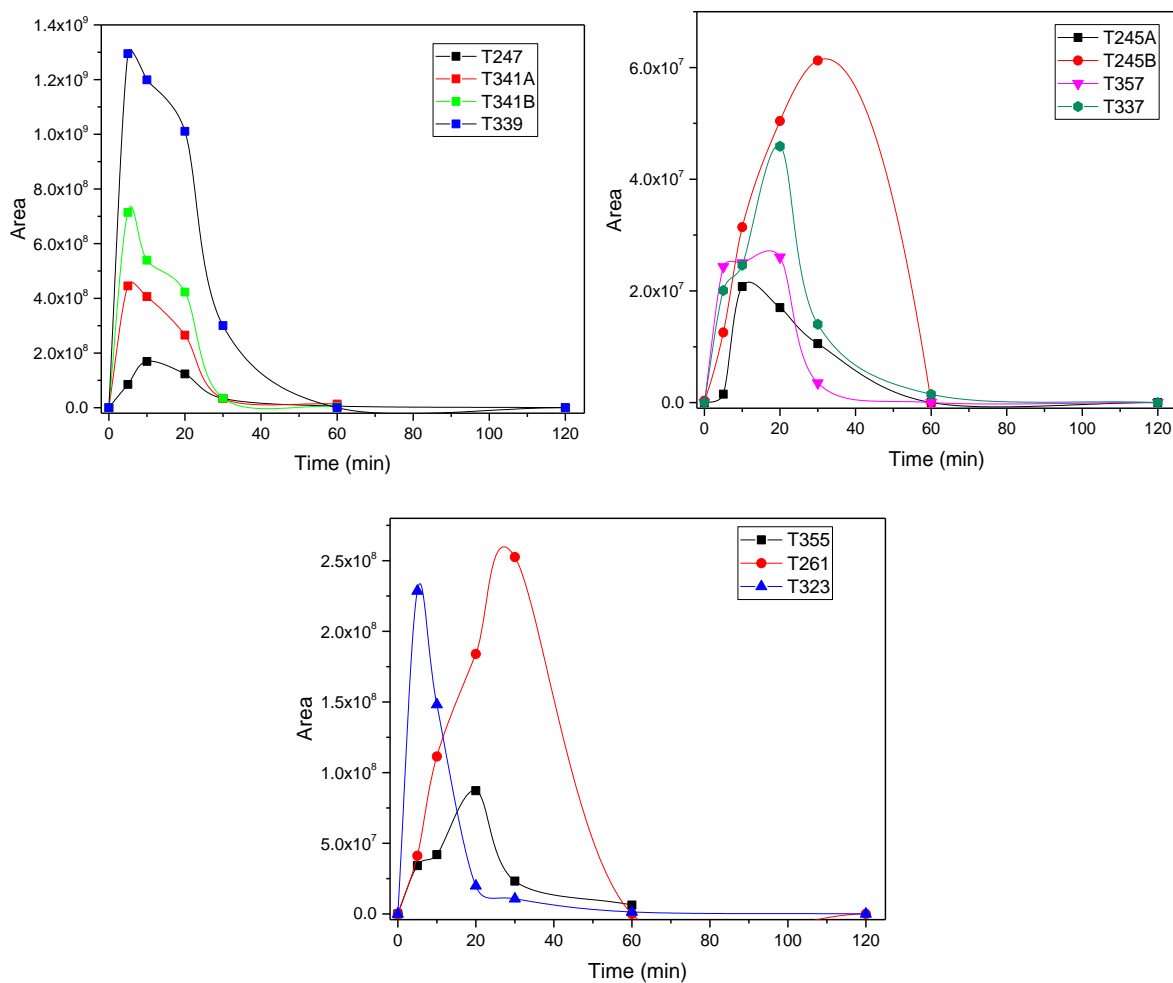


Figure S13. Time evolution of TPs detected during the photocatalytic treatment.

1. Osawa, R.A.; Carvalho, A.P.; Monteiro, O.C.; Oliveira, M.C.; Florêncio, M.H. Transformation products of citalopram: Identification, wastewater analysis and in silico toxicological assessment. *Chemosphere***2019**, *217*, 858–868, doi:10.1016/j.chemosphere.2018.11.027.
2. Hörsing, M.; Kosjek, T.; Andersen, H.R.; Heath, E.; Ledin, A. Fate of citalopram during water treatment with O₃, ClO₂, UV and fenton oxidation. *Chemosphere***2012**, *89*, 129–135, doi:10.1016/j.chemosphere.2012.05.024.
3. Jiménez-Holgado, C.; Sakkas, V.; Richard, C. Phototransformation of three psychoactive drugs in presence of sedimental water extractable organic matter. *Molecules***2021**, *26*, 1–17, doi:10.3390/molecules26092466.

References

- [1] <https://www.un.org/sustainabledevelopment/>.
- [2] Montes-Grajales, D.; Fennix-Agudelo, M.; Miranda-Castro, W. Occurrence of personal care products as emerging chemicals of concern in water resources: A review. *Sci. Total Environ.* 2017, 595, 601–614, doi:10.1016/j.scitotenv.2017.03.286.
- [3] Ebele, A.J.; Abou-Elwafa Abdallah, M.; Harrad, S. Pharmaceuticals and personal care products (PPCPs) in the freshwater aquatic environment. *Emerg. Contam.* 2017, 3, 1–16, doi:10.1016/j.emcon.2016.12.004.
- [4] Hörsing, M.; Kosjek, T.; Andersen, H.R.; Heath, E.; Ledin, A. Fate of citalopram during water treatment with O₃, ClO₂, UV and fenton oxidation. *Chemosphere* 2012, 89, 129–135, doi:10.1016/j.chemosphere.2012.05.024.
- [5] Patel, M.; Kumar, R.; Kishor, K.; Mlsna, T.; Pittman, C.U.; Mohan, D. Pharmaceuticals of Emerging Concern in Aquatic Systems: Chemistry, Occurrence, Effects, and Removal Methods. *Chem. Rev.* 2019, 119, 3510–3673, doi:10.1021/acs.chemrev.8b00299.
- [6] Osawa, R.A.; Carvalho, A.P.; Monteiro, O.C.; Oliveira, M.C.; Florêncio, M.H. Transformation products of citalopram: Identification, wastewater analysis and in silico toxicological assessment. *Chemosphere* 2019, 217, 858–868, doi:10.1016/j.chemosphere.2018.11.027.
- [7] Kwon, J.W.; Armbrust, K.L. Degradation of citalopram by simulated sunlight. *Environ. Toxicol. Chem.* 2005, 24, 1618–1623, doi:10.1897/04-522R.1.
- [8] Hossain, M.S.; Kubec, J.; Guo, W.; Roje, S.; Ložek, F.; Grabicová, K.; Randák, T.; Kouba, A.; Buřič, M. A combination of six psychoactive pharmaceuticals at environmental concentrations alter the locomotory behavior of clonal marbled crayfish. *Sci. Total Environ.* 2021, 751, 141383, doi:10.1016/j.scitotenv.2020.141383.
- [9] Molé, R.A.; Good, C.J.; Stebel, E.K.; Higgins, J.F.; Pitell, S.A.; Welch, A.R.; Minarik, T.A.; Schoenfuss, H.L.; Edmiston, P.L. Correlating effluent concentrations and bench-scale experiments to assess the transformation of endocrine active compounds in wastewater by UV or chlorination disinfection. *Chemosphere* 2019, 226, 565–575, doi:10.1016/j.chemosphere.2019.03.145.
- [10] Canonica, S.; Jans, U.R.S.; Stemmler, K.; Hoigne, J. Transformation Kinetics of Phenols in Water: Photosensitization. *Environ. Sci. Technol.* 1995, 29, 1822–1831.
- [11] Vaughan, P.P.; Blough, N. V. Photochemical formation of hydroxyl radical by constituents of natural waters. *Environ. Sci. Technol.* 1998, 32, 2947–2953, doi:10.1021/es9710417.
- [12] Mopper, K.; Zhou, X. Hydroxyl radical photoproduction in the sea and its potential impact on marine processes. *Science (80-.)*. 1990, 250, 661–664, doi:10.1126/science.250.4981.661.
- [13] Vione, D.; Minella, M.; Maurino, V.; Minero, C. Indirect photochemistry in sunlit surface waters:

- Photoinduced production of reactive transient species. *Chem. - A Eur. J.* 2014, 20, 10590–10606, doi:10.1002/chem.201400413.
- [14] Zepp, R.G.; Schlotzhauer, P.F.; Sink, R.M. Photosensitized Transformations Involving Electronic Energy Transfer in Natural Waters: Role of Humic Substances. *Environ. Sci. Technol.* 1985, 19, 74–81, doi:10.1021/es00131a008.
- [15] Peterson, B.M.; McNally, A.M.; Cory, R.M.; Thoemke, J.D.; Cotner, J.B.; McNeill, K. Spatial and temporal distribution of singlet oxygen in Lake Superior. *Environ. Sci. Technol.* 2012, 46, 7222–7229, doi:10.1021/es301105e.
- [16] Cooper, W.J.; Zika, R.G.; Petasne, R.G.; Plane, J.M. Photochemical formation of hydrogen peroxide in natural waters exposed to sunlight. *Environ. Sci. Technol.* 1988, 22, 1156–1160.
- [17] Minguez, L.; Farcy, E.; Ballandonne, C.; Lepailleur, A.; Serpentine, A.; Lebel, J.M.; Bureau, R.; Halm-Lemeille, M.P. Acute toxicity of 8 antidepressants: What are their modes of action? *Chemosphere* 2014, 108, 314–319, doi:10.1016/j.chemosphere.2014.01.057.
- [18] Ziegler, M.; Knoll, S.; Köhler, H.-R.; Tisler, S.; Huhn, C.; Zwiener, C.; Triebkorn, R. Impact of the antidepressant citalopram on the behaviour of two different life stages of brown trout., doi:10.7717/peerj.8765.
- [19] Styris, B.; Halling-Sørensen, B.; Ingerslev, F. Environmental risk assessment of three selective serotonin reuptake inhibitors in the aquatic environment: A case study including a cocktail scenario. *Environ. Toxicol. Chem.* 2011, 30, 254–261, doi:10.1002/etc.372.
- [20] Suarez, S.; Lema, J.M.; Omil, F. Removal of Pharmaceutical and Personal Care Products (PPCPs) under nitrifying and denitrifying conditions. *Water Res.* 2010, 44, 3214–3224, doi:10.1016/j.watres.2010.02.040.
- [21] Boreen, A.L.; Arnold, W.A.; McNeill, K. Photodegradation of pharmaceuticals in the aquatic environment: A review. *Aquat. Sci.* 2003, 65, 320–341, doi:10.1007/s00027-003-0672-7.
- [22] Patel, M.; Kumar, R.; Kishor, K.; Mlsna, T.; Pittman, C.U.; Mohan, D. Pharmaceuticals of Emerging Concern in Aquatic Systems: Chemistry, Occurrence, Effects, and Removal Methods. *Chem. Rev.* 2019, 119, 3510–3673, doi:10.1021/acs.chemrev.8b00299.
- [23] Trawiński, J.; Skibiński, R. Studies on photodegradation process of psychotropic drugs: a review. *Environ. Sci. Pollut. Res.* 2017, 24, 1152–1199, doi:10.1007/s11356-016-7727-5.
- [24] Gopinath, K.P.; Madhav, N.V.; Krishnan, A.; Malolan, R.; Rangarajan, G. Present applications of titanium dioxide for the photocatalytic removal of pollutants from water: A review. *J. Environ. Manage.* 2020, 270, 110906, doi:10.1016/j.jenvman.2020.110906.
- [25] Kanan, S.; Moyet, M.A.; Arthur, R.B.; Patterson, H.H. Recent advances on TiO₂-based photocatalysts toward the degradation of pesticides and major organic pollutants from water bodies. *Catal. Rev.* 2020, 62, 1–65, doi:10.1080/01614940.2019.1613323.

- [26] Takeda, K.; Takedoi, H.; Yamaji, S.; Ohta, K.; Sakugawa, H. Determination of Hydroxyl Radical Photoproduction Rates in Natural Waters. *Anal. Sci.* 2004, 20, 153–158, doi:10.2116/analsci.20.153.
- [27] Jiménez-Holgado, C.; Sakkas, V.; Richard, C. Phototransformation of three psychoactive drugs in presence of sedimental water extractable organic matter. *Molecules* 2021, 26, 1–17, doi:10.3390/molecules26092466.
- [28] Kotnik, K.; Kosjek, T.; Žegura, B.; Filipič, M.; Heath, E. Photolytic fate and genotoxicity of benzophenone-derived compounds and their photodegradation mixtures in the aqueous environment. *Chemosphere* 2016, 147, 114–123, doi:10.1016/j.chemosphere.2015.12.068.
- [29] Konstantinou, I.K.; Zarkadis, A.K.; Albanis, T.A. Organic Compounds in the Environment Photodegradation of Selected Herbicides in Various Natural Waters and Soils under Environmental Conditions. *Publ. J. Environ. Qual* 2001, 30, 121–130.
- [30] Zonja, B.; Gonçalves, C.; Pérez, S.; Delgado, A.; Petrovic, M.; Alpendurada, M.F.; Barceló, D. Evaluation of the phototransformation of the antiviral zanamivir in surface waters through identification of transformation products. *J. Hazard. Mater.* 2014, 265, 296–304, doi:10.1016/j.jhazmat.2013.10.008.
- [31] Beretsou, V.G.; Psoma, A.K.; Gago-Ferrero, P.; Aalizadeh, R.; Fenner, K.; Thomaidis, N.S. Identification of biotransformation products of citalopram formed in activated sludge. *Water Res.* 2016, 103, 205–214, doi:10.1016/j.watres.2016.07.029.
- [32] Calza, P.; Medana, C.; Padovano, E.; Giancotti, V.; Minero, C. Fate of selected pharmaceuticals in river waters. *Environ. Sci. Pollut. Res.* 2013, 20, 2262–2270, doi:10.1007/s11356-012-1097-4.
- [33] Schymanski, E.L.; Jeon, J.; Gulde, R.; Fenner, K.; Ruff, M.; Singer, H.P.; Hollender, J. Identifying small molecules via high resolution mass spectrometry: Communicating confidence. *Environ. Sci. Technol.* 2014, 48, 2097–2098, doi:10.1021/es5002105.
- [34] Calza, P.; Jiménez-Holgado, C.; Cocha, M.; Chrimatopoulos, C.; Dal Bello, F.; Medana, C.; Sakkas, V. Study of the photoinduced transformations of sertraline in aqueous media. *Sci. Total Environ.* 2021, 756, 143805, doi:10.1016/j.scitotenv.2020.143805.
- [35] Brown, A.K.; Challis, J.K.; Wong, C.S.; Hanson, M.L. Selective serotonin reuptake inhibitors and β -blocker transformation products may not pose a significant risk of toxicity to aquatic organisms in wastewater effluent-dominated receiving waters. *Integr. Environ. Assess. Manag.* 2015, 11, 618–639, doi:10.1002/ieam.1637.

Chapter 6. Exploring the photolytic and photocatalytic transformation of Clozapine: kinetics, degradation mechanism and toxicity assessment

6.1. Introduction

The presence of psychotropic pharmaceuticals in environmental waters is a hot topic. Due to the lack of legislation and guidelines, as well as the understanding about their fate in the environment and effective removal methods in WWTPs, these compounds still classified as Contaminant of Emergency Concern (CEC). Therefore, the presence of pharmaceuticals in samples such as lake, seawater, river or WW has been well reported in the literature [1–4]. Their consumption in developed countries has increased greatly to treat mental illnesses such as panic disorder, depression or anorexia.

Clozapine (8-chloro-11-(4-methylpiperazin-1-yl)-5H-dibenzo[b,e][1,4]diazepine), is the first atypical antipsychotic sold into the market in the 1960s as a successful medication in the treatment of schizophrenia [5]. CLO has been detected in natural aqueous samples ranging from a few ng/L to a dozen µg/L[6,7]. Several studies have shown that this drug has the ability to accumulate in the tissues of aquatic organisms [8,9], in addition to being toxic, for *Fathead minnow*[10] and green algae

[11]. Clozapine can be induced by solar light because absorbs solar radiations between 295 and 450 nm [12]. According to the literature data, irradiation with simulated solar light in pure water yielded a half-life of 8 h for CLO [13] but it depends on some factors such as the pH of sample, the temperature, the concentration of the pollutant among other [5,6,14,15].

Once realized in the environment, they can undergo to biotic and abiotic degradation processes, among which hydrolysis, photodegradation and microbiological degradation are most common. Chromophoric dissolved organic matter (DOM) have been of interest for the scientific community since the 1970s. CDOM can sensitize the degradation of micropollutant through the formation of reactive intermediates (RIs) such as hydroxyl radical ($\bullet\text{OH}$) [16–18], singlet oxygen ($^1\text{O}_2$) [19,20], superoxide radical anion (O_2^-) [21], hydrogen peroxide (H_2O_2) [22] and excited triplet states ($^3\text{DOM}^*$) [12].

The low efficiency of the elimination procedures currently used in WWTPs implies the search for new and more effective methods [23,24]. Then, due to the photostability of CLO, processes more efficient such as Advance Oxidation Processes are being employed. Nowadays, the AOPs more used is heterogeneous photocatalysis. This process is based on the interaction of radiation of appropriate wavelength (depending on the band-gap of the semiconductor) with the surface of the semiconductor that acts as a photocatalyst. The pollutants are expected to be completely mineralized as a result of this process. Numerous studies have shown that the use of heterogeneous photocatalysis yielded promising results in the elimination of persistent pharmaceuticals from the environment [25]. TiO_2 is one of the most used and efficient catalyst. The popularity of this photocatalyst could be attributed to its many advantages, such as high photostability, photoreactivity, low toxicity, or low cost [26]. J Trawinski was the first author to use TiO_2 combined with CLO, and after 20 minutes of irradiation, both, parent molecule and its TPs were practically completely eliminated [13].

6.2. Materials and methods

6.2.1. Materials

Clozapine (8-Chloro-11-(4-methyl-1-piperazinyl)-5H-dibenzo[b,e][1,4]-diazepine),(CLO), was purchased from TCI Tokyo Chemical Industry (Tokyo, Japan) with a purity higher than 98%. For analytical purposes, a stock solution containing 1000 mg/L of CLO was dissolved in methanol. The solution was stored in glass-stopped bottles at $-20\text{ }^{\circ}\text{C}$ in the dark. Standard working solutions were prepared, daily. Ultrapure water used was produced by a Milli-Q system (Evoqua, Pittsburg, USA). Photosensitizers: humic acid, nitrate (NaNO_3) and bicarbonates (NaHCO_3) were purchased from Sigma-Aldrich (Athens, Greece). Irradiation procedures of CLO were carried out by experimental solutions that were prepared by dissolving CLO directly in ultrapure water, ultrapure water+sensitizers, WWTP effluent and Pamvotis lake. Acetonitrile ($\geq 99.9\%$) was purchased from Merck Life Science S.r.l. (Milan, Italy). TiO_2 P25 (Evonik Industries, Italy) was used as photocatalyst.

6.2.2. Sample collection

Samples from WWTPs effluent were collected from the WWTP of the city of Ioannina in amber glass bottles prerinsed with deionized water. Up on their arrival in the laboratory, were centrifuged (4000 rpm, $25\text{ }^{\circ}\text{C}$, 10 min) and filtered with $0.45\text{ }\mu\text{m}$ polypropylene (PP) filters to eliminate the particulate matter.

Lake samples were collected from Pamvotis lake, located in Ioannina, NW Greece. All the samples were collected in clean amber glass bottles, transported to the laboratory and immediately filtered with polyamide filters of $0.45\text{ }\mu\text{m}$ and placed in the refrigerator at $5\text{ }^{\circ}\text{C}$. Wastewater and Lake samples were characterized and values are compiled at Table S1 and S2 of Chapter 5.

6.2.3. Irradiation experiments

6.2.3.1. Natural solar light

To simulate the degradation processes that take place in the environment, photodegradation and hydrolysis experiments were carried out under natural solar irradiation. For this, 1 L of samples were spiked with 10 mg/L of CLO in MQ water as well as natural waters (WWTP and Lake). These samples were put into capped Pyrex glass bottles and homogenized under magnetic stirring conditions, and finally placed on the terrace of the Department of Chemistry of Ioannina University in 2018. Dark control experiments were also carried out. For this, amber glass bottles were exposed with the same concentration and covered with aluminum foil, in order to obtain the same environmental conditions (Figure 6.1).

At certain times, aliquots of 2 mL were collected from the bottles. The average total daily short-wave radiation was 286 and 273 W/m² for July and August, respectively, while the sunshine duration from sunrise to sunset was 10 and 11 h, for the two months, respectively. The mean daily air temperature was 23 and 26 °C, with minimum air temperature at 17 and 18 °C and maximum air temperature at 26 and 32 °C, for July and August, respectively. Experiments were carried out in duplicate.



Figure 6.1. Samples at the terrace in the University of Ioannina exposed to natural solar light.

6.2.3.2. Artificial solar irradiation

Photodegradation experiments were conducted in a sunlight simulator (Solarbox, CO.FO.Me.Gra, Milan) equipped with a xenon lamp (1500 W) with a cut-off filter at below 340 nm (Figure 6.2). On top of the solutions the irradiance was 18 W m^{-2} in the 295–400 nm range (like the natural sunlight UV irradiance at middle European latitude in sunny days). Irradiation was carried out in magnetically stirred cylindrical closed cells (Pyrex glass, 40 mm i.d. 25 mm), on 5 mL aqueous solutions containing 10 mg/L of CLO and were subjected to different irradiation times.

The differences between the photodegradation rates of CLO in the presence of dissolved organic matter (DOM) was studied. Solutions of MQ water of 1 mg/L of CLO, containing DOM, nitrate and bicarbonate ions (10 mg/L each) were exposed to the same irradiation conditions than the previous experiments. All experiments were carried out in triplicate including dark controls that were performed under the same conditions.



Figure 6.2. Sunlight simulator used during my secondment at the University of Turin.

To calculate the degradation rate constant, the equation (1) was used:

$$C_t = C_0 e^{-kt} \quad (1)$$

where C_t is the concentration at time t and C_0 the initial concentration. At the time, that concentration reduces to 50 % of its initial amount and the half-life is calculated by:

$$t_{1/2} = \ln 2 / k \quad (2)$$

6.2.3.3. Photocatalysis

Photocatalytic degradation experiments were conducted in the same cylindrical closed cells on 5 mL aqueous solutions containing 20 mg/L of CLO and 400 mg/L TiO_2 . Samples were subjected to different irradiation times (ranging from 5 min to 3 h), using the 40 W Philips TL K05 lamp (Figure 6.3). After irradiation, the samples were filtered through 0.45 μm Millex LCR hydrophilic PTFE membranes (Millipore) before the analysis. The lamp irradiance over the irradiated solutions was around 30 W/m^2 in the wavelength range of 290–400 nm (measured with a power meter from CO.FO.ME.GRA., Milan, Italy).



Figure 6.3. 40 W Philips lamp used during for irradiation purposes (University of Turin).

6.2.4. Irradiation experiments

Concentrations of CLO under all irradiation conditions was monitored with a Merck-Hitachi chromatograph equipped with Rheodyne injector (20 μ L sample loop), L-6200 and L-6200A pumps for high-pressure gradients, L-4200 UV-vis detector, and RP-C18 column (Lichrospher, 4mm i.d. \times 125 mm long, from Merck). Isocratic elution (1 mL/min flow rate) was carried out with 85% of 0.01 M phosphoric acid solution at pH 2.8 and 15 % acetonitrile. The detector wavelength chosen was 245 nm.

The formation of ionic products in samples irradiated with simulated solar light, was followed by a suppressed ion chromatography, employing a Dionex DX 500 instrument (Thermo Scientific) equipped with a conductimeter detector (ED 40, Dionex). The anions (nitrate and nitrite) have been analysed by using an AS9HC anionic column (200 mm long \times 4 mm i.d.) using an aqueous solution of K_2CO_3 (9 mM) as mobile phase; the elution was performed at 30 $^{\circ}C$, at a flow rate of 1mL/min. The determination of ammonium ions was performed by employing a CS12A column, using methanesulfonic acid 25mM as eluent, at a flow rate of 1mL/min.

The evolution of the dissolved organic carbon (DOC) during the irradiation process runs was followed using a Shimadzu TOC-V CSH (catalytic oxidation on Pt at 680°C) equipped with a Shimadzu ASI-V autosampler. Calibration was achieved by injection of known amounts of potassium phthalate.

6.2.5. Toxicity

The toxicity was evaluated with a Microtox Model 500 Toxicity Analyzer (Milan, Italy). Acute toxicity was evaluated with a bioluminescence inhibition assay using the marine bacterium *Vibrio fischeri* (Figure 6.4) by monitoring changes in the natural emission of the luminescent bacteria when challenged with toxic compounds. Freeze-dried bacteria, reconstitution solution, diluent (2% NaCl) and an adjustment solution (non-toxic 22% sodium chloride) were obtained from Azur (Milan, Italy).

Samples were tested in a medium containing 2% sodium chloride, in five dilutions, and luminescence was recorded after 5, 15, and 30 min of incubation at 15°C. Since no substantial change in luminescence was observed between 5 and 30 min, the results related to 15 min of contact are reported below. Inhibition of luminescence, compared with a toxic-free control to give the percentage inhibition, was calculated following the established protocol using the Microtox calculation program.

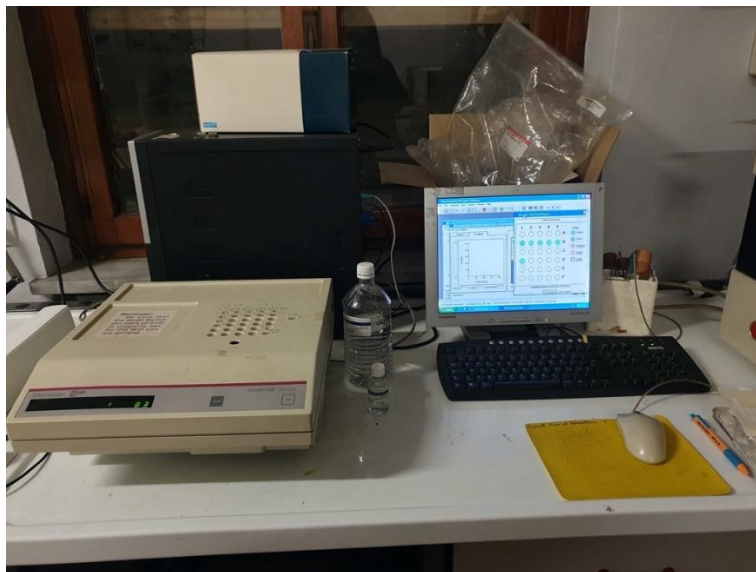


Figure 6.4. Microtox Model 500 Toxicity Analyzer (University of Turin).

6.3. Results and Discussion

6.3.1. Natural sunlight Irradiation

The degradation of CLO can be induced by solar light because it absorbs solar radiations between 295 and 375 nm, as previously reported [12]. The results obtained during natural solar irradiation of CLO (10 mg/L) in MQ water and natural waters (lake and WWTP samples) are presented in Figure 6.5. The photodegradation rates constant of CLO are listed in the following order: MQ water < Lake < WWTP. Considering the quality parameters of natural waters (Table S1 and S2 of Chapter 5), the content of DOM (11.7 and 23.2 mg/L) and NO_3^- (10.5 and 86.1 mg/L) in lake and WWTP samples respectively, these two parameters are much higher in WWTP than in lake and MQ samples, implying the presence of photoactive compounds called photosensitizers [27]. As we can see from the Figure 6.5, the degradation of CLO is clearly faster in WWTP samples, with a half-life of 14 days compared to the half-life in lake samples, 58 days and in MQ water, 481 days. This fact confirmed that the photosensitizers present in the environmental waters when are irradiated under

natural solar light, can generate reactive oxygen species (ROS) such hydroxyl radical ($\bullet\text{OH}$), singlet oxygen ($^1\text{O}_2$), and CDOM triplet states ($^3\text{CDOM}^*$), which can cause pollutant transformation [18]. The same behavior has been observed by other authors for CLO [5,13,28]. Dark control samples were collected to evaluate if there was another degradation process than photolysis during the experiment, and less than the 10% was degraded in the 3 matrices over the exposure period, indicating that other processes such as volatilization and biodegradation did not occur. Then, CLO could be considered as a stable compound in the environment.

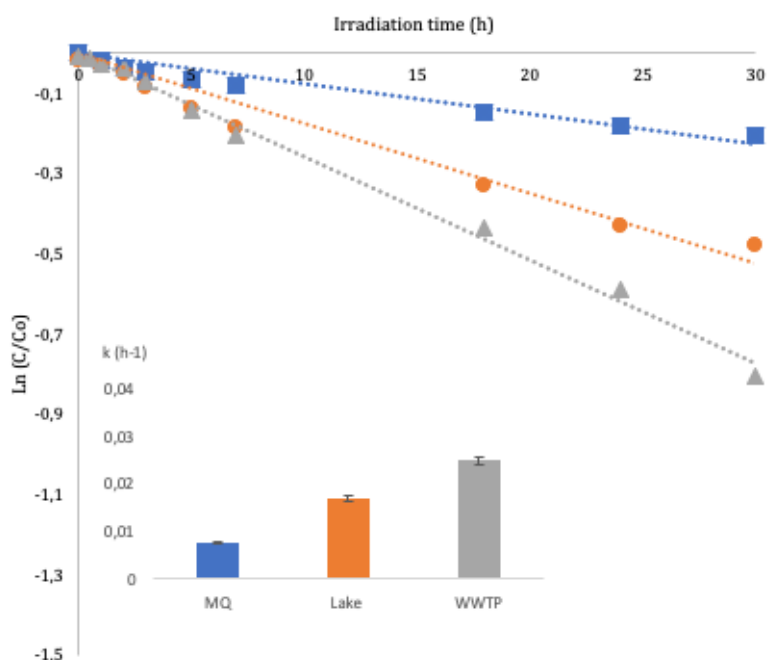


Figure 6.5. Kinetics and rate constants (h^{-1}) of CLO in MQ water (blue), lake sample (orange) and WWTP sample (grey) under natural solar light.

In order to further elucidate this photosensitization effect on the performance of the photolytic process, solutions of CLO (1 mg/L) were irradiated in the presence of NOM, and as a representative standard, humic acid (HA, 10 mg/L) was used. As well, solutions of CLO were irradiated under simulated solar light in the presence of nitrate and bicarbonate ions (10 mg/L each).

6.3.2. Artificial solar irradiation

According to J. Trawiński, the lamp of Xe should be considered as the most relevant for the environment, since it allows evaluating both the environmental fate and the treatment aspects of waste water [25]. Table 6.1 presents the photodegradation rate constants along with half-lives and coefficient standards, exposed to simulated and natural sunlight, presenting the influence of different aqueous matrices.

Table 6.1. Kinetics of the photolysis of CLO in different aqueous media

Photolysis	$t_{1/2}$ (hrs)	k (hrs ⁻¹)	R^2
<i>Simulated solar irradiation (solar box)</i>			
MQ water	91.20	0.0076	0.9703
Lake Pamvotis	40.77	0.0170	0.9775
WWTP water	27.73	0.0258	0.9944
HA 10 mg/L	34.66	0.0200	0.9937
CO ₃ ²⁻ 10 mg/L	63.01	0.0110	0.9904
NO ₃ ⁻ 10 mg/L	46.21	0.0150	0.9955
<i>Natural solar irradiation (outdoor)</i>			
MQ water	11552.45	0.0001	0.9854
Lake Pamvotis	1386.29	0.0005	0.9958
WWTP water	346.57	0.0020	0.9947

Photodegradation of CLO in MQ water, lake and WWTP followed pseudo-first order kinetics, with r^2 generally above 0.9703. Figure 6.6 shows the photolytic behavior of CLO over the time and the rate constant in different matrices. Results showed that the degradation order in natural sunlight is in good agreement with the irradiation experiments done in artificial-laboratory, suggesting that laboratory-scale experiments using artificial irradiation can help to predict the behavior of CLO in

natural waters [29,30]. However, the rate of photodegradation of each sample cannot be directly compared due to differences in the irradiation spectrum and the variation of daily light (night-day circle) [31,32] [25, 26]. But it gives us a better understanding of the photodegradation that actually occurs in the natural environment.

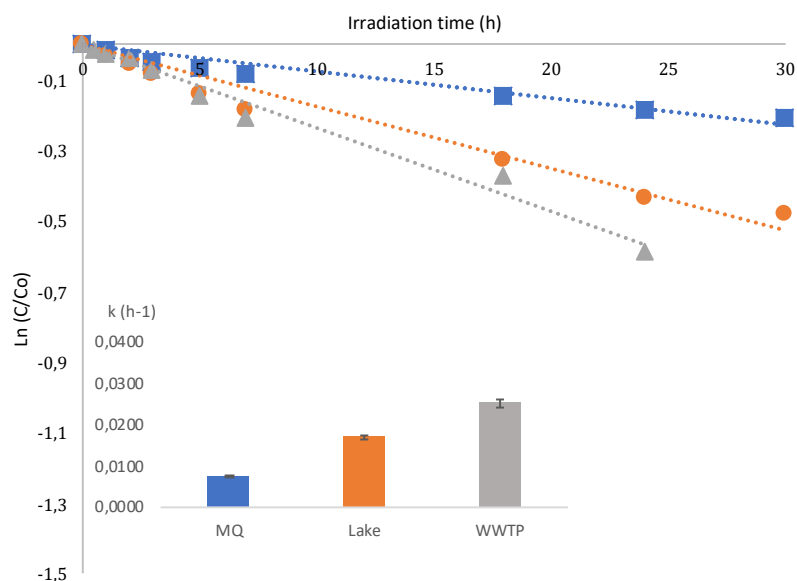


Figure 6.6. Kinetics and rate constants (h^{-1}) of CLO in MQ water (blue), lake sample (orange) and WWTP sample (grey) under artificial solar irradiation.

Photodegradation of CLO under simulated solar irradiation follows a pseudo first order kinetic in the three different matrices, with r^2 generally above 0.9703. The rate constants were of the same order as in the experiment under natural sunlight: MQ water < Lake < WWTP, suggesting that the photosensitizers present in environmental waters promote the degradation of CLO. As before, dark control experiments were carried out and no hydrolysis effect was observed. When CLO was exposed under artificial light in wastewater samples, the photodegradation rate of CLO was 3.3 times faster compared to MQ water. This acceleration due to a sensitization effect was also observed in the lake water. The CLO photodegradation rate was almost 2.2 times higher in lake water compared to MQ, indicating a photosensitization effect in the respective aqueous matrices. From Table S1 and S2 of Chapter 5, it can be seen how the concentration of organic matter follows the order: WWTP >

lake> MQ water, suggesting that the higher concentration of NOM, higher will be the rate of photolysis, according with our findings.

In order to study the role of organic matter of the photolytic process, solutions of CLO (1 mg/L) containing HA, CO_3^{2-} and NO_3^- ions (10 mg/L each) were irradiated and the results are presented in the Table 6.1. Once again, the concentration of NOM and nitrates in natural aqueous samples clearly accelerates the kinetics of CLO. Figure 6.7 presents de kinetics and the rate constants of CLO in the presence of the photosensitizers under artificial solar irradiation. As it was expecting, the presence of HA accelerates the degradation process of CLO considerably, specifically, CLO photodegradation rate was 2.6 times faster in samples containing HA, 1.5 times those containing CO_3^- and twice as fast for those containing NO_3^{2-} , compared to the experimental rate constant obtained for MQ water. CLO is still considered a photostable molecule in the natural aqueous medium, although it degrades a bit in the presence of photosensitizers and under the presence of light. Therefore, it is necessary to study other alternatives, such as Advanced Oxidation Processes (AOPs), for the total elimination of CLO from the environment.

6.3.3. Photocatalysis

TiO_2 is the most used catalyst today due to its features such as it is highly photostable, photoreactive, non-toxic, chemically and biologically inert, and inexpensive. The introduction of the semiconductor (200 mg / L) together with CLO (20 mg / L) in MQ water drastically accelerated its kinetics (Figure 6.9) and after 30 min of irradiation, CLO concentration was less than 5% of the initial concentration.

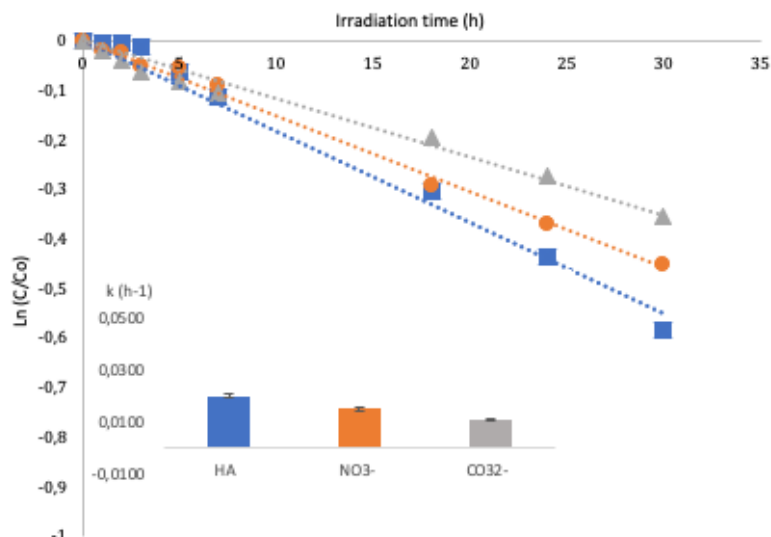


Figure 6.7. Kinetics and rate constants (h^{-1}) of CLO in the presence of HA (blue), NO_3^- (orange) and CO_3^{2-} (blue) ions in different matrices under artificial solar irradiation.

In terms of the mineralization process, the TOC was 5% of the initial organic carbon after 5 hours of irradiation (Figure 6.8). This delay between the TOC evolution and the photocatalytic degradation is due to the formation of intermediate photoproducts. Chlorine is released faster than nitrogen and after 5 hours they reach the stoichiometric amount. Interestingly, nitrogen is released in a small proportion as NO_3^- and remains constant throughout the irradiation process, but instead, ammonia is released in a higher proportion. These results imply that Advance Oxidation Processes, such as photocatalysis, should be examined to overcome the limits of primary and secondary treatment processes in WWTPs for removing CLO residues.

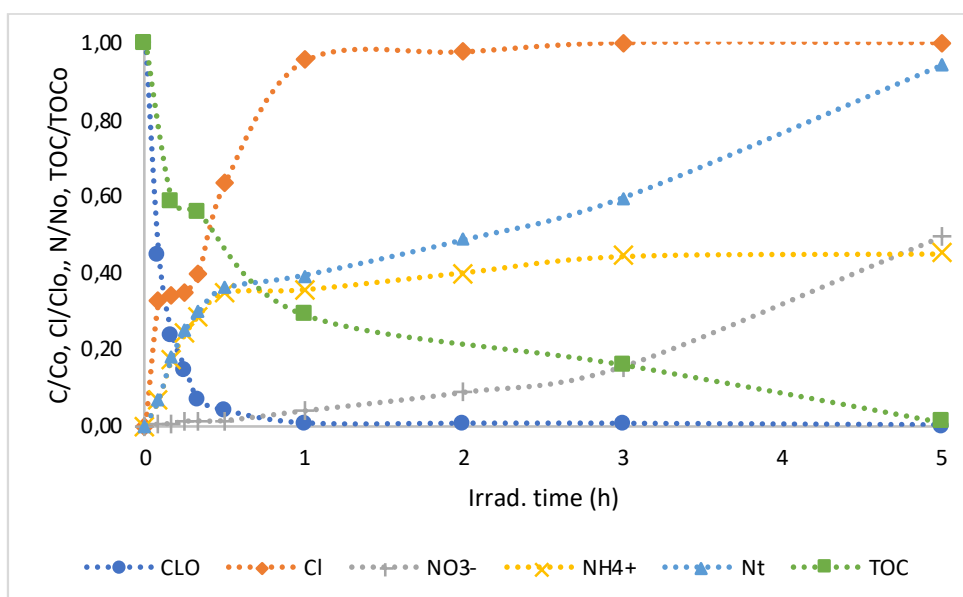


Figure 6.8. Time evolution of primary process of CLO, end-inorganic products (nitrate, ammonium, and chloride) and organic carbon during the photocatalytic degradation of CLO.

6.3.4. Toxicity assessment

The toxicity of CLO in MQ water and TiO₂ was studied by monitoring changes in the natural emission of the luminescent bacteria *V. fischeri* when challenged with toxic compounds. Samples were submitted to degradation process at different irradiation times and analyzed to estimate the percentage of inhibition of each sample. In the first 10 min of irradiation, there was an increase in the inhibition of the toxicity, reaching a maximum of 47% (Figure 6.9). After that time, the toxicity of the solution decreased slowly and after 1h, the toxicity is less than 10%. After 3 hours of irradiation, it seemed that the molecule and its photoproducts have been completely degraded, since the toxicity was 0%, showing the efficiency of the photocatalytic process in the detoxification of the irradiated solution. These observations demonstrate that during the photocatalytic treatment, in the period 0–10 min, compounds more toxic than CLO were formed, in accordance with previously demonstrated observations [33]. There is no data related to the toxicity assessment for CLO in water in the literature, so this was the first attempt to study the toxicity of clozapine.

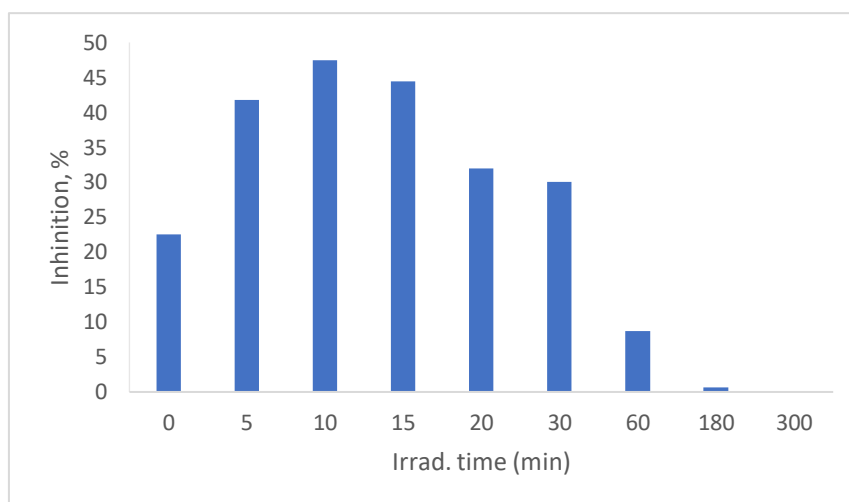


Figure 6.9. Toxicity assessed for CLO as a function of the irradiation times.

6.4. Conclusions

In this study, the degradation of clozapine (CLO), an atypical antipsychotic, using direct and indirect photolysis and heterogeneous photocatalysis (TiO_2 in dispersion), under natural and simulated solar light radiation, was investigated. Various matrices were used: MQ water, lake and WWTP samples, affecting the degradation rate of the target compound during the applied processes. The rate constants of CLO photo-decomposition reactions, were well described by the pseudo-first-order kinetic model. Half-lives of CLO ranged from 91.20 h in MQ to 40.77 and 27.73 h in lake and WWTP samples, respectively, when they were irradiated under artificial solar light, confirming an acceleration effect in the presence of photosensitizers and under the presence of light. The addition of TiO_2 drastically accelerated the degradation rate of CLO and after 30 min of irradiation, CLO was almost completely degraded. Finally, toxicity measurements were conducted using Microtox bioassay in order to evaluate the potential risk of CLO to aqueous organisms. Although, the acute toxicity increased during the first stages of treatment the final outcome led to very low toxicity levels even within 60 min of TiO_2 treatment. Concluding, the obtained results suggest that the photocatalytic

degradation of CLO can lead to its complete elimination and simultaneously to the detoxification of the solution.

References

- [1] R. Loos, J. Wollgast, T. Huber, G. Hanke, Polar herbicides, pharmaceutical products, perfluorooctanesulfonate (PFOS), perfluorooctanoate (PFOA), and nonylphenol and its carboxylates and ethoxylates in surface and tap waters around Lake Maggiore in Northern Italy, *Anal. Bioanal. Chem.* 387 (2007) 1469–1478. <https://doi.org/10.1007/s00216-006-1036-7>.
- [2] R. Moreno-González, S. Rodríguez-Mozaz, M. Gros, E. Pérez-Cánovas, D. Barceló, V.M. León, Input of pharmaceuticals through coastal surface watercourses into a Mediterranean lagoon (Mar Menor, SE Spain): Sources and seasonal variations, *Sci. Total Environ.* 490 (2014) 59–72. <https://doi.org/10.1016/j.scitotenv.2014.04.097>.
- [3] D. Munaron, N. Tapie, H. Budzinski, B. Andral, J.L. Gonzalez, Pharmaceuticals, alkylphenols and pesticides in Mediterranean coastal waters: Results from a pilot survey using passive samplers, *Estuar. Coast. Shelf Sci.* 114 (2012) 82–92. <https://doi.org/10.1016/j.ecss.2011.09.009>.
- [4] S.E. Musson, T.G. Townsend, Pharmaceutical compound content of municipal solid waste, *J. Hazard. Mater.* 162 (2009) 730–735. <https://doi.org/10.1016/j.jhazmat.2008.05.089>.
- [5] R. Skibiński, J. Trawiński, Ł. Komsta, K. Bajda, Characterization of forced degradation products of clozapine by LC-DAD/ESI-Q-TOF, *J. Pharm. Biomed. Anal.* 131 (2016) 272–280. <https://doi.org/10.1016/j.jpba.2016.09.007>.
- [6] S. Yuan, X. Jiang, X. Xia, H. Zhang, S. Zheng, Detection, occurrence and fate of 22 psychiatric pharmaceuticals in psychiatric hospital and municipal wastewater treatment plants in Beijing, China, *Chemosphere.* 90 (2013) 2520–2525. <https://doi.org/10.1016/j.chemosphere.2012.10.089>.
- [7] S. Matongo, G. Birungi, B. Moodley, P. Ndungu, Occurrence of selected pharmaceuticals in water and sediment of Umgeni River, KwaZulu-Natal, South Africa, *Environ. Sci. Pollut. Res.* 22 (2015) 10298–10308. <https://doi.org/10.1007/s11356-015-4217-0>.
- [8] A. David, A. Lange, C.R. Tyler, E.M. Hill, Concentrating mixtures of neuroactive pharmaceuticals and altered neurotransmitter levels in the brain of fish exposed to a wastewater effluent, *Sci. Total Environ.* 621 (2018) 782–790. <https://doi.org/10.1016/j.scitotenv.2017.11.265>.
- [9] G.C. Nallani, R.E. Edziyie, P.M. Paulos, B.J. Venables, L.A. Constantine, D.B. Huggett, Bioconcentration of two basic pharmaceuticals, verapamil and clozapine, in fish, *Environ. Toxicol. Chem.* 35 (2016) 593–603. <https://doi.org/10.1002/etc.3244>.
- [10] M.D. Overturf, C.L. Overturf, D. Baxter, D.N. Hala, L. Constantine, B. Venables, D.B. Huggett,

- Early life-stage toxicity of eight pharmaceuticals to the fathead minnow, *pimephales promelas*, *Arch. Environ. Contam. Toxicol.* 62 (2012) 455–464.
<https://doi.org/10.1007/s00244-011-9723-6>.
- [11] J. Villain, L. Minguez, M.P. Halm-Lemeille, G. Durrieu, R. Bureau, Acute toxicities of pharmaceuticals toward green algae. mode of action, biopharmaceutical drug disposition classification system and quantile regression models, *Ecotoxicol. Environ. Saf.* 124 (2016) 337–343. <https://doi.org/10.1016/j.ecoenv.2015.11.009>.
- [12] C. Jim, V. Sakkas, C. Richard, Phototransformation of Three Psychoactive Drugs in Presence of Sedimental Water Extractable Organic Matter, (2021) 1–17.
- [13] J. Trawiński, Jakub Skibiński, Rapid degradation of clozapine by heterogeneous photocatalysis. Comparison with direct photolysis, kinetics, identification of transformation products and scavenger study, *Sci. Total Environ.* 665 (2019) 557–567.
<https://doi.org/10.1016/j.scitotenv.2019.02.124>.
- [14] C. Jiménez-Holgado, C. Chrimatopoulos, V. Stathopoulos, V. Sakkas, Investigating the utility of fabric phase sorptive extraction and hplc-uv-vis/dad to determine antidepressant drugs in environmental aqueous samples, *Separations.* 7 (2020) 1–14.
<https://doi.org/10.3390/separations7030039>.
- [15] J. Rafael, Photodegradation and phototoxicity of the drug clozapine, 9 (2001) 79–87.
- [16] P.P. Vaughan, N. V. Blough, Photochemical formation of hydroxyl radical by constituents of natural waters, *Environ. Sci. Technol.* 32 (1998) 2947–2953.
<https://doi.org/10.1021/es9710417>.
- [17] K. Mopper, X. Zhou, Hydroxyl radical photoproduction in the sea and its potential impact on marine processes, *Science (80-.)*. 250 (1990) 661–664.
<https://doi.org/10.1126/science.250.4981.661>.
- [18] D. Vione, M. Minella, V. Maurino, C. Minero, Indirect photochemistry in sunlit surface waters: Photoinduced production of reactive transient species, *Chem. - A Eur. J.* 20 (2014) 10590–10606. <https://doi.org/10.1002/chem.201400413>.
- [19] R.G. Zepp, P.F. Schlotzhauer, R.M. Sink, Photosensitized Transformations Involving Electronic Energy Transfer in Natural Waters: Role of Humic Substances, *Environ. Sci. Technol.* 19 (1985) 74–81. <https://doi.org/10.1021/es00131a008>.
- [20] B.M. Peterson, A.M. McNally, R.M. Cory, J.D. Thoemke, J.B. Cotner, K. McNeill, Spatial and temporal distribution of singlet oxygen in Lake Superior, *Environ. Sci. Technol.* 46 (2012) 7222–7229. <https://doi.org/10.1021/es301105e>.
- [21] F.L. Rosario-Ortiz, S. Canonica, Probe compounds to assess the photochemical activity of dissolved organic matter, *Environ. Sci. Technol.* 50 (2016) 12532–12547.

- <https://doi.org/10.1021/acs.est.6b02776>.
- [22] W.J. Cooper, R.G. Zika, R.G. Petasne, J.M. Plane, Photochemical formation of hydrogen peroxide in natural waters exposed to sunlight, *Environ. Sci. Technol.* 22 (1988) 1156–1160.
- [23] V.M. Monsalvo, J.A. McDonald, S.J. Khan, P. Le-Clech, Removal of trace organics by anaerobic membrane bioreactors, *Water Res.* 49 (2014) 103–112.
<https://doi.org/10.1016/j.watres.2013.11.026>.
- [24] S. Yang, F.I. Hai, W.E. Price, J. McDonald, S.J. Khan, L.D. Nghiem, Occurrence of trace organic contaminants in wastewater sludge and their removals by anaerobic digestion, *Bioresour. Technol.* 210 (2016) 153–159. <https://doi.org/10.1016/j.biortech.2015.12.080>.
- [25] J. Trawiński, R. Skibiński, Studies on photodegradation process of psychotropic drugs: a review, *Environ. Sci. Pollut. Res.* 24 (2017) 1152–1199. <https://doi.org/10.1007/s11356-016-7727-5>.
- [26] J. Fenoll, P. Flores, P. Hellín, C.M. Martínez, S. Navarro, Photodegradation of eight miscellaneous pesticides in drinking water after treatment with semiconductor materials under sunlight at pilot plant scale, *Chem. Eng. J.* 204–205 (2012) 54–64.
<https://doi.org/10.1016/j.cej.2012.07.077>.
- [27] I.P. Pozdnyakov, Y.E. Tyutereva, M. V. Parkhats, V.P. Grivin, Y. Fang, L. Liu, D. Wan, F. Luo, Y. Chen, Mechanistic investigation of humic substances assisted photodegradation of imipramine under simulated sunlight, *Sci. Total Environ.* 738 (2020) 140298.
<https://doi.org/10.1016/j.scitotenv.2020.140298>.
- [28] Q.L. Zhao, H. Ito, T. Kondo, T. Uehara, M. Ikeda, H. Abe, J.I. Saitoh, K. Noguchi, M. Suzuki, M. Kurachi, Antipsychotic drugs scavenge radiation-induced hydroxyl radicals and intracellular ROS formation, and protect apoptosis in human lymphoma U937 cells, *Free Radic. Res.* 53 (2019) 304–312. <https://doi.org/10.1080/10715762.2019.1572889>.
- [29] C.I. Kosma, D.A. Lambropoulou, T.A. Albanis, Photochemical transformation and wastewater fate and occurrence of omeprazole: HRMS for elucidation of transformation products and target and suspect screening analysis in wastewaters, *Sci. Total Environ.* 590–591 (2017) 592–601. <https://doi.org/10.1016/j.scitotenv.2017.02.233>.
- [30] K. Kotnik, T. Kosjek, B. Žegura, M. Filipič, E. Heath, Photolytic fate and genotoxicity of benzophenone-derived compounds and their photodegradation mixtures in the aqueous environment, *Chemosphere.* 147 (2016) 114–123.
<https://doi.org/10.1016/j.chemosphere.2015.12.068>.
- [31] B. Zonja, C. Gonçalves, S. Pérez, A. Delgado, M. Petrovic, M.F. Alpendurada, D. Barceló, Evaluation of the phototransformation of the antiviral zanamivir in surface waters through identification of transformation products, *J. Hazard. Mater.* 265 (2014) 296–304.

<https://doi.org/10.1016/j.jhazmat.2013.10.008>.

- [32] V.G. Beretsou, A.K. Psoma, P. Gago-Ferrero, R. Aalizadeh, K. Fenner, N.S. Thomaidis, Identification of biotransformation products of citalopram formed in activated sludge, *Water Res.* 103 (2016) 205–214. <https://doi.org/10.1016/j.watres.2016.07.029>.
- [33] A.K. Brown, J.K. Challis, C.S. Wong, M.L. Hanson, Selective serotonin reuptake inhibitors and β -blocker transformation products may not pose a significant risk of toxicity to aquatic organisms in wastewater effluent-dominated receiving waters, *Integr. Environ. Assess. Manag.* 11 (2015) 618–639. <https://doi.org/10.1002/ieam.1637>.

Chapter 7. General conclusions

The main goals of this PhD project were successfully achieved by the development of a green microextraction method for the determination of the target analytes in environmental samples as well the study of their photolytic and photocatalytic fate as well as the elucidation of their degradation pathways.

The determination and preconcentration of the target analytes were achieved with an innovative fabric phase sorptive extraction (FPSE) followed by high performance liquid chromatography (HPLC) with a diode-array detector (DAD). The behavior of different substrates has been studied such as laboratory filter paper as well as 3D-printed PLA, a biodegradable and low-cost material. The set-up of the extraction process and the type of coating were the variables exerting the most prominent effects in the repeatability and the yield of the extraction, respectively. The chromatographic separation was carried using a mobile phase consisted of methanol and water acidified with phosphate buffer of pH 3.0 at a flow rate 0.3 mL/min on SpeedCore C18 50x2.1 mm column. The analytical method was optimized with the aid of chemometric tools such as experimental design and response surface methodology to tease out the factors that are statistically

significant in either mode of extraction, and to determine what combination of levels produces the optimum. In accordance with the obtained results, the optimum conditions for FPSE procedure were as follow: sample volume of 1 mL with an ionic strength of 0% at pH 12, an extraction time of 30 min and elution with 0.10 mL of methanol for 10 min at stirring conditions (300 rpm).

In addition, the mechanisms of sertraline, clozapine and citalopram photo-transformation were studied when they are irradiated in the presence of natural organic matter. Water extractable organic matter (WEOM) was extracted from sediments of Pamvotis Lake under mild conditions. Water extractable NOM (WEOM) was recovered by stirring sediments at room temperature overnight in phosphate buffer at pH 9-9.5. UV-visible and fluorescence spectra confirmed the humic-like nature of WEOM.

The capacity of WEOM to generate oxidant species under simulated solar light was determined using probe molecules. Then, we investigated the ability of WEOM to sensitize the photodegradation of the three target compounds. It was observed that Extracted WEOM generate triplet WEOM, singlet oxygen and hydroxyl radicals upon irradiation around 365 nm. Formations were quantified using trimethylphenol, furfuryl alcohol and terephthalic acid as probe molecules. It can be said that the CECS were mainly oxidized by OH radicals upon irradiation in the presence of WEOM. Many photoproducts were identified by HPLC-HRMS; such non-specific reaction confirms the involvement of hydroxyl radicals.

Moreover, the photoinduced degradation of sertraline, citalopram and clozapine under simulated solar radiation was studied. Photolysis was studied under different experimental conditions to explore its photolytic fate in the aqueous environment. Photolytic degradation kinetics were carried out in ultrapure water, wastewater effluent, lake water, as well as in the presence of dissolved organic matter (humic acids), bicarbonate and nitrate ions which enabled their assessment on sertraline photooxidation. Direct photolysis was not shown to play a key role, while the reaction of the target analytes with photoactive compounds accelerated drugs transformation. The

introduction of TiO₂ as a catalyst dramatically accelerated the degradation rate of the three drugs even at mild conditions (400 mg/L) and after 1 h of irradiation, parent molecules were totally removed.

Finally, toxicity assessment of the three molecules showed that at the beginning of the irradiation, the toxicity is increased. However, afterwards the toxicity slowed down settling at negligible value at the end of treatment in agreement with the organic carbon content reduction. For the three molecules, irradiation treatments can result in compounds that are more harmful than the parent substance.

Summary of PhD activities

Conferences attended

- 1-4 September, 2021. 17th International Conference on Environmental Science and Technology.

Oral presentation: "Aquatic phototransformation of psychoactive drugs by organic matter extracted from sediments of Pamvotis lake". Athens, Greece.

- 3-6 May, 2021. SETAC Europe 31st Annual meeting. Oral presentation: "Effect of water extractable organic matter from sediment of lake Pamvotis of psychoactive drugs under simulated solar light".

Virtual conference.

- 1-12 June, 2020. 68th American Society for Mass Spectrometry Annual Conference (ASMS). Oral presentation: "Photodegradation of contaminants of emerging concern enhanced by dissolved organic matter derived from Pamvotis Lake sediments". Virtual conference.

- 3-7 May, 2020. SETAC Europe 30th Annual meeting. Poster and Flash presentation:

"Photodegradation of contaminants of emerging concern by simulated solar irradiation enhanced by dissolved organic matter derived from Pamvotis Lake sediments (NW Greece)". Virtual conference.

- 22-25 September, 2019. 11th International Conference on "Instrumental Methods of Analysis" (IMA 2019). Oral presentation: "Fabric phase sorptive extraction for the determination of antidepressant drugs in environmental samples prior to HPLC-DAD". Ioannina, Greece.

- 2-6 September, 2019. International Conference on Chemical Energy and Semiconductor Photochemistry. Trabzon, Turkey.

- 4-7 September, 2019. 16th International Conference on Environmental Science and Technology (CEST 2019). Oral presentation: "Optimization of fabric phase sorptive extraction for the determination of selected pharmaceuticals in environmental waters". Rhodes, Greece.
- 16-20 June, 2019. 17th International Conference on Chemistry and the Environment (ICCE 2019). Oral presentation: "Fabric phase sorptive extraction followed by high-performance liquid chromatography (HPLC-DAD) for the determination of psychoactive drugs in environmental samples". Thessaloniki, Greece.

Attending courses and training activities

- Webinar: "Estudio de las aguas residuales con fines epidemiológicos." organized by FACSAs in cooperation with Universitat Jaume I, Castellón, Spain - UJI. 28th January, 2021. Online.
- Webinar: "Preparation and characterization of photocatalysts for environmental application" organized by Universitat Politècnica de Valencia, Spain. 27th January, 2021. Online.
- Webinar: "EU versus Italian water management" organized by SMAT, Italy. 18th January, 2021. Online.
- Research Italian Night: "La sfida di AQUALITY: rimuovere i contaminanti di ultima generazione dalle acque". Torino, Italy. 27th November, 2020.
- Summer School: "Introduction to Basic Statistical Tools and Data Analysis in Research". Organized by Ioannina University and Università Piemonte Orientale. 23-24th September, 2020. Online.
- Webinar. "ESOF 2020, "The emotional roller coaster of building a Career in Science", SCI Giovani session, dedicated to Mental Health of young researchers." 6th September, 2020. Online.
- Webinar: "Open science and the reward system: how can they be aligned?". Webinar- organized by BrighTALK. 2nd July, 2020. Online.
- Webinar: "Innovative Water Week-2020". 22-26th June, 2020. Online.

- Webinar: NanoCommons Online Jaqot webinar on nanotoxicity prediction: "Take your research from bench to the community by making yours models available as a web service". NanoCommons. 3rd June, 2020. Online.
- Course: "Estaciones de Depuración de Aguas Residuales (EDAR): Funcionamiento y Explotación". FACSA with Universitat Jaume I, Spain. 9-30th April, 2020. Online.
- Training on Method Development HPLC-DAD (24 h). University of Ioannina, Greece. 15-17th April, 2019.
- Training on Method Development GC-MS (24 h). University of Ioannina, Greece. 9-11th April, 2019.
- Training on Lab safety (8 h). University of Ioannina, Greece. 8th April 2019.
- Workshop on "Prioritisation of Emerging Contaminants in Urban Wastewater". Palaiseau, Paris, France. 6th March, 2019.
- Winter School on Mass Spectrometry, École Polytechnique de Paris. Paris, France. 4-8th March, 2019.
- Summer School on "Micropollutant analysis and emerging technologies for their abatement". Aalborg, Denmark. 27-29th August, 2018.
- Summer School on "Photochemistry and depollution: direct and sensitized photolysis, fundamental aspects and examples". Clermont Ferrand, France. 25-27th April 2018.

Periods Abroad

- October-December, 2020. Università degli Studi di Torino, Italy. "Identification of intermediate products of Contaminants of Emerging Concern photodegradation at Pamvotis Lake during the case study". Tutor: Prof. Debora Fabbri.
- October-March, 2020. CNRS, Clermont-Ferrand, France. "Isolation and characterization of the dissolved organic carbon from Pamvotis Lake and investigation of the photochemical fate of the

Contaminants of Emerging Concern in aqueous matrices of different composition”. Tutor: Prof. Claire Richard

- MIRTEC S.A, Chalkida, Greece. “Development of advanced green analytical methods (materials characterization) for the determination of Contaminants of Emerging Concern”. October-November 2018. Tutor: Prof. Vassilis Stathopoulos.

